

Summer 8-31-2003

Thermochemistry and kinetic analysis on radicals of acetaldehyde + O₂, allyl radical + O₂ and diethyl and chlorodiethyl sulfides

Jongwoo Lee
New Jersey Institute of Technology

Follow this and additional works at: <https://digitalcommons.njit.edu/dissertations>

 Part of the [Chemical Engineering Commons](#)

Recommended Citation

Lee, Jongwoo, "Thermochemistry and kinetic analysis on radicals of acetaldehyde + O₂, allyl radical + O₂ and diethyl and chlorodiethyl sulfides" (2003). *Dissertations*. 592.
<https://digitalcommons.njit.edu/dissertations/592>

This Dissertation is brought to you for free and open access by the Electronic Theses and Dissertations at Digital Commons @ NJIT. It has been accepted for inclusion in Dissertations by an authorized administrator of Digital Commons @ NJIT. For more information, please contact digitalcommons@njit.edu.

Copyright Warning & Restrictions

The copyright law of the United States (Title 17, United States Code) governs the making of photocopies or other reproductions of copyrighted material.

Under certain conditions specified in the law, libraries and archives are authorized to furnish a photocopy or other reproduction. One of these specified conditions is that the photocopy or reproduction is not to be “used for any purpose other than private study, scholarship, or research.” If a user makes a request for, or later uses, a photocopy or reproduction for purposes in excess of “fair use” that user may be liable for copyright infringement,

This institution reserves the right to refuse to accept a copying order if, in its judgment, fulfillment of the order would involve violation of copyright law.

Please Note: The author retains the copyright while the New Jersey Institute of Technology reserves the right to distribute this thesis or dissertation

Printing note: If you do not wish to print this page, then select “Pages from: first page # to: last page #” on the print dialog screen

The Van Houten library has removed some of the personal information and all signatures from the approval page and biographical sketches of theses and dissertations in order to protect the identity of NJIT graduates and faculty.

ABSTRACT

THERMOCHEMISTRY AND KINETIC ANALYSIS ON RADICALS OF ACETALDEHYDE + O₂, ALLYL RADICAL + O₂ AND DIETHYL AND CHLORODIETHYL SULFIDES

by
Jongwoo Lee

Thermochemical properties for reactants, intermediates, products and transition states important in the radicals of acetaldehyde + O₂ and allyl radical + O₂ reaction systems are analyzed with density functional and *ab initio* calculations, to evaluate the reaction paths and kinetics in oxidation and pyrolysis. Ketene is one important product resulting from acetaldehyde oxidation; thus thermochemistry plus isomerization and conversion reactions of ketene are also analyzed. Enthalpies of formation are determined using isodesmic reaction analysis at the CBSQ composite and density functional levels. Entropies and heat capacities are determined using geometric parameters and vibration frequencies obtained at the HF/6-31G(d') or B3LYP/6-31G(d,p) level of theory. Internal rotor contributions are included in calculation of entropy, S°_{298} , and heat capacities, $C_p(T)$. Rate constants are estimated as a function of pressure and temperature using multifrequency quantum Rice-Ramsperger-Kassel analysis for $k(E)$ and master equation analysis for falloff. A mechanism for pyrolysis and oxidation of acetaldehyde and its' corresponding radicals is constructed. The competition between reactions of radicals of acetaldehyde with O₂ versus unimolecular decomposition is evaluated versus temperature and pressure.

Thermodynamic parameters, enthalpies, entropies and heat capacities are evaluated for C₁ and C₂ chlorocarbon molecules and radicals. These thermodynamic

properties are used in evaluation and comparison of $\text{Cl}_2 + \text{R}\bullet \rightleftharpoons \text{Cl}\bullet + \text{RCl}$ reaction rate constants from the kinetics literature for comparison with empirical analysis. Data from some 20 reactions in the literature show linearity on a plot of $E_{a,\text{fwd}}$ vs. $\Delta H_{\text{rxn},\text{fwd}}$, yielding a slope of (0.38 ± 0.04) and an intercept of (10.12 ± 0.81) kcal/mol.

The use of Density Functional Theory, B3LYP/6-31g(d,p), with isodesmic working reactions for enthalpy of formation of sulfur hydrocarbons is evaluated using a set of known sulfur hydrocarbon / radical species. Thermodynamic and kinetic parameters for reactants, transition states, and products from unimolecular dissociations of sulfur species related to the chemical agent: $\text{CH}_3\text{CH}_2\text{SCH}_2\text{CH}_3$, $\text{CH}_3\text{CH}_2\text{SCH}_2\text{CH}_2\text{Cl}$, and $\text{CH}_2\text{ClCH}_2\text{SCH}_2\text{CH}_2\text{Cl}$ and corresponding radicals are analyzed. Standard enthalpy, ΔH_f° , for the molecules and radicals are determined using isodesmic reaction analysis at the B3LYP/6-31G(d,p) level, with S°_{298} and $C_p(T)$ determined using geometric parameters and vibrational frequencies obtained at this same level of theory. Potential barriers for the internal rotor potentials are also calculated at the B3LYP/6-31G(d,p) level, and the hindered rotation contributions to S°_{298} and $C_p(T)$ are calculated.

**THERMOCHEMISTRY AND KINETIC ANALYSIS ON RADICALS OF
ACETALDEHYDE + O₂, ALLYL RADICAL + O₂ AND
DIETHYL AND CHLORODIETHYL SULFIDES**

by
Jongwoo Lee

**A Dissertation
Submitted to the Faculty of New Jersey Institute of Technology
in Partial Fulfillment of the Requirements for the Degree of
Doctor of Philosophy**

Department of Chemical Engineering

August 2003

Copyright © 2003 by Jongwoo Lee

ALL RIGHTS RESERVED

APPROVAL PAGE

THERMOCHEMISTRY AND KINETIC ANALYSIS ON RADICALS OF ACETALDEHYDE + O₂, ALLYL RADICAL + O₂ AND DIETHYL AND CHLORODIETHYL SULFIDES

Jongwoo Lee

Dr. Joseph W. Bozzelli, Advisor Date
Distinguished Professor and Chairperson of Chemistry and Environmental Science, NJIT

Dr. Tamara M. Gund Date
Professor of Chemistry, NJIT

Dr. Dana E. Knox Date
Associate Professor and Associate Chairperson of Chemical Engineering, NJIT

Dr. Michael C. Y. Huang Date
Assistant Professor of Chemical Engineering, NJIT

Dr. Edward Ritter Date
Associate Professor of Chemical Engineering, Villanova University, PA

BIOGRAPHICAL SKETCH

Author: Jongwoo Lee
Degree: Doctor of Philosophy
Date: August 2003

Undergraduate and Graduate Education:

- Doctor of Philosophy in Chemical Engineering,
New Jersey Institute of Technology, Newark, NJ, 2003
- Master of Science in Chemical Engineering,
New Jersey Institute of Technology, Newark, NJ, 1999
- Bachelor of Science in Chemical Engineering,
Yonsei University, Seoul, Korea, 1995

Major: Chemical Engineering

Publications:

Lee, J.; Bozzelli, J. W., "Thermochemical and Kinetic Analysis of the Formyl Methyl Radical + O₂ Reaction System" *Journal of Physical Chemistry A*, Volume 107, Issue 19, 2003, pp. 3778-3791.

Lee, J.; Bozzelli, J. W., "Reaction of H + Ketene to Formyl Methyl and Acetyl Radicals and Reverse Dissociations" *International Journal of Chemical Kinetics*, Volume 35, Issue 1, 2003, pp. 20-44.

Lee, J.; Chen, C.; Bozzelli, J. W., "Thermochemical and Kinetic Analysis of the Acetyl Radical (CH₃C●O) + O₂ Reaction System" *Journal of Physical Chemistry A*, Volume 106, Issue 31, 2002, pp. 7155-7170.

Lee, J.; Bozzelli, J. W.; Sawerysyn, J. P., “*Ab initio* Calculations and Thermochemical Analysis on Cl Atom Abstractions of Chlorine from Chlorocarbons and the Reverse Alkyl Abstractions: $\text{Cl}_2 + \text{R}\bullet \leftrightarrow \text{Cl}\bullet + \text{RCl}$ ” *International Journal of Chemical Kinetics*, Volume 32, Issue 9, 2000, pp. 548-565.

Presentations:

Lee, J.; Bozzelli, J. W.; Pitz, W., “Thermochemical Properties, Reaction Pathways, and Kinetics of the Allyl Radical with O_2 Reaction System”, *AIChE Annual Meeting*; Indianapolis, IN; November 3-8, 2002, 392a, Oral Presentation.

Lee, J.; Bozzelli, J. W., “Thermochemical Properties, Reaction Pathways, and Kinetics of the Formyl Methyl Radical + O_2 Reaction System”, *AIChE Annual Meeting*; Indianapolis, IN; November 3-8, 2002, 223b, Poster.

Lee, J.; Bozzelli, J. W., “Thermochemical Properties, Reaction Pathways, and Kinetics of the Ketene + H Reaction System”, *AIChE Annual Meeting*; Indianapolis, IN; November 3-8, 2002, 373ab, Poster.

Lee, J.; Bozzelli, J. W., “Thermochemical Properties, Reaction Pathways, and Kinetics of the Acetyl Radical + O_2 Reaction System”, *17th International Symposium on Gas Kinetics*; Essen, Germany; August 24-29, 2002, AP.10, Poster.

Lee, J.; Bozzelli, J. W., “Thermodynamic Properties of Acetyl and Ethyl Hydroperoxides and Peroxyacetyl and Peroxyethyl Nitrite”, *223rd ACS National Meeting*; Orlando, FL; April 7-11, 2002, 180, Poster.

Lee, J.; Bozzelli, J. W., “Thermodynamic and Kinetic Analysis using *Ab initio* Calculations on Formyl Methyl Radical + O_2 Reaction System”, *Fifth International Conference on Chemical Kinetics*; Gaithersburg, MD; July 16-20, 2001, 295-296, Oral Presentation.

Lee, J.; Bozzelli, J. W.; Pitz, W., “Thermochemical and Kinetic Analysis on Allyl Radical + O_2 Reaction System”, *Fifth International Conference on Chemical Kinetics*; Gaithersburg, MD; July 16-20, 2001, 157-158, Poster.

Lee, J.; Bozzelli, J. W.; Sawerysyn, J. P., “*Ab initio* Calculations and Thermodynamic Analysis on Cl Atom Abstractions of Chlorine from Chlorocarbons and the Reverse Alkyl Abstractions: $\text{Cl}_2 + \text{R}\bullet \leftrightarrow \text{Cl}\bullet + \text{RCl}$ ”, *The Fall Technical Meeting of the Eastern States Section of the Combustion Institute*; Raleigh, NC; October 10-13, 1999, 41-44, Oral Presentation.

This thesis is dedicated to
my parents, Nam-Ki Lee and Jung-Yeul Kang,
my wife, Bo-Young Noh, and
my son, Bryan Jaewon Lee

ACKNOWLEDGMENT

First and foremost, I wish to express my appreciation to my advisor, Professor Joseph W. Bozzelli, not only for his professional advice but also his encouragement, patience, and support throughout this research. I also wish to thank Mrs. Bozzelli for her kindness.

I would also like to thank to my dissertation committee members, Professor Tamara Gund, Professor Dana Knox, Professor Michael Huang, and Professor Edward Ritter for their helpful corrections and suggestions.

The author is exceptionally appreciative to the members of Bozzelli Research Group who have provided friendship, assistance and encouraging conversations during my studies include Dr. Larry Lay, Dr. Chiung-Chu Chen, Dr. Takahiro Yamada, Dr. Chad Sheng, Dr. Byung-Ik Park, Dr. Samuel Chern, Dr. Li Zhu, and Hongyan Sun.

In particular, I must appreciate constant love, prayers, support and encouragement my parents have given me over years, as well as freedom to allow me to pursue my dreams. I would also like to thank my wife, Bo-young Noh and my son, Bryan Jaewon Lee for being patient, always providing encouragement and being there for me.

Of course, I must Thank God and Praise the Lord Jesus Christ, for without Him, nothing would be possible.

TABLE OF CONTENTS

Chapter	Page
1 INTRODUCTION.....	1
1.1 Background.....	1
1.2 Previous Studies.....	3
2 THERMOCHEMICAL KINETICS.....	7
2.1 Overview.....	7
2.2 Computational Chemistry.....	8
2.3 Kinetics.....	10
2.3.1 Lindemann-Hinshelwood Mechanism for Unimolecular Reactions..	10
2.3.2 Slater Theory.....	14
2.3.3 RRK Theory of Unimolecular Reactions.....	15
2.3.4 RRKM Theory of Unimolecular Reactions.....	17
2.3.5 Chemical Activation Reactions.....	17
2.3.6 QRRK Analysis for Unimolecular and Chemical Activation Reactions.....	21
3 THERMOCHEMICAL AND KINETIC ANALYSYS OF THE ACETYL RADICAL + O ₂ REACTION SYSTEM.....	24
3.1 Background.....	24
3.2 Calculation Methods.....	26
3.2.1 Determination of Enthalpy of Formation.....	27
3.2.2 Determination of Entropy and Heat Capacity.....	29
3.2.3 High-Pressure Limit A Factor (A_{∞}) and Rate Constant (k_{∞}) Determination.....	30
3.2.4 Kinetic Analysis.....	31

TABLE OF CONTENTS
(Continued)

Chapter	Page
3.3 Results and Discussion	32
3.3.1 Transition States.....	32
3.3.2 Enthalpy of Formation ($\Delta H_f^\circ_{298}$) using Calculated Total Energies and Isodesmic Reactions.....	33
3.3.3 Entropy ($S^\circ_{(298)}$) and Heat Capacity ($C_p(T)$, $300 \leq T/K \leq 1500$).....	34
3.3.4 Energy Diagram for $\text{CH}_3\text{C}\bullet\text{O} + \text{O}_2$ Reaction System.....	38
3.3.5 Comparison of $\text{C}_2\text{H}_5 + \text{O}_2$ and $\text{CH}_3\text{C}\bullet\text{O} + \text{O}_2$	41
3.3.6 Analysis of Chemical Activation Reaction in Acetyl + O_2	45
3.3.7 Abstraction of Methyl Hydrogen in $\text{CH}_3\text{C}\bullet\text{O}$ by O_2	46
3.3.8 Unimolecular Dissociation of Acetyl Peroxy and Formyl Methyl Hydroperoxide Radicals.....	50
3.3.9 Acetyl Radical Unimolecular Dissociation.....	57
3.3.10 Detailed Mechanism of Acetyl Radical Reactions.....	61
3.3.11 Importance of $\text{CH}_3\text{C}\bullet\text{O} + \text{O}_2$ Relative to Unimolecular Dissociation of $\text{CH}_3\text{C}\bullet\text{O}$	62
3.4 Summary	66
4 THERMOCHEMICAL AND KINETIC ANALYSIS OF THE FORMYL METHYL RADICAL + O_2 REACTION SYSTEM.....	67
4.1 Background	67
4.2 Calculation Methods	69
4.2.1 Determination of Enthalpy of Formation.....	71
4.2.2 Determination of Entropy and Heat Capacity	72

TABLE OF CONTENTS
(Continued)

Chapter	Page
4.2.3 High-Pressure Limit A Factors (A_∞) and Rate Constants (k_∞) Determination	73
4.2.4 Kinetic Analysis	74
4.3 Results and Discussion	75
4.3.1 Geometries of Parent Hydroperoxide Aldehyde, Two Intermediate Radicals and Transition States	75
4.3.2 Enthalpy of Formation ($\Delta H_f^\circ_{298}$) using Calculated Total Energies and Isodesmic Reactions	77
4.3.3 Entropy ($S^\circ_{(298)}$) and Heat Capacity ($C_p(T)$, $300 \leq T/K \leq 1500$).....	82
4.3.4 Energy Diagram for $C\bullet H_2CHO + O_2$ Reaction System	82
4.3.5 Comparison of $C\bullet H_2CHO + O_2$, $CH_3C\bullet O + O_2$ and $C_2H_5 + O_2$	86
4.3.6 Analysis of the $C\bullet H_2CHO + O_2$ Chemical Activation Reaction	86
4.3.7 Abstraction of a Hydrogen from the $-CHO$ Group of $C\bullet H_2CHO$ by O_2	90
4.3.8 Unimolecular Dissociation of Formyl Methyl Peroxy and Acetyl Hydroperoxide Radicals	94
4.3.9 Formyl Methyl Radical Unimolecular Dissociation	95
4.3.10 Detailed Mechanism of Formyl Methyl Radical Oxidation Reactions.....	96
4.3.11 Comparison of $C\bullet H_2CHO + O_2$ with Unimolecular Dissociation of $C\bullet H_2CHO$	101
4.4 Summary	104
5 REACTION OF H + KETENE TO FORMYL METHYL RADICAL AND ACETYL RADICALS AND REVERSE DISSOCIATIONS.....	106
5.1 Background	106

TABLE OF CONTENTS
(Continued)

Chapter	Page
5.2 Calculation Methods	109
5.2.1 Determination of Enthalpy of Formation.....	110
5.2.2 Determination of Entropy and Heat Capacity	111
5.2.3 High-Pressure Limit A Factor (A_{∞}) and Rate Constant (k_{∞}) Determination	112
5.2.4 Kinetic Analysis.....	113
5.3 Results and Discussion	114
5.3.1 Geometries of Intermediate Radicals and Transition States	114
5.3.2 Enthalpy of Formation ($\Delta H_f^{\circ}_{298}$) using Calculated Total Energies and Isodesmic Reactions.....	120
5.3.3 Entropy ($S^{\circ}_{(298)}$) and Heat Capacity ($C_p(T)$)	123
5.3.4 Potential Energy Diagram for $\text{CH}_2=\text{C}=\text{O} + \text{H}$ / Formyl Methyl and Acetyl Radical System	126
5.3.5 Analysis of Chemical Activation Reaction in $\text{CH}_2=\text{C}=\text{O} + \text{H}$ via TS1 and TS2	127
5.3.6 Abstraction of Hydrogen Atom in $\text{CH}_2=\text{C}=\text{O}$ by H.....	134
5.3.7 Radical Dissociations.....	138
5.4 Summary	144
6 THERMOCHEMICAL PROPERTIES, REACTION PATHWAYS AND KINETICS OF THE ALLYL RADICAL WITH O_2 REACTION SYSTEM.....	145
6.1 Background	145
6.2 Calculation Methods	148
6.2.1 Determination of Enthalpy of Formation.....	149

TABLE OF CONTENTS
(Continued)

Chapter	Page
6.2.2	150
6.2.3	151
6.2.4	151
6.3	152
6.3.1	152
6.3.2	160
6.3.3	165
6.3.4	168
6.3.5	172
6.3.6	176
6.4	180
7	181
7.1	181
7.2	182
7.3	184
7.3.1	184
7.3.2	184
7.3.3	185

TABLE OF CONTENTS
(Continued)

Chapter	Page
7.3.4 Thermodynamic Properties	185
7.3.5 Thermodynamic Analysis for the Reactions	188
7.4 Results and Discussion	188
7.4.1 <i>Ab initio</i> Calculations of Thermodynamic Properties in Reactions of CH ₃ and C ₂ H ₅ with Cl ₂	188
7.4.2 Estimation of Entropy and Heat Capacity for Transition States and Adducts	190
7.4.3 Calculated Enthalpies of Formation.....	192
7.4.4 Thermodynamic Analysis for Reactions of CH ₃ and C ₂ H ₅ with Cl ₂	192
7.4.5 Atomic Charges in reactants, Adducts, Transition States, and Products CH ₃ + Cl ₂ ---> CH ₃ Cl + Cl and C ₂ H ₅ + Cl ₂ ---> C ₂ H ₅ Cl + Cl Reactions.....	197
7.4.6 Thermodynamics of Literature Data and Comparison.....	203
7.5 Summary	210
8 INTERNAL ROTOR ANALYSIS, THERMODYNAMIC PROPERTIES, BOND ENERGIES, DISSOCIATION PATHS AND KINETICS ON DIETHYL AND CHLORODIETHYL SULFIDES: CH₃CH₂SCH₂CH₃, CH₃CH₂SCH₂CH₂CL, AND CH₂CLCH₂SCH₂CH₂CL.....	212
8.1 Overview.....	212
8.2 Background	213
8.3 Calculation Methods	214
8.3.1 Geometries and Vibration Frequencies.....	214
8.3.2 Enthalpies of Formation.....	217
8.3.3 Entropy and Heat Capacity	222

TABLE OF CONTENTS
(Continued)

Chapter	Page
8.3.4 High-Pressure Limit A Factors (A_∞) and Rate Constants (k_∞) Determination	222
8.4 Results and Discussion	224
8.4.1 Rotational Barriers	224
8.4.2 Entropy ($S^\circ_{(298)}$) and Heat Capacity ($C_p(T)$)	228
8.4.3 Hydrogen Bond Dissociation Energies (BDEs) in CH_3SH , $\text{CH}_3\text{CH}_2\text{SH}$, CH_3SCH_3 , $\text{CH}_3\text{CH}_2\text{SCH}_2\text{CH}_3$, and $\text{CH}_3\text{CH}_2\text{SCH}_2\text{CH}_2\text{Cl}$	231
8.4.4 Unimolecular Dissociation Reactions on $\text{CH}_3\text{CH}_2\text{SCH}_2\text{CH}_3$, $\text{CH}_3\text{CH}_2\text{SCH}_2\text{CH}_2\text{Cl}$, and $\text{CH}_2\text{ClCH}_2\text{SCH}_2\text{CH}_2\text{Cl}$	233
8.5 Summary	241
APPENDIX A $\text{CH}_3\text{C}(=\text{O})\text{OO}\bullet$ AND $\text{C}\bullet\text{H}_2\text{C}(=\text{O})\text{OOH}$ DISSOCIATIONS	242
APPENDIX B GEOMETRIES AND $\text{C}(\text{OO}\bullet)\text{H}_2\text{CHO}$ AND $\text{C}(\text{OOH})\text{H}_2\text{C}\bullet\text{O}$ DISSOCIATIONS.....	253
APPENDIX C GEOMETRIES, VIBRATIONAL FREQUENCIES AND MOMENTS OF INERTIA.....	263
APPENDIX D INTERNAL ROTATION, THERMODYNAMIC AND KINETIC ANALYSIS	272
APPENDIX E PARTIAL INSTRUCTION SET FOR CHEMRATE	286
REFERENCES	300

LIST OF TABLES

Table		Page
3.1	Activation Energies and Enthalpies of Transition States in CBSQ Calculation ^a	30
3.2	Enthalpies of Formation for Reference Molecules in the Isodesmic Reactions.....	34
3.3	Reaction Enthalpies and Enthalpies of Formation in the Isodesmic Reactions ^a	35
3.4	Ideal Gas Phase Thermodynamic Properties Obtained by CBSQ Calculation and by Therm ^a	36
3.5	Moments of Inertia (amu-Å ²) and Rotational Barriers (kcal/mol) for Internal Rotors.....	38
3.6	The Comparison of Bond Energies between CH ₃ C(=O)OOH and C ₂ H ₅ OOH ^a	40
3.7	Input Parameters ^a and High-Pressure Limit Rate Constants (k_{∞}) ^b for QRRK Calculations ^c	42
3.8	Resulting Rate Constants in QRRK Calculations.....	43
3.9	Products Ratios from C•H ₂ C(=O)OOH Dissociation at 1 atm and 1000 K.....	50
3.10	Detailed Mechanism	58
4.1	Enthalpies of Formation for Reference Molecules in the Isodesmic Reactions.....	78
4.2	Reaction Enthalpies and Enthalpies of Formation in the Isodesmic Reactions.....	78
4.3	The Comparison of Bond Energies between C(OOH)H ₂ C(=O)H, C ₂ H ₅ OOH, and CH ₃ C(=O)OOH.....	80
4.4	Activation Energies and Enthalpies of Transition States in CBSQ Calculation ^a	81
4.5	Ideal Gas Phase Thermodynamic Properties Obtained by CBSQ Calculation and by Therm ^a	83

LIST OF TABLES
(Continued)

Table	Page
4.6 Comparison of C•H ₂ CHO, CH ₃ C•(=O) and C ₂ H ₅ with O ₂ ^a	85
4.7 Input Parameters ^a and High-Pressure Limit Rate Constants (k_{∞}) ^b for QRRK Calculations ^c	87
4.8 Resulting Rate Constants in QRRK Calculations	88
4.9 Detailed Mechanism	97
5.1 List of Total Energy, ZPVE, and Thermal Correction of CBS-QCI/APNO Calculation ^a	121
5.2 List of Total Energy, ZPVE, and Thermal Correction of CBSQ Calculation ^a	121
5.3 Enthalpies of Formation for Reference Molecules in the Isodesmic Reactions	122
5.4 Reaction Enthalpies and Enthalpies of Formation in the Isodesmic Reactions	122
5.5 Activation Energies and Enthalpies of Transition States in CBS-QCI/APNO Calculation (Units: kcal/mol)	123
5.6 Ideal Gas Phase Thermodynamic Properties Obtained by CBSQ-QCI/ APNO, CBSQ Calculation and by Therm ^a	124
5.7 Thermochemical Properties ^a (50 K ≤ T ≤ 5000 K)	125
5.8 Input Parameters ^a and High-Pressure Limit Rate Constants (k_{∞}) ^b for QRRK Calculations ^c	128
5.9 Resulting Rate Constants in QRRK Calculations ^a for CH ₂ =C=O + H via TS1	129
5.10 Comparison of Rate Constants with Experimental Data	130
5.11 Resulting Rate Constants in QRRK Calculations ^a for CH ₂ =C=O + H via TS2	132

LIST OF TABLES
(Continued)

Table	Page
6.1 Enthalpies of Formation for Reference Molecules in the Isodesmic Reactions.....	161
6.2 Reaction Enthalpies and Enthalpies of Formation in the Isodesmic Reactions.....	162
6.3 Comparison of Bond Energies between CH ₂ =CHCH ₂ OOH, C(OOH)H ₂ C(=O)H, C ₂ H ₅ OOH, and CH ₃ C(=O)OOH	164
6.4 Ideal Gas Phase Thermodynamic Properties Obtained by CBSQ Calculation ^a	166
6.5 Comparison of CH ₂ =CHC•H ₂ , C•H ₂ CHO, CH ₃ C•O, and C ₂ H ₅ with O ₂	172
6.6 Input Parameters ^a and High-Pressure Limit Rate Constants (k_{∞}) ^b for QRRK Calculations ^c	173
6.7 Resulting Rate Constants in QRRK Calculations ^a	174
7.1 Evaluated Thermodynamic Property Data	186
7.2 Cl ₂ + Radicals -----> Products + Cl	187
7.3 Ideal Gas Phase Thermodynamic Properties ^a : $\Delta H_f^{\circ}_{298}$: CBSQ//MP2/ 6-311G(d,p), S°_{298} and Cp(T) : MP2/6-311G(d,p).....	191
7.4 Thermodynamic and Kinetic Analysis for Reactions of CH ₃ and C ₂ H ₅ and Cl ₂ Comparing with Experiment Data ^a	193
7.5 Calculated Atomic Charges, Bond Lengths(Å) and Bond Angles(deg) MP2/6-311G(d,p).....	198
7.6 Comparison of Calculated Structures and Thermodynamic Parameters: Methyl and Ethyl Radical + Cl ₂	202
7.7 Cl ₂ + Radicals -----> Products + Cl (C-Cl Bond Energy).....	210
8.1 Geometries of Transition States Optimized at B3LYP/6-31G(d,p).....	215
8.2 Comparison of Enthalpies of Formation at B3LYP/6-31G(d,p) with Literature Value	219

LIST OF TABLES
(Continued)

Table	Page
8.3 Enthalpies of Formation for Reference Molecules in the Isodesmic Reactions.....	220
8.4 Reaction Enthalpies and Enthalpies of Formation in the Isodesmic Reactions.....	221
8.5 Comparison of Activation Energies (Units in kcal/mol)	223
8.6 Ideal Gas Phase Thermodynamic Properties Obtained by B3LYP/6-31G(d,p) Calculation ^a	228
8.7 Bond Energies at 298K	232
B.1 Geometries of Radicals and TS Optimized at MP2/6-31G(d') ^a	254
C.1 Geometries of Intermediate Radicals and Transition States Optimized at B3LYP/6-31G(d,p).....	264
C.2 Vibrational Frequencies and Moments of Inertia at B3LYP/6-31G(d,p) level.....	270
D.1 Total Energy and Internal Rotation Barriers of CH ₃ CH ₂ SCH ₂ CH ₂ Cl and CH ₂ ClCH ₂ SCH ₂ CH ₂ Cl.....	273
D.2 Coefficients of Truncated Fourier Series Expansions for Internal Rotation Potentials ^a	275
D.3 Vibrational Frequencies and Moments of Inertia at B3LYP/6-31G(d,p) level.....	276
D.4 Thermodynamic and Kinetic Analysis vs. Temperature in Retro-ene and HCl Eliminations	278
D.5 Thermodynamic and Kinetic Analysis vs. Temperature in Bond Cleavage Reactions.....	284

LIST OF FIGURES

Figure		Page
2.1	Potential energy diagram of $\text{CH}_3\text{C}\bullet\text{O} + \text{O}_2$	18
3.1	Potential energy diagram $\text{CH}_3\text{C}\bullet\text{O} + \text{O}_2$	39
3.2	Bond dissociation energy of $\text{CH}_3\text{C}(=\text{O})\text{OOH}$ (Units : kcal/mol)	40
3.3	$\text{CH}_3\text{C}\bullet\text{O} + \text{O}_2 \rightarrow$ products k vs. $1000/T$ at 1atm.....	47
3.4	$\text{CH}_3\text{C}\bullet\text{O} + \text{O}_2 \rightarrow$ products k vs. pressure at 298K.....	48
3.5	$\text{CH}_3\text{C}\bullet\text{O} + \text{O}_2 \rightarrow$ products k vs. pressure at 1000K.....	49
3.6	Comparison of rate constants between Chemaster and ChemRate with pressure in 800K with $\text{CH}_3\text{C}(=\text{O})\text{OO}\bullet$ dissociation	52
3.7	Comparison of rate constants between Chemaster and ChemRate with pressure in 1000K with $\text{CH}_3\text{C}(=\text{O})\text{OO}\bullet$ dissociation	53
3.8	Comparison of rate constants between Chemaster and ChemRate with pressure in 800K with $\text{C}\bullet\text{H}_2\text{C}(=\text{O})\text{OOH}$ dissociation	55
3.9	Comparison of rate constants between Chemaster and ChemRate with pressure in 1000K with $\text{C}\bullet\text{H}_2\text{C}(=\text{O})\text{OOH}$ dissociation	56
3.10	Potential energy diagram of acetyl and formyl methyl radical unimolecular isomerization/ dissociations (Units : kcal/mol)	57
3.11	Chemkin kinetic calculations: concentration vs. time	60
3.12	Chemkin kinetic calculations: concentration vs. time	64
3.13	Chemkin kinetic calculations: concentration vs. time	65
4.1	Bond dissociation energy of $\text{C}(\text{OOH})\text{H}_2\text{CHO}$ (Units : kcal/mol).....	80
4.2	Potential energy diagram $\text{C}\bullet\text{H}_2\text{CHO} + \text{O}_2$	85
4.3	$\text{C}\bullet\text{H}_2\text{CHO} + \text{O}_2 \rightarrow$ products k vs. $1000/T$ at 1atm.....	91
4.4	$\text{C}\bullet\text{H}_2\text{CHO} + \text{O}_2 \rightarrow$ products k vs. pressure at 298K.....	92
4.5	$\text{C}\bullet\text{H}_2\text{CHO} + \text{O}_2 \rightarrow$ products k vs. pressure at 1000K.....	93

LIST OF FIGURES
(Continued)

Figure		Page
4.6	Potential energy diagram of acetyl and formyl methyl radical unimolecular isomerization/ dissociations (Units : kcal/mol)	96
4.7	Chemkin kinetic calculations: concentration vs. time	99
4.8	Chemkin kinetic calculations: concentration vs. time	100
4.9	Chemkin kinetic calculations: concentration vs. time	103
5.1	Structure for TS1 [$\text{CH}_2=\text{C}=\text{O} + \text{H} \rightarrow \text{TS1} \rightarrow \text{CH}_3\text{C}\bullet\text{O}$].....	115
5.2	Structure for TS2 [$\text{CH}_2=\text{C}=\text{O} + \text{H} \rightarrow \text{TS2} \rightarrow \text{C}\bullet\text{H}_2\text{CHO}$].....	116
5.3	Structure for TS3 [$\text{C}\bullet\text{H}_2\text{CHO} \rightarrow \text{TS3} \rightarrow \text{CH}_3\text{C}\bullet\text{O}$].....	117
5.4	Structure for TS4 [$\text{CH}_3\text{C}\bullet\text{O} \rightarrow \text{TS4} \rightarrow \text{CH}_3 + \text{CO}$]	119
5.5	Potential energy diagram of $\text{CH}_2=\text{C}=\text{O} + \text{H}$	126
5.6	Arrhenius plot for the reaction $\text{CH}_2=\text{C}=\text{O} + \text{H} \rightarrow \text{CH}_3 + \text{CO}$	131
5.7	$\text{CH}_2=\text{C}=\text{O} + \text{H} \rightarrow$ products (via TS2) k vs. $1000/T$ at 1 atm	135
5.8	$\text{CH}_2=\text{C}=\text{O} + \text{H} \rightarrow$ products (via TS2) k vs. pressure at 298 K.....	136
5.9	$\text{CH}_2=\text{C}=\text{O} + \text{H} \rightarrow$ products (via TS2) k vs. pressure at 1000 K.....	137
5.10	$\text{C}\bullet\text{H}_2\text{CHO}$ dissociation k vs. $1000/T$ at 1 atm	139
5.11	$\text{C}\bullet\text{H}_2\text{CHO}$ dissociation k vs. pressure at 1000 K.....	140
5.12	Comparison of rate constants between Chemaster and ChemRate with pressure in 600 K with $\text{C}\bullet\text{H}_2\text{CHO}$ dissociation.....	142
5.13	Comparison of rate constants between Chemaster and ChemRate with pressure in 1000 K with $\text{C}\bullet\text{H}_2\text{CHO}$ dissociation.....	143
6.1	Bond dissociation energy of $\text{CH}_2=\text{CHCH}_2\text{OOH}$ (Units : kcal/mol).....	163
6.2A	Potential energy diagram for allyl + O_2 (a) Isomerizations via H shifts	170

LIST OF FIGURES
(Continued)

Figure	Page
6.2B Potential energy diagram for allyl + O ₂ (b) cyclization pathways to form cyclic adducts and further reactions	171
6.3 CH ₂ =CHC•H ₂ + O ₂ -> products <i>k</i> vs. 1000/T at 1 atm	177
6.4 CH ₂ =CHC•H ₂ + O ₂ -> products <i>k</i> vs. pressure at 298 K.....	178
6.5 CH ₂ =CHC•H ₂ + O ₂ -> products <i>k</i> vs. pressure at 1000 K.....	179
7.1 Reaction path diagrams in CH ₃ with Cl ₂ and C ₂ H ₅ with Cl ₂	189
7.2 log <i>k</i> vs. 1000/T on CH ₃ + Cl ₂ ----> CH ₃ Cl + Cl•.....	195
7.3 log <i>k</i> vs. 1000/T on C ₂ H ₅ + Cl ₂ ----> C ₂ H ₅ Cl + Cl•	196
7.4A Calculated atomic charges at MP2/6-311G(d,p) CH ₃ + Cl ₂ ----> CH ₃ Cl + Cl•.....	199
7.4B Calculated atomic charges at MP2/6-311G(d,p) C ₂ H ₅ + Cl ₂ ----> C ₂ H ₅ Cl + Cl•.....	200
7.5 E _{a,fwd} vs. ΔH ^o _{rxn, fwd}	204
7.6 Hydrocarbons	205
7.7 C ₁ chlorocarbons.....	207
7.8 C ₂ chlorocarbons.....	208
8.1 Potential barriers for four internal rotations about CH ₃ CH ₂ SCH ₂ CH ₂ Cl.....	225
8.2 Potential barriers for two internal rotations about CH ₂ ClCH ₂ SCH ₂ CH ₂ Cl...	227
8.3 Potential energy diagram (units in kcal/mol).....	234
8.4 Bond dissociation energies ^a (kcal/mol) of CH ₃ CH ₂ SCH ₂ CH ₃ ^b and CH ₃ CH ₂ SCH ₂ CH ₂ Cl ^c	236
8.5 CH ₃ CH ₂ SCH ₂ CH ₃ dissociation <i>k</i> vs. 1000/T at 1 atm.....	238
8.6 CH ₃ CH ₂ SCH ₂ CH ₂ Cl dissociation <i>k</i> vs. 1000/T at 1 atm.....	239

LIST OF FIGURES
(Continued)

Figure	Page
8.7	CH ₂ ClCH ₂ SCH ₂ CH ₂ Cl dissociation <i>k</i> vs. 1000/T at 1 atm 240
A.1	CH ₃ C(=O)OO• dissociation <i>k</i> vs. 1000/T at 1atm..... 243
A.2	CH ₃ C(=O)OO• dissociation <i>k</i> vs. pressure at 298K 244
A.3	CH ₃ C(=O)OO• dissociation <i>k</i> vs. pressure at 1000K 245
A.4	C•H ₂ C(=O)OOH dissociation <i>k</i> vs. 1000/T at 1atm..... 246
A.5	C•H ₂ C(=O)OOH dissociation <i>k</i> vs. pressure at 298K 247
A.6	C•H ₂ C(=O)OOH dissociation <i>k</i> vs. pressure at 1000K 248
A.7	Potential barriers for internal rotation in CH ₃ C(=O)OONO ₂ at B3LYP/6-31G(d') level of theory 249
A.8	Potential barriers for internal rotation in C ₂ H ₅ OONO ₂ at B3LYP/6-31G(d') level of theory 251
B.1	C(OO•)H ₂ CHO dissociation <i>k</i> vs. 1000/T at 1atm 257
B.2	C(OO•)H ₂ CHO dissociation <i>k</i> vs. pressure at 298K 258
B.3	C(OO•)H ₂ CHO dissociation <i>k</i> vs. pressure at 1000K 259
B.4	C(OOH)H ₂ C•O dissociation <i>k</i> vs. 1000/T at 1atm 260
B.5	C(OOH)H ₂ C•O dissociation <i>k</i> vs. pressure at 298K 261
B.6	C(OOH)H ₂ C•O dissociation <i>k</i> vs. pressure at 1000K 262
E.1	Collision efficiency vs. temperature for C•H ₂ CHO stabilization in CH ₂ CO + H reaction system 298
E.2	Collision efficiency vs. temperature for CH ₃ C(=O)OO• stabilization in CH ₃ C•O + O ₂ reaction system..... 299

CHAPTER 1

INTRODUCTION

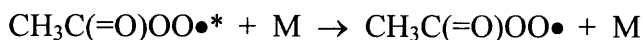
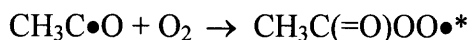
1.1 Background

Important initial products from pyrolysis, oxidation, or photochemical reactions of saturated and unsaturated hydrocarbons are the corresponding radicals. The subsequent reactions of the hydrocarbon radicals with molecular oxygen are complex and often difficult to study experimentally. These reactions often represent the principal pathways of the radical conversion in hydrocarbon combustion^{1,2} and atmosphere oxidation.

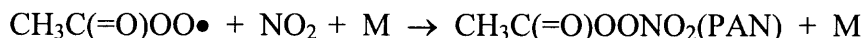
Acetaldehyde (CH_3CHO) and the radical species that result through loss of hydrogen atoms from the carbon sites in CH_3CHO are common products (intermediates) from oxidation of higher molecular weight hydrocarbon species in combustion and in atmospheric chemistry. Oxidation of methane also forms these species as a result of methyl radical combination and subsequent reactions of the ethane. The association reaction of these radicals with molecular oxygen ($^3\text{O}_2$) will form chemically activated peroxy adducts that can be stabilized, or the adduct may react via either isomerization or dissociation to new products before stabilization. The adducts can also dissociate back to initial reactants. These reactions are complex, because of competition between the pressure dependent stabilization versus unimolecular reaction to new products or reverse dissociation.^{1,2} The isomerization, dissociation and bimolecular reactions of the stabilized adduct provide further complexity. The reactions of radicals from acetaldehyde with oxygen also serve as model reactions for some reaction paths of larger aldehydic molecule systems.

Acetaldehyde (CH_3CHO) is of particular interest in atmospheric chemistry because it is formed as a product of the reaction of O_3 and/or OH with naturally occurring, nonmethane hydrocarbons, especially higher olefins such as isoprene and terpenes.^{3,4} The photo-oxidation of hydrocarbons in photochemical smog also produces acetaldehyde as a major intermediate product. Acetaldehyde is, in addition, a significant product of incomplete combustion processes in diesel engines, aircraft exhausts, power plants, waste combustion, and many other oxidation processes. Acetaldehyde is also one of the important oxidation products of ethane and ethylene. Acetaldehyde and acetyl radicals are important intermediates in the overall breakdown processes of higher molecular weight and C_1 hydrocarbons to CH_2O , CO , CO_2 , and H_2O .

Acetylperoxy radicals, $\text{CH}_3\text{C}(=\text{O})\text{OO}\bullet$ (often represented as $\text{CH}_3\text{CO}_3\bullet$ or CH_3CO_3), are formed as a result of $\text{CH}_3\text{C}\bullet\text{O}$ radical reaction with O_2 and subsequent stabilization of the energized adduct. These peroxy radicals play an important role in atmospheric photooxidation processes:



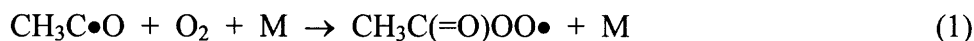
These stabilized peroxy radicals react with NO_x when it is present in the atmosphere and in the clean troposphere with other peroxy radicals. Acetylperoxy radicals are the precursor of peroxyacetylnitrite (PAN) an important constituent of photochemical smog and an air pollutant having important physiological effects. PAN is formed by combination with NO_2 ⁵:



Because of its thermal stability at lower temperatures and its photochemical inertness under tropospheric conditions, PAN can act as a temporary reservoir for NO_x and serve as a carrier for transport in colder regions of the troposphere.

1.2 Previous Studies

One absolute measurement of k_I has been reported in the literature; McDade et al.⁶ determined $k_I = (1.2 \pm 0.2) \times 10^{12} \text{ cm}^3/(\text{mol s})$ in 1-4 Torr He at 298 K. The high-pressure limit value of $k_I = (3.01 \pm 1.5) \times 10^{12} \text{ cm}^3/(\text{mol s})$ recommended by the IUPAC panel is based on the absolute measurements of McDade et al.⁶ and the pressure dependence of the C₂H₅• + O₂ reaction.⁷ The results from two other studies, on the relative reactivity of CH₃C•O with O₂ and Cl₂⁵, and on the rate constant for CH₃C•O with Cl₂,⁸ have been combined to give a high-pressure limit rate constant of $k_I = (1.9 \pm 0.4) \times 10^{12} \text{ cm}^3/(\text{mol s})$ at room temperature.



Tyndall et al.⁹ studied the reaction of the OH radical with methyl glyoxal and acetaldehyde in a low-pressure (ca. 3 Torr) flow reactor between 260 and 333 K. They report rate constants for OH abstractions from the parent molecules and also report data on further reactions of the radicals formed from the abstractions. They infer that only the acetyl radical is formed (no indication of formyl methyl radical) and further reaction of acetyl radical with O₂ leads to noticeable regeneration of OH based on observations showing reduced loss of the OH versus time. Chamber experiments by the same group at atmospheric pressure using FTIR detection showed no evidence of OH radical production.⁹

Absolute rate constants of fluorine atom reaction with acetaldehyde were studied by Sehested and co-workers,¹⁰ who report $k_f = (2.65 \pm 0.4) \times 10^{12} \text{ cm}^3/(\text{mol s})$ at 295K and 1000 mbar total pressure of SF₆ using pulse radiolysis combined with transient ultraviolet absorption. They report production of two radicals: formyl methyl at 35% and acetyl at 65% (both $\pm 9\%$).

Reactions where a chlorine atom is abstracting a hydrogen atom usually have similar A factors to that of fluorine and low *E_a*'s, when the reactions are exothermic, as they are in this study. In the case of acetaldehyde, for example, k_{298} for Cl atom abstraction is reported as 4.58×10^{13} [11] at 298K, while abstraction by F atom is 5.00×10^{13} [12]. The H—Cl bond is 103 kcal/mol, whereas the carbonyl C—H and methyl C—H bonds on acetaldehyde are 88.7 and 95.3 kcal/mol, respectively. Although one might expect some abstraction of the methyl hydrogen's by chlorine considering statistical factors, the discussion below suggests this is small and maybe insignificant at atmospheric temperature.

Michael et al.¹³ studied the reaction of OH with acetaldehyde in a low-pressure discharge flow reactor using resonance fluorescence to monitor OH. They also studied the further reaction of product radical(s) (generated via the OH reaction) with O₂. The total reaction rate constant for OH with acetaldehyde was $A = 3.3 \times 10^{12}$, with a small negative energy of activation of 610 cal/mol. Michael et al.¹³ also report near complete regeneration of the OH radical in the OH + acetaldehyde experiments when O₂ was initially present to further react with the product radical. This OH regeneration was also observed in studies where the Cl atom was used to generate the acetyl radical from acetaldehyde. They considered and rejected possible formation of formyl methyl radicals

based on work of Gutman's research group.¹⁴ Slagle and Gutman¹⁴ studied formation of the acetyl radical from acetaldehyde in the reaction of Cl atoms and monitored the radical profiles with photoionization mass spectrometry. Verification of the $\text{CH}_3\text{C}\bullet\text{O}$ radical versus formyl methyl was by use of deuterated acetaldehyde, CD_3CHO . They observed $\text{CD}_3\text{C}\bullet\text{O}$ and could not detect $\text{C}\bullet\text{D}_2\text{CHO}$; although they did not report lower limits of detection, they did indicate $\text{CD}_3\text{C}\bullet\text{O}$ was readily detected.

Alvarez-Idaboy et al.¹⁵ have recently characterized the abstraction reaction of $\text{OH} + \text{acetaldehyde}$ at the $\text{CCSD(T)/6-311++G(d,p)//MP2(FC)/6-311++G(d,p)}$ level of theory. The reaction rate constant was calculated as $k = 8.72 \times 10^{12}$ with a small negative energy of activation, 1.71 kcal/mol. They used the canonical transition state theory as applied to a mechanism involving the formation of a prereactive complex to reproduce the reported experimental results. They indicated that the reaction predominantly occurs by hydrogen abstraction from the carbonyl site, and that OH addition to the carbonyl carbon is unfavorable. The energetics of abstraction of H's on acetaldehyde by OH was also studied by Aloisio and Francisco¹⁶ at the $\text{B3LYP//6-311++G(3df,3pd)}$ level of theory. Binding energy (D_0) for $\text{CH}_3\text{CHO-HO}$ prereactive complex was calculated as 4.0 kcal/mol.

Although the abstraction can occur at two sites, both studies^{15,16} report that the dominant reaction is the abstraction from the carbonyl site. They reported that the position of the OH hydrogen atom in the prereactive complex is very far from the methyl hydrogen. In addition, the energy of the methyl C—H bond is about 5 kcal/mol larger than that of the carbonyl C—H bond. (This difference is 6.6 kcal/mol at the CBSQ level of theory in this study.)

Formyl methyl was generated by photodissociation of methyl vinyl ether, at 298 K by Zhu and Johnston¹⁷; $\text{CH}_3\text{-O-C}_2\text{H}_3 + h\nu \rightarrow \text{CH}_3 + \text{C}_2\text{H}_3\text{O}$. Here the vinoxy radical undergoes rapid electron rearrangement to the lower energy form (ca. 16 kcal/mol lower) formyl methyl structure. Kinetic studies on this formyl methyl radical with O_2 show a slower reaction, $k = 1.2 \times 10^{11} \text{ cm}^3/(\text{mol s})$, relative to those reported¹⁸ for acetyl radical, $k = 2.65 \times 10^{12} \text{ cm}^3/(\text{mol s})$. This suggests that formyl methyl radicals produced in experiments on Cl or OH reaction with acetaldehyde will react about one tenth as fast with O_2 , probably requiring a small or no correction to kinetic data of the faster acetyl + O_2 reactions. It also suggests that a barrier to the association may exist or that there is a very low well depth for the formyl methyl + O_2 adduct.

CHAPTER 2

THERMOCHEMICAL KINETICS

2.1 Overview

Reaction kinetic models with detailed mechanisms, based on fundamental thermochemical and kinetic principles are presently used and being developed by researchers attempting to optimize or more fully understand a number of systems comprised of many complex chemical reactions. These include combustion, flame inhibition, ignition, atmospheric smog formation and transport, stratospheric ozone depletion, municipal and hazardous wastes incineration, chemical vapor deposition, semiconductor etching, rocket propulsion and other related fields.

To have accurate thermochemical property data for molecules, intermediate radicals and transition states is one of the most important requirements for modeling and simulation of these systems. These data provide determination of equilibrium, and reverse rate constants from the forward rate constant and the equilibrium constant. *Ab initio* and density functional calculations provide an opportunity to accurately estimate thermochemical properties of reactants, intermediate radicals, and products, plus estimate properties for transition states which is often impossible to obtain through experiment.

2.2 Computational Chemistry

Ab initio molecular orbital theory is concerned with predicting the properties of atomic and molecular systems. It is based upon the fundamental laws of quantum mechanics and uses a variety of mathematical transformation and approximation techniques to solve the fundamental equations, i.e. Schrödinger partial differential equation,

$$H\Psi = E\Psi$$

Here H is the *Hamiltonian*, a differential operator representing the total energy. E is the numerical value of the energy of the state, in terms of kinetic energy symbolized by T and potential energy V . Ψ is the wavefunction.

Model chemistries are characterized by the combination of a theoretical procedure and a basis set.¹⁹ A basis set is a mathematical representation of the molecular orbitals within a molecule. The basis set can be interpreted as restricting each electron to a particular region of space. Large basis sets impose fewer constraints on electrons and more accurately approximate exact molecular orbitals. The computation of atomic or molecular properties with large basis sets requires correspondingly more computational resources.

Standard basis sets for electronic structure calculation use linear combinations of Gaussian functions to form the orbitals.¹⁹ Basis sets assign a group of basis functions to each atom within a molecule to approximate its orbitals. These basis functions themselves are composed of a linear combination of Gaussian functions. The linear combined basis functions are referred to as contracted functions, and the component Gaussian functions are referred to as primitives. A basis function consisting of a single

Gaussian function is termed uncontracted. Explanation of the nomenclature of 6-31G basis set is:

- Six primitive Gaussians in the core function,
- Two sets of function in the valence region (one function consisting of three primitive Gaussian, one consisting of one primitive Gaussian).

The 6-31G(d) indicates it is the 6-31G basis set with one d polarization function added to the heavy atoms (now hydrogen atoms). The 6-311+G(3df,2p) is three d functions and one f function on heavy atoms (+ means adding diffuse functions to heavy atoms), and 2 p functions added on the hydrogen atoms. If 6-311++G(3df,2p), then the one more + means also adding diffuse functions to hydrogen atoms.

The Hartree-Fock (HF) calculation method does not include a full treatment of the effects of electron correlation, i.e. it does not include the energy contributions arising from electrons interacting with one another (electron – electron repulsion). A variety of theoretical methods, such as Møller-Plesset perturbation (MP2), and density functional have been developed which include some effects of electron correlation. Traditionally, such methods are referred as post-SCF (Self-Consistent Field) methods because they add this electron correlation correction to the basic Hartree-Fock model.

Density functional theory (DFT) methods have recently gained widespread use in computational chemistry. DFT methods compute electron correlation via general functionals of the electron density. These DFT functionals partition the electronic energy into several components, which are computed separately. They include the kinetic energy, the electron-nuclear interaction, the coulomb repulsion, and an exchange-correlation term accounting for the remainder of the electron-electron interactions (the

exchange-correlation term is, itself, also divided into separate exchange and correlation components in most actual DFT functions). A variety of functionals have been defined, generally distinguished by the way that they treat exchange and correlation components.¹⁹

- *Local* exchange and correlation functionals involve only the values of the electron spin densities.
- *Gradient-corrected* functionals involve both the values of electron spin densities and their gradients. Such functionals are also referred to as non-local in literature. A popular gradient-corrected exchange functional is one proposed by Becke²⁰; a widely used gradient-corrected correlation functional is the LYP functional of Lee, Yang and Parr. The combination of the two forms the B-LYP method. B3LYP is Becke-style 3-parameter density functional theory (using the Lee-Yang-Parr correlation functional).

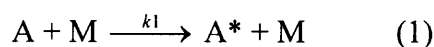
2.3 Kinetics

2.3.1 Lindemann-Hinshelwood Mechanism for Unimolecular Reactions

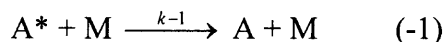
A general theory for thermal unimolecular reactions that forms the basis for the current theory of thermal unimolecular rates was proposed by Lindemann²¹ in 1922. He proposed that molecules become energized by bimolecular collisions, with a time lag between the moment of collisional energy transfer and the time the molecule decomposes. Energized molecules could then undergo deactivating collisions before decomposition occurred. Steinfeld et al.²² indicated that “A major achievement of Lindemann’s theory is its ability to explain the experimental finding that the reaction rate changes from first to second order in going from the high- to low-pressure limit.”

Steinfeld et al.²² and Robinson et al.²³ explained briefly the main concepts of the Lindemann theory as follows:

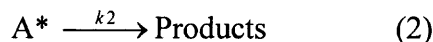
(a) A certain fraction of the molecules become energized by collision, i.e. gain energy in excess of a critical quantity E_0 . The rate of the energization process depends upon the rate of bimolecular collisions. M represents a product molecule, an added “inert” gas molecule, or a second molecule of reactant. In the simple Lindemann theory k_1 is taken to be energy-independent and is calculated from the simple collision theory equation.



(b) Energized molecules are de-energized by collision, which is a reverse reaction of process (1). The rate constant k_{-1} is taken to be energy-independent, and is equated with the collision number Z_1 by assuming that every collision of A^* leads to a de-energized state. This is known as “strong collision assumption” for de-energizing collisions.



(c) There is a time-lag between the energization and unimolecular dissociation or isomerization of the energized molecule. This unimolecular dissociation process also occurs with a rate constant k_2 independent of the energy content of A^* .



If the steady-state hypothesis is applied to the concentration of A^* , the overall rate of reaction becomes

$$\text{Rate} = k_{\text{uni}}[A] = k_2[A^*] = \frac{k_1 k_2 [A][M]}{k_{-1}[M] + k_2}$$

The overall concept can be expressed by the equations below, where M can represent a generic bath gas molecule, an added “inert” gas molecule; it may also represent a second molecule of reactant or product. In the simple Lindemann theory k_1 , along with k_{-1} and k_2 are taken to be energy-independent and are calculated from the simple collision theory equation.

Application of the steady-state hypothesis to the concentration of A*, allows the unimolecular rate constant and the high-pressure and low-pressure limit rate and rate constants to be determined as follows:

$$\text{Rate} = k_{\text{uni}}[A] = k_2[A^*] = \frac{k_1 k_2 [A][M]}{k_{-1}[M] + k_2}$$

$$k_{\text{uni}} = \frac{k_1 k_2 [M]}{k_{-1}[M] + k_2}$$

High-pressure limit rate, $[M] \rightarrow \infty$, $k_{\text{uni}} = k_{\infty} = k_1 k_2 / k_{-1}$

Low-pressure limit rate, $[M] \rightarrow 0$, $k_{\text{uni}} = k_0 = k_1 [M]$

The unimolecular rate constant is then written as $k_{\text{uni}} = k_{\infty} / (1 + k_{\infty} / k_1 [M])$.

One can expect the Lindemann theory to predict a linear change in the initial rate of a unimolecular reaction with respect to concentration of M at low pressure. The transition from high-pressure rate constant to low pressure is called “falloff region”.

The k_1 in the original Lindemann theory is taken from the collision theory expression ($k_1 = Z_1 \exp(-E_0/k_B T)$) with $Z_1 = (\sigma_d^2 N_A / R)(8\pi N_A k / \mu)^{1/2} (1/T)^{1/2}$, where Z_1 will be in $\text{Torr}^{-1} \cdot \text{s}^{-1}$ (consistent with $[M]$ in Torr and k_2 in s^{-1}) when σ_d = collision diameter in cm; μ = reduced molar mass in $\text{g} \cdot \text{mol}^{-1} = (1/M_A + 1/M_B)^{-1}$; T = temperature in Kelvin; N_A

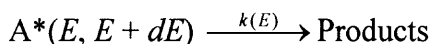
is Avogadro constant $6.022 \times 10^{23} \text{ mol}^{-1}$; R is gas constant $6.2326 \times 10^4 \text{ cm}^3\text{-Torr-K}^{-1}\text{-mol}^{-1}$ or $0.082 \text{ atm-lit/mol-K}$; k_B (Boltzmann constant) = $1.3805 \times 10^{-16} \text{ erg-K}^{-1}$.

The Lindemann theory, unfortunately, predicts the falloff in k_{uni} to occur at much higher pressures than what is observed experimentally.

Based on the Lindemann's suggestion that k_1 could be increased by assuming that the required energy (energized molecules) could be drawn in part from the internal degrees of freedom (mainly vibration) of the reactant molecule, Hinshelwood²⁴ increases k_1 by using a much higher probability of a molecule possessing total energy $\geq E_0$ in s classical degrees of freedom, $\exp(-E_0/k_B T)(E_0/k_B T)^{s-1}/(s-1)!$, than the simpler $\exp(-E_0/k_B T)$ Lindemann used. The result is

$$k_1 = [Z_1/(s-1)!](E_0/k_B T)^{s-1} \exp(-E_0/k_B T)$$

Since k_1 increases with s classical degrees of freedom in the Lindemann-Hinshelwood theory, then $k_2 = k_{\infty}k_1/k_1$ should decrease with s . Thus the lifetime of the energized molecule $t \approx 1/k_2$ increases when the molecule can store energy among a greater number of degrees of freedom. Then k_2 is expected to depend on the energy of A^* . Making k_2 energy-dependent, expressed as $k(E)$, the energy interval from E to $E + dE$ is considered:



$$\text{Then } dk_{\text{uni}}(E, E + dE) = k(E)(dk_1/k_1) / (1 + k(E)/k_1 [M])$$

It is assumed that for all pressure dk_1/k_{-1} represents the equilibrium probability and that the A^* has energy between E and $E + dE$. This probability may be denoted $P(E)dE$. Also, $k_{-1} [M]$ is the collision frequency ω between A^* and M , then

$$k_{\text{uni}} = \omega \int_{E_0}^{\infty} k(E)P(E)dE / (k(E) + \omega)$$

In order to make accurate quantitative predictions of the fall-off behavior of a unimolecular reaction it is essential to take into account the energy dependence of the rate constant $k(E)$ for the conversion of energized molecules into activated complexes where products result from decomposition or reaction of the energized complex.

Steinfeld et al.²² noted that two quite different approaches may be taken to determine $k(E)$. One is to consider the explicit nature of the intramolecular motion of highly energized molecules, such as Slater theory. The other approach is based on statistical assumptions, such as RRK (Rice-Ramsperger-Kassel) theory and its extension, RRKM (Marcus) theory. Most modern theories of unimolecular reaction rates, including the Slater theory, the RRK theory and the RRKM theory, are based on the fundamental Lindemann mechanism involving collision energy transfer of the reactant molecules, and more specifically on Hinshelwood's development.

2.3.2 Slater Theory

Slater²⁵ pictured a molecule as an assembly of harmonic oscillators in 1939. Decomposition is assumed to occur when a critical coordinate (i.e. a bond length or bond angle) attains a critical displacement. The attainment of the reaction coordinate critical extension is not a statistical random process as in RRKM Theory, but depends on the

energies and phases of the specific normal mode excited. Since energy does not flow freely within the molecule, the theory predicts intrinsic non-RRKM behavior.

Overall, the Slater Theory is not successful in interpreting experiments.

2.3.3 RRK Theory of Unimolecular Reactions

The RRK theory was developed independently by Rice and Ramsperger²⁶ and Kassel.²⁷⁻²⁹

Both Rice and Ramsperger theory and Kassel theory consider that for reaction to occur a critical energy E_0 must become concentrated in one part (specific vibration) of the molecule. They used the basic Lindemann-Hinshelwood mechanism of collision energy transfer and de-energization, but assumed more realistically that the rate constant for conversion of an energized molecule to products is proportional to a specific probability. This is a finite statistical probability that energy, E_0 , is found in the relevant part of the energized molecule which contains total energy, E , is greater than E_0 since E of the molecule under consideration is assumed to be rapidly redistributed around the molecule. This probability will increase with E and make k_2 a function of its energy content; k_2 is not “energy” dependent.

The difference between the two models (Rice and Ramsperger versus Kassel) is two-fold. First, Rice and Ramsperger used classical statistical mechanics throughout, while Kassel used classical methods and also developed a quantum treatment. The quantum method turns out to be much more realistic and accurate. Second, different assumptions were made about the part of the molecule into which the critical energy E_0 has to be concentrated. The Kassel’s model seems slightly more realistic by assuming the energy had to be concentrated into one oscillator. The quantum version of the Kassel theory serves as a theoretical basis for calculations performed in this thesis.

The classical RRK theory is based on the notion that the probability that a molecule of s classical oscillators with total energy E has energy greater than E_0 in one chosen oscillator, which is the critical mode leading to reaction. The assumptions used to derive the quantum RRK rate constant are similar to those for classical theory. In the quantum theory it is assumed there are s identical oscillators in the molecule, all having frequency ν . The energized molecule has n quanta, so $E = nh\nu$. The critical oscillator must have m quanta for dissociation occurrence, $m = E_0/h\nu$.

The probability that one oscillator contains at least m quanta; probability (energy $\geq m$ quanta in chosen oscillator) is then equal to^{22,23}:

$$\text{Probability} = \frac{n!(n - m + s - 1)!}{(n - m)!(n + s - 1)!}$$

Where s is identical oscillators. Hence,

$$k_{\alpha}(nh\nu) = A \frac{n!(n - m + s - 1)!}{(n - m)!(n + s - 1)!}$$

Where A is a proportion constant.

The corresponding $k_1(E)$ of the Hinshelwood expression is now derived. It refers to energy transfer into a specific quantum state rather than into an energy range E to $E + dE$, as

$$k_1(E) = k_1(nh\nu) = k_2 \alpha^n (1-\alpha)^s \frac{(n + s - 1)!}{n!(s - 1)!}$$

where $\alpha = \exp(-h\nu/k_B T)$.

Both classical and quantum versions RRK theory were developed, and in the limit of a large excitation energy E the two versions become identical.

In RRK theory, the assumption is made that the rate of conversion of energized molecules into products is related to the probability that the critical energy E_0 is concentrated in one part of the molecule, e.g. in one oscillator (Kassel theory) or in one squared term (Rice-Ramsperger theory). This probability is a function of the total energy E of the energized molecule, and the total vibrations among which the vibration energy quanta can be distributed.

2.3.4 RRKM Theory of Unimolecular Reactions

The Rice-Ramsperger-Kassel-Marcus (RRKM) theory was developed using the RRK model and extending it to consider explicitly vibrational and rotational energies and to include zero point energies. Several minor modifications of the theory have been made, primarily as a result of improved treatments of external degrees of freedom.

The RRKM theory is a microcanonical transition state theory.



Where A^\ddagger is the transition state.

Different experimental techniques, including static pyrolysis, carrier (flow) techniques, shock tube methods, and very low-pressure pyrolysis, have been used to measure k_{uni} as a function of temperature and pressure. One of the most significant achievements of RRKM theory is its ability to match measurements of k_{uni} with pressure.

2.3.5 Chemical Activation Reactions

The energization methods other than by molecular collision, such as photoactivation and chemical activation, may produce a non-equilibrium situation in which molecules acquire energies far in excess of the average thermal energy. This presence of excess energy in

the energized adduct makes chemical activation reactions much more important in these systems. A treatment for the rate of conversion, which includes decomposition of energized adduct to product(s) (including back to reactant) and the competing rate of its collision stabilization, is needed.

An example of a chemically activated reaction system is $\text{CH}_3\text{C}\cdot\text{O}$ with O_2 . As is discussed by Lee et al.,³⁰ $\text{CH}_3\text{C}\cdot\text{O}$ radical reacts with O_2 to form a chemically activated, energized adduct $[\text{CH}_3\text{CO}_3\cdot^*]$, this process of forming adduct is much more efficient than that by thermal molecular collision, and adduct contains excess energy from the new bond formed in this chemical (addition) reaction. The energized adduct $[\text{CH}_3\text{CO}_3\cdot^*]$ could go back to reactant $\text{CH}_3\text{C}\cdot\text{O} + \text{O}_2$, or could go to products $\text{CH}_2\text{CO} + \text{HO}_2$ via an intramolecular H shift. The QRRK analysis ($\text{A} + \text{BC} \rightarrow \text{ABC}^*$) shows that the chemical activation process is more important than thermal dissociation process.

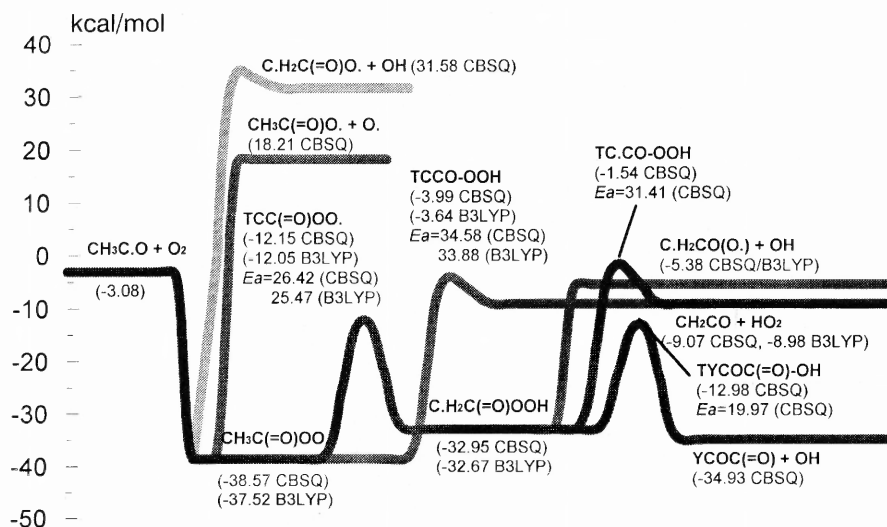


Figure 2.1 Potential energy diagram of $\text{CH}_3\text{C}\cdot\text{O} + \text{O}_2$.

The basic idea of the treatment of a chemical activation system is that a vibrationally excited molecule ABC^* formed by an association of reactants can reform reactants $A + BC$ with a rate constant $k'(E)$, form decomposition products, $AB + C$, with a rate constant $k_a(E)$ or be de-energized to stable molecules ABC , $\times k_{stab}(M)$.

In the strong collision assumption the first order rate constant for de-energization is equal to the collision frequency, $\omega = Zp$ where p is the total pressure and Z is collision number. (see “2.3.1 Lindemann-Hinshelwood Mechanism for Unimolecular Reactions”) This assumes that stabilization occurs at each collision.

Suppose that the fraction of molecules which are energized per unit time into the energy range between E and $E + dE$ is $f(E)dE$. To simplify, one can consider decomposition path (back to reactant, $A + BC$, as the decomposition path), then the fraction of ABC^* decomposing (path $A + BC$) compared with those stabilized (path ABC) is $k(E)/ [k(E)+\omega]$. The fraction of molecules in the energy range between E and $E+dE$ decomposing to products is therefore $\{k(E)/[k(E)+\omega]\}f(E)dE$, and the total number of molecules decomposing per unit time (D), at all energies above the critical energy E_0 , is:

$$D = \int_{E_0}^{\infty} \frac{k(E)}{k(E) + \omega} f(E) dE$$

Corresponding, the total rate of stabilization (S) is:

$$S = \int_{E_0}^{\infty} \frac{\omega}{k(E) + \omega} f(E) dE$$

Considering an average rate constant $\langle k \rangle$ for all energies above E_0 , one would have:

$$\frac{\langle k \rangle}{\omega} = \frac{D}{S} = \frac{\text{No. molecules decomposing per unit time}}{\text{No. of molecules being stabilized per unit time}}$$

So,

$$\langle k \rangle = \omega \frac{\int_{E_0}^{\infty} \{k(E)/[k(E) + \omega]\} f(E) dE}{\int_{E_0}^{\infty} \{\omega/[k(E) + \omega]\} f(E) dE}$$

The $f(E)$ is the distribution function of energized molecules in the energy range between E and $E + dE$. In the thermal energy transfer systems, this distribution function is simply the thermal quantum Boltzmann distribution $K(E)$ and the rate of energy transfer into the energy range between E and $E + dE$ is $K(E)dE = dk_1/k_2$. For the chemically activated system described here, the distribution function can be derived by applying the principle of detailed balancing to the reverse process to reactants. Consider a situation in which other processes can be ignored and equilibrium is established between A^* and reactants. Then the fraction of molecules with energy between E and $E + dE$ is Boltzmann distribution $K(E)dE$, so the rate of dissociation to reactants is then $K'(E)K(E)dE$, and by the principle of detailed balancing this also gives the rate of combination of reactants to give A^* in this energy range. The total rate of energy transfer to all levels above the minimum energy E_{\min} (the minimum energy of A^*) is:

$$\text{Total rate of energization} = \int_{E_0}^{\infty} k'(E)K(E)dE$$

Therefore, the distribution function is given by:

$$f(E)dE = \frac{k'(E)K(E)dE}{\int_{E_0}^{\infty} k'(E)K(E)dE}$$

The $f(E)dE$ can be incorporated into QRRK theory for $k(E)$ and $k_1(E)$ serves as a basis for the calculations for chemical activation reaction systems.

2.3.6 QRRK Analysis for Unimolecular and Chemical Activation Reactions

Multifrequency quantum Rice-Ramsperger-Kassel (QRRK) analysis, as initially presented by Dean³¹⁻³³ combined with the modified strong collision approach of Gilbert et al.³⁴⁻³⁶, to compute rate constants for both chemical activation and unimolecular reactions, over a range of temperature and pressure. The computer program, CHEMDIS, based on the QRRK theory outlined as above, and unimolecular dissociation and chemical activation formalism carries out all unimolecular and chemical activation reactions involved in this thesis. The input parameters for CHEMDIS are: (1) High-pressure limit rate constants (Arrhenius A factor and activation energy Ea) for each reaction included for analysis; (2) A reduced set of three vibration frequencies and their associated degeneracy; (3) Lennard-Jones transport parameters, s (Angstroms) and e/k (Kelvin)), and (4) molecular weight of well species.

2.3.6.1 Input Information Requirements for QRRK Calculation. High pressure limit rate constants (k_∞ 's) are fitted by three parameters A , n , and Ea over temperature range from 298 to 2000K, $k_\infty = A_\infty(T)^n \exp(-Ea/RT)$. Entropy differences between reactant and transition state are used to determine the pre-exponential factor, A , via canonical Transition State Theory (TST):

$$A = (k_B T/h) \exp(\Delta S^\ddagger/R), \quad Ea = \Delta H^\ddagger$$

Where h is the Planck constant and k_B is the Boltzmann constant. $\Delta S^\ddagger = S(\text{TST}) - S(\text{reactants})$ and $\Delta H^\ddagger = H(\text{TST}) - H(\text{reactants})$. Treatment of the internal rotors for S and $C_p(T)$ of reactants and the TST's is important here because these internal rotors are often lost in the cyclic transition state structures. Pre-exponential factors (A), are calculated from structures determined by Density Functional Theory (DFT) or estimated from the

literature and from trends in homologous series of reactions. Activation energies come from DFT plus evaluated endothermicity of reaction ΔU_{rxn} , from analysis of Evans-Polanyi relationships for abstractions plus evaluation of ring strain energy, and from analogy to similar reactions with known energies. Thermochemical properties are provided for each system.

Reduced sets of three vibration frequencies and their associated degeneracies are computed from fits to heat capacity data, as described by Ritter and Bozzelli et al.^{37,38} These have been shown by Ritter to accurately reproduce molecular heat capacities, $C_p(T)$, and by Bozzelli et al.³⁸ to yield accurate ratios of density of states to partition coefficient, $\rho(E)/Q$.

Lennard-Jones parameters, sigma (angstroms) and ϵ/k (Kelvin's), are obtained from tabulations³⁹ and from a calculation method based on molar volumes and compressibility.⁴⁰

When necessary, estimation is done in a consistent and uniform manner via use of generic reaction rate constants with reference to literature, experiment or theoretical calculation in each case. The QRRK calculation input parameters and their references are listed in the table associated with the respective reaction system.

2.3.6.2 Quantum RRK /Master Equation Calculation. The quantum RRK (QRRK) /master equation analysis is described by Chang et al.^{31,41} The QRRK code utilizes a reduced set of three vibration frequencies which accurately reproduce the molecule's (adduct) heat capacity; the code includes contribution from one external rotation in calculation of the ratio of the density of states to the partition coefficient $\rho(E)/Q$.

Comparisons of ratios of these $\rho(E)/Q$ with direct count $\rho(E)/Q$'s are shown to be in good agreement.³⁸ Rate constant results from the quantum RRK - Master equation analysis are shown to accurately reproduce (model) experimental data on several complex systems. They also provide a reasonable method to estimate rate constants for numerical integration codes by which the effects of temperature and pressure can be evaluated in complex reaction systems.

Multifrequency quantum Rice-Ramsperger-Kassel (QRRK) analysis is used to calculate $k(E)$ with master equation analysis⁴¹ for fall-off. A 500 cal. energy grain interval is used for the energy intervals. Rate constants are obtained as a function of temperature and pressure for the chemical activation and dissociation reactions. The master equation analysis⁴¹ uses an exponential-down model for the energy transfer function with $(\Delta E)^\circ_{\text{down}} = 1000$ cal/mol (for N₂ as bath gas). Troe et al.^{42,43} conclude that $(\Delta E)^\circ_{\text{down}}$ is independent of temperature (293 – 866 K) for the rare and diatomic bath gases and Hann et al.⁴⁴ recently determined a value of $(\Delta E)^\circ_{\text{down}} = 500$ cm⁻¹ for matching the two-dimensional master equation solutions to the experimental fall-off behavior in the C₃H₃ + O₂ system with N₂ bath gas. Knyazev and Slagle⁴⁵ reported that $(\Delta E)^\circ_{\text{down}}$ changes with temperature; they compared three models, two of which are $(\Delta E)^\circ_{\text{down}} = \alpha T$ and $(\Delta E)^\circ_{\text{down}} = \text{constant}$, in reaction of n-C₄H₉ \leftrightarrow C₂H₅ + C₂H₄ with He as bath gas. The difference between the values of the energy barrier height (E) needed to fit the experimental data with these two models (temperature dependent versus non-temperature dependent) for $(\Delta E)^\circ_{\text{down}}$ is only 0.4 kJ/mol; but this is over a relatively narrow temperature range (560 – 620 K). A larger temperature range of 298 – 2000 K and a constant $(\Delta E)^\circ_{\text{down}}$ (where N₂ is the third body) are used in this study.

CHAPTER 3

THERMOCHEMICAL AND KINETIC ANALYSIS OF THE ACETYL RADICAL + O₂ REACTION SYSTEM

3.1 Background

Several studies have illustrated that the reactions of ethyl⁴⁹⁻⁵⁵ and isopropyl⁵⁶ radicals at pressures from 1 to 6000 Torr and temperatures from 300 to 900 K, exhibit significant negative temperature dependence (NTD) and complex falloff with pressure. Acetyl radical reaction with O₂ is expected to have similar complexities.

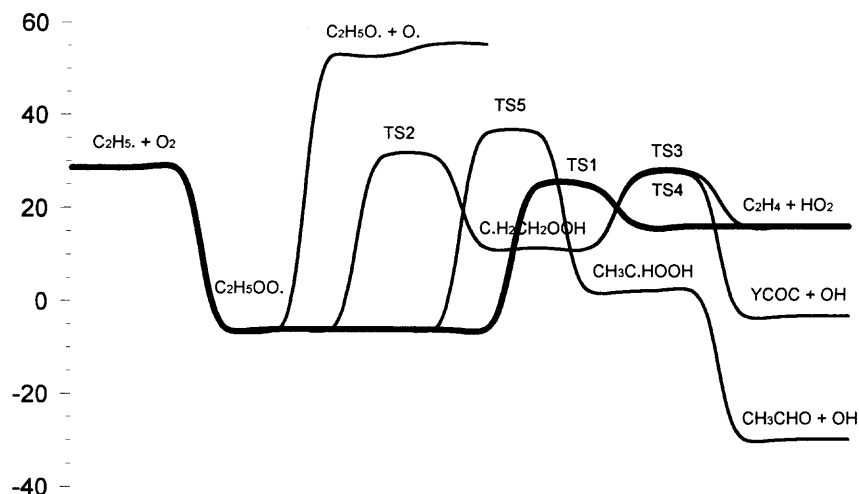
The ethyl radical + O₂ reaction is the system best characterized in the literature, and it is a useful model with which to compare CH₃C•O + O₂ reaction paths and kinetics. Analysis of the C₂H₅• + O₂ reaction system⁵⁷⁻⁵⁹ invokes formation of a chemically activated adduct (C₂H₅OO•*), which can be stabilized, dissociate back to C₂H₅• + O₂, undergo concerted elimination to C₂H₄ + HO₂, or undergo intramolecular hydrogen transfer to hydroperoxide alkyl radical (C•H₂CH₂OOH*). The C•H₂CH₂OOH* isomer can be stabilized, react to an epoxide YCOC + OH (Y=cyclic), or undergo elimination to ethylene + HO₂. The stabilized adduct (C₂H₅OO•) can undergo the same reactions as C₂H₅OO•*, but at a lower rate because of its lower energy (Scheme 3.1).

The rate of ethyl radical loss decreases significantly with temperature⁵⁰, but increases with pressure; this is explained by invoking reversible formation of a weakly bound adduct. The C₂H₅OO•* adduct is readily stabilized at low temperatures

and atmospheric pressure; but dissociates back to reactants at higher temperatures.

This rapid dissociation of the peroxy adduct is used in the explanation of the observed

Scheme 3.1 Potential Energy Diagram of Ethyl Radical + O₂ (CBSQ//B3LYP/6-31G(d,p))



negative temperature dependence (NTD) regime in hydrocarbon oxidation. The epoxide (YCOC) is an observed product in this reaction system⁶⁰ at least in part formed from the HO₂ addition to ethylene path⁶¹ because in this reaction system, C₂H₅• + O₂, C₂H₄ + HO₂, as well as adducts C₂H₅OO• and C•H₂CH₂OOH will often exist in a quasiequilibrium under combustion conditions. The Arrhenius A factor for direct HO₂ elimination is much lower than that for dissociation of the complex to reactants, but the barrier height is also lower. Stabilization and dissociation back to reactants are dominant paths for the chemically activated adduct, whereas concerted HO₂ elimination is the important reaction channel for the stabilized adduct at lower temperature.

There is very little information on the chemical activation reaction of $\text{CH}_3\text{C}\bullet\text{O}$ radicals with O_2 relative to the ethyl + O_2 system.⁶² The oxidation process involves formation of a chemically activated peroxyacetyl radical, $\text{CH}_3\text{C}(=\text{O})\text{OO}\bullet$, which can undergo reactions similar to the ethyl peroxy system.

This chapter focuses on the reaction mechanism of the acetyl radical association with O_2 . Thermochemical properties are estimated for reactants, intermediates, products and transition states in the reaction paths using ab initio and density functional calculations. The thermochemical parameters are used to calculate high-pressure limit rate constants using canonical Transition State Theory (TST). Rate constants as a function of temperature and pressure are estimated using a multifrequency quantum RRK analysis for $k(E)$ and the master equation analysis for falloff. The data at relevant pressures and temperatures should be useful to both atmospheric and combustion models.

3.2 Calculation Methods

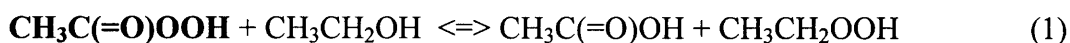
Enthalpies of formation ($\Delta H_f^\circ_{298}$) for reactants, intermediate radicals, transition states and products are calculated using the CBS-Q composite method and density functionals. The initial structure of each compound or transition state is determined using ROHF or UHF/PM3 in MOPAC,⁶³ followed by optimization and vibrational frequency calculation at the HF/6-31G(d') level of theory using GAUSSIAN 94.⁶⁴ The prime in 6-31G(d') indicates the basis set orbitals of Petersson et al.^{65,66} Transition state geometries are identified by the existence of only one imaginary frequency, structure information, and the TST reaction coordinate vibration

information. Zero-point vibrational energies (ZPVE) are scaled by 0.91844 as recommended by Petersson et al.⁶⁷ Single-point energy calculations are carried out at the B3LYP/6-31G(d). The complete basis set (CBS-Q) method of Petersson and co-workers for computing accurate energies^{68,69} is chosen as the determining enthalpies used in this kinetic analysis.

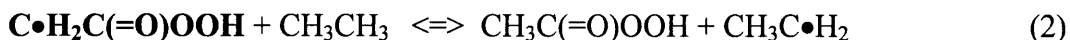
The CBS-Q calculation sequence is performed on a geometry determined at the MP2/6-31G(d') level followed by single-point calculations at the theory level of QCISD(T)/6-31+G(d'), MP4(SDQ)/CBSB4, and MP2/CBSB3 CBSExtrap = (Nmin=10,Pop) including corrections for unpaired electron and spin contamination in intermediate overlap (i.e., $0 < {}^{\alpha\beta}S_{ij} < 1$) between the α and β spin orbitals.⁷⁰

3.2.1 Determination of Enthalpy of Formation

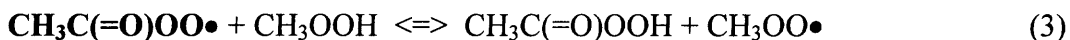
Isodesmic reactions are used to determine the enthalpy of formation ($\Delta H_f^\circ_{298}$) for parent and radical species. $\Delta H_f^\circ_{298}$ for estimation of **CH₃C(=O)OOH** is by



$\Delta H_f^\circ_{298}$ for estimation of **C•H₂C(=O)OOH** [**•** : radical site] is by



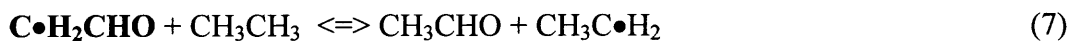
$\Delta H_f^\circ_{298}$ for estimation of **CH₃C(=O)OO•** is by



The working reactions for estimation of $\Delta H_f^\circ_{298}$ on **CH₃C•O** are



The working reactions for estimation of $\Delta H_f^\circ_{298}$ on $\text{C}\cdot\text{H}_2\text{CHO}$ are



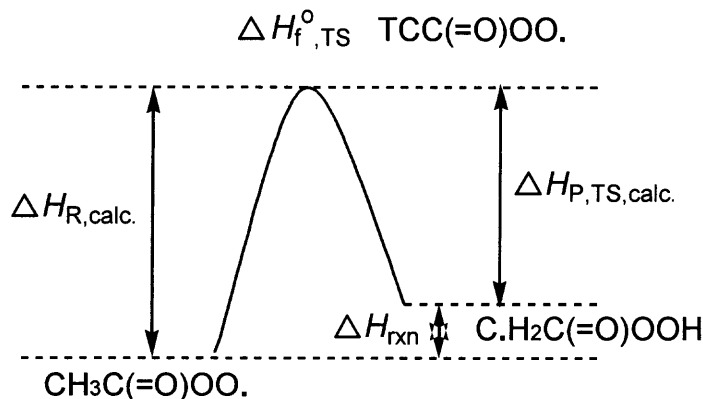
The method of isodesmic reactions relies upon the similarity of the bonding environments in the reactants and products that leads to cancellation of systematic errors from the *ab initio* MO calculations.⁷¹ It also results in a higher accuracy in estimates of $\Delta H_f^\circ_{298}$ than heats of atomization. The basic requirement of the isodesmic reaction is that the number of bonds of each formal chemical bond type is conserved in the reaction. In reaction (1), *ab initio* calculations with ZPVE and thermal correction are performed on all four compounds in the reaction. $\Delta H_f^\circ_{298}$ of three of the compounds in reaction (1), excepting the target molecule, $\text{CH}_3\text{C}(=\text{O})\text{OOH}$ in (1), have been experimentally or theoretically determined. The unknown $\Delta H_f^\circ_{298}$ of $\text{CH}_3\text{C}(=\text{O})\text{OOH}$ is obtained with the calculated $\Delta H^\circ_{\text{rxn}(298)}$ and known $\Delta H_f^\circ_{298}$ of the three reference compounds. The $\text{C}\cdot\text{H}_2\text{C}(=\text{O})\text{OOH}$, $\text{CH}_3\text{C}(=\text{O})\text{OO}\cdot$, $\text{CH}_3\text{C}\cdot\text{O}$, and $\text{C}\cdot\text{H}_2\text{CHO}$ radicals are calculated in the same manner.

3.2.1.1 Enthalpies of Transition States. Enthalpies of transition state structures are estimated by evaluation of $\Delta H_f^\circ_{298}$ of the stable radical adducts from the working reaction analysis above, plus the difference of total energies with ZPVE and thermal correction between these radical species and the transition state. The method is illustrated for the H-shift transition state $\text{TCC}(=\text{O})\text{OO}\cdot$ in Scheme 3.2 below.

Calculation of the enthalpy of formation for $\text{TCC}(=\text{O})\text{OO}\cdot$ is not taken as the calculated energy difference between reactant and transition state. The absolute

enthalpies of reactant and product are first estimated using isodesmic reaction analysis [(3) and (4)]. ΔH_{rxn} is taken from ΔH_f° values determined from the separate isodesmic reactions. $\Delta H_{R',\text{TS,calc.}}$ is the difference between the calculated energy of the transition state and reactant plus ΔH_{rxn} ($\Delta H_f^\circ_{\text{product}} - \Delta H_f^\circ_{\text{reactant}}$). $\Delta H_{P,\text{TS,calc.}}$ is the difference between the calculated energy of the transition state and product. $\Delta H_f^\circ_{\text{TS}}$ is calculated by an average of two values $\Delta H_{R',\text{TS,calc.}}$ and $\Delta H_{P,\text{TS,calc.}}$. (Table 3.1)

Scheme 3.2 $\Delta H_f^\circ_{\text{TS}}$ (TCC(=O)OO•) Calculation



$$\Delta H_{R',\text{TS,calc.}} = \Delta H_{\text{rxn}} (\text{Reactant} \rightarrow \text{TS}) + \Delta H_{\text{rxn}}$$

$$\Delta H_{P,\text{TS,calc.}} = \Delta H_{\text{rxn}} (\text{Product} \rightarrow \text{TS})$$

$$\Delta H_f^\circ_{\text{TS}} = (\Delta H_{R',\text{TS,calc.}} + \Delta H_{P,\text{TS,calc.}}) / 2$$

3.2.2 Determination of Entropy and Heat Capacity

The contributions of external rotation and vibrations to entropies and heat capacities are calculated from scaled vibration frequencies and moments of inertia for the optimized HF/6-31G(d') structures. Contributions from frequencies corresponding to hindered internal rotation are replaced with values calculated from the method of

Pitzer and Gwinn⁷² for S and $C_p(T)$. The number of optical isomers and spin degeneracy of unpaired electrons are also incorporated.

Table 3.1 Activation Energies and Enthalpies of Transition States in CBSQ Calculation^a

Reactant	Transition State (TS)	Product	E_a	$\Delta H_f^{\circ}_{298}$ of TS
CH ₃ C(=O)OO.	TCC(=O)OO.	C.H ₂ C(=O)OOH	26.42	-12.15
CH ₃ C(=O)OO.	TCCO-OOH ^a		34.58	-3.99
C.H ₂ C(=O)OOH	TYCOC(=O)-OH ^a		19.97	-12.98
C.H ₂ C(=O)OOH	TC.CO-OOH ^a		31.41	-1.54

^a : Units in kcal/mol

^b : The activation energy and enthalpy for this transition state is estimated by taking the difference of total energy with ZPVE and thermal correction between the transition state and reactant (peroxy/hydroperoxide isomer).

3.2.3 High-Pressure Limit A Factor (A_{∞}) and Rate Constant (k_{∞}) Determination

For the reactions where thermochemical properties of transition state are calculated by ab initio or density functional methods, k_{∞} 's are fit by three parameters A, n, and E_a over temperature range from 298 to 2000K, $k_{\infty} = A (T)^n \exp(-E_a / RT)$. Entropy differences between reactant and transition state are used to determine the pre-exponential factor, A, via canonical Transition State Theory (TST)

$$A = (k_b T / h_p) \exp(\Delta S^{\ddagger} / R), E_a = \Delta H^{\ddagger}$$

(h_p is the Planck constant and k_b is the Boltzmann constant.) Treatment of the internal rotors for S and $C_p(T)$ is important here because these internal rotors are often lost in the cyclic transition state structures.

3.2.4 Kinetic Analysis

The potential energy surface and thermochemical properties are evaluated, and forward or reverse rate constants (high-pressure limit) for each, elementary reaction step are determined. Multifrequency quantum Rice-Ramsperger-Kassel (QRRK) analysis for $k(E)$ with the master equation analysis⁴¹ for falloff with a 0.5 kcal energy grain is used to obtain rate constants as a function of temperature and pressure, for the separate chemical activation and dissociation reactions.

The QRRK analysis is described by Chang et al.³¹ It is shown to yield reasonable results and provides a framework by which the effects of temperature and pressure can be evaluated in complex reaction systems. The QRRK code utilizes a reduced set of three vibration frequencies which accurately reproduce the molecules' (adduct) heat capacity and include one external rotation in calculation of density of states $\rho(E)/Q$. Comparisons of ratios of these $\rho(E)/Q$ (partition function Q) with direct count $\rho(E)/Q$ are shown to be in good agreement.⁷³ Nonlinear Arrhenius effects resulting from changes in the thermochemical properties of the respective transition state, relative to the adduct with temperature are incorporated using a two parameter Arrhenius preexponential factor (A, n) in AT^n .

Tunneling is applied for the intramolecular hydrogen atom transfer reactions of $TCC(=O)OO\bullet$ and $TC\bullet CHOS$ and hydrogen atom dissociation reactions, $TC\bullet CHO-H$ and $TCC\bullet O-H$. Tunneling effects are taken into account using the Erwin-Henry code⁷⁴ to determine high-pressure limit rate constant (k_∞). This program is based on Eckart's one-dimensional potential function.⁷⁵ Eckart evaluated in closed form, an expression for the probability $k(E)$ of crossing the barrier for a particle of

energy E . The Erwin-Henry code requires input of vibrational frequencies, moments of inertia, and total energies at 0 K of reactants, transition states, and products; imaginary frequencies are also required. Total energies are obtained from the CBSQ composite method, vibrational frequencies and moments of inertia are obtained from HF/6-31G(d') level of calculation. Schwartz et al. note that calculated vibrational frequencies corresponding to the reaction coordinate at the HF/6-31G(d) level of theory need to be reduced by one-half to one-third for calculated rate constant to match experimental data in abstraction reactions.⁷⁶

3.3 Results and Discussion

3.3.1 Transition States

Transition States are identified as follows:

TCC(=O)OO• : peroxy radical $\text{CH}_3\text{C}(=\text{O})\text{OO}\bullet$ isomerizes to form a $\text{C}\bullet\text{H}_2\text{C}(=\text{O})\text{OOH}$ isomer via hydrogen shift.

TCCO-OOH : peroxy radical $\text{CH}_3\text{C}(=\text{O})\text{OO}\bullet$ decomposes to products, $\text{CH}_2\text{CO} + \text{HO}_2$ via concerted HO_2 elimination.

TC•CO-OOH : $\text{C}\bullet\text{H}_2\text{C}(=\text{O})\text{OOH}$ isomer undergoes β -scission to products, $\text{CH}_2\text{CO} + \text{HO}_2$

TYCOC(=O)-OH : $\text{C}\bullet\text{H}_2\text{C}(=\text{O})\text{OOH}$ isomer reacts to products, $\text{YCOC}(=\text{O}) + \text{OH}$ via intramolecular addition and OH elimination.

TC•CHOS : formyl methyl radical $\text{C}\bullet\text{H}_2\text{CHO}$ isomerizes to form a $\text{CH}_3\text{C}\bullet\text{O}$ isomer via hydrogen shift.

TC•CHO-H : $\text{C}\bullet\text{H}_2\text{CHO}$ undergoes β -scission to products, $\text{CH}_2\text{CO} + \text{H}$

TCC•O-H : CH₃C•O isomer undergoes β-scission to products, CH₂CO + H

TCH₃-CO : CH₃C•O isomer decomposes to products, CH₃ + CO

3.3.2 Enthalpy of Formation ($\Delta H_f^\circ_{298}$) using Calculated Total Energies and Isodesmic Reactions

The evaluated enthalpies of formation for the reference molecules and radicals in the isodesmic reactions are listed in Table 3.2. The evaluated reaction enthalpies and enthalpies of formation in the isodesmic reactions are listed in Table 3.3.

A low or zero $\Delta H^\circ_{\text{rxn},298}$ in the working reactions suggests good cancellation of errors in the reaction analysis leading to accurate $\Delta H_f^\circ_{298}$ values, and supports the hypothesis of group additivity. As an example, $\Delta H_f^\circ_{298}[\text{CH}_3\text{C(=O)OOH}]$ is evaluated from

$$\Delta H_f^\circ_{\text{rxn},298} = \Delta H_f^\circ_{298} [\text{CH}_3\text{C(=O)OH}] + \Delta H_f^\circ_{298} [\text{CH}_3\text{CH}_2\text{OOH}] - \Delta H_f^\circ_{298} [\text{CH}_3\text{C(=O)OOH}] - \Delta H_f^\circ_{298} [\text{CH}_3\text{CH}_2\text{OH}]$$

$$\Delta H_f^\circ_{\text{rxn},298} = -2.29(\text{CBSQ}) \text{ and } -3.88(\text{B3LYP})$$

$$\Delta H_f^\circ_{\text{rxn},298} = -103.56 + (-39.70) - X - (-56.17) \text{ kcal/mol} \quad (10)$$

The enthalpies of formation of CH₃C(=O)OOH obtained are -84.80 and -83.21 kcal/mol by CBSQ and B3LYP/6-31G(d), respectively.

Enthalpies of formation of the two intermediate radicals, C•H₂C(=O)OOH and CH₃C(=O)OO• by CBSQ and B3LYP/6-31G(d) are obtained from the use of isodesmic reactions (2) and (3) and values of reference species in Table 3.2. The bond dissociation energies of reference species in these reactions are as follows: C₂H₅—H and CH₃OO—H are 101.1 and 86.6 kcal/mol, respectively.^{80,81,84} The data results in enthalpy values of -32.95 and -32.67 for C•H₂C(=O)OOH, -38.57 and -37.52 for

$\text{CH}_3\text{C}(=\text{O})\text{OO}\bullet$, by CBSQ and B3LYP/6-31G(d), respectively, with bond energies being surprisingly strong, 103.95 and 98.33, respectively.

The working reactions (4) to (6) and (7) to (9) are used to estimate enthalpy of $\text{CH}_3\text{C}\bullet\text{O}$ and $\text{C}\bullet\text{H}_2\text{CHO}$ radical species with the CBSQ composite method.

The average values of $\Delta H_f^\circ_{298}$ from three isodesmic reactions for $\text{CH}_3\text{C}\bullet\text{O}$ and $\text{C}\bullet\text{H}_2\text{CHO}$ are -3.08 and 3.52 kcal/mol by CBSQ, respectively (Table 3.3).

Table 3.2 Enthalpies of Formation for Reference Molecules in the Isodesmic Reactions

Compounds	$\Delta H_f^\circ_{298}$ (kcal/mol)	Compounds	$\Delta H_f^\circ_{298}$ (kcal/mol)
$\text{CH}_3\text{CH}_2\text{OH}$	-56.17 ± 0.10^a [77]	$\text{CH}_3\text{CH}_2\text{OOH}$	-39.70 ± 0.16 [61]
$\text{CH}_3\text{C}(=\text{O})\text{OH}$	-103.56 ± 0.32 (Avg. of -103.32 [77], -103.44 [78], -103.92 [79])		
CH_3CH_3	-20.24 ± 0.10^a [80]	$\text{CH}_3\text{C}\bullet\text{H}_2$	28.80 ± 0.50 [81]
CH_3CHO	-39.72 ± 0.12^a [77]	CH_3OH	-48.16 ± 0.07 [78]
$\text{C}\bullet\text{H}_2\text{OH}$	-3.97 ± 0.22 [82]	$\text{CH}_3\text{C}(=\text{O})\text{CH}_3$	-51.94 ± 0.17 [78]
$\text{C}\bullet\text{H}_2\text{C}(=\text{O})\text{CH}_3$	-8.53 ± 1.15 [83]		

^a The uncertainties are evaluated from ref.[78]

3.3.3 Entropy ($S^\circ_{(298)}$) and Heat Capacity ($Cp(T)$, $300 \leq T/K \leq 1500$)

Entropy and heat capacities are calculated based on vibration frequencies and moments of inertia of the optimized HF/6-31G(d') structures.

The calculation results using MP2/6-31G(d') determined geometries and HF/6-31G(d') determined frequencies are summarized in Table 3.4. TVR represents the sum of the contributions from translation, vibrations and external rotations for $S^\circ_{(298)}$ and $Cp(T)$'s. Symmetry, number of optical isomers and electronic spin are

incorporated in the estimation of $S^{\circ}_{(298)}$ as described in Table 3.4. Torsion frequency vibrations are omitted in these calculations, instead, contributions from internal rotation for $S^{\circ}_{(298)}$ and $Cp(T)$'s are calculated based on rotational barrier heights, moments of inertia of the rotors using the method of Pitzer and Gwinn,⁷² data on these parameters are listed in Table 3.5 with internal rotor contributions noted in Table 3.4.

Table 3.3 Reaction Enthalpies and Enthalpies of Formation in the Isodesmic Reactions^a

Working Reaction Series	$\Delta H^{\circ}_{\text{rxn},298}$		$\Delta H^{\circ}_{\text{f},298}$	
	B3LYP	CBSQ	B3LYP	CBSQ
$\text{CH}_3\text{C(=O)OOH} + \text{CH}_3\text{CH}_2\text{OH} \rightleftharpoons \text{CH}_3\text{C(=O)OH} + \text{CH}_3\text{CH}_2\text{OOH}$	-3.88	-2.29	-83.21	-84.80
$\text{C.H}_2\text{C(=O)OOH} + \text{CH}_3\text{CH}_3 \rightleftharpoons \text{CH}_3\text{C(=O)OOH} + \text{CH}_3\text{C.H}_2$	-1.54	-2.85	-32.67	-32.95
$\text{CH}_3\text{C(=O)OO.} + \text{CH}_3\text{OOH} \rightleftharpoons \text{CH}_3\text{C(=O)OOH} + \text{CH}_3\text{OO.}$	-11.19	-11.73	-37.52	-38.57
$\text{CH}_3\text{C.O} + \text{CH}_3\text{CH}_3 \rightleftharpoons \text{CH}_3\text{CHO} + \text{CH}_3\text{C.H}_2$	-	12.26	-	-2.94
$\text{CH}_3\text{C.O} + \text{CH}_3\text{OH} \rightleftharpoons \text{CH}_3\text{CHO} + \text{C.H}_2\text{OH}$	-	7.25	-	-2.78
$\text{CH}_3\text{C.O} + \text{CH}_3\text{C(=O)CH}_3 \rightleftharpoons \text{CH}_3\text{CHO} + \text{C.H}_2\text{C(=O)CH}_3$	-	7.20	-	-3.51
	Average for CH₃C.O :			-3.08 ± 0.38
$\text{C.H}_2\text{CHO} + \text{CH}_3\text{CH}_3 \rightleftharpoons \text{CH}_3\text{CHO} + \text{CH}_3\text{C.H}_2$	-	5.66	-	3.66
$\text{C.H}_2\text{CHO} + \text{CH}_3\text{OH} \rightleftharpoons \text{CH}_3\text{CHO} + \text{C.H}_2\text{OH}$	-	0.65	-	3.82
$\text{C.H}_2\text{CHO} + \text{CH}_3\text{C(=O)CH}_3 \rightleftharpoons \text{CH}_3\text{CHO} + \text{C.H}_2\text{C(=O)CH}_3$	-	0.60	-	3.09
	Average for C.H₂CHO :			3.52 ± 0.38

^a : Units in kcal/mol

Table 3.4 Ideal Gas Phase Thermodynamic Properties Obtained by CBSQ Calculation and by Therm^a

Species (s, e, OI) ^g		ΔH_f° ₂₉₈ ^b	S° ₂₉₈ ^c	Cp_{300} ^c	Cp_{400}	Cp_{500}	Cp_{600}	Cp_{800}	Cp_{1000}	Cp_{1500}
CH ₃ CHO (3,0,1)	TVR ^d		57.97 ^e	11.58	14.29	16.88	19.20	22.98	25.80	30.10
	Internal Rotor 1 ^f		5.16	1.44	1.30	1.23	1.17	1.10	1.07	1.03
	Total	-39.72	63.13	13.02	15.59	18.11	20.37	24.08	26.87	31.13
	THERM	-39.18	63.13	13.22	15.71	18.22	20.47	24.22	26.97	
CH ₃ C=O (3,1/2,1)	TVR		58.82	11.12	13.24	15.24	17.01	19.90	22.07	25.39
	Internal Rotor 1		5.45	1.16	1.10	1.06	1.04	1.02	1.01	1.00
	Total	-3.08	64.27	12.28	14.34	16.30	18.05	20.92	23.08	26.39
	THERM	-2.54	64.27	12.28	14.34	16.30	18.05	20.92	23.08	
C.H ₂ CHO (1,1/2,1)	TVR		61.99	13.10	15.79	18.04	19.86	22.63	24.62	27.66
	Total	3.52	61.99	13.10	15.79	18.04	19.86	22.63	24.62	27.66
	THERM	4.06	61.99	13.10	15.79	18.04	19.86	22.63	24.62	
CH ₃ C(=O)OOH (3,0,2)	TVR		66.93	15.50	19.22	22.49	25.25	29.52	32.59	37.27
	Internal Rotor 1,2,3		9.65	5.53	6.06	6.27	6.30	6.06	5.64	4.70
	Total	-84.80	76.58	21.03	25.28	28.76	31.55	35.58	38.23	41.97
	THERM	-84.80	76.58	21.03	25.28	28.76	31.55	35.58	38.23	
CH ₃ C(=O)OO. (3,1/2,1)	TVR		66.69	15.34	18.84	21.87	24.38	28.18	30.86	34.77
	Internal Rotor 1,2		8.87	4.14	4.38	4.46	4.43	4.21	3.90	3.22
	Total	-38.57	75.56	19.48	23.22	26.33	28.81	32.39	34.76	37.99
	THERM	-38.57	75.56	19.48	23.22	26.33	28.81	32.39	34.76	
C.H ₂ C(=O)OOH (1,1/2,2)	TVR		70.45	15.79	19.14	21.85	24.01	27.19	29.43	32.85
	Internal Rotor 1,2,3		8.80	6.00	6.39	6.50	6.46	6.15	5.69	4.72
	Total	-32.95	79.25	21.79	25.53	28.35	30.47	33.34	35.12	37.57
	THERM	-32.95	78.02	22.07	25.82	28.60	30.67	33.46	35.17	
CH ₂ CO (2,0,1)	TVR		57.57	12.26	14.10	15.61	16.85	18.81	20.29	22.61
	Total		57.57	12.26	14.10	15.61	16.85	18.81	20.29	22.61
	THERM	-11.80	57.81	12.68	14.77	16.43	17.75	19.65	20.92	22.91
TCC(=O)OO. (1,1/2,2)	TVR		72.28	18.52	22.50	25.75	28.32	32.02	34.46	37.79
	Total	-12.15	72.28	18.52	22.50	25.75	28.32	32.02	34.46	37.79
TCCO-OOH (1,1/2,2)	TVR		76.34	20.04	23.37	26.14	28.41	31.83	34.20	37.57
	Total	-3.99	76.34	20.04	23.37	26.14	28.41	31.83	34.20	37.57
TC.CO-OOH (1,1/2,2)	TVR		74.11	18.14	20.96	23.20	25.00	27.76	29.80	33.03
	Internal Rotor 1,2		5.07	3.83	4.19	4.41	4.52	4.47	4.20	3.47
	Total	-1.54	79.18	21.97	25.15	27.61	29.52	32.23	34.00	36.50
CH ₃ C(=O)O. (3,1/2,1)	TVR		62.80	12.71	15.42	17.91	21.10	23.58	26.16	30.15
	Internal Rotor 1		5.62	1.08	1.05	1.03	1.02	1.01	1.00	1.00
	Total	-41.35	68.42	13.79	16.47	18.94	22.12	24.59	27.16	31.15
YCOC(=O) (1,0,1)	TVR		62.29	11.95	14.65	17.06	19.06	22.10	24.24	27.42
	Total	-44.42	62.29	11.95	14.65	17.06	19.06	22.10	24.24	27.42
C.H ₂ C(=O)O. (1,1,1)	TVR		66.14	14.53	17.17	19.34	21.10	23.69	25.50	28.17
	Total	-14.87	66.14	14.53	17.17	19.34	21.10	23.69	25.50	28.17

Table 3.4 Ideal Gas Phase Thermodynamic Properties Obtained by CBSQ Calculation and by Therm^a (Continued)

Species (s, e, OI) ^g		ΔH_f^0 ₂₉₈ ^b	S^0 ₂₉₈ ^c	Cp_{300} ^c	Cp_{400}	Cp_{500}	Cp_{600}	Cp_{800}	Cp_{1000}	Cp_{1500}
TYCOC(=O)-OH (1,1/2,1)	TVR		73.08	18.74	21.97	24.50	26.48	29.39	31.47	34.77
	Internal Rotor 1		4.31	1.46	1.30	1.20	1.14	1.08	1.05	1.02
	Total	-12.98	77.39	20.20	23.27	25.70	27.62	30.47	32.52	35.79
TC.CHOS (1,1/2,1)	TVR		61.32	12.12	14.47	16.59	18.40	21.21	23.21	26.11
	Total	43.03	61.32	12.12	14.47	16.59	18.40	21.21	23.21	26.11
TC.CHO-H (1,1/2,1)	TVR		64.09	15.29	17.59	19.33	20.71	22.79	24.31	26.64
	Total	44.01	64.09	15.29	17.59	19.33	20.71	22.79	24.31	26.64
TCC.O-H (1,1/2,1)	TVR		63.25	14.69	17.05	18.88	20.34	22.53	24.12	26.54
	Total	40.09	63.25	14.69	17.05	18.88	20.34	22.53	24.12	26.54
TCH ₃ -CO (3,1/2,1)	TVR		60.70	12.22	13.92	15.42	16.75	18.99	20.78	23.69
	Internal Rotor 1		5.45	1.16	1.10	1.06	1.04	1.02	1.01	1.00
	Total	13.56	66.15	13.38	15.02	16.48	17.79	20.01	21.79	24.69
CH ₃ C(=O)OONO ₂ (3,0,1)	TVR		72.70	20.72	26.00	30.33	33.83	38.94	42.43	47.38
	I. R. 1,2,3,4		21.31	6.90	7.01	7.02	6.94	6.57	6.12	5.00
	Total		94.01	27.62	33.01	37.35	40.77	45.51	48.55	52.38
C ₂ H ₅ OONO ₂ (3,0,1)	TVR		70.93	19.33	24.89	29.79	33.88	40.08	44.48	50.98
	I. R. 1,2,3,4		21.86	8.97	8.47	7.82	7.20	6.13	5.33	3.96
	Total		92.79	28.30	33.36	37.61	41.08	46.21	49.81	54.94

a : Thermodynamic properties are referred to a standard state of an ideal gas of pure enantiomer at 1 atm.

Therm values for stable species are included for comparison (refs 37 and 85).

b : Units in kcal/mol c : Units in cal/mol-K

d : Sum of contributions from translations, vibrations, and external rotations.

f : Contribution from internal rotation

g : Symmetry number, optical isomer and electronic spin are taken into account, -Rln(s), Rln2, Rln2, respectively. s = number of symmetry, e = electronic spin, OI = number of optical isomer.

Table 3.5 Moments of Inertia ($\text{amu}\cdot\text{\AA}^2$) and Rotational Barriers (kcal/mol) for Internal Rotors

Species	Rotor	I_A	I_B	V	n^a
CH ₃ CHO	CH ₃ --C(=O)H	3.12	18.90	1.20	6
CH ₃ C.O ^b	CH ₃ --C.(=O)	3.12	12.63	0.55	3
CH ₃ C(=O)OOH ^c	CH ₃ --C(=O)OOH	3.12	130.14	3.18	3
	CH ₃ C(=O)--OOH	44.19	1.56	5.46	1
	CH ₃ C(=O)O--OH	100.00	0.92	7.15	1
CH ₃ C(=O)OO.	CH ₃ --C(=O)OO.	3.12	126.74	4.00	3
	CH ₃ C(=O)--OO.	44.19	23.30	7.00	1
C.H ₂ C(=O)OOH	C.H ₂ --C(=O)OOH	1.75	130.14	3.18	2
	C.H ₂ C(=O)--OOH	42.44	1.56	5.46	2
	C.H ₂ C(=O)O--OH	100.00	0.92	7.15	1
TC.CO-OOH	C.H ₂ C(=O)--OOH	42.44	1.56	5.46	2
	C.H ₂ C(=O)O--OH	100.00	0.92	7.15	1
CH ₃ C(=O)O.	CH ₃ --C(=O)O.	3.12	38.12	0.48	6
TYCOC(=O)-OH	OH--YCOC(=O)	0.98	61.8	1	2
TCH ₃ -CO	CH ₃ --C.(=O)	3.12	12.63	0.55	3

^a n : foldness.

^b "." stands for radical site.

^c "=" stands for double bonding(C=O).

3.3.4 Energy Diagram for CH₃C•O + O₂ Reaction System

The overall energy diagram for the CH₃C•O + O₂ reaction is illustrated in Figure 3.1

where enthalpies of formation are from CBSQ calculations and in units of kcal/mol.

The acetyl radical CH₃C•O ($\Delta H_f^\circ_{298} = -3.08$ kcal/mol) adds to O₂ to form a CH₃C(=O)OO• peroxy radical with a 35.5 kcal/mol well depth. This peroxy radical can undergo dissociation back to reactants, decompose to products, CH₂CO + HO₂

via concerted HO_2 elimination with a barrier, ($E_a = 34.58$) or isomerize via hydrogen shift ($E_a = 26.42$) to form a $\text{C}\cdot\text{H}_2\text{C}(=\text{O})\text{OOH}$ isomer ($\Delta H_f^\circ_{298} = -32.95$).

The $\text{C}\cdot\text{H}_2\text{C}(=\text{O})\text{OOH}$ isomer can undergo β scission to products, $\text{CH}_2\text{CO} + \text{HO}_2$ ($E_a = 31.41$), decompose to a cyclic ketone, $\text{YCOC}(=\text{O}) + \text{OH}$ via OH elimination ($E_a = 19.97$, $\text{Y}=\text{cyclic}$), decompose to a diradical, $\text{C}\cdot\text{H}_2\text{CO}(\text{O}\cdot) + \text{OH}$ via simple RO-OH bond cleavage ($E_a = 27.57$), or isomerize via hydrogen shift ($E_a = 20.80$), to form a $\text{CH}_3\text{C}(=\text{O})\text{OO}\cdot$ isomer.

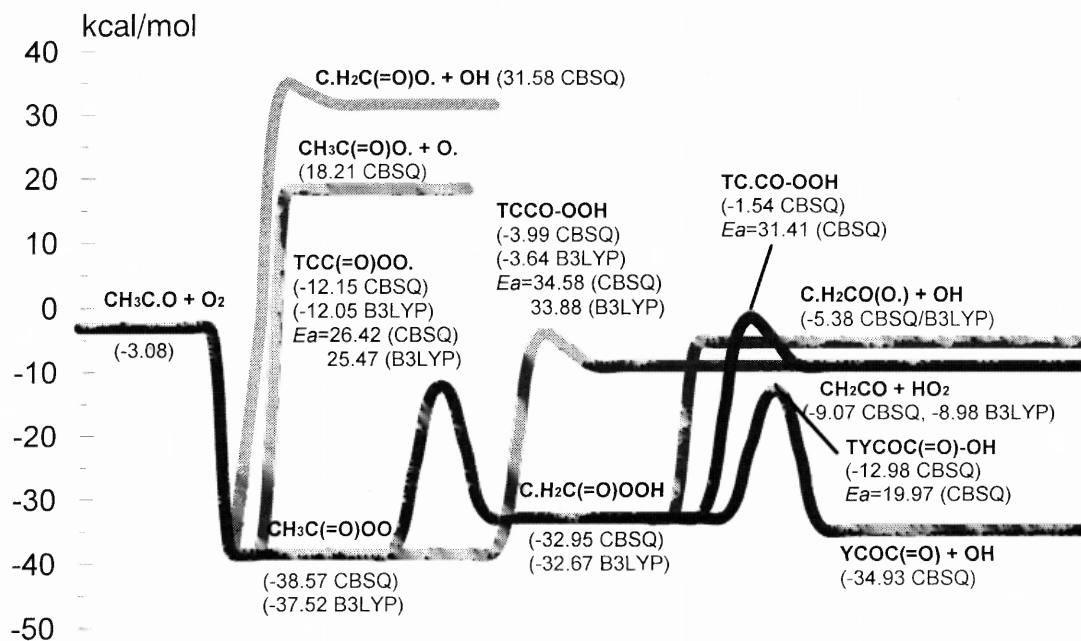


Figure 3.1 Potential energy diagram $\text{CH}_3\text{C}\cdot\text{O} + \text{O}_2$.

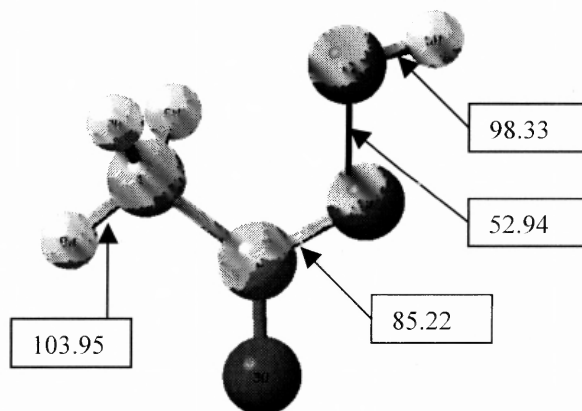


Figure 3.2 Bond dissociation energy of CH₃C(=O)OOH (Units : kcal/mol).

Table 3.6 The Comparison of Bond Energies between CH₃C(=O)OOH and C₂H₅OOH^a

	CH ₃ C(=O)OOH	C ₂ H ₅ OOH
ROO-H	98.33	85.27
RO-OH	52.94	45.12
R-OOH	85.22	71.35
H-CH ₂ C(=O)OOH or H-CH ₂ CH ₂ OOH	103.95	103.21

^a : Units in kcal/mol

3.3.5 Comparison of $C_2H_5 + O_2$ and $CH_3C\bullet O + O_2$

The $C_2H_5\bullet + O_2$ ⁴¹ and $CH_3C\bullet O + O_2$ reaction systems have some similarities and some significant differences. The $C_2H_5\bullet + O_2$ and $CH_3C\bullet O + O_2$ reactions have similar well depths 35.3 and 35.5 kcal/mol, respectively. The H shift isomerization and concerted HO_2 elimination reaction paths for the $C_2H_5OO\bullet$ and $CH_3C(=O)OO\bullet$ have major differences in the barriers. The hydrogen shift in ethylperoxy, $C_2H_5OO\bullet$, to $C\bullet H_2CH_2OOH$ and the barrier for HO_2 molecular elimination, to $C_2H_4 + HO_2$, are 37.05 and 30.93 kcal/mol, respectively. The HO_2 elimination is clearly a more important first step in the ethyl system. In our acetyl radical system, the H shift from $CH_3C(=O)OO\bullet$ to $C\bullet H_2C(=O)OOH$ and HO_2 molecular elimination to $CH_2CO + HO_2$ have barriers, 26.42 and 34.58 kcal/mol, respectively. The lowering of the H shift barrier is partially due to the lower C—H bond of the methyl in the acetyl system. The hydrogen shift is important in this acetyl radical system.

Rienstra-Kiracofe et al.⁵⁷ recently studied the $C_2H_5\bullet + O_2$ reaction system with the CCSD and CCSD(T) ab initio methods. They showed that the concerted HO_2 elimination path from $C_2H_5OO\bullet$ is energetically preferred and is also the only mechanism consistent with experimental observations of a negative temperature coefficient¹⁴. They reported a 30.5 kcal/mol well depth at 0 K; we use vibration frequencies of $C_2H_5\bullet$, O_2 and $C_2H_5OO\bullet$ from the HF/6-31G(d') level, and estimate a well depth at 298 K from their data of 31.9 kcal/mol. This is 3.4 kcal/mol different from Sheng et al.,⁴¹ whose value is closer to data of Knyazev and Slagle,⁸⁶ 35.5 kcal/mol, Miller et al.,⁸⁷ 35.3 kcal/mol and Blanksby et al.,⁸⁸ 35.7 kcal/mol.

Table 3.7 Input Parameters^a and High-Pressure Limit Rate Constants (k_{∞})^b for QRRK Calculations^c

Input parameters for QRRK calculations with master equation analysis for fall-off			
Reaction (kcal/mol)	A	k_{∞}	
		n	E_a
1 $\text{CH}_3\text{C}\cdot\text{O} + \text{O}_2 \Rightarrow \text{CH}_3\text{C}(=\text{O})\text{OO}\cdot^{\text{d}}$	2.65E+12	0.0	0.0
-1 $\text{CH}_3\text{C}(=\text{O})\text{OO}\cdot \Rightarrow \text{CH}_3\text{C}\cdot\text{O} + \text{O}_2^{\text{e}}$	3.37E+14	0.0	32.44
2 $\text{CH}_3\text{C}(=\text{O})\text{OO}\cdot \Rightarrow \text{C}\cdot\text{H}_2\text{C}(=\text{O})\text{OOH}^{\text{f}}$	1.29E+06	2.00	24.57
3 $\text{CH}_3\text{C}(=\text{O})\text{OO}\cdot \Rightarrow \text{CH}_2\text{CO} + \text{HO}_2^{\text{f}}$	9.47E+09	1.17	34.45
4 $\text{C}\cdot\text{H}_2\text{C}(=\text{O})\text{OOH} \Rightarrow \text{YCOC}(=\text{O}) + \text{OH}^{\text{f}}$	4.87E+13	-0.29	20.77
5 $\text{C}\cdot\text{H}_2\text{C}(=\text{O})\text{OOH} \Rightarrow \text{CH}_2\text{CO} + \text{HO}_2^{\text{f}}$	5.98E+11	0.52	31.79
6 $\text{C}\cdot\text{H}_2\text{C}(=\text{O})\text{OOH} \Rightarrow \text{C}\cdot\text{H}_2\text{CO}(\text{O}\cdot) + \text{OH}^{\text{f}}$	4.50E+15 ^g	0.00	24.59

[units] k_1 : $\text{cm}^3/(\text{mol}\times\text{sec})$, $k_{-1} \rightarrow k_6$: sec^{-1}

^aGeometric mean frequency (from CPFIT, Ref.[73]: $361.7 \text{ cm}^{-1}(6.059)$; $1143.8 \text{ cm}^{-1}(8.297)$; $2566.9 \text{ cm}^{-1}(2.645)$). Lennard-Jones parameters: $\sigma_{ij}=5.19\text{\AA}$, $\epsilon/k=533.08\text{K}$, Ref.[89])

^bThe units of A factors and rate constants k are sec^{-1} for unimolecular reactions and $\text{cm}^3/(\text{mol}\times\text{sec})$ for bimolecular reactions.

^c ΔE down of 1000 cal/mol is used, N_2 for bath gas.

^d $k_{\infty,1}$: Sehested et al.[10]

^e $k_{\infty,-1}$: Thermodynamics and microscopic reversibility.

^f A is calculated using TST and entropy of transition state, $\Delta S_{298}^{\ddagger}$ from HF/6-31G(d'); E_a is from CBSQ calculation (see Table 3.4 and description for determination of E_a in Scheme 3.2). All parameters A, n, E_a , are fit over the temperature range of 298-2000K.

^g Ref.[90]

Table 3.8 Resulting Rate Constants in QRRK Calculations

1) Calculated Reaction Parameters at P = 0.01 atm,
 $k = A(T/K)^n \exp(-Ea/RT)$ ($298 \leq T/K \leq 2000$)

Reaction	A	n	Ea (kcal/mol)	k_{298}
1 $\text{CH}_3\text{C}\bullet\text{O} + \text{O}_2 \Rightarrow \text{CH}_3\text{C}(=\text{O})\text{OO}\bullet$	9.04E+72	-20.57	13.54	1.35E+12
7 $\text{CH}_3\text{C}\bullet\text{O} + \text{O}_2 \Rightarrow \text{CH}_2\text{CO} + \text{HO}_2$	2.21E+09	0.72	2.82	1.15E+09
8 $\text{CH}_3\text{C}\bullet\text{O} + \text{O}_2 \Rightarrow \text{YCOC}(=\text{O}) + \text{OH}$	7.60E+24	-4.76	3.42	3.97E+10
9 $\text{CH}_3\text{C}\bullet\text{O} + \text{O}_2 \Rightarrow \text{C}\bullet\text{H}_2\text{C}(=\text{O})\text{OOH}$	2.78E+69	-19.51	14.89	1.79E+10
10 $\text{CH}_3\text{C}\bullet\text{O} + \text{O}_2 \Rightarrow \text{C}\bullet\text{H}_2\text{CO}(\text{O}\bullet) + \text{OH}$	7.79E+17	-1.92	2.42	2.32E+11
2 $\text{CH}_3\text{C}(=\text{O})\text{OO}\bullet \Rightarrow \text{C}\bullet\text{H}_2\text{C}(=\text{O})\text{OOH}$	3.03E+39	-9.08	32.73	1.02E-07
3 $\text{CH}_3\text{C}(=\text{O})\text{OO}\bullet \Rightarrow \text{CH}_2\text{CO} + \text{HO}_2$	4.42E+56	-15.38	42.76	1.69E-13
4 $\text{C}\bullet\text{H}_2\text{C}(=\text{O})\text{OOH} \Rightarrow \text{YCOC}(=\text{O}) + \text{OH}$	8.62E+10	-0.36	16.62	7.17E-03
5 $\text{C}\bullet\text{H}_2\text{C}(=\text{O})\text{OOH} \Rightarrow \text{CH}_2\text{CO} + \text{HO}_2$	6.43E-18	6.33	19.96	6.79E-17
6 $\text{C}\bullet\text{H}_2\text{C}(=\text{O})\text{OOH} \Rightarrow \text{C}\bullet\text{H}_2\text{CO}(\text{O}\bullet) + \text{OH}$	2.03E-05	4.67	13.99	3.97E-04

The units of A factors and rate constants k are sec^{-1} for unimolecular reactions and $\text{cm}^3/(\text{mol}\times\text{sec})$ for bimolecular reactions.

2) Calculated Reaction Parameters at P = 0.1 atm,
 $k = A(T/K)^n \exp(-Ea/RT)$ ($298 \leq T/K \leq 2000$)

Reaction	A	n	Ea (kcal/mol)	k_{298}
1 $\text{CH}_3\text{C}\bullet\text{O} + \text{O}_2 \Rightarrow \text{CH}_3\text{C}(=\text{O})\text{OO}\bullet$	3.41E+69	-18.90	14.40	1.62E+12
7 $\text{CH}_3\text{C}\bullet\text{O} + \text{O}_2 \Rightarrow \text{CH}_2\text{CO} + \text{HO}_2$	1.65E+12	-0.10	4.60	3.93E+08
8 $\text{CH}_3\text{C}\bullet\text{O} + \text{O}_2 \Rightarrow \text{YCOC}(=\text{O}) + \text{OH}$	4.14E+27	-5.49	6.17	3.20E+09
9 $\text{CH}_3\text{C}\bullet\text{O} + \text{O}_2 \Rightarrow \text{C}\bullet\text{H}_2\text{C}(=\text{O})\text{OOH}$	2.50E+64	-17.49	15.49	5.81E+09
10 $\text{CH}_3\text{C}\bullet\text{O} + \text{O}_2 \Rightarrow \text{C}\bullet\text{H}_2\text{CO}(\text{O}\bullet) + \text{OH}$	1.47E+21	-2.83	4.97	3.33E+10
2 $\text{CH}_3\text{C}(=\text{O})\text{OO}\bullet \Rightarrow \text{C}\bullet\text{H}_2\text{C}(=\text{O})\text{OOH}$	1.17E+35	-7.46	32.25	9.07E-08
3 $\text{CH}_3\text{C}(=\text{O})\text{OO}\bullet \Rightarrow \text{CH}_2\text{CO} + \text{HO}_2$	1.25E+54	-13.84	44.10	3.22E-13
4 $\text{C}\bullet\text{H}_2\text{C}(=\text{O})\text{OOH} \Rightarrow \text{YCOC}(=\text{O}) + \text{OH}$	8.89E+15	-1.86	18.15	1.09E-02
5 $\text{C}\bullet\text{H}_2\text{C}(=\text{O})\text{OOH} \Rightarrow \text{CH}_2\text{CO} + \text{HO}_2$	1.54E-16	6.15	18.35	8.81E-15
6 $\text{C}\bullet\text{H}_2\text{C}(=\text{O})\text{OOH} \Rightarrow \text{C}\bullet\text{H}_2\text{CO}(\text{O}\bullet) + \text{OH}$	5.44E+07	0.99	17.22	3.61E-03

Table 3.8 Resulting Rate Constants in QRRK Calculations (Continued)

3) Calculated Reaction Parameters at P = 1 atm,
 $k = A(T/K)^n \exp(-Ea/RT)$ ($298 \leq T/K \leq 2000$)

Reaction	A	n	<i>Ea</i> (kcal/mol)	<i>k</i> ₂₉₈
1 CH ₃ C•O + O ₂ => CH ₃ C(=O)OO•	5.79E+61	-16.07	13.40	1.50E+12
7 CH ₃ C•O + O ₂ => CH ₂ CO + HO ₂	2.04E+15	-0.95	7.04	6.20E+07
8 CH ₃ C•O + O ₂ => YCOC(=O) + OH	3.24E+27	-5.37	8.27	1.43E+08
9 CH ₃ C•O + O ₂ => C•H ₂ C(=O)OOH	7.40E+56	-14.88	14.87	1.40E+09
10 CH ₃ C•O + O ₂ => C•H ₂ CO(O•) + OH	8.24E+22	-3.26	7.48	2.31E+09
2 CH ₃ C(=O)OO• => C•H ₂ C(=O)OOH	2.89E+29	-5.55	31.11	8.15E-08
3 CH ₃ C(=O)OO• => CH ₂ CO + HO ₂	1.38E+47	-11.15	43.62	3.64E-13
4 C•H ₂ C(=O)OOH => YCOC(=O) + OH	6.24E+13	-0.99	18.10	1.17E-02
5 C•H ₂ C(=O)OOH => CH ₂ CO + HO ₂	2.30E-24	9.22	14.95	1.62E-12
6 C•H ₂ C(=O)OOH => C•H ₂ CO(O•) + OH	3.67E+08	1.12	18.28	8.52E-03

4) Calculated Reaction Parameters at P = 10 atm,
 $k = A(T/K)^n \exp(-Ea/RT)$ ($298 \leq T/K \leq 2000$)

Reaction	A	n	<i>Ea</i> (kcal/mol)	<i>k</i> ₂₉₈
1 CH ₃ C•O + O ₂ => CH ₃ C(=O)OO•	5.07E+52	-12.96	11.56	1.46E+12
7 CH ₃ C•O + O ₂ => CH ₂ CO + HO ₂	4.22E+15	-0.97	8.82	5.71E+06
8 CH ₃ C•O + O ₂ => YCOC(=O) + OH	1.04E+25	-4.53	9.89	3.57E+06
9 CH ₃ C•O + O ₂ => C•H ₂ C(=O)OOH	4.47E+49	-12.44	14.33	2.29E+08
10 CH ₃ C•O + O ₂ => C•H ₂ CO(O•) + OH	1.99E+22	-2.98	9.62	7.36E+07
2 CH ₃ C(=O)OO• => C•H ₂ C(=O)OOH	4.44E+23	-3.62	29.68	8.43E-08
3 CH ₃ C(=O)OO• => CH ₂ CO + HO ₂	1.31E+39	-8.32	42.28	3.33E-13
4 C•H ₂ C(=O)OOH => YCOC(=O) + OH	6.67E+08	0.77	17.23	1.23E-02
5 C•H ₂ C(=O)OOH => CH ₂ CO + HO ₂	1.95E-21	9.04	16.14	6.65E-11
6 C•H ₂ C(=O)OOH => C•H ₂ CO(O•) + OH	3.30E+05	2.43	18.35	1.17E-02

The bond energies of $\text{CH}_3\text{C(=O)OOH}$ (Figure 3.2) and $\text{C}_2\text{H}_5\text{OOH}$ are compared in Table 3.6. The C–O, O–O, and O–H bond energies in $\text{CH}_3\text{C(=O)OOH}$ are 7 – 14 kcal/mol higher than those in $\text{C}_2\text{H}_5\text{OOH}$, probably because of coupling with the C=O bond in $\text{CH}_3\text{C(=O)OOH}$.

3.3.6 Analysis of Chemical Activation Reaction in Acetyl + O_2

The QRRK calculations for $k(E)$ and the master equation analysis for falloff are performed on this $\text{CH}_3\text{C}\bullet\text{O} + \text{O}_2$ reaction system to estimate rate constants and to determine important reaction paths as a function of temperature and pressure (Tables 3.7 and 3.8).

The master equation analysis⁴¹ uses an exponential-down model for the energy transfer function with $(\Delta E)^\circ_{\text{down}} = 1000 \text{ cal/mol}$,^{42,45} where N_2 is the third body (Table 3.7). Rate constants at 1 atm pressure versus $1000/T$ are illustrated in Figure 3.3. Stabilization to $(\text{CH}_3\text{C(=O)OO}\bullet)$ is important below 600 K, with reverse dissociation important at higher temperatures. The diradical, $\text{C}\bullet\text{H}_2\text{CO(O}\bullet)$, + OH product via RO-OH bond cleavage is also important above 1000 K, but it is 1 order of magnitude lower than reverse dissociation at 1000 K.

Plots of calculated rate constants for $\text{CH}_3\text{C}\bullet\text{O} + \text{O}_2$ at 298 K versus pressure are illustrated in Figure 3.4. Stabilization is the dominant path above 0.01 atm, whereas reverse dissociation is important below 0.01 atm. $\text{C}\bullet\text{H}_2\text{CO(O}\bullet)$ + OH is also important below 0.001 atm; but it is not important at atmospheric pressure, in agreement with Tyndall et al.⁹

Rate constants at 1000 K versus pressure are illustrated in Figure 3.5. Reverse dissociation is the dominant path at both high and low pressures. $\text{C}\bullet\text{H}_2\text{CO(O}\bullet)$ + OH

is more than one order of magnitude below reverse dissociation at 0.1 atm. Stabilization decreases as pressure is decreased (as expected).

A high-pressure limit value of $k_1 = 2.65 \times 10^{12} \text{ cm}^3/(\text{mol}\cdot\text{s})$ is selected for the acetyl radical + O₂ association as noted in Table 3.7 and described earlier. This results in a total forward rate constant of $(2.13 \pm 0.05) \times 10^{12} \text{ cm}^3/(\text{mol}\cdot\text{s})$ under the conditions of McDade et al.⁶ and is about factor of 2 higher than their reported value of $(1.2 \pm 0.2) \times 10^{12} \text{ cm}^3/(\text{mol}\cdot\text{s})$ in 1-4 Torr He at 298K.

3.3.7 Abstraction of Methyl Hydrogen in CH₃C•O by O₂



A transition state for direct abstraction of methyl hydrogens on CH₃C•O by O₂ to form, ketene plus HO₂ is identified with a barrier of 10 kcal/mol, at only the B3LYP/6-31G(d) level. This abstraction channel to form ketene + HO₂ is not competitive with the chemical activation CH₃C•O by O₂ (association) rate constant to the same product set below 1400K at 1 atm.

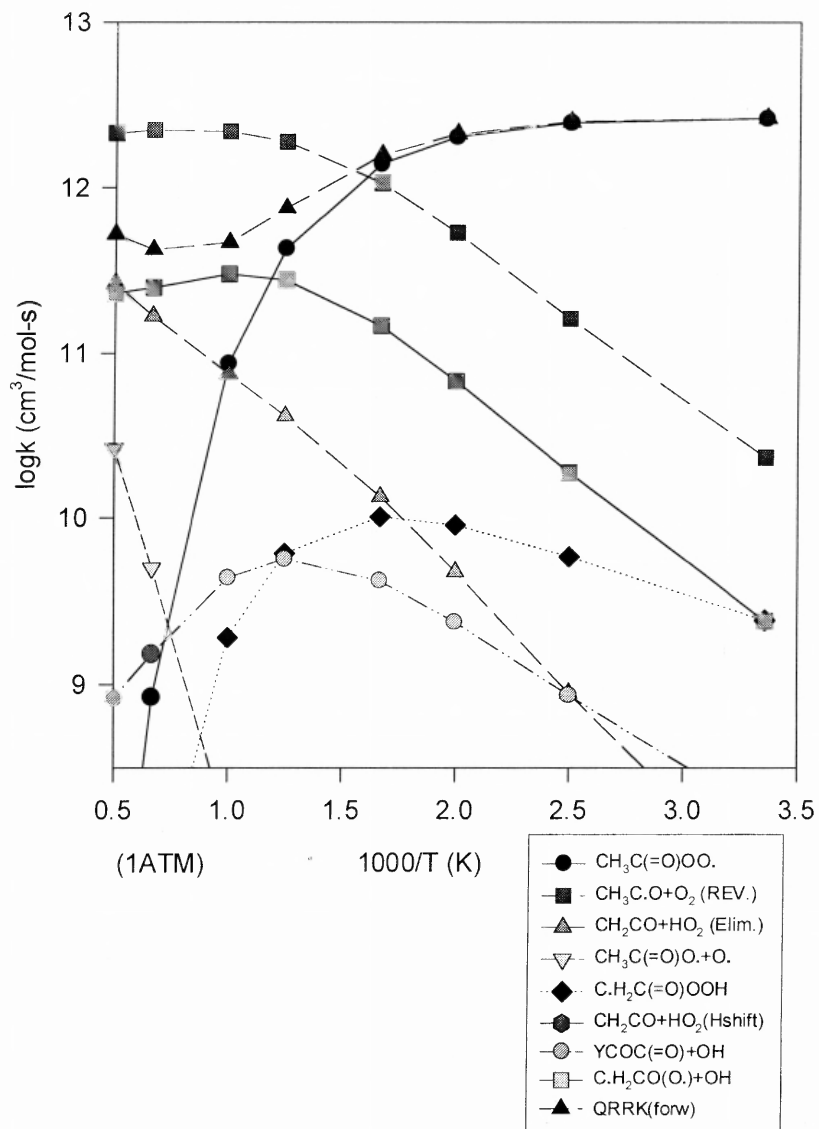


Figure 3.3 $\text{CH}_3\text{C}\cdot\text{O} + \text{O}_2 \rightarrow \text{products}$ k vs. $1000/T$ at 1 atm.

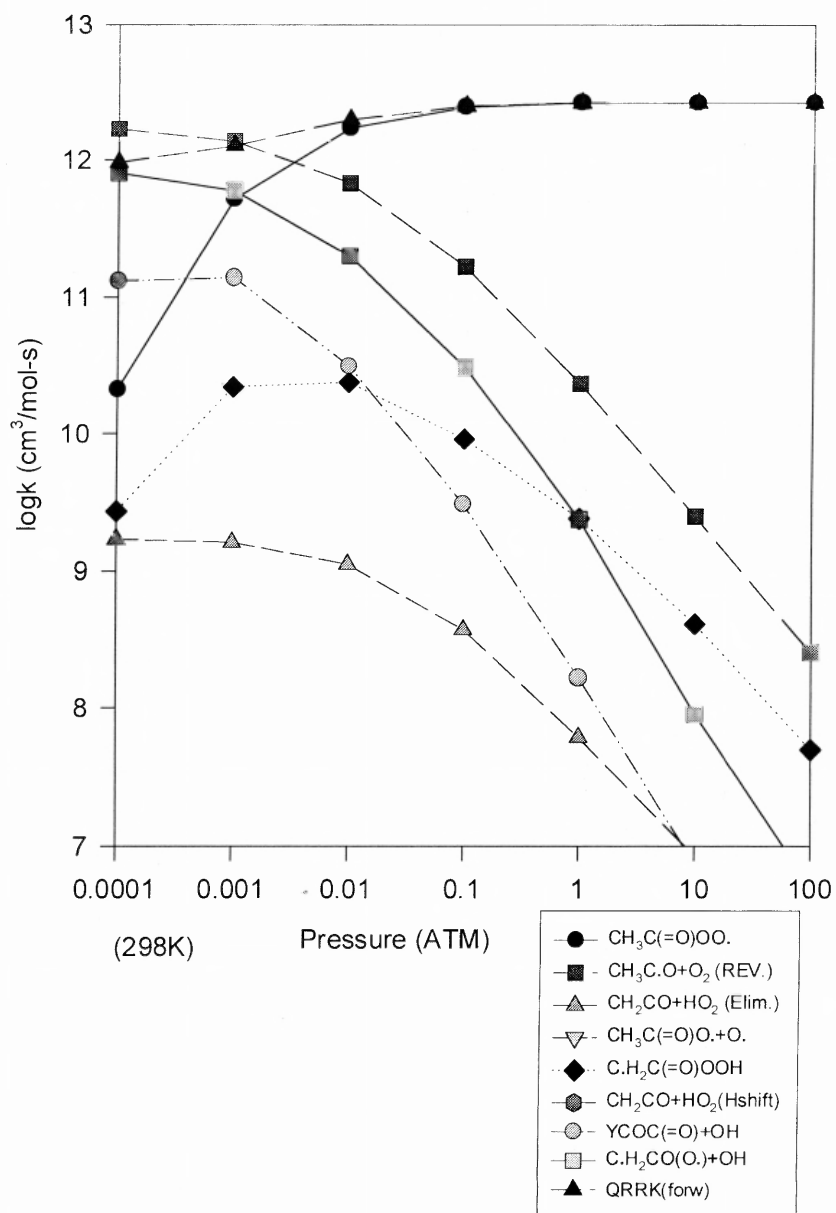


Figure 3.4 $\text{CH}_3\text{C}\cdot\text{O} + \text{O}_2 \rightarrow \text{products}$ k vs. pressure at 298K.

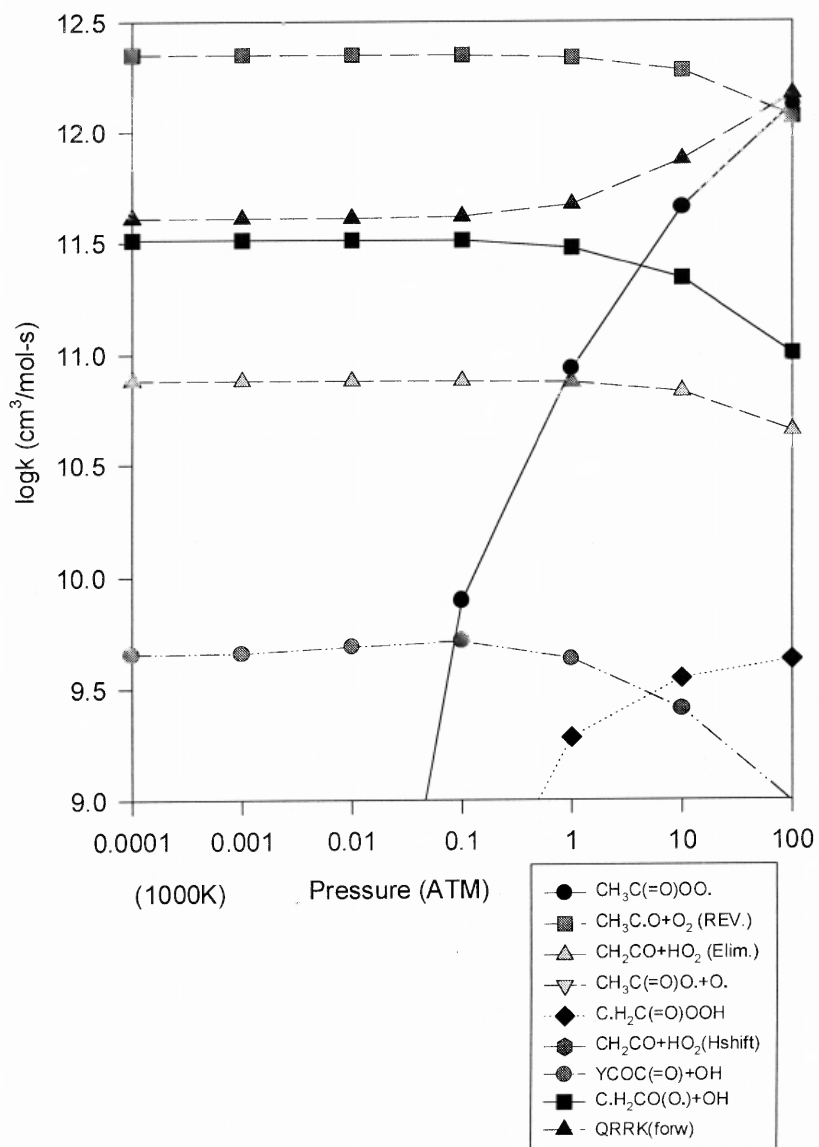


Figure 3.5 $\text{CH}_3\text{C}\cdot\text{O} + \text{O}_2 \rightarrow \text{products}$ k vs. pressure at 1000K.

3.3.8 Unimolecular Dissociation of Acetyl Peroxy and Formyl Methyl Hydroperoxide Radicals

Stabilization of the adducts is observed to be important at lower temperature and moderate pressure conditions. Dissociation rate constants of the stabilized adducts are, therefore, of value. These dissociation rate parameters are estimated using QRRK analysis for $k(E)$ with master equation for falloff with a 0.5 kcal energy grain.

(1) $\text{CH}_3\text{C(=O)OO}\bullet$ Dissociation. Plots of rate constants for $\text{CH}_3\text{C(=O)OO}\bullet$ dissociation at 1atm pressure versus $1000/T$ and rate constants at 298 and 1000 K versus pressure are illustrated in Figures A.1, A.2, and A.3, respectively (Appendix A). H shift isomerization to $\text{C}\bullet\text{H}_2\text{C(=O)OOH}$ is important below 500 K at 1atm pressure. Reverse dissociation and $\text{C}\bullet\text{H}_2\text{CO(O}\bullet) + \text{OH}$ are important above 1000 K.

Table 3.9 Products Ratios from $\text{C}\bullet\text{H}_2\text{C(=O)OOH}$ Dissociation at 1 atm and 1000 K

Reactant	Activated Intermediate	Product	Ratio(%)
$\text{C}\bullet\text{H}_2\text{C(=O)OOH}$	$\Rightarrow \text{C}\bullet\text{H}_2\text{C(=O)OOH}^*$	$\Rightarrow \text{YCOC(=O)} + \text{OH}$	11.3
$\text{C}\bullet\text{H}_2\text{C(=O)OOH}$	$\Rightarrow \text{C}\bullet\text{H}_2\text{C(=O)OOH}^*$	$\Rightarrow \text{C}\bullet\text{H}_2\text{CO(O}\bullet) + \text{OH}$	86.3
$\text{C}\bullet\text{H}_2\text{C(=O)OOH}$	$\Rightarrow \text{C}\bullet\text{H}_2\text{C(=O)OOH}^*$	$\Rightarrow \text{CH}_2\text{CO} + \text{HO}_2$	0.0
$\text{C}\bullet\text{H}_2\text{C(=O)OOH}$	$\Rightarrow \text{CH}_3\text{C(=O)OO}\bullet^*$	$\Rightarrow \text{CH}_3\text{C}\bullet\text{O} + \text{O}_2$	0.04
$\text{C}\bullet\text{H}_2\text{C(=O)OOH}$	$\Rightarrow \text{CH}_3\text{C(=O)OO}\bullet^*$	$\Rightarrow \text{CH}_2\text{CO} + \text{HO}_2$	0.0
$\text{C}\bullet\text{H}_2\text{C(=O)OOH}$	$\Rightarrow \text{CH}_3\text{C(=O)OO}\bullet^*$	$\Rightarrow \text{CH}_3\text{C(=O)OO}\bullet$	2.4

(2) $\text{C}\cdot\text{H}_2\text{C}(=\text{O})\text{OOH}$ Dissociation. Rate constants for $\text{C}\cdot\text{H}_2\text{C}(=\text{O})\text{OOH}$ dissociation at 1 atm pressure versus $1000/T$ and rate constants at 298 and 1000 K versus pressure are illustrated in Figures A.4, A.5, and A.6, respectively (Appendix A). At 1 atm, the diradical ($\text{C}\cdot\text{H}_2\text{CO}(\text{O}\cdot)$) + OH product set is the dominant path above 800 K; with the $\text{YCOC}(=\text{O}) + \text{OH}$ also important below 400 K.

Products from the low-temperature reaction at both high and low pressure are $\text{YCOC}(=\text{O}) + \text{OH}$ products via OH elimination and H shift to the peroxy radical. The diradical ($\text{C}\cdot\text{H}_2\text{CO}(\text{O}\cdot)$) + OH from $\text{RO}-\text{OH}$ cleavage is also important above 1 atm at low temperature. At higher temperatures, the diradical ($\text{C}\cdot\text{H}_2\text{CO}(\text{O}\cdot)$) + OH is the dominant path, as a result of the loose transition state structure. Products ratios from $\text{C}\cdot\text{H}_2\text{C}(=\text{O})\text{OOH}$ dissociation at 1 atm and 1000 K are listed in Table 3.9.

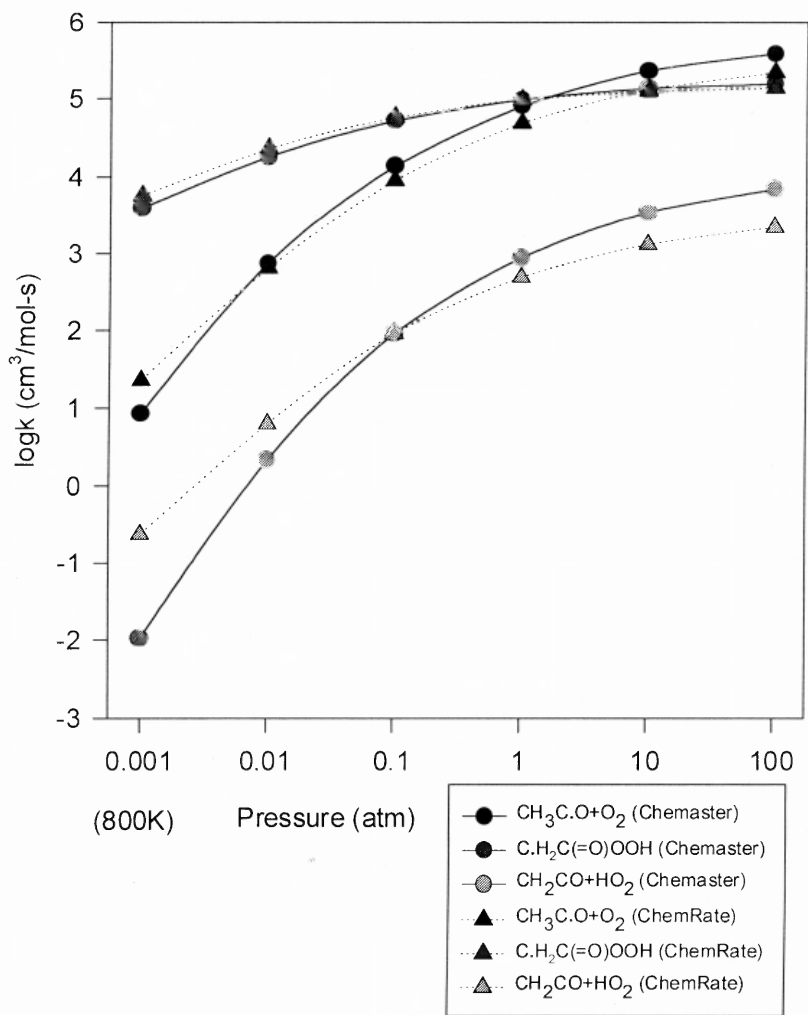


Figure 3.6 Comparison of rate constants between Chemaster and ChemRate with pressure in 800K with $\text{CH}_3\text{C}(\text{O})\text{OO}\cdot$ dissociation.

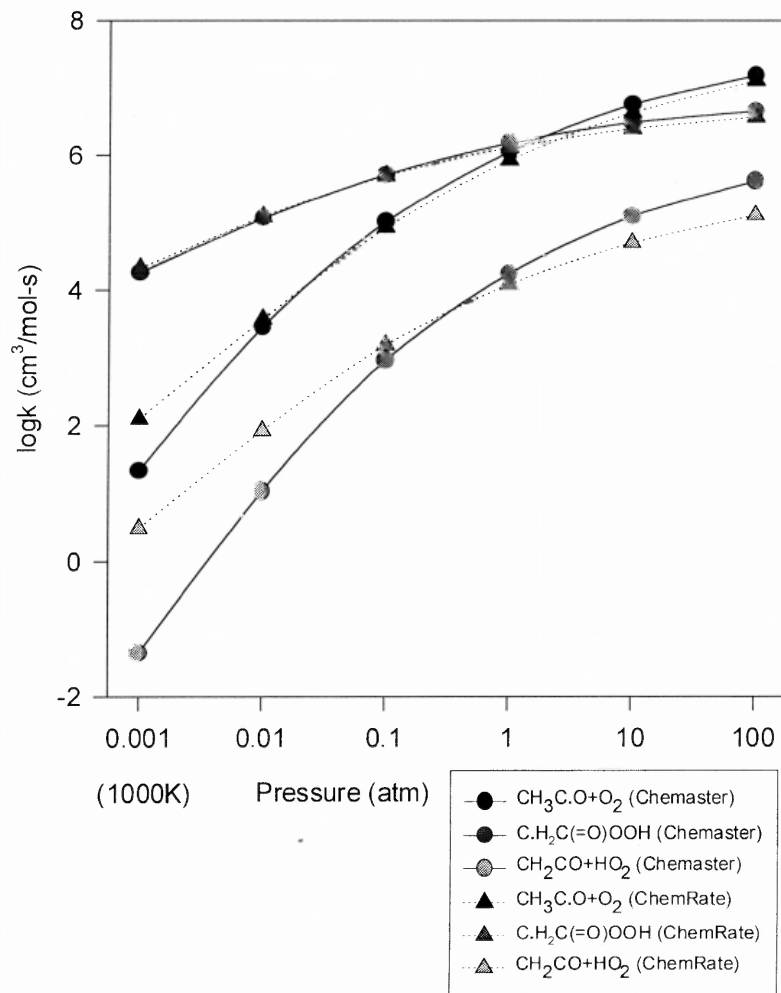


Figure 3.7 Comparison of rate constants between Chemaster and ChemRate with pressure in 1000K with $\text{CH}_3\text{C}(\text{=O})\text{OO}\bullet$ dissociation.

(3) Comparison of Dissociation Rate Constants between QRRK with Master Equation and ChemRate (RRKM with Master Equation).

Dissociation rate constants at 800 and 1000 K versus pressure are compared between QRRK with the master equation and ChemRate⁴⁶ (Rice-Ramsperger-Kassel-Marcus (RRKM) with master equation) on $\text{CH}_3\text{C}(=\text{O})\text{OO}\bullet$ dissociations in Figures 3.6 and 3.7, and for $\text{C}\bullet\text{H}_2\text{C}(=\text{O})\text{OOH}$ in Figures 3.8 and 3.9, respectively.

Calculated rate constants from the two methods versus pressure for $\text{CH}_3\text{C}(=\text{O})\text{OO}\bullet$ dissociation are compared in Figure 3.6 (800 K) and Figure 3.7 (1000 K). The rate constants to $\text{C}\bullet\text{H}_2\text{C}(=\text{O})\text{OOH}$ (H shift isomerization) show very good agreement, with reasonable agreement also observed for predictions on dissociation to $\text{CH}_3\text{C}\bullet\text{O} + \text{O}_2$. Chemrate predicts a slightly broader falloff for all the three reaction paths, with the largest variation for the lowest rate channel of HO_2 elimination. This is amplified a bit in the 1000 K data of Figure 3.7.

The $\text{C}\bullet\text{H}_2\text{C}(=\text{O})\text{OOH}$ dissociation rate constants versus pressure are compared in Figures 3.8 and 3.9 for 800 K and 1000 K, respectively. The $\text{YCOC}(=\text{O}) + \text{OH}$ products via OH elimination and H shift isomerization ($\text{CH}_3\text{C}(=\text{O})\text{OO}\bullet$) show agreement above 1 atm. The rate constants of ChemRate are 1.5 – 2 times higher than those calculated by use of QRRK with master equation below 0.1 atm in both figures.

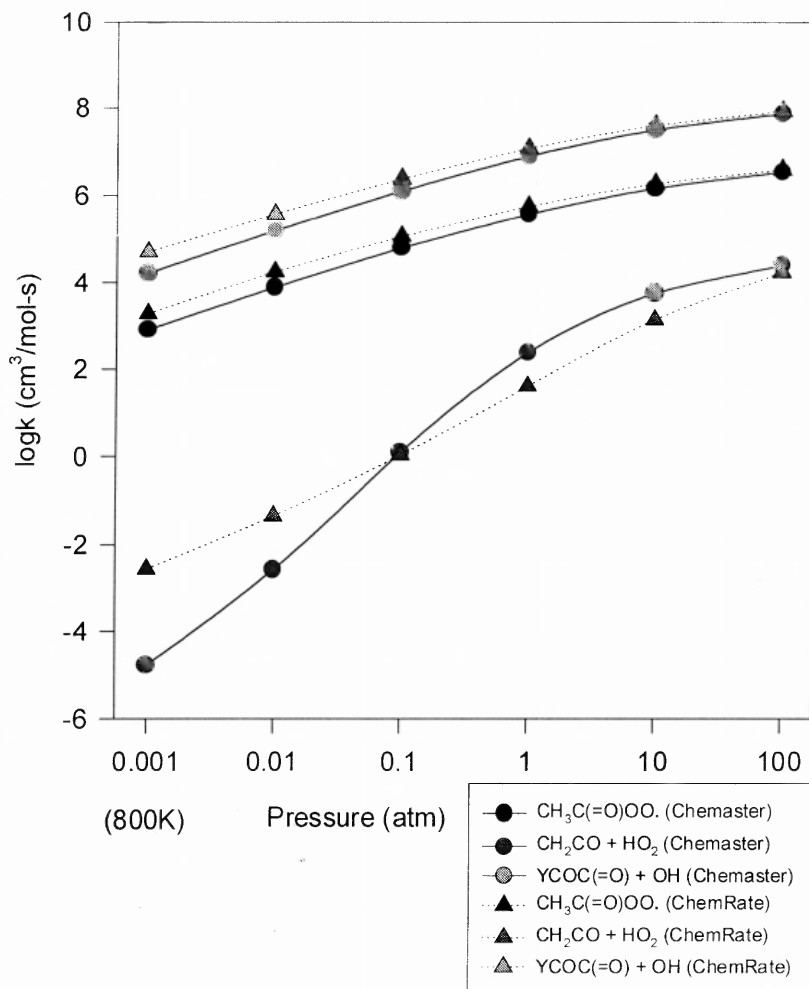


Figure 3.8 Comparison of rate constants between Chemaster and ChemRate with pressure in 800K with $\text{C}\cdot\text{H}_2\text{C}(=\text{O})\text{OOH}$ dissociation.

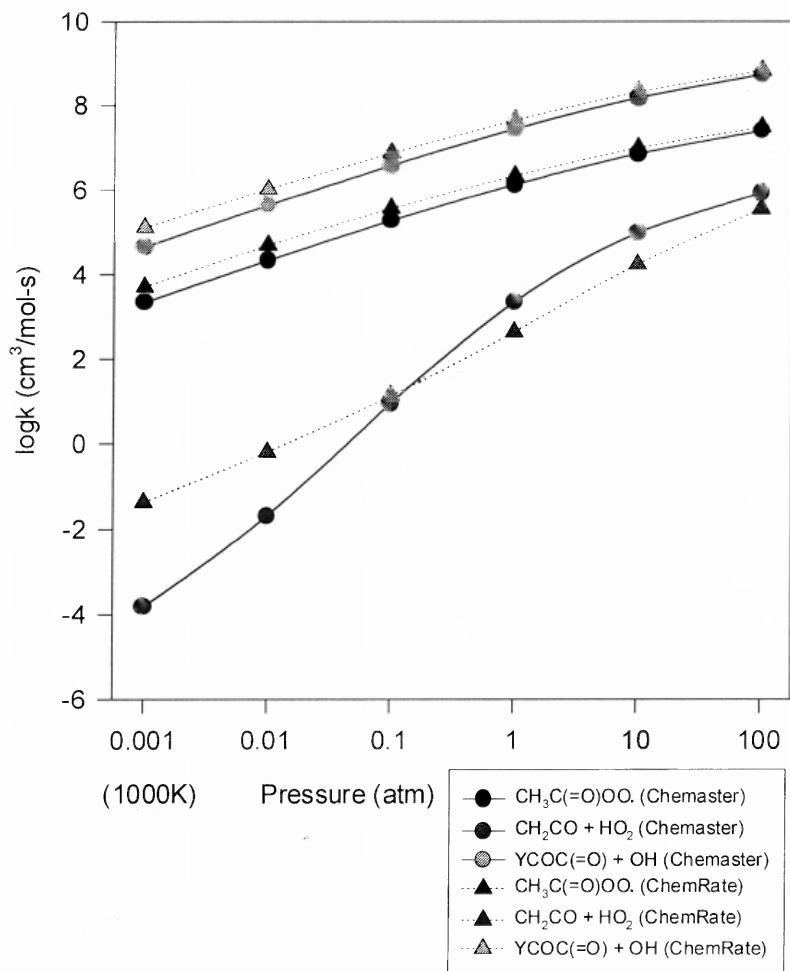


Figure 3.9 Comparison of rate constants between Chemaster and ChemRate with pressure in 1000K with $\text{C}\cdot\text{H}_2\text{C}(=\text{O})\text{OOH}$ dissociation.

3.3.9 Acetyl Radical Unimolecular Dissociation

The energy diagram for acetyl radical unimolecular dissociation is illustrated in Figure 3.10. The acetyl radical $\text{CH}_3\text{C}\cdot\text{O}$ ($\Delta H_f^\circ_{298} = -3.08$ kcal/mol in CBSQ) can decompose to $\text{CH}_3 + \text{CO}$ ($E_a = 16.64$), undergo β scission to products, $\text{CH}_2\text{CO} + \text{H}$ ($E_a = 43.17$) or isomerize via hydrogen shift ($E_a = 46.11$) to form the slightly higher energy $\text{C}\cdot\text{H}_2\text{CHO}$ isomer ($\Delta H_f^\circ_{298} = 3.52$).

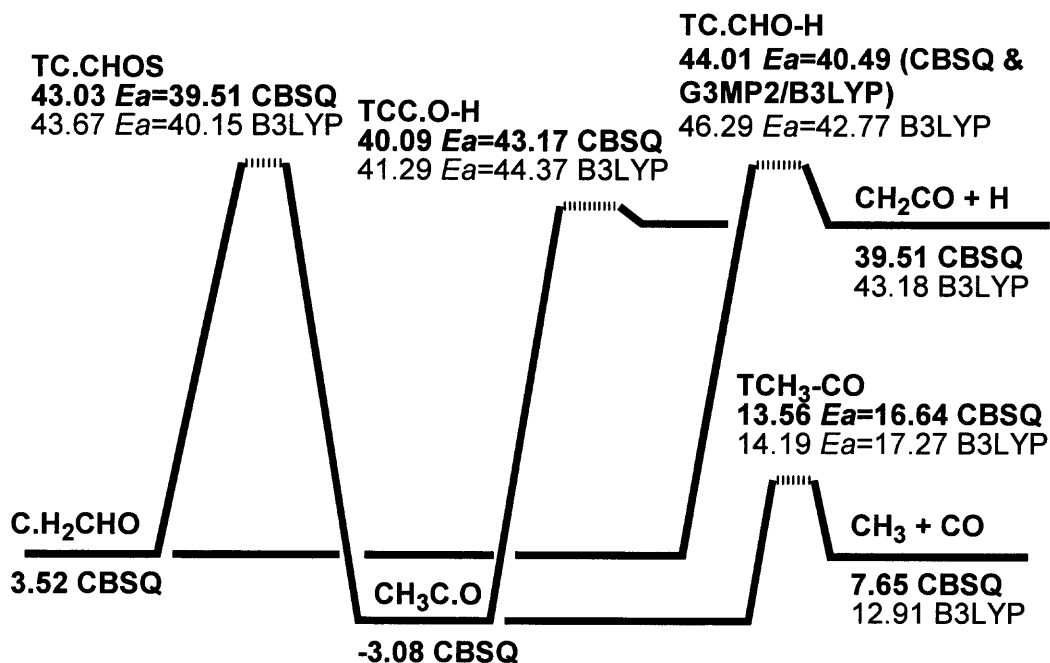


Figure 3.10 Potential energy diagram of acetyl and formyl methyl radical unimolecular isomerization/ dissociations (Units : kcal/mol).

Table 3.10 Detailed Mechanism

Reactions	A	n	<i>E_a</i>	References
CH ₃ CHO = CH ₃ +HCO	6.99E+44	-9.82	88320	a
CH ₃ CHO = CH ₃ C•O+H	7.50E+44	-11.49	92652	a
CH ₃ CHO+O ₂ = CH ₃ C•O+HO ₂	3.01E+13	0.0	39143	b
HCO = H+CO	7.94E+17	-3.51	16326	a
CH ₃ CHO+OH = CH ₃ C•O+H ₂ O	3.37E+12	0.0	-536	c
CH ₃ CHO+O = CH ₃ C•O+OH	1.08E+13	0.0	2186	c
CH ₃ CHO+H = CH ₃ C•O+H ₂	4.00E+13	0.0	4206	d
CH ₃ CHO+HO ₂ = CH ₃ C•O+H ₂ O ₂	3.01E+12	0.0	8000	b
CH ₃ CHO+CH ₃ = CH ₃ C•O+CH ₄	1.86E+8	0.0	2464	b
CH ₃ CHO+OH = C•H ₂ CHO+H ₂ O	4.31E+11	0.0	1000	e
CH ₃ CHO+H = C•H ₂ CHO+H ₂	2.4E+8	1.5	2103	f
CH ₃ CHO+O = C•H ₂ CHO+OH	5.85E+12	0.0	1808	b
CH ₃ CHO+HO ₂ = C•H ₂ CHO+H ₂ O ₂	1.4E+4	2.69	14068	f
CH ₃ CHO+CH ₃ = C•H ₂ CHO+CH ₄	8.1E+5	1.87	5251	f
CH ₃ C•O+O ₂ = CH ₃ C(=O)OO•	1.90E+76	-22.20	12775	a
CH ₃ C•O+O ₂ = CH ₂ CO+HO ₂	3.29E+08	0.96	2341	a
CH ₃ C•O+O ₂ = CH ₃ C(=O)O•+O•	8.17E+13	-0.33	21744	a
CH ₃ C•O+O ₂ = C•H ₂ C(=O)OOH	3.91E+72	-20.99	13932	a
CH ₃ C•O+O ₂ = CH ₂ CO+HO ₂	1.23E+06	0.88	6367	a
CH ₃ C•O+O ₂ = YCOC(=O)+OH	4.27E+21	-3.84	1444	a
CH ₃ C•O+O ₂ = C•H ₂ CO(O•)+OH	1.11E+16	-1.40	1250	a
CH ₃ C(=O)OO• = CH ₃ C•O+O ₂	1.65E+25	-5.53	28017	a
CH ₃ C(=O)OO• = CH ₂ CO+HO ₂	8.37E+23	-5.98	29810	a
CH ₃ C(=O)OO• = CH ₃ C(=O)O•+O•	9.18E+07	-6.66	46289	a
CH ₃ C(=O)OO• = C•H ₂ C(=O)OOH	2.05E+17	-2.30	24938	a
C•H ₂ C(=O)OOH = CH ₂ CO+HO ₂	4.06E+07	-3.17	27150	a
C•H ₂ C(=O)OOH = YCOC(=O)+OH	4.78E+20	-3.73	19179	a
C•H ₂ C(=O)OOH = C•H ₂ CO(O•)+OH	1.18E+20	-3.77	20459	a
C•H ₂ C(=O)OOH = CH ₃ C(=O)OO•	8.33E+14	-1.99	19173	a
CH ₃ C(=O)O• = CH ₃ +CO ₂	3.41E+15	-0.48	17466	a
C•H ₂ CO(O•) = CH ₂ +CO ₂	1.24E+11	-0.85	16563	a
C•H ₂ CHO+O ₂ = CH ₂ (OO•)CHO	4.15E+64	-18.13	15908	a
C•H ₂ CHO+O ₂ = CH ₂ CO+HO ₂	2.56E+05	2.57	23785	a
C•H ₂ CHO+O ₂ = CH ₂ (OOH)C•(=O)	2.67E+50	-18.89	15625	a
C•H ₂ CHO+O ₂ = CH ₂ CO+HO ₂	2.88E-03	2.06	4400	a
C•H ₂ CHO+O ₂ = CO+CH ₂ O+OH	5.77E+14	-0.96	5752	a
CH ₂ (OO•)CHO = C•H ₂ CHO +O ₂	2.75E+51	-13.62	33711	a
CH ₂ (OO•)CHO = CH ₂ CO+HO ₂	1.81E+29	-12.65	46998	a
CH ₂ (OO•)CHO = CH ₂ (OOH)C•(=O)	5.31E+34	-8.00	26153	a
CH ₂ (OOH)C•(=O) = CH ₂ CO+HO ₂	3.02E+03	-4.73	21783	a
CH ₂ (OOH)C•(=O) = CO+CH ₂ O+OH	3.93E+18	-3.43	8668	a
CH ₂ (OOH)C•(=O) = CH ₂ (OO•)CHO	2.14E+06	-4.59	16759	a
CH ₃ C•O = CH ₂ CO+H	2.33E-23	1.64	38980	a
CH ₃ C•O = CH ₃ +CO	4.87E+06	0.33	12525	a
CH ₃ C•O = C•H ₂ CHO	7.10E-25	1.48	39974	a
C•H ₂ CHO = CH ₂ CO+H	1.43E+38	-8.75	46719	a

Table 10 Detailed Mechanism (Continued)

Reactions	A	n	<i>E_a</i>	References
$C\bullet H_2CHO = CH_3C\bullet O$	5.84E+38	-9.08	46719	a
$2CH_3C(=O)OO\bullet = 2CH_3C(=O)O\bullet + O_2$	8.51E+10	0.0	248	g
$CH_3CHO + CH_3C(=O)OO\bullet = CH_3C(=O)OOH + CH_3C\bullet O$	2.4E+8	1.5	3643	f
$CH_3CHO + CH_3C(=O)OO\bullet = CH_3C(=O)OOH + C\bullet H_2CHO$	2.4E+8	1.5	7933	f
$CH_2(OO\bullet)CHO + NO = CH_2(O\bullet)CHO + NO_2$	1.26E+12	0.0	1133	h
$CH_2(O\bullet)CHO = CH_2O + HCO$	8.72E+22	-4.9	12378	a
$CH_2(O\bullet)CHO = CHOCHO + H$	2.94E+13	-2.2	28503	a
$CH_3C(=O)OO\bullet + NO = CH_3C(=O)O\bullet + NO_2$	1.26E+12	0.0	1133	h
$C\bullet H_2C(=O)OOH + O_2 = (\bullet OO)H_2CC(=O)OOH$	1.10E+11	0.0	0	i
$(\bullet OO)H_2CC(=O)OOH + NO = (\bullet O)H_2CC(=O)OOH + NO_2$	1.26E+12	0.0	1133	h
$(\bullet O)H_2CC(=O)OOH = C\bullet H(=O)OOH + CH_2O$	1.35E+12	0.0	20800	a
$C\bullet H(=O)OOH = CO + HO_2$	1.73E+10	0.0	16550	a
$C\bullet H(=O)OOH = CO_2 + OH$	3.34E+12	0.0	24290	a
$CH_3 + O_2 = CH_2O + OH$	2.61E+08	1.01	12487	j
$CH_3 + O_2 = CH_3OO$	1.99E+31	-6.72	4212	j
$CH_3OO = CH_2O + OH$	1.99E+20	-7.76	47315	a
$CH_3 + CH_2O = HCO + CH_4$	5.54E+03	2.81	5862	k
$CH_3 + HO_2 = CH_3O + OH$	1.81E+13	0.0	0	b
$CH_3O = CH_2O + H$	6.13E+28	-5.65	31351	j
$CH_3O + HO_2 = CH_2O + H_2O_2$	3.01E+11	0.0	0	k
$CH_2O + O = OH + HCO$	1.81E+13	0.0	3080	k
$CH_2O + H = H_2 + HCO$	2.29E+10	1.05	3279	b
$CH_2O + OH = H_2O + HCO$	3.44E+09	1.18	-447	b
$HCO + O_2 = CO + HO_2$	6.25E+15	-1.15	2018	j
$HCO + O_2 = CO_2 + OH$	5.45E+14	-1.15	2018	j
$CO + O = CO_2$	6.17E+14	0.0	3001	k
$CO + OH = CO_2 + H$	6.32E+06	1.5	-497	k
$CO + HO_2 = CO_2 + OH$	1.51E+14	0.0	23650	k
$CO + O_2 = CO_2 + O$	2.53E+12	0.0	47693	k
$H + O_2 + M = HO_2 + M$	1.41E+18	-0.8	0	b
$H + O_2 = OH + O$	1.99E+14	0.0	16802	b
$OH + OH = O + H_2O$	1.51E+09	1.14	99	b
$H_2 + OH = H_2O + H$	1.02E+08	1.6	3300	b
$H + OH + M = H_2O + M$	2.21E+22	-2.0	0	b
$O + HO_2 = OH + O_2$	1.75E+13	0.0	-397	l
$OH + HO_2 = H_2O + O_2$	1.45E+16	-1.0	0	k
$H + HO_2 = OH + OH$	1.69E+14	0.0	874	k
$H + HO_2 = H_2 + O_2$	6.62E+13	0.0	2126	k
$H + HO_2 = H_2O + O$	3.01E+13	0.0	1721	b
$H + O + M = OH + M$	4.71E+18	-1.0	0	k
$H_2O_2 + M = OH + OH + M$	1.21E+17	0.0	45507	b
$H_2O_2 + OH = H_2O + HO_2$	1.75E+12	0.0	318	l
$H_2O_2 + O = OH + HO_2$	9.63E+06	2.0	3974	k
$H_2O_2 + H = OH + H_2O$	2.41E+13	0.0	3974	k
$H_2O_2 + H = HO_2 + H_2$	4.82E+13	0.0	7949	k
$CH_4 + HO_2 = H_2O_2 + CH_3$	9.04E+12	0.0	24641	b
$2HO_2 = 2OH + O_2$	1.00E+12	0.0	11500	j
$HO_2 + HO_2 = H_2O_2 + O_2$	1.87E+12	0.0	1540	b
$H + H + M = H_2 + M$	5.44E+18	-1.3	0	k
$O + H_2 = OH + H$	5.12E+04	2.67	6285	b

^a From QRRK calculations (1 torr, 298-2000K). ^b Reference 93. ^c Reference 94. ^d Reference 95. ^e Reference 96. ^f Estimate in this study. ^g $2C_2H_5OO\bullet = 2C_2H_5O\bullet + O_2$ (ref 41). ^h Reference 97. ⁱ $0.7 \times 1.57E+11(C\bullet H_2CHO + O_2)$. ^j Reference 90. ^k Reference 98. ^l Reference 99.

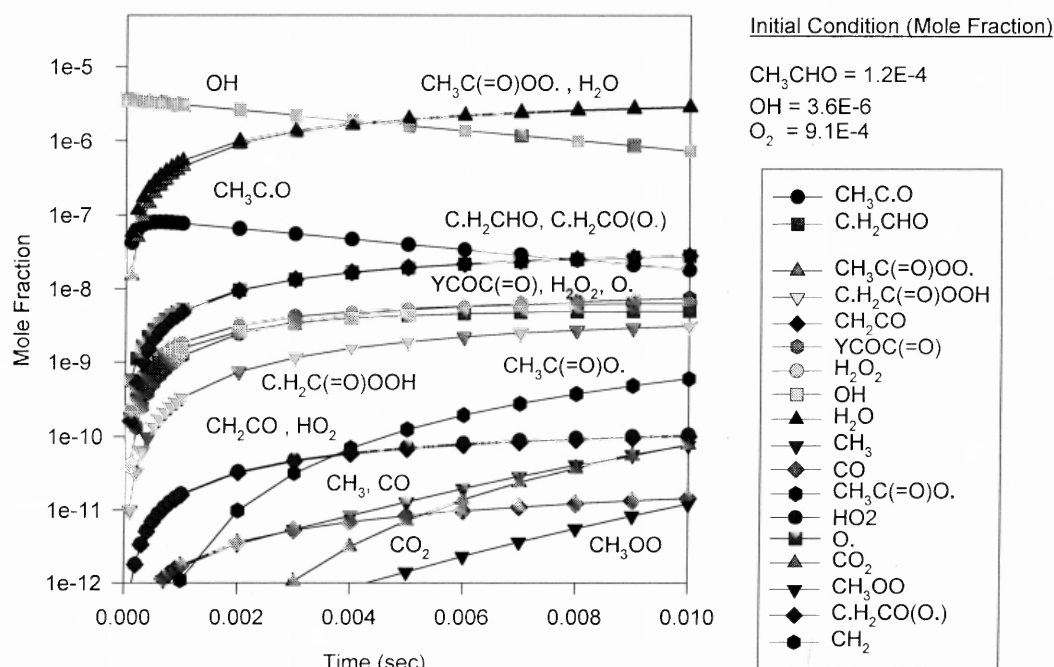


Figure 3.11 Chemkin kinetic calculations: concentration vs. time.

3.3.10 Detailed Mechanism of Acetyl Radical Reactions

A small detailed mechanism including the reactions evaluated in this study is assembled and listed in Table 3.10. The mechanism consists of 98 reactions and 37 species with each elementary reaction evaluated and referenced. The CHEMKIN II integrator computer code⁹¹ is used to model the reaction conditions of Tyndall et al.⁹ Abstraction reactions by O, H, OH, HO₂, O₂ and CH₃ radicals are taken from evaluated literature wherever possible. A procedure from Dean and Bozzelli⁹² is used to estimate abstraction rate constants by H, HO₂, CH₃, and CH₃C(=O)OO• radicals when no literature data are available. Abstraction reactions are not considered pressure dependent and therefore do not require falloff analysis.

The reactions of CH₃CHO + OH → CH₃C•O and → C•H₂CHO + H₂O are analyzed to model conditions of Tyndall et al., 0 – 0.01 s, 300 K, and 3 Torr, both with and without added O₂. The reaction with no O₂ added (mole fraction: CH₃CHO = 1.2E-4, OH = 3.6E-6) shows 99% CH₃C•O, acetyl radical, and 1% C•H₂CHO, formyl methyl radical, at 0.01 s via OH abstraction paths.

Data on concentration versus time for reaction conditions identical to those above, plus 3 Torr of O₂ (mole fraction= 9.1E-4) are illustrated in Figure 3.11. CH₃C(=O)OO•, C•H₂CO(O•), and YCOC(=O), which result from the acetyl radical reaction with O₂, are the major products. In the mechanism, the diradical, C•H₂CO(O•), dissociates to ³CH₂ + CO₂ which is 13 kcal/mol endothermic. Under these O₂ conditions, it is observed that only 20 % of the OH radical is regenerated through the acetyl radical with O₂ reaction. Tyndall et al.⁹ and Michael et al.¹³ both report almost complete regeneration of OH in their experiments.

Chemkin calculation of complete OH regeneration requires adjustment of the computed barrier from 26.42 down to 11.42 kcal/mol for reaction ($\text{CH}_3\text{C}(=\text{O})\text{OO}\bullet \rightarrow \text{TCC}(=\text{O})\text{OO}\bullet$) that forms OH. This adjustment of the barrier is unreasonable.

3.3.11 Importance of $\text{CH}_3\text{C}\bullet\text{O} + \text{O}_2$ Relative to Unimolecular Dissociation of $\text{CH}_3\text{C}\bullet\text{O}$

The competition between unimolecular dissociation of $\text{CH}_3\text{C}\bullet\text{O} \rightarrow \text{CH}_3 + \text{CO}$ versus association of $\text{CH}_3\text{C}\bullet\text{O}$ with O_2 as a function of reactor temperature is considered. The mechanism is used for this evaluation because the reaction system is complex; it involves reactions of chemical activated and stabilized $\text{CH}_3\text{C}(=\text{O})\text{OO}\bullet$. The $\text{C}\bullet\text{H}_2\text{C}(=\text{O})\text{OOH}$ isomer has low barriers for both forward and reverse reactions resulting in a quasiequilibrium system. In addition, $\text{CH}_3\text{C}\bullet\text{O}$ has a low energy dissociation path ($E_a = 16.64$ kcal/mol).

Several reaction condition sets are evaluated, one similar to those of Tyndall et al.⁹ is 0.01 s with mole fraction of $\text{CH}_3\text{CHO} = 1.2\text{E-}4$, $\text{OH} = 3.6\text{E-}6$, and $\text{O}_2 = 9.1\text{E-}4$. The reactions are evaluated at two pressures 1 Torr and 1 atm. The fraction of acetyl radical that reacts with O_2 versus unimolecular dissociation is summarized in Scheme 3.3. It shows that the two reaction channels, oxidation and dissociation, are competitive around 500 K. The unimolecular dissociation channel accounts for more than 80% of the reaction at 600 K.

The second condition set considers the competition between oxidation and dissociation at concentrations more relative to combustion. Mole fractions: ($\text{CH}_3\text{C}\bullet\text{O} = 1.0\text{E-}5$, $\text{O}_2 = 0.15$, $\text{N}_2 = 0.80$, and $\text{CH}_4(\text{fuel}) = 0.05$). Plots of concentration versus time for 10 ns, at 300 K, and 1 atm are illustrated in Figure 3.12. The $\text{CH}_3\text{C}\bullet\text{O}$

radicals decrease slowly with time, from the oxidation with effectively no unimolecular dissociation. At 0.1 s time, the ratio of oxidation to unimolecular dissociation products, $\text{CH}_3\text{C}(=\text{O})\text{OO}\bullet$: CO is $2.0\text{E}+7$: 1. The $\text{CH}_3\text{C}\bullet\text{O}$ radicals decrease by 3 orders magnitudes at 40 ns. The major product is stabilized $\text{CH}_3\text{C}(=\text{O})\text{OO}\bullet$ which results from acetyl radical reaction with O_2 .

Scheme 3.3 The Fraction of Oxidation and Dissociation of Acetyl Radical ($t = 0.01$ s, mole fraction : $\text{CH}_3\text{CHO} = 1.2\text{E}-4$, $\text{OH} = 3.6\text{E}-6$, and $\text{O}_2 = 9.1\text{E}-4$)

T / %	Oxidation		Dissociation	
	1 Torr	1 atm	1 Torr	1 atm
400K	93.3	99.8	6.7	0.2
450K	66.5	98.7	33.5	1.3
475K	46.3	96.6	53.7	3.4
500K	28.8	91.2	71.2	8.8
550K	9.7	43.1	90.3	56.9
600K	3.4	17.1	96.6	82.9

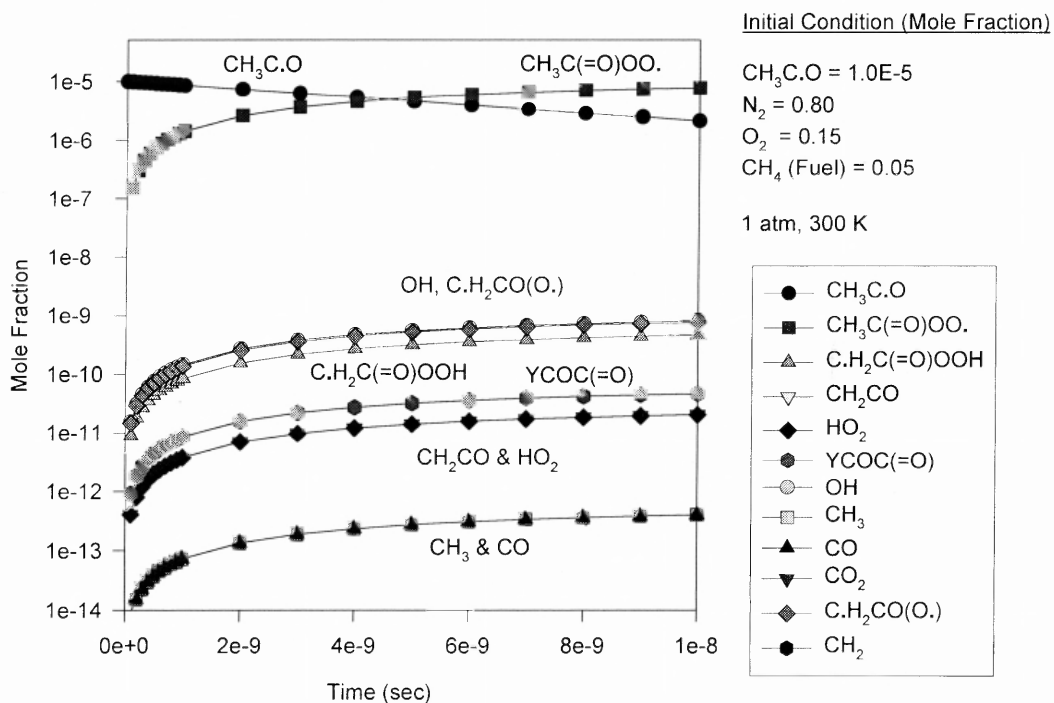


Figure 3.12 Chemkin kinetic calculations: concentration vs. time.

Products are illustrated in Figure 3.13 for reaction at higher temperature, 750K, and 1 atm. The major products are $\text{CH}_3\text{C(=O)OO.}$, CH_3 , and CO ; these result from both acetyl radical reaction with O_2 and from $\text{CH}_3\text{C.O}$ unimolecular dissociation to $\text{CH}_3 + \text{CO}$. Above 800K, the major products are CH_3 and CO from the unimolecular dissociation. The oxidation and dissociation channels are competitive around 750 K under these conditions. Ratios of the product sets are summarized in Scheme 3.4 at varied temperature. These data are in reasonable agreement with the relative rate constant at these conditions.

Scheme 3.4 The Fraction of Oxidation and Dissociation of Acetyl Radical ($t = 10$ ns, mole fraction : $\text{CH}_3\text{C}\cdot\text{O} = 1.0\text{E-}5$, $\text{O}_2 = 0.15$, $\text{N}_2 = 0.80$, and $\text{CH}_4(\text{fuel}) = 0.05$)

T / %	Oxidation	Dissociation	Disso./ Oxi.
300K	100.0	0.0	0.00
500K	99.9	0.1	0.00
600K	97.8	2.2	0.02
700K	73.0	27.0	0.37
750K	43.6	56.4	1.29
800K	19.4	80.6	4.16
900K	2.8	97.2	34.93
1000K	0.4	99.6	232.51

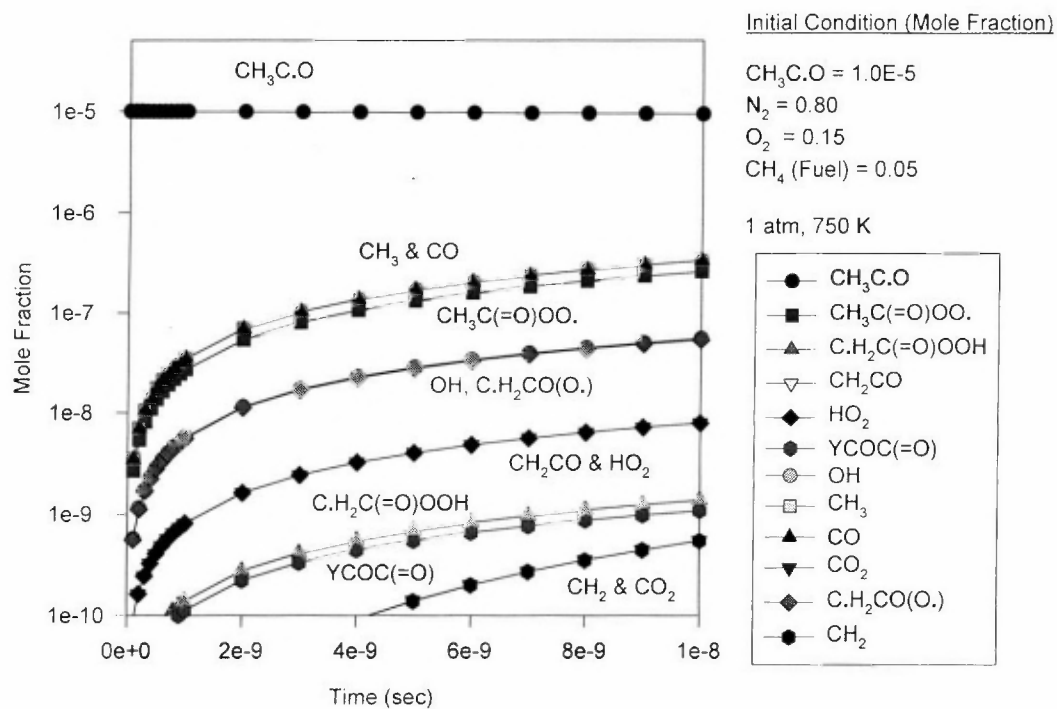


Figure 3.13 Chemkin kinetic calculations: concentration vs. time.

Scheme 3.4 The Fraction of Oxidation and Dissociation of Acetyl Radical ($t = 10$ ns, mole fraction : $\text{CH}_3\text{C}\cdot\text{O} = 1.0\text{E-}5$, $\text{O}_2 = 0.15$, $\text{N}_2 = 0.80$, and $\text{CH}_4(\text{fuel}) = 0.05$)

T / %	Oxidation	Dissociation	Disso./ Oxi.
300K	100.0	0.0	0.00
500K	99.9	0.1	0.00
600K	97.8	2.2	0.02
700K	73.0	27.0	0.37
750K	43.6	56.4	1.29
800K	19.4	80.6	4.16
900K	2.8	97.2	34.93
1000K	0.4	99.6	232.51

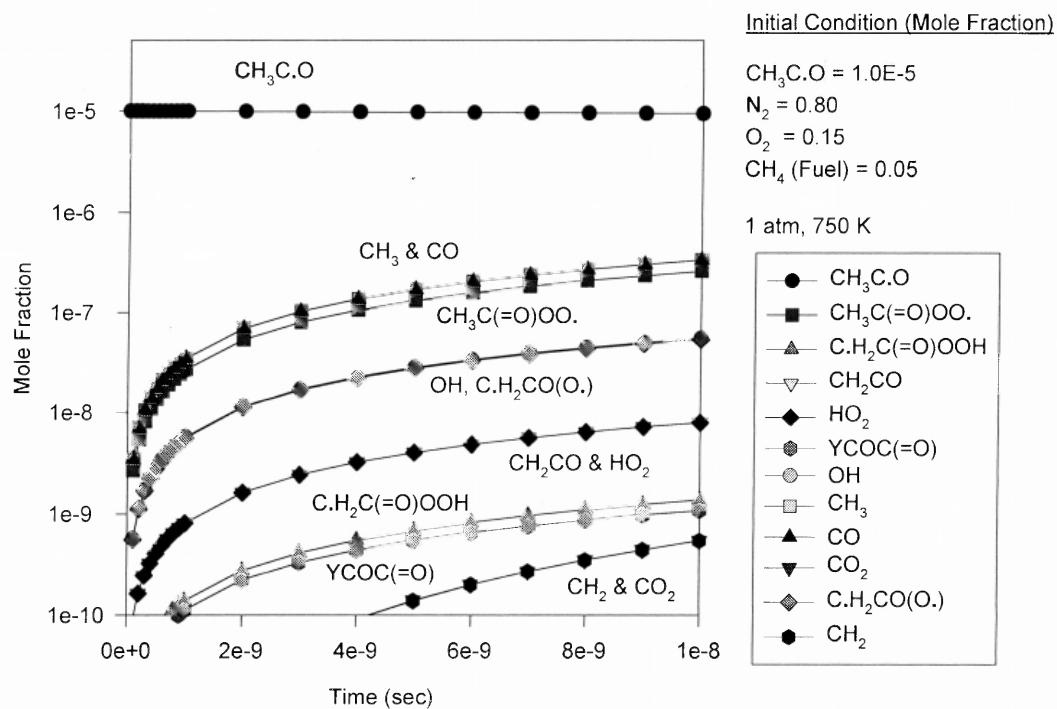


Figure 3.13 Chemkin kinetic calculations: concentration vs. time.

Scheme 3.4 The Fraction of Oxidation and Dissociation of Acetyl Radical ($t = 10$ ns, mole fraction : $\text{CH}_3\text{C}\cdot\text{O} = 1.0\text{E-}5$, $\text{O}_2 = 0.15$, $\text{N}_2 = 0.80$, and $\text{CH}_4(\text{fuel}) = 0.05$)

T / %	Oxidation	Dissociation	Disso./ Oxi.
300K	100.0	0.0	0.00
500K	99.9	0.1	0.00
600K	97.8	2.2	0.02
700K	73.0	27.0	0.37
750K	43.6	56.4	1.29
800K	19.4	80.6	4.16
900K	2.8	97.2	34.93
1000K	0.4	99.6	232.51

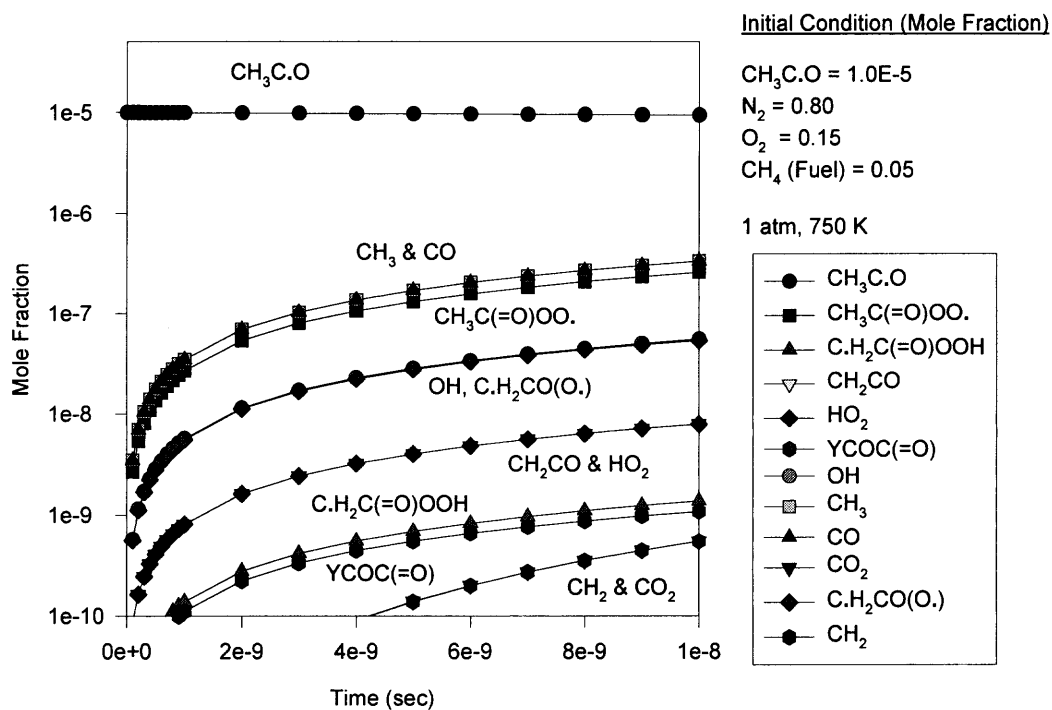


Figure 3.13 Chemkin kinetic calculations: concentration vs. time.

3.4 Summary

Thermochemical properties of stable radicals and transition states on the $\text{CH}_3\text{C}\bullet\text{O} + \text{O}_2$ reaction system are calculated using density functional and ab initio methods with enthalpies of formation ($\Delta H_f^\circ_{298}$) at the CBSQ level. Entropies (S°_{298}) and heat capacities ($C_p^\circ(T)$) are also determined, with inclusion of internal rotor contributions. The acetyl + O_2 system has a similar well depth to that of the more studied ethyl + O_2 system, but subsequent reaction barriers are significantly different. Reaction paths and kinetics are analyzed on $\text{CH}_3\text{C}\bullet\text{O} + \text{O}_2$ reaction system using QRRK for $k(E)$ and the master equation for fall-off. Reaction to products is evaluated versus both pressure and temperature.

The major reaction path at 1 atm pressure is the stabilization of peroxy adduct ($\text{CH}_3\text{C}(=\text{O})\text{OO}\bullet$) below 600 K. Reverse dissociation exhibits the highest rate constant for both the energized and stabilized adduct above 800 K. The major product channels are the diradical, ($\text{C}\bullet\text{H}_2\text{C}(=\text{O})\text{O}\bullet$), + OH and ketene + HO_2 paths above 1000 K at 1 atm. It is important to further analyze the reaction products that result from this diradical.

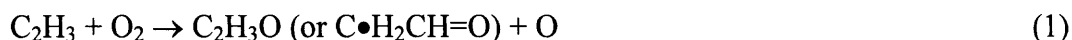
A detailed reaction mechanism is constructed with pressure dependence for the acetyl radical reaction with O_2 . Several paths lead to formation (regeneration) of the OH radical as reported in experimental studies, but use of the mechanism for evaluation of the OH regeneration shows results that are low compared to experiment. The mechanism is also used to compare the competition between acetyl radical decomposition and acetyl radical reaction with O_2 with temperature.

CHAPTER 4

THERMOCHEMICAL AND KINETIC ANALYSIS OF THE FORMYL METHYL RADICAL + O₂ REACTION SYSTEM

4.1 Background

Bozzelli et al.^{18,31} and Mebel et al.¹⁰⁰ have separately reported that the formyl methyl radical is an important intermediate from reaction of vinyl radicals, e.g. C₂H₃ + O₂ reaction system. The C₂H₃O + O product set is important at low pressures and it is important above 900 K at atmospheric pressure.



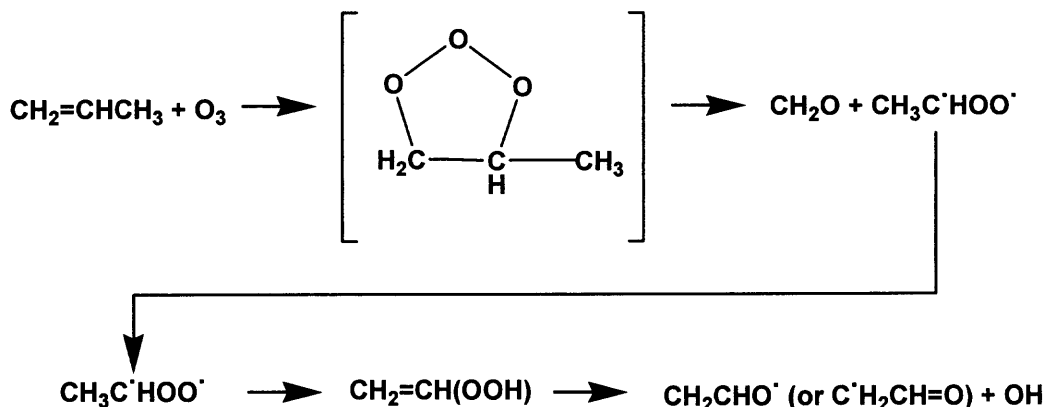
The C•H₂CH=O radical is also formed in a number of peroxide reactions important in intermediate temperature combustion and thermal oxidation.^{101,102}

Olzmann et al.¹⁰³ and Atkinson et al.^{104,105} have shown that formyl methyl radicals are formed in ozone reactions of olefins; where the Criegee intermediate CH₃C•HOO• undergoes a H shift to form a vinyl peroxide which dissociates rapidly through cleavage of the weak CH₂CHO—OH bond. An example formation of C•H₂CH=O in one reaction path for propene with ozone is illustrated in Scheme 4.1.

Reactions involving abstraction of H atoms from acetaldehyde by Cl, F, and OH radicals, have been studied by several research groups.⁹⁻¹⁶ While the abstraction can occur at two sites, these studies all report that the dominant reaction at atmospheric temperature is the abstraction from the carbonyl site to produce acetyl radicals. Sehested et al.¹⁰ are one group that have reported data for the abstraction of hydrogen atoms, by atomic fluorine, on the methyl radicals. They reported formyl methyl radical production at 35% and acetyl at 65% (both ± 9%) at 295 K and 1000

mbar. Abstraction from the methyl group producing formyl methyl radical should become important, at increased temperatures; because of the higher degeneracy and reduced influence of the activation energy (E_a).

Scheme 4.1 One Reaction Path for Propene + Ozone



Thermochemical properties are estimated for reactants, intermediates, products and transition states in the reaction paths using ab initio and density functional calculations. The thermochemical parameters are used to calculate high-pressure limit rate constants using canonical Transition State Theory (TST). Rate constants as a function of temperature and pressure are estimated using a multi-frequency quantum RRK analysis for $k(E)$ and master equation analysis for falloff. The thermochemical and kinetic data at relevant pressures and temperatures should be useful to both atmospheric and combustion models.

4.2 Calculation Methods

Enthalpies of formation ($\Delta H_f^\circ_{298}$) for reactants, intermediate radicals, transition states and products are calculated using CBS-Q composite method and density functional (B3LYP/6-31G(d)) calculations. The initial structure of each compound or transition state is determined using ROHF or UHF/PM3 in MOPAC,⁶³ followed by optimization and vibrational frequency calculation at HF/6-31G(d') level of theory using GAUSSIAN 94⁶⁴ for the CBS-Q analysis. The prime in 6-31G(d') indicates the basis set orbitals of Petersson et al.^{65,66} Transition state geometries are identified by the existence of only one imaginary frequency, structure information and the TST reaction coordinate vibration information. Zero-point vibrational energies (ZPVE) are scaled by 0.91844 as recommended by Ochterski et al.⁶⁷ Single point energy calculations are carried out at the B3LYP/6-31G(d).

Ochterski et al.⁶⁷ have developed several, high level, complete basis set (CBS) composite methods, denoted as CBS-QCI/APNO and CBS-Q. They indicate that CBS-Q is the most accurate, for molecules with several heavy atoms, where CBS-QCI/APNO is more accurate, but can only be used on smaller molecules. The mean absolute deviations from experiment for the 125 energies of the G2 test set are 0.5 and 1.0 kcal/mol for CBS-QCI/APNO and CBS-Q, respectively. Curtiss and coworkers⁶⁸ also have evaluated the CBS-Q method using isodesmic bond separation reactions, rather than atomization energies, on the G2 neutral test set of 148 molecules. The average absolute deviation between experiment and the CBS-Q calculated enthalpies was 1.57 kcal/mol. They reported that the combination of such bond balance reactions with G2 theory leads to a dramatic improvement in the

accuracy of theoretically evaluated enthalpies of formation.⁶⁹ It is noted that similar isodesmic reactions are used in this study. $\Delta H_f^\circ_{298}$ values of hydrocarbons, substituted hydrocarbons, and corresponding radicals have been studied^{41,106-108} and shown^{106,107} that the CBS-Q values are in agreement with accepted literature values. The CBS-Q enthalpies are more consistent than QCISD(T)/6-31G(d,p) single point calculations when values of one species are compared through a series of different work reactions. A comparison of ($\Delta H_f^\circ_{298}$) values from CBS-Q, CBS-QCI/APNO, and G2 methods with experimental values on several oxygenated hydrocarbons is listed in Scheme 4.2.

Scheme 4.2 Enthalpies of Formation at CBS-Q, CBS-QCI/APNO, and G2 Methods with Experimental Values

Species	Enthalpies of Formation ($\Delta H_f^\circ_{298}$) in kcal/mol				
	CBS-Q	CBS-QCI/APNO	G2	Ref.	Exp. [ref]
CH ₃ C(=O)•	-3.08 ± 0.38	-3.27 ± 0.28	-	108	-2.90 ± 0.70 [109]
C•H ₂ CHO	3.52 ± 0.38	3.08 ± 0.28	-	108	3.55 ± 1.00 [110]
CH ₃ OO•	0.3 ± 2.4	1.2 ± 1.7	-	41	2.15 ± 1.22 [86]
CH ₃ CH ₂ OOH	-39.9 ± 1.5	-	-40.1 ± 1.8	41	-39.7 ± 0.3 ^a [61]
CH ₃ CH ₂ OO•	-6.7 ± 2.3	-	-6.8 ± 2.7	41	-6.8 ± 2.3 [88]
C•H ₂ CH ₂ OOH	11.2 ± 2.1	-	10.5 ± 2.4	41	10.96 ± 1.06 ^a [61]

^a calculation values

The CBS-Q calculation sequence has the following steps at the noted levels (Scheme 4.3). It also includes a correction for spin contamination and an empirical correction (for the absolute overlap integral and the intra-orbital interference factor). The CBS-Q calculation is indicated as being equivalent to a QCISD(T)/6-311+G(3df,2p) calculation.^{70,111} The complete basis set (CBS-Q) method of Petersson

and coworkers for computing accurate energies^{66,67,112} is chosen as the determining enthalpies used in this kinetic analysis.

Scheme 4.3 CBS-Q calculation sequence

	Level of Theory
Optimized Geometry	MP2/6-31G(d')
Single Point Calculation	QCISD(T)/6-31+G(d')
	MP4(SDQ)/CBSB4 ^a
	MP2/CBSB3 ^b CBSExtrap = (Nmin ^c =10, Pop ^d)

^a 6-31+G(d(f),d,p). ^b H, He 311+G(2p), Li-Ne 6-311+G(2df).

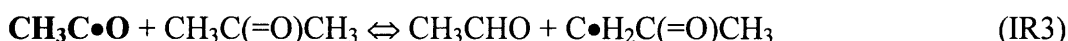
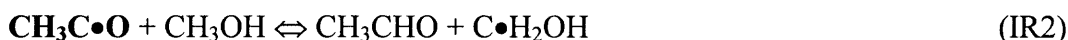
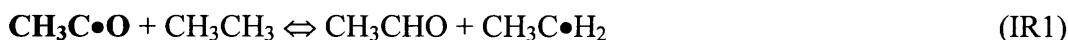
^c the minimum number of natural orbital configurations used for CBS extrapolations.

^d use population localization.

4.2.1 Determination of Enthalpy of Formation

The method of isodesmic reactions is used to determine the enthalpy of formation ($\Delta H_f^\circ_{298}$) for parent and radical species. It provides higher accuracy for estimates of $\Delta H_f^\circ_{298}$ than heats of atomization.³⁹⁻⁴³

The working reactions for estimation of $\Delta H_f^\circ_{298}$ on $\text{CH}_3\text{C}\bullet\text{O}$ are



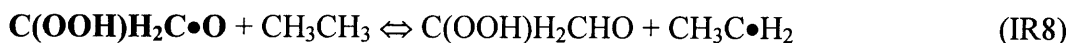
The working reactions for estimation of $\Delta H_f^\circ_{298}$ on $\text{C}\bullet\text{H}_2\text{CHO}$ are



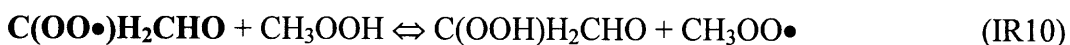
$\Delta H_f^\circ_{298}$ for estimation of **C(OOH)H₂CHO** is by



$\Delta H_f^\circ_{298}$ for estimation of **C(OOH)H₂C•O** [**•** : radical site] is by



$\Delta H_f^\circ_{298}$ for estimation of **C(OO•)H₂CHO** is by



Ab initio calculations for ZPVE and thermal correction energy are performed on all of four compounds in the reaction. The three reference compounds in the working reaction (IR1), excepting the target molecule, **CH₃C•O** in (IR1), have experimental or theoretical determined values of $\Delta H_f^\circ_{298}$. The unknown $\Delta H_f^\circ_{298}$ of **CH₃C•O** is obtained with the calculated $\Delta H^\circ_{\text{rxn}(298)}$ and known $\Delta H_f^\circ_{298}$ of the three reference compounds. The **C•H₂CHO**, **C(OOH)H₂CHO**, **C(OOH)H₂C•O**, and **C(OO•)H₂CHO** are calculated in the same manner.

4.2.2 Determination of Entropy and Heat Capacity

The contributions of vibrations and external rotation to entropies and heat capacities are calculated from scaled vibration frequencies and moments of inertia for the optimized HF/6-31G(d') structures. Contributions to S and $C_p(T)$ from torsion frequencies corresponding to hindered internal rotation are replaced with values calculated from the method of Pitzer and Gwinn.⁷² Number of optical isomers and spin degeneracy of unpaired electrons are also incorporated.

4.2.3 High-Pressure Limit A Factors (A) and Rate Constants (k_∞) Determination

For the reactions where thermochemical properties of transition states are calculated by *ab initio* or density functional methods, k_∞ 's are fit by three parameters A, n, and E_a over temperature range from 298 to 2000K, $k_\infty = A (T)^n \exp(-E_a / RT)$. Entropy differences between reactant and transition state are used to determine the pre-exponential factor, A, via canonical Transition State Theory (TST)

$$A = (k_b T / h_p) \exp(\Delta S^\ddagger / R), \quad E_a = \Delta H^\ddagger$$

(h_p is the Planck constant and k_b is the Boltzmann constant.) Treatment of the internal rotors for S and $C_p(T)$ is important here because these internal rotors are often lost in the cyclic transition state structures.

4.2.3.1 Tunneling. Corrections for H atom tunneling are applied for the intramolecular hydrogen atom transfer reactions of T₁HS and TC•CHOS and hydrogen atom dissociation reactions, TC•CHO-H and TCC•O-H. The tunneling corrections are determined using the Erwin-Henry computer code⁷⁴ that is based on Eckart's one-dimensional potential function.⁷⁵ The Erwin-Henry code requires input of vibrational frequencies, moments of inertia, symmetries, electronic degeneracies, and total energies at 0 K of reactants, transition states, and products; imaginary frequencies are also required. Schwartz et al.⁷⁶ note that calculated vibrational frequencies using HF/6-31G(d) level of theory need to be reduced by one-half to one-third in order for calculated transition states rate constant to match experimental data in abstraction reactions from fluorinated methane's.

4.2.4 Kinetic Analysis

Thermochemical properties for each species on the potential energy surface for the reaction system are evaluated. Forward or reverse rate constants (high-pressure limit) for each, elementary reaction step are determined from the calculations and use of literature data for enthalpies of stable molecules. Reverse rate constants are calculated from microscopic reversibility.

Multifrequency quantum Rice-Ramsperger-Kassel (QRRK) analysis is used to calculate $k(E)$ with a master equation analysis⁴¹ for falloff in order to obtain rate constants as a function of temperature and pressure. This kinetic analysis is for the chemical activation and the dissociation reaction systems. The master equation analysis⁴¹ uses an exponential-down model for the energy transfer function with $(\Delta E)^\circ_{\text{down}} = 1000 \text{ cal/mol}$,^{42,45} for N_2 as the third body and a 500 cal energy grain is used.

The QRRK/master equation analysis is described by Chang et al.^{31,41} The QRRK code utilizes a reduced set of three vibration frequencies which accurately reproduce the molecules' heat capacity; the code includes contribution from one external rotation in calculation of the ratio of the density of states to the partition coefficient $\rho(E)/Q$.

Comparisons of ratios of these $\rho(E)/Q$ with direct count $\rho(E)/Q$'s have been shown to result in good agreement.⁷³ Rate constant results from the quantum RRK-Master equation analysis are shown to accurately reproduce (model) experimental data on several complex systems.^{31,41,92} They also provide a reasonable method to

estimate rate constants for numerical integration codes by which the effects of temperature and pressure can be incorporated in these chemical activation systems.

4.3 Results and Discussion

4.3.1 Geometries of Parent Hydroperoxide Aldehyde, Two Intermediate Radicals and Transition States

Tables B.1 [a] to [c] (Appendix B) show the MP2/6-31G(d') optimized geometries of the C(OOH)H₂CHO and the two intermediate radicals, C(OO•)H₂CHO and C(OOH)H₂C•O, respectively. All remaining structures are from MP2/6-31G(d') determined geometries except transition states: T₁E(HO₂), T₂E(C•H₂OOH), and T₂D(CO+CH₂O+OH), which are determined from B3LYP/6-31G(d) calculations. Energies of Activation (E_a) reported below are relative to the corresponding stabilized adduct.

The transition state (TS) structure, TC•H₂CHO-O₂, is for C•H₂CHO addition to O₂ to form the C(OO•)H₂CHO peroxy radical. There is a small barrier to reaction, 2.97 kcal/mol, and the well depth is 27.5 kcal/mol. The C•H₂CHO structure is planar with the O₂ group perpendicular to the plane and the forming O₇-C₁ bond is calculated as 1.91Å.

The TS structure, T₁E(HO₂), shows the B3LYP/6-31G(d) geometry of the TS structure for direct HO₂ elimination from the peroxy adduct: C(OO•)H₂CHO to CH₂CO + HO₂. The O₇-O₈ bond shortens from 1.32 to 1.26Å while the O₇-C₁ and H₆-C₂ cleaving bonds lengthen to 2.31 and 1.31Å, respectively. The E_a is 48.13 kcal/mol.

The H shift isomerization: $C(OO\bullet)H_2CHO \rightarrow C(OOH)H_2C\bullet O$ is T_1HS . The H_4 atom is in a bridge structure shifting from C_2 to the radical site O_5 . The leaving H_4-C_2 bond is 1.29\AA and the forming H_4-O_5 bond is 1.36\AA . The imaginary frequency is 3104 cm^{-1} at HF/6-31G(d') and the E_a is 20.25 kcal/mol . The $C(OOH)H_2C\bullet O$ isomer is only slightly, 1.4 kcal/mol , higher in energy than the peroxy isomer.

The TS structure for HO_2 elimination from the hydroperoxide acetyl radical adduct is $T_2E(HO_2)$: $C(OOH)H_2C\bullet O \rightarrow CH_2CO + HO_2$. The cleaving O_6-C_1 bond is 1.86\AA and the C_1-C_4 bond shortens from 1.54 to 1.35\AA . The CH_2CO is planar with the HO_2 group perpendicular to the plane.

The TS structure for β scission of $C(OOH)H_2C\bullet O$ to products, $CO + C\bullet H_2OOH$ is $T_2E(C\bullet H_2OOH)$. The cleaving C_1-C_2 bond is 2.32\AA and the transition state C_2-O_3 is moving to a double bond at 1.36\AA . The E_a is 10.32 kcal/mol . The TS structure for $C(OOH)H_2C\bullet O$ decomposition to products, $CO + CH_2O + OH$ is $T_2D(CO + CH_2O + OH)$. The leaving C_2-C_3 and O_7-O_4 bonds are 1.69 and 1.81\AA , respectively. The E_a is 16.80 kcal/mol .

The TS structure for hydrogen abstraction from the $-CHO$ group of $C\bullet H_2CHO$ by O_2 to form ketene plus HO_2 (Bimolecular Reaction): $C\bullet H_2CHO + O_2 \rightarrow CH_2CO + HO_2$ is $TC\bullet H_2CO-HO_2$. The H_6 atom is in a bridge structure shifting from C_2 to O_7 . The transition state C_1-C_2 bond is 1.42\AA and the leaving H_6-C_2 and the forming H_6-O_7 bonds are 1.35 and 1.28\AA , respectively. The imaginary frequency is 3425 cm^{-1} at HF/6-31G(d') and the E_a is 29.03 kcal/mol .

The TS structure, TCC•O-H, is the transition state for CH₃C•O reaction to CH₂CO + H. The C₁-C₄ bond is 1.34Å and the cleaving C₁-H₅ bond is 1.70Å. The CH₂CO is planar with the hydrogen perpendicular to the plane.

The TS structure for β scission of C•H₂CHO to CH₂CO + H is TC•CHO-H. The cleaving C₄-H₅ bond is 1.64Å. The CH₂CO is planar with the hydrogen perpendicular to the plane. The *E_a* is 40.49 kcal/mol.

The H shift isomerization in formyl methyl radical, C•H₂CHO → CH₃C•O is identified as TC•CHOS. The H₄ atom is in a bridge structure shifting from C₂ to the radical site on C₁. The imaginary frequency is 2401 cm⁻¹ at HF/6-31G(d') and the *E_a* is 39.51 kcal/mol.

The TS structure, TCH₃-CO, is for unimolecular decomposition of acetyl radical, CH₃C•O → CH₃ + CO. The leaving C₁-C₂ and the forming CO bond lengths are 2.11 and 1.16Å, respectively. The *E_a* and Δ*H_f*^o_{rxn,298} are 16.64 and 10.73 kcal/mol, respectively.

4.3.2 Enthalpy of Formation (Δ*H_f*^o₂₉₈) using Calculated Total Energies and Isodesmic Reactions

The evaluated enthalpies of formation for the reference molecules and radicals in the isodesmic reactions are listed in Table 4.1. The evaluated reaction enthalpies and enthalpies of formation in the isodesmic reactions are listed in Table 4.2.

The working reactions (IR1) to (IR3) and (IR4) to (IR6) are used to estimate enthalpies of CH₃C•O and C•H₂CHO radical species with the CBSQ composite method.

Table 4.1 Enthalpies of Formation for Reference Molecules in the Isodesmic Reactions

Compounds	$\Delta H_f^\circ_{298}$ (kcal/mol)	Compounds	$\Delta H_f^\circ_{298}$ (kcal/mol)
C ₂ H ₆	-20.24 ± 0.10 ^a [80]	CH ₃ CHO	-39.72 ± 0.12 ^a [77]
C ₂ H ₅ OOH	-39.70 ± 0.3 [61]	CH ₃ C.H ₂	28.80 ± 0.50 [81]
CH ₃ OOH	-31.80 [84]	CH ₃ OO.	2.15 ± 1.22 [86]
CH ₃ OH	-48.16 ± 0.07 [78]	C.H ₂ OH	-3.97 ± 0.22 [82]
CH ₃ C(=O)CH ₃	-51.94 ± 0.17 [78]	C.H ₂ C(=O)CH ₃	-8.53 ± 1.15 [83]
C ₂ H ₅ OO.	-6.72 ± 2.3 [41]	C ₂ H ₅ OH	-56.17 ± 0.10 ^a [77]
CH ₃ C(=O)OH	-103.56 ± 0.32 ^b	C ₂ H ₅ O.	-3.90 ± 1.27 [114]

^a The uncertainties are evaluated from reference [78].

^b Average of -103.32 [77], -103.44 [78], and -103.92 [79].

Table 4.2 Reaction Enthalpies and Enthalpies of Formation in the Isodesmic Reactions

Working Reaction Series (units in kcal/mol)	$\Delta H^\circ_{\text{rxn},298}$		$\Delta H_f^\circ_{298}$	
	B3LYP	CBSQ	B3LYP	CBSQ
CH ₃ C.O + CH ₃ CH ₃ <=> CH ₃ CHO + CH ₃ C.H ₂	-	12.26	-	-2.94
CH ₃ C.O + CH ₃ OH <=> CH ₃ CHO + C.H ₂ OH	-	7.25	-	-2.78
CH ₃ C.O + CH ₃ C(=O)CH ₃ <=> CH ₃ CHO + C.H ₂ C(=O)CH ₃	-	7.20	-	-3.51
Average for CH ₃ C.O :				-3.08 ± 0.38 (CBSQ)
C.H ₂ CHO + CH ₃ CH ₃ <=> CH ₃ CHO + CH ₃ C.H ₂	-	5.66	-	3.66
C.H ₂ CHO + CH ₃ OH <=> CH ₃ CHO + C.H ₂ OH	-	0.65	-	3.82
C.H ₂ CHO + CH ₃ C(=O)CH ₃ <=> CH ₃ CHO + C.H ₂ C(=O)CH ₃	-	0.60	-	3.09
Average for C.H ₂ CHO :				3.52 ± 0.38 (CBSQ)
C(OOH)H ₂ CHO + C ₂ H ₆ <=> CH ₃ CHO + C ₂ H ₅ OOH	-3.16	-2.99	-56.02	-56.19
C(OOH)H ₂ C.O + C ₂ H ₆ <=> C(OOH)H ₂ CHO + CH ₃ C.H ₂	13.29	12.46	-20.27	-19.61
C(OOH)H ₂ C.O + CH ₃ CHO <=> C(OOH)H ₂ CHO + CH ₃ C.O	1.01	0.12	-20.39	-19.67
				-20.33 ± 0.09 (B3LYP)
Average for C(OOH)H ₂ C.O :				-19.64 ± 0.04 (CBSQ)
C(OO.)H ₂ CHO + CH ₃ OOH <=> C(OOH)H ₂ CHO + CH ₃ OO.	-1.14	-1.40	-20.93	-20.84
C(OO.)H ₂ CHO + C ₂ H ₅ OOH <=> C(OOH)H ₂ CHO + C ₂ H ₅ OO.	-1.45	-2.03	-21.59	-21.18
				-21.26 ± 0.47 (B3LYP)
Average for C(OO.)H ₂ CHO :				-21.01 ± 0.24 (CBSQ)

The average values of $\Delta H_f^\circ_{298}$ from three isodesmic reactions for $\text{CH}_3\text{C}\cdot\text{O}$ and $\text{C}\cdot\text{H}_2\text{CHO}$ are -3.08 and 3.52 kcal/mol by CBSQ, respectively.

A low or zero $\Delta H^\circ_{\text{rxn},298}$ in working reactions where the central atom environments are similar on both sides, suggests good cancellation of errors due to similarity in the reaction environment. This should lead to accurate $\Delta H_f^\circ_{298}$ values. This also supports the hypothesis of group additivity. As an example, $\Delta H_f^\circ_{298}[\text{C}(\text{OOH})\text{H}_2\text{CHO}]$ is evaluated from

$$\begin{aligned} \Delta H_f^\circ_{\text{rxn},298} &= \Delta H_f^\circ_{298} [\text{CH}_3\text{CHO}] + \Delta H_f^\circ_{298} [\text{C}_2\text{H}_5\text{OOH}] \\ &\quad - \Delta H_f^\circ_{298} [\text{C}(\text{OOH})\text{H}_2\text{CHO}] - \Delta H_f^\circ_{298} [\text{C}_2\text{H}_6] \end{aligned}$$

$$\Delta H_f^\circ_{\text{rxn},298} = -2.99(\text{CBSQ}) \text{ and } -3.16(\text{B3LYP})$$

The enthalpies of formation for $\text{C}(\text{OOH})\text{H}_2\text{CHO}$ are -56.19 and -56.02 kcal/mol by CBSQ and B3LYP/6-31G(d), respectively. The enthalpy of formation for the parent hydroperoxide is important because it allows the evaluation of relative stabilities in the peroxy radicals.

The bond energies of $\text{C}(\text{OOH})\text{H}_2\text{CHO}$ (Figure 4.1), $\text{C}_2\text{H}_5\text{OOH}$ and $\text{CH}_3\text{C}(=\text{O})\text{OOH}$ are compared in Table 4.3. The R-OOH bond energy in $\text{C}(\text{OOH})\text{H}_2\text{CHO}$ is 8 kcal/mol lower than that of $\text{C}_2\text{H}_5\text{OOH}$, because radical site is resonantly stabilized. The RO-OH and ROO-H bonds in $\text{C}(\text{OOH})\text{H}_2\text{CHO}$ are 45.1 and 87.3 kcal/mol, similar to those in $\text{C}_2\text{H}_5\text{OOH}$, 45.1 and 85.3 kcal/mol, respectively. However, the C-O, O-O, and O-H bond energies in $\text{CH}_3\text{C}(=\text{O})\text{OOH}$ are 22, 6 and 11 kcal/mol higher than those in $\text{C}(\text{OOH})\text{H}_2\text{CHO}$, respectively, because of coupling with the C=O carbonyl bond.

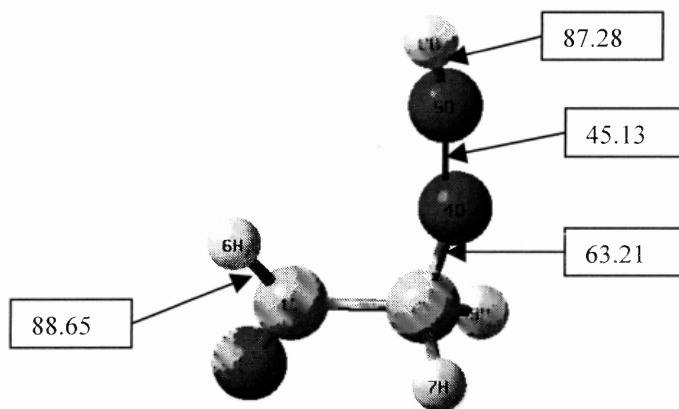


Figure 4.1 Bond dissociation energy of C(OOH)H₂CHO (Units : kcal/mol).

Table 4.3 The Comparison of Bond Energies between C(OOH)H₂C(=O)H, C₂H₅OOH, and CH₃C(=O)OOH

(units in kcal/mol)	C(OOH)H ₂ CHO ^a	C ₂ H ₅ OOH ^b	CH ₃ C(=O)OOH ^c
ROO--H	87.28	85.27	98.33
RO--OH	45.13	45.12	50.95
R--OOH	63.21	71.35	85.22
C(OOH)H ₂ C(=O)--H,	88.65	-	-
H--CH ₂ CH ₂ OOH,	-	103.21	-
H--CH ₂ C(=O)OOH	-	-	103.95
CH ₃ CH ₂ O--H,	-	104.7 ± 0.8 ^d	-
CH ₃ C(=O)O--H	-	-	112.32 ^c

^a in this study ^b Reference 41. ^c Reference 30. ^d Reference 115.

^e $\Delta H_f^\circ_{298}$ of CH₃C(=O)OH = -103.56 (average of references 77, 78, and 79),

CH₃C(=O)O, = -43.34 (CBSQ with isodesmic reaction, CH₃C(=O)O. + C₂H₅OH <=> CH₃C(=O)OH + C₂H₅O.)

The enthalpies of formation of the two intermediate radicals, C(OOH)H₂C•O and C(OO•)H₂CHO by CBSQ and B3LYP/6-31G(d) are obtained from use of isodesmic reactions (IR8) to (IR11) and values of reference species in Table 4.1. The data results in enthalpy values of -19.64 and -20.33 for C(OOH)H₂C•O, -21.01 and -21.26 for C(OO•)H₂CHO, by CBSQ and B3LYP/6-31G(d), respectively. The similar $\Delta H_f^\circ_{298}$ values for these two radicals infer near identical bond energies at the respective radical sites (within 1.4 kcal/mol and a thermo-neutral reaction for the H shift).

Table 4.4 Activation Energies and Enthalpies of Transition States in CBSQ Calculation^a

Reactant	Transition State (TS)	Product	<i>E_a</i>	$\Delta H_f^\circ_{298}$ of TS
C(OO.)H ₂ CHO	T ₁ HS	C(OOH)H ₂ C.O	20.25	-0.76
C(OO.)H ₂ CHO	T ₁ E(HO ₂) ^{b,c}		48.31	27.30
C(OOH)H ₂ C.O	T ₂ E(HO ₂) ^b		23.53	3.89
C(OOH)H ₂ C.O	T ₂ E(C.H ₂ OOH) ^{b,c}		10.32	-9.32
C(OOH)H ₂ C.O	T ₂ D(CO+CH ₂ O+OH) ^{b,c}		16.80	-2.84
C.H ₂ CHO + O ₂	TC.H ₂ CO-HO ₂	CH ₂ CO + HO ₂	28.84	32.36

^a units in kcal/mol

^b The activation energy and enthalpy for this transition state is estimated by taking the difference of total energy with ZPVE and thermal correction between the transition state and reactant (peroxy/hydroperoxide isomer).

^c CBS-Q//B3LYP/6-31G(d) Calculation

The activation energies and enthalpies of transition states at CBS-Q level are summarized in Table 4.4. All *E_a*'s are at CBS-Q level except the transition states: T₁E(HO₂), T₂E(C•H₂OOH), and T₂D(CO+CH₂O+OH), which are determined from

CBS-Q//B3LYP/6-31G(d) calculations; because all attempts at MP2 optimization failed.

4.3.3 Entropy ($S^{\circ}_{(298)}$) and Heat Capacity ($C_p(T)$, $300 \leq T/K \leq 1500$)

Entropy and heat capacities are calculated based on vibration frequencies and moments of inertia from the optimized HF/6-31G(d') structures.

The calculation results using MP2/6-31G(d') determined geometries and HF/6-31G(d') determined frequencies are summarized in Table 4.5. TVR represents the sum of the contributions from translation, vibrations and external rotations for $S^{\circ}_{(298)}$ and $C_p(T)$'s. Symmetry, number of optical isomers and electronic spin are incorporated in estimation of $S^{\circ}_{(298)}$ as described in Table 4.5. Torsion frequency vibrations are omitted in these calculations; instead, contributions from internal rotation for $S^{\circ}_{(298)}$ and $C_p(T)$'s are calculated based on rotational barrier heights, moments of inertia of the rotors using the method of Pitzer and Gwinn.⁷²

4.3.4 Energy Diagram for C•H₂CHO + O₂ Reaction System

The energy diagram for the C•H₂CHO + O₂ reaction system is illustrated in Figure 4.2, where enthalpies of formation are from CBSQ calculations in units of kcal/mol. The formyl methyl radical C•H₂CHO ($\Delta H_f^{\circ}_{298} = 3.52$ kcal/mol) adds to O₂ ($E_a = 2.97$) to form a C(OO•)H₂CHO peroxy radical with a 27.5 kcal/mol well depth. This peroxy radical can undergo dissociation back to reactants, decompose to products, CH₂CO + HO₂ via concerted HO₂ elimination with a barrier, ($E_a = 48.31$) or isomerize via hydrogen shift ($E_a = 20.25$) to form a C(OOH)H₂C•O isomer ($\Delta H_f^{\circ}_{298} = -19.64$).

Table 4.5 Ideal Gas Phase Thermodynamic Properties Obtained by CBSQ Calculation and by Therm^a

Species (s, e, OI) ^b		ΔH_f° ₂₉₈ ^c	S° ₂₉₈ ^d	Cp_{300} ^d	Cp_{400}	Cp_{500}	Cp_{600}	Cp_{800}	Cp_{1000}	Cp_{1500}
CH ₃ CHO (3,0,1)	TVR ^e		57.97 ^b	11.58	14.29	16.88	19.20	22.98	25.80	30.10
	I. R. 1 ^f		5.16	1.44	1.30	1.23	1.17	1.10	1.07	1.03
	Total	-39.72	63.13	13.02	15.59	18.11	20.37	24.08	26.87	31.13
	THERM	-39.18	63.13	13.22	15.71	18.22	20.47	24.22	26.97	
CH ₃ C.O (3,1/2,1)	TVR		58.82	11.12	13.24	15.24	17.01	19.90	22.07	25.39
	I. R. 1		5.45	1.16	1.10	1.06	1.04	1.02	1.01	1.00
	Total	-3.08	64.27	12.28	14.34	16.30	18.05	20.92	23.08	26.39
	THERM	-2.54	64.27	12.28	14.34	16.30	18.05	20.92	23.08	
C.H ₂ CHO (1,1/2,1)	TVR		61.99	13.10	15.79	18.04	19.86	22.63	24.62	27.66
	Total	3.52	61.99	13.10	15.79	18.04	19.86	22.63	24.62	27.66
	THERM	4.06	61.99	13.10	15.79	18.04	19.86	22.63	24.62	
C(OOH)H ₂ CHO (1,0,2)	TVR		69.25	15.10	18.82	22.20	25.05	29.44	32.58	37.30
	I. R. 1,2,3		13.56	3.99	5.82	5.92	5.93	5.84	5.68	5.20
	Total	-56.19	82.81	19.09	24.64	28.12	30.98	35.28	38.26	42.50
	THERM	-55.77	82.81	19.09	24.64	28.12	30.98	35.28	38.26	42.50
C(OO.)H ₂ CHO (1,1/2,1)	TVR		68.78	14.86	18.37	21.49	24.10	28.05	30.81	34.77
	I. R. 1,2		11.20	2.27	4.13	3.98	3.84	3.68	3.62	3.48
	Total	-21.01	79.98	17.13	22.50	25.47	27.94	31.73	34.43	38.25
	THERM	-20.17	79.98	17.13	22.50	25.47	27.94	31.73	34.43	38.25
C(OOH)H ₂ C.O (1,1/2,2)	TVR		70.40	14.64	17.81	20.58	22.89	26.39	28.88	32.62
	I. R. 1,2,3		11.38	5.90	6.35	6.49	6.45	6.09	5.59	4.59
	Total	-19.64	81.78	20.54	24.16	27.07	29.34	32.48	34.47	37.21
	THERM	-18.73	81.78	20.54	24.16	27.07	29.34	32.48	34.47	
C.H ₂ OOH (1,1/2,2)	TVR		61.46	11.15	13.22	15.05	16.57	18.93	20.68	23.52
	I. R. 1,2		4.77	3.61	4.05	4.33	4.48	4.45	4.19	3.44
	Total		66.23	14.76	17.27	19.38	21.05	23.38	24.87	26.96
	THERM	15.20	65.41	15.60	18.12	20.15	21.79	24.14	25.65	27.65
CH ₂ O.C.O (1,1,1)	TVR		66.26	13.36	15.79	17.84	19.53	22.10	23.91	26.53
	I. R. 1		5.91	2.19	1.95	1.74	1.58	1.37	1.25	1.12
	Total	11.01	72.17	15.55	17.74	19.58	21.11	23.47	25.16	27.65
HC.=C=O (1,1/2,1)	TVR		59.79	12.48	13.44	14.23	14.90	15.98	16.79	18.06
	Total	41.98	59.79	12.48	13.44	14.23	14.90	15.98	16.79	18.06
T ₁ HS (1,1/2,2)	TVR		70.09	17.85	21.71	24.96	27.58	31.41	33.98	37.51
	Total	-0.76	70.09	17.85	21.71	24.96	27.58	31.41	33.98	37.51
T ₁ E(HO ₂) (1,1/2,2)	TVR		81.23	22.66	25.70	28.18	30.17	33.12	35.15	38.05
	Total	27.30	81.23	22.66	25.70	28.18	30.17	33.12	35.15	38.05
T ₂ E(HO ₂) (1,1/2,2)	TVR		70.81	16.98	19.98	22.41	24.37	27.35	29.52	32.89
	I. R. 1,2		5.34	3.60	4.06	4.33	4.46	4.37	4.07	3.33
	Total	3.89	76.15	20.58	24.04	26.74	28.83	31.72	33.59	36.22
T ₂ E(C.H ₂ OOH) (1,1/2,2)	TVR		85.82	20.33	22.39	24.17	25.69	28.12	30.01	33.10
	I. R. 1,2,3		11.38	5.90	6.35	6.49	6.45	6.09	5.59	4.59
Total	-9.32	97.20	26.23	28.74	30.66	32.14	34.21	35.60	37.69	

Table 4.5 Ideal Gas Phase Thermodynamic Properties Obtained by CBSQ Calculation and by Therm^a (Continued)

Species (s, e, OI) ^b		ΔH_f° ₂₉₈ ^c	S° ₂₉₈ ^d	Cp ₃₀₀ ^d	Cp ₄₀₀	Cp ₅₀₀	Cp ₆₀₀	Cp ₈₀₀	Cp ₁₀₀₀	Cp ₁₅₀₀
T ₂ D(CO+CH ₂ O+OH)	TVR		77.30	19.77	22.25	24.44	26.29	29.20	31.36	34.77
(1,1/2,1)	I. R. 1		2.16	1.98	2.13	2.23	2.29	2.28	2.14	1.75
	Total	-2.84	79.46	21.75	24.38	26.67	28.58	31.48	33.50	36.52
TC.H ₂ CHO-O ₂	TVR		70.53	15.82	19.16	21.97	24.22	27.55	29.88	33.29
(1,1/2,1)	I. R. 1,2		11.20	2.27	4.13	3.98	3.84	3.68	3.62	3.48
	Total	6.49	81.73	18.09	23.29	25.95	28.06	31.23	33.50	36.77
TC.CHOS	TVR		61.32	12.12	14.47	16.59	18.40	21.21	23.21	26.11
(1,1/2,1)	Total	43.03	61.32	12.12	14.47	16.59	18.40	21.21	23.21	26.11
TC.CHO-H	TVR		64.09	15.29	17.59	19.33	20.71	22.79	24.31	26.64
(1,1/2,1)	Total	44.01	64.09	15.29	17.59	19.33	20.71	22.79	24.31	26.64
TCC.O-H	TVR		63.25	14.69	17.05	18.88	20.34	22.53	24.12	26.54
(1,1/2,1)	Total	40.09	63.25	14.69	17.05	18.88	20.34	22.53	24.12	26.54
TCH ₃ -CO	TVR		60.70	12.22	13.92	15.42	16.75	18.99	20.78	23.69
(3,1/2,1)	I. R. 1		5.45	1.16	1.10	1.06	1.04	1.02	1.01	1.00
	Total	13.56	66.15	13.38	15.02	16.48	17.79	20.01	21.79	24.69
TC.H ₂ CHO-HO ₂	TVR		71.57	17.14	20.32	22.96	25.10	28.28	30.46	33.62
(1,1/2,1)	I. R. 1,2		6.31	4.15	4.41	4.44	4.34	3.96	3.57	2.91
	Total	32.36	77.88	21.29	24.73	27.40	29.44	32.24	34.03	36.53

a : Thermodynamic properties are referred to a standard state of an ideal gas of pure enantiomer at 1 atm. Therm values for stable species are included for comparison (refs 37, 85).

b : Symmetry number, optical isomer and electronic spin are taken into account, $-\text{Rln}(s)$, $\text{Rln}2$, and $\text{Rln}2$, respectively. s = number of symmetry, e = electronic spin, OI = number of optical isomer.

c : Units in kcal/mol d : Units in cal/mol-K

e : Sum of contributions from translations, vibrations, and external rotations.

f : Contribution from internal rotation

The C(OOH)H₂C•O isomer can undergo β -scission to products, CH₂CO + HO₂ ($E_a = 23.53$), decompose to CO + C•H₂OOH (C•H₂OOH rapidly dissociates to CH₂O + OH with little or no barrier) ($E_a = 10.32$) via T₂E(C•H₂OOH), decompose directly to CO + CH₂O + OH ($E_a = 16.80$) via T₂D(CO+CH₂O+OH), decompose to a diradical, CH₂O•C•O + OH via simple RO—OH bond cleavage ($E_a = 40.14$), or isomerize via hydrogen shift ($E_a = 18.88$), to form a C(OO•)H₂CHO isomer.

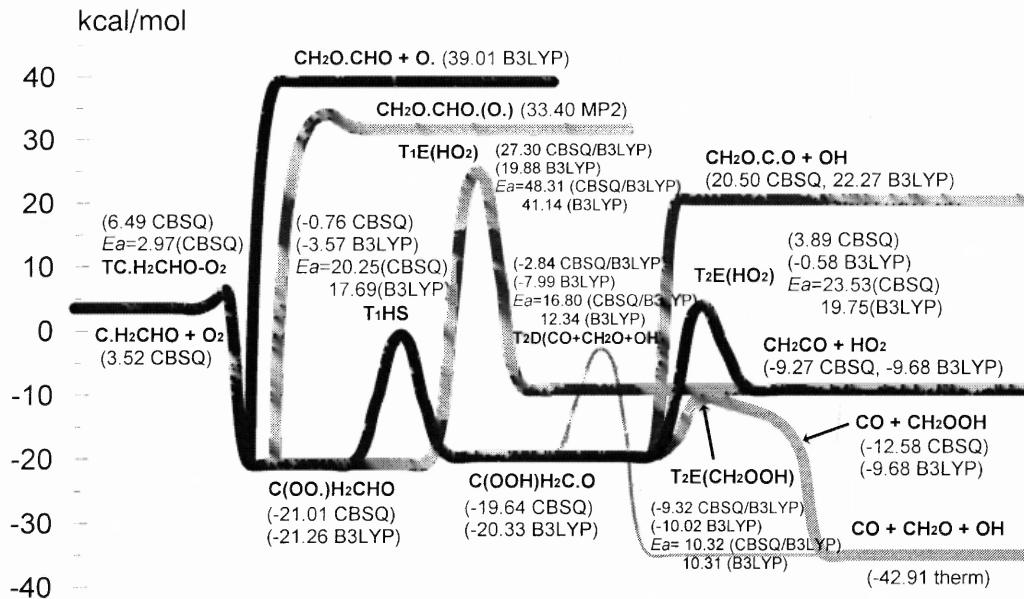


Figure 4.2 Potential energy diagram $C\bullet H_2CHO + O_2$.

Table 4.6 Comparison of $C\bullet H_2CHO$, $CH_3C\bullet(=O)$ and C_2H_5 with O_2^a

	$C\bullet H_2CHO + O_2$	$CH_3C\bullet(=O) + O_2$	$C_2H_5 + O_2$
Well Depth	27.5	35.5	35.3
H Shift ^b	20.25	26.42	36.36
HO_2 Elimination ^b	48.31	34.58	30.48

^a units in kcal/mol

^b H shift and HO_2 elimination for the $C(OO\bullet)H_2CHO$, $CH_3C(=O)OO\bullet$, and $C_2H_5OO\bullet$.

4.3.5 Comparison of $C\bullet H_2CHO + O_2$, $CH_3C\bullet O + O_2$ and $C_2H_5 + O_2$

The $C\bullet H_2CHO + O_2$, $CH_3C\bullet O + O_2$,³⁰ and $C_2H_5 + O_2$ ⁴¹ reaction systems have significant differences. The $C\bullet H_2CHO + O_2$ reaction system of this study has a lower well depth of 27.5 kcal/mol compared to $CH_3C\bullet O + O_2$ and $C_2H_5 + O_2$: 35.5 and 35.3 kcal/mol, respectively.

The H shift barriers in the $C(OO\bullet)H_2CHO$ and $CH_3C(=O)OO\bullet$ peroxy radicals are both lower than those of concerted HO_2 elimination, whereas in $C_2H_5OO\bullet$, direct HO_2 elimination has a lower barrier than the H shift.

The well depth and barriers of H shift and HO_2 elimination in the $C\bullet H_2CHO$, $CH_3C\bullet O$ and $C_2H_5\bullet$ with O_2 reaction systems are compared in Table 4.6.

4.3.6 Analysis of the $C\bullet H_2CHO + O_2$ Chemical Activation Reaction

The QRRK calculations for $k(E)$ and master equation analysis for falloff are performed on this $C\bullet H_2CHO + O_2$ reaction system to estimate rate constants and to determine important reaction paths as a function of temperature and pressure. Table 4.7 presents high-pressure limit kinetic parameters used as input data and Table 4.8 presents results versus temperature and pressure.

Rate constants at 1atm pressure versus $1000/T$ are illustrated in Figure 4.3. Stabilization ($C(OO\bullet)H_2CHO$) is important below 500 K, with reverse dissociation and $CO + CH_2O + OH$ products important above 1000 K. The ketene + HO_2 product set via direct HO_2 elimination is also important above 1500 K.

Plots of calculated rate constants for $C\bullet H_2CHO + O_2$ at 298 K versus pressure are illustrated in Figure 4.4. Stabilization is the dominant path above 0.1 atm, whereas

Table 4.7 Input Parameters^a and High-Pressure Limit Rate Constants (k_{∞})^b for QRRK Calculations^c

Input Parameters for QRRK Calculations with Master Equation Analysis for Falloff			
Reaction (kcal/mol)	High-Pressure Limit Rate Constants		
	A	n	E_a
1 C•H ₂ CHO + O ₂ => C(OO•)H ₂ CHO ^d	3.74E+07	1.55	3.12
-1 C(OO•)H ₂ CHO => C•H ₂ CHO + O ₂ ^d	2.54E+11	0.80	27.81
2 C(OO•)H ₂ CHO => C(OOH)H ₂ C•O ^d	1.04E+04	2.22	17.67
3 C(OO•)H ₂ CHO => CH ₂ CO + HO ₂ ^d	4.35E+08	1.76	48.24
4 C(OOH)H ₂ C•O => CO + CH ₂ O + OH ^d	8.47E+10	2.04	10.10
5 C(OOH)H ₂ C•O => CH ₂ CO + HO ₂ ^d	1.47E+10	0.65	23.82

^aGeometric mean frequency (from CPFIT, ref 41: 740.8 cm⁻¹(7.239); 725.6 cm⁻¹ (4.899); 2180.4 cm⁻¹ (4.862). Lennard-Jones parameters: σ_{ij} =5.19Å, ϵ/k =533.08K, ref 89]

^bThe units of A factors and rate constants k are s⁻¹ for unimolecular reactions and cm³/(mol s) for bimolecular reactions.

^c ΔE down of 1000 cal/mol is used, N₂ for bath gas. [Units] k_1 : cm³/(mol s), k_{-1} -> k_5 : s⁻¹

^d A is calculated using TST and entropy of transition state, $\Delta S^{\ddagger}_{298}$ from HF/6-31G(d'); E_a is from CBSQ calculation (see Table 4.5). All parameters A, n, E_a , are fit over the temperature range of 298-2000K.

Table 4.8 Resulting Rate Constants in QRRK Calculations^a

1) Calculated Reaction Parameters at P = 0.01 atm,

$$k = A(T/K)^n \exp(-Ea/RT) \quad (298 \leq T/K \leq 2000)$$

Reaction	A	n	Ea (kcal/mol)	k ₂₉₈
1 C•H ₂ CHO + O ₂ => C(OO•)H ₂ CHO	1.58E+77	-21.90	19.35	6.68E+08
6 C•H ₂ CHO + O ₂ => CH ₂ CO + HO ₂	1.88E+05	2.37	23.73	5.43E-07
7 C•H ₂ CHO + O ₂ => CO + CH ₂ O + OH	2.68E+17	-1.84	6.53	1.21E+08
8 C•H ₂ CHO + O ₂ => C(OOH)H ₂ C•O	3.64E+65	-21.87	19.02	3.16E-03
2 C(OO•)H ₂ CHO => C(OOH)H ₂ C•O	8.27E+30	-6.65	24.50	3.13E-04
3 C(OO•)H ₂ CHO => CH ₂ CO + HO ₂	2.05E+40	-13.31	52.15	1.35E-31
4 C(OOH)H ₂ C•O => CO + CH ₂ O + OH	2.36E+17	-2.95	8.10	1.37E+04
5 C(OOH)H ₂ C•O => CH ₂ CO + HO ₂	1.12E+07	-3.76	21.68	6.99E-19

^aThe units of A factors and rate constants *k* are s⁻¹ for unimolecular reactions and cm³/(mol s) for bimolecular reactions.

2) Calculated Reaction Parameters at P = 0.1 atm,

$$k = A(T/K)^n \exp(-Ea/RT) \quad (298 \leq T/K \leq 2000)$$

Reaction	A	n	Ea (kcal/mol)	k ₂₉₈
1 C•H ₂ CHO + O ₂ => C(OO•)H ₂ CHO	3.88E+69	-18.84	19.24	7.33E+08
6 C•H ₂ CHO + O ₂ => CH ₂ CO + HO ₂	1.88E+05	2.37	23.73	5.43E-07
7 C•H ₂ CHO + O ₂ => CO + CH ₂ O + OH	1.52E+20	-2.58	8.98	1.62E+07
8 C•H ₂ CHO + O ₂ => C(OOH)H ₂ C•O	3.64E+58	-19.00	19.09	3.53E-03
2 C(OO•)H ₂ CHO => C(OOH)H ₂ C•O	1.73E+26	-4.99	23.76	2.92E-04
3 C(OO•)H ₂ CHO => CH ₂ CO + HO ₂	5.72E+45	-14.00	52.20	6.80E-28
4 C(OOH)H ₂ C•O => CO + CH ₂ O + OH	2.38E+18	-2.95	8.10	1.37E+05
5 C(OOH)H ₂ C•O => CH ₂ CO + HO ₂	1.10E+08	-3.76	21.68	6.92E-18

Table 4.8 Resulting Rate Constants in QRRK Calculations^a (Continued)

3) Calculated Reaction Parameters at P = 1 atm,
 $k = A(T/K)^n \exp(-Ea/RT)$ ($298 \leq T/K \leq 2000$)

Reaction	A	n	Ea (kcal/mol)	k_{298}
1 C•H ₂ CHO + O ₂ => C(OO•)H ₂ CHO	7.80E+59	-15.40	17.65	7.04E+08
6 C•H ₂ CHO + O ₂ => CH ₂ CO + HO ₂	2.51E+05	2.33	23.80	5.15E-07
7 C•H ₂ CHO + O ₂ => CO + CH ₂ O + OH	1.65E+19	-2.22	10.34	1.37E+06
8 C•H ₂ CHO + O ₂ => C(OOH)H ₂ C•O	6.65E+48	-15.55	17.46	3.51E-03
2 C(OO•)H ₂ CHO => C(OOH)H ₂ C•O	9.03E+19	-2.92	22.17	2.97E-04
3 C(OO•)H ₂ CHO => CH ₂ CO + HO ₂	4.16E+55	-15.76	55.08	1.68E-24
4 C(OOH)H ₂ C•O => CO + CH ₂ O + OH	2.51E+19	-2.95	8.11	1.42E+06
5 C(OOH)H ₂ C•O => CH ₂ CO + HO ₂	9.20E+08	-3.73	21.63	7.43E-17

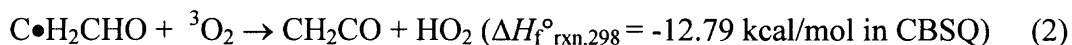
4) Calculated Reaction Parameters at P = 10 atm,
 $k = A(T/K)^n \exp(-Ea/RT)$ ($298 \leq T/K \leq 2000$)

Reaction	A	n	Ea (kcal/mol)	k_{298}
1 C•H ₂ CHO + O ₂ => C(OO•)H ₂ CHO	3.05E+50	-12.20	15.63	6.86E+08
6 C•H ₂ CHO + O ₂ => CH ₂ CO + HO ₂	7.05E+07	1.63	25.29	2.16E-07
7 C•H ₂ CHO + O ₂ => CO + CH ₂ O + OH	8.95E+13	-0.60	10.12	1.11E+05
8 C•H ₂ CHO + O ₂ => C(OOH)H ₂ C•O	4.80E+38	-12.14	14.96	4.72E-03
2 C(OO•)H ₂ CHO => C(OOH)H ₂ C•O	1.43E+16	-1.67	21.21	2.94E-04
3 C(OO•)H ₂ CHO => CH ₂ CO + HO ₂	1.12E+61	-16.04	60.01	2.23E-23
4 C(OOH)H ₂ C•O => CO + CH ₂ O + OH	4.16E+20	-3.02	8.24	1.27E+07
5 C(OOH)H ₂ C•O => CH ₂ CO + HO ₂	2.09E+09	-3.55	21.22	9.46E-16

stabilization, reverse dissociation, and CO + CH₂O + OH products are important below 0.01 atm.

Rate constants at 1000 K versus pressure are illustrated in Figure 4.5. Reverse dissociation and CO + CH₂O + OH products are most important at both high and low pressures. Stabilization decreases as pressure is decreased.

4.3.7 Abstraction of a Hydrogen from the –CHO Group of C•H₂CHO by O₂



A transition state for direct abstraction of a hydrogen from the –CHO group of C•H₂CHO by O₂ to form ketene plus HO₂ is identified with a barrier of ca. 29 kcal/mol, at the CBSQ level. (This TS is calculated as doublet.) This barrier seems high for a reaction, which is this exothermic, so further calculations were performed. The species structures and the barrier are further calculated using the recently published KMLYP density functional method¹¹⁶ with the /6-311G(d,p) basis set. The barrier is calculated relative to the reactants and relative to the HO₂ elimination transition state (T₂E(HO₂)). Comparison of the two calculation results for the three methods (B3LYP, KMLYP and CBSQ) is listed in Scheme 4.4. The barrier of 28.8 kcal/mol at CBSQ is similar in both comparisons. This value is 4.3 kcal/mol lower than the value from KMLYP and 4.1 kcal/mol higher than B3LYP. Kang et al.¹¹⁶ reported comparisons between the B3LYP barriers and experiment show that B3LYP is less accurate than KMLYP in estimating barriers, it has a tendency to underestimate barriers as reported in several studies.¹¹⁷⁻¹¹⁹ The value at CBSQ level is chosen.^{66,67,112}

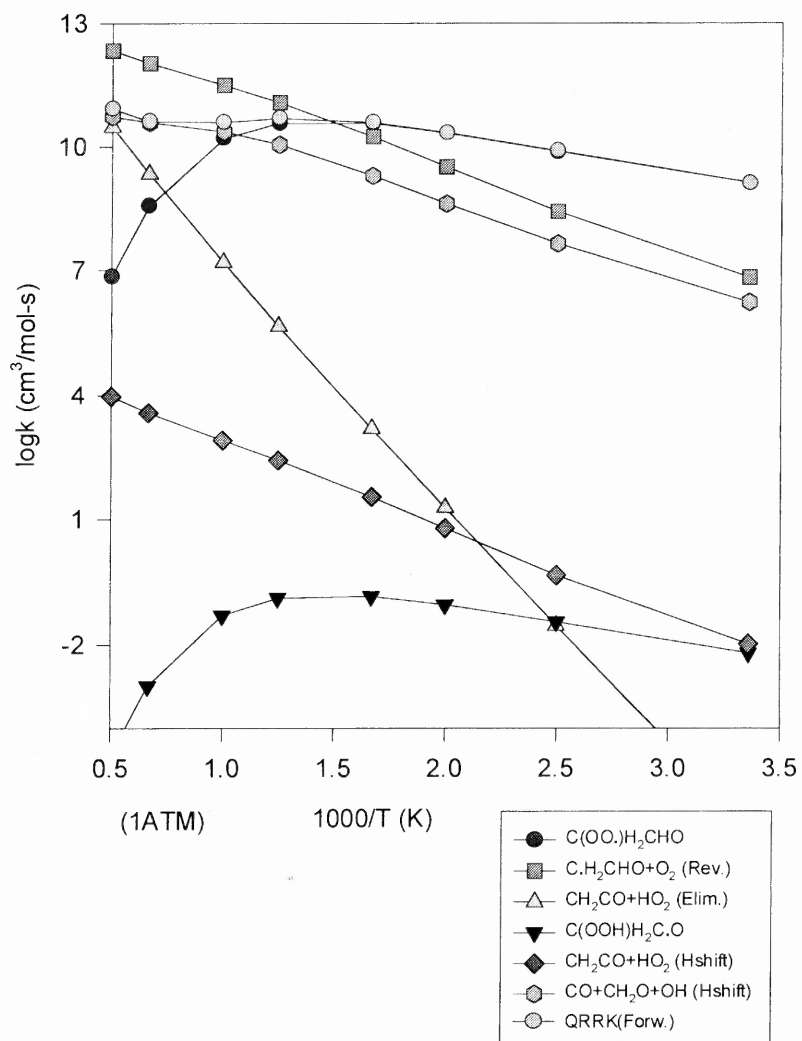


Figure 4.3 C•H₂CHO + O₂ → products k vs. $1000/T$ at 1 atm.

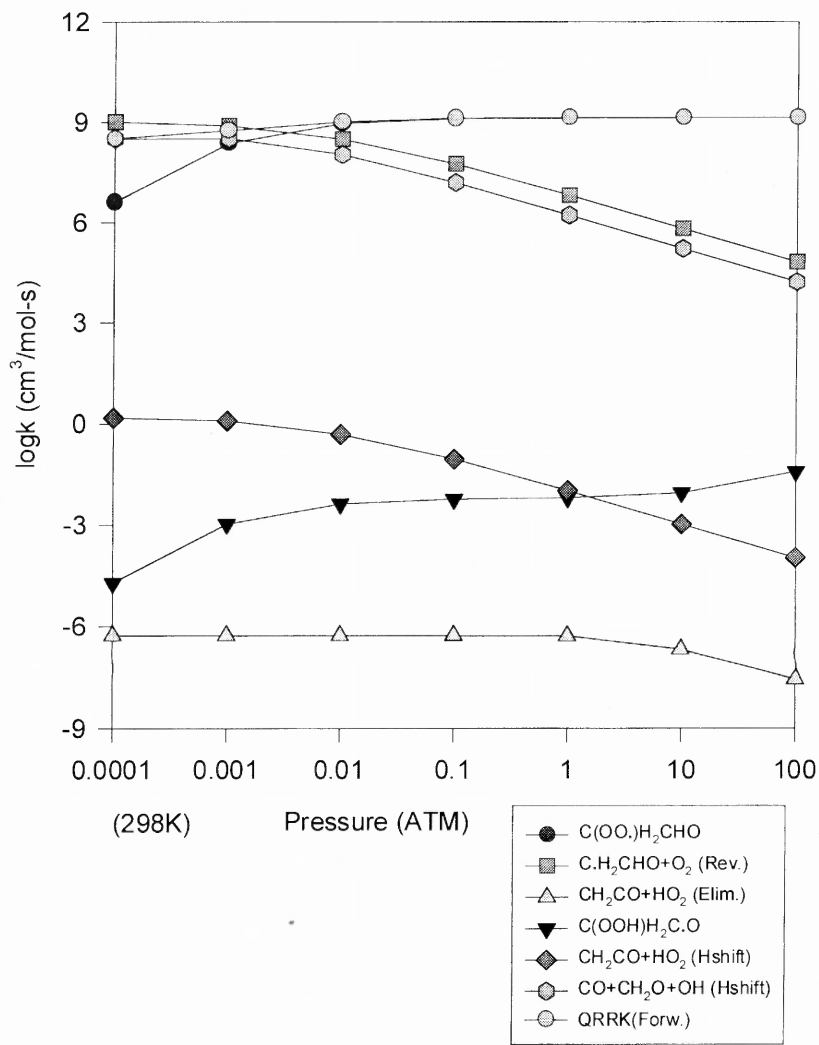


Figure 4.4 $C\bullet H_2CHO + O_2 \rightarrow$ products k vs. pressure at 298K.

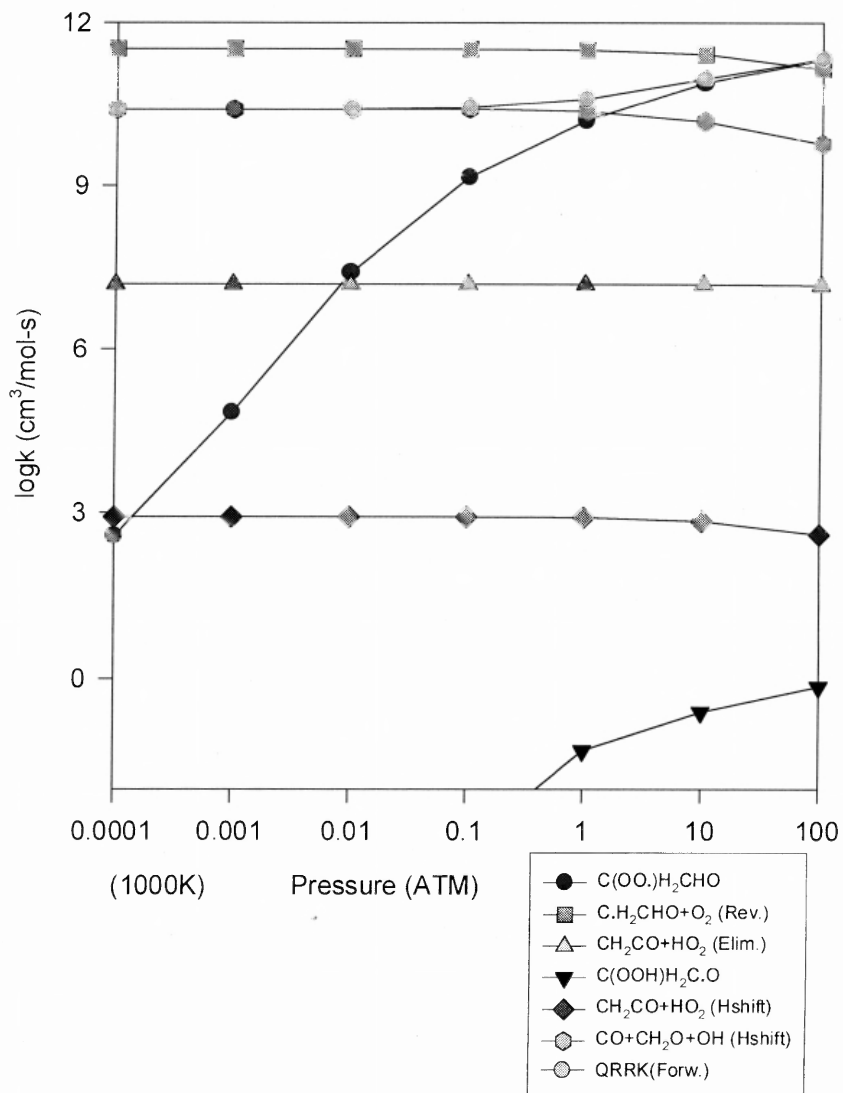


Figure 4.5 $\text{C}\cdot\text{H}_2\text{CHO} + \text{O}_2 \rightarrow \text{products}$ k vs. pressure at 1000K.

The barrier is determined to be high in all the calculation methods. The high barrier is interpreted as due to the non-initiation of the new C=C Π bond in the TS structure, where some re-arrangement is required to form the ketene structure, for this direct hydrogen abstraction by O₂ from the -CH(=O). The forming C=C bond is 1.42 Å in the transition state structure and is 1.47 Å in the stable C•H₂CHO radical.

Scheme 4.4 Comparison of the Activation Energies
[Ea's are calculated from (a) C•H₂CHO + ³O₂ → TS (Bimolecular Reaction) and (b) Relative to T₂E(HO₂) (Unimolecular Reaction)]

Units (kcal/mol)	(a) Ea	(b) Ea
CBSQ	28.84	28.61
KMLYP/6-311G(d,p)	33.10	25.55
B3LYP/6-31G(d)	24.67	15.76

This direct abstraction channel to form ketene + HO₂ is not competitive with the chemical activation C•H₂CHO by O₂ (association) rate constant to the same product set below 1500K at 1 atm.

4.3.8 Unimolecular Dissociation of Formyl Methyl Peroxy and Acetyl Hydroperoxide Radicals

Stabilization of the adducts is observed to be important at lower temperature and moderate pressure conditions. Important dissociation products of the adducts and the rate constants are, therefore, of value.

(1) C(OO•)H₂CHO Dissociation Reaction. Plots of rate constants for C(OO•)H₂CHO dissociation at 1atm pressure versus 1000/T, and rate constants at

298 K and 1000K versus pressure are illustrated in Figures B.1, B.2, and B.3, respectively (Appendix B). $\text{C}\bullet\text{H}_2\text{CHO} + \text{O}_2$ and $\text{CO} + \text{CH}_2\text{O} + \text{OH}$ products via H shift are important above 500 K at both high and low pressures. $\text{CO} + \text{CH}_2\text{O} + \text{OH}$ products via H shift is the dominant path below 500 K where the ketene + HO_2 products increase as temperature is increased at 1atm pressure.

(2) $\text{C}(\text{OOH})\text{H}_2\text{C}\bullet\text{O}$ Dissociation Reaction. Rate constants for $\text{C}(\text{OOH})\text{H}_2\text{C}\bullet\text{O}$ dissociation at 1atm pressure versus $1000/T$, and rate constants at 298 K and 1000K versus pressure are illustrated in Figures B.4, B.5, and B.6, respectively (Appendix B). The $\text{CO} + \text{CH}_2\text{O} + \text{OH}$ product set is most important at both high and low temperatures and decrease as temperature is decreased. Isomerization to $(\text{C}(\text{OO}\bullet)\text{H}_2\text{CHO})$ shows falloff above 600K. At 298 K and 1000K, the $\text{CO} + \text{CH}_2\text{O} + \text{OH}$ product set is the dominant path at both high and low pressures.

4.3.9 Formyl Methyl Radical Unimolecular Dissociation

The energy diagram for formyl methyl radical unimolecular dissociation is illustrated in Figure 4.6. The formyl methyl radical, $\text{C}\bullet\text{H}_2\text{CHO}$ can undergo β scission to products, $\text{CH}_2\text{CO} + \text{H}$ ($E_a = 40.49$) or isomerize via H shift ($E_a = 39.51$) to form the slightly lower energy $\text{CH}_3\text{C}\bullet\text{O}$ isomer. The barriers of these two channels are similar. This $\text{CH}_3\text{C}\bullet\text{O}$ isomer can decompose to $\text{CH}_3 + \text{CO}$ ($E_a = 16.64$), undergo β scission to products, $\text{CH}_2\text{CO} + \text{H}$ ($E_a = 43.17$) or isomerize via H shift ($E_a = 46.11$) to form the $\text{C}\bullet\text{H}_2\text{CHO}$ isomer. The barrier of $\text{CH}_3\text{C}\bullet\text{O}$ decomposition to $\text{CH}_3 + \text{CO}$ is 26.5 kcal/mol lower than barrier for β scission to products, $\text{CH}_2\text{CO} + \text{H}$; thus the $\text{CH}_3 + \text{CO}$ product set is the dominant path for $\text{CH}_3\text{C}\bullet\text{O}$ dissociation.

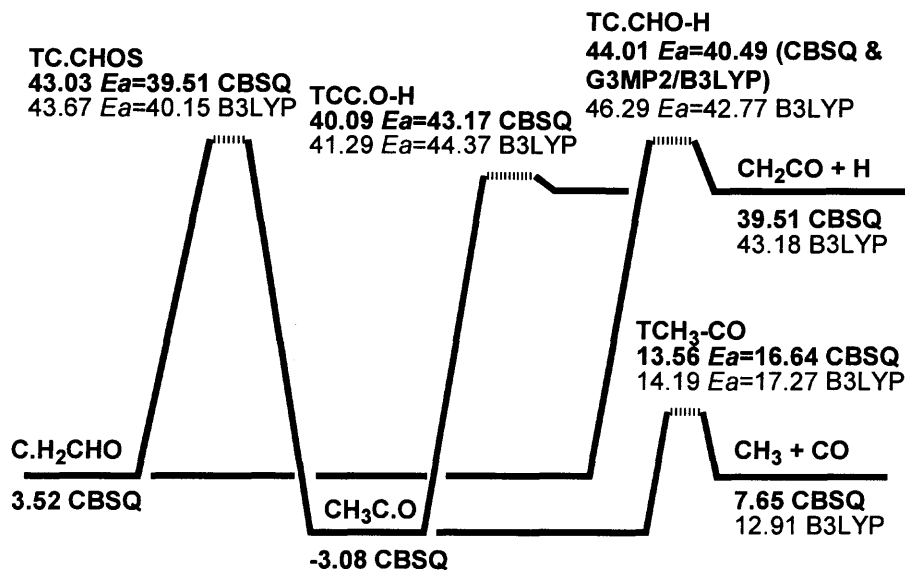


Figure 4.6 Potential energy diagram of acetyl and formyl methyl radical unimolecular isomerization/ dissociations (units: kcal/mol).

4.3.10 Detailed Mechanism of Formyl Methyl Radical Oxidation Reactions

A small detailed mechanism including the reactions evaluated in this study is assembled and listed in Table 4.9. The mechanism consists of 72 reactions and 31 species with each elementary reaction evaluated and referenced. The CHEMKIN II integrator code⁹¹ is used to model typical low-pressure flow reactor conditions⁹ in this study on formyl methyl radical + O₂ reaction system. The acetyl radical + O₂ reaction system was previously modeled under similar conditions.³⁰ Abstraction reactions by O, H, OH, HO₂, O₂ and CH₃ radicals are taken from evaluated literature wherever possible. A procedure from Dean and Bozzelli⁹² is used to estimate abstraction rate constants by H, HO₂, CH₃, and CH₃C(=O)OO• radicals when no literature data are available.

Table 4.9 Detailed Mechanism

Reactions	A	n	<i>E_a</i>	References
CH ₃ CHO = CH ₃ +HCO	6.99E+44	-9.82	88320	a
CH ₃ CHO = CH ₃ C•O+H	7.50E+44	-11.49	92652	a
CH ₃ CHO+O ₂ = CH ₃ C•O+HO ₂	3.01E+13	0.0	39143	b
HCO = H+CO	7.94E+17	-3.51	16326	a
CH ₃ CHO+OH = C•H ₂ CHO+H ₂ O	4.31E+11	0.0	1000	c
CH ₃ CHO+H = C•H ₂ CHO+H ₂	2.4E+8	1.5	2103	d
CH ₃ CHO+O = C•H ₂ CHO+OH	5.85E+12	0.0	1808	b
CH ₃ CHO+HO ₂ = C•H ₂ CHO+H ₂ O ₂	1.4E+4	2.69	14068	d
CH ₃ CHO+CH ₃ = C•H ₂ CHO+CH ₄	8.1E+5	1.87	5251	d
C•H ₂ CHO+O ₂ = C(OO•)H ₂ CHO	8.22E+90	-27.02	21062	a
C•H ₂ CHO+O ₂ = CH ₂ CO+HO ₂	1.88E+05	2.37	23728	a
C•H ₂ CHO+O ₂ = C(OOH)H ₂ C•(=O)	6.62E+73	-26.06	20125	a
C•H ₂ CHO+O ₂ = CH ₂ CO+HO ₂	1.15E-03	2.21	3493	a
C•H ₂ CHO+O ₂ = CO+CH ₂ O+OH	1.18E+15	-1.16	5109	a
C•H ₂ CHO+O ₂ = CH ₂ O•C•O+OH	3.24E-01	2.43	14700	a
C(OO•)H ₂ CHO = C•H ₂ CHO +O ₂	4.45E+74	-21.35	39750	a
C(OO•)H ₂ CHO = CH ₂ CO+HO ₂	3.26E+49	-19.88	53147	a
C(OO•)H ₂ CHO = CH ₂ (OOH)C•(=O)	8.57E+32	-7.48	24373	a
C(OOH)H ₂ C•(=O) = CH ₂ CO+HO ₂	9.55E+02	-4.58	22116	a
C(OOH)H ₂ C•(=O) = CO+CH ₂ O+OH	1.39E+18	-3.32	8482	a
C(OOH)H ₂ C•(=O) = CH ₂ O•C•O+OH	8.21E-05	-5.22	36056	a
C(OOH)H ₂ C•(=O) = C(OO•)H ₂ CHO	9.60E+04	-3.41	14091	a
CH ₂ O•C•O = CH ₂ O+CO	2.02E+10	-1.08	2552	a
C(OOH)H ₂ C•(=O)+O ₂ = C(OOH)H ₂ C(=O)OO•	3.38E+68	-21.47	7828	a
C(OOH)H ₂ C•(=O)+O ₂ = CHOC(=O)OOH+OH	2.06E+16	-1.43	1083	a
C(OOH)H ₂ C(=O)OO• = C(OOH)H ₂ C•(=O)+O ₂	4.99E+50	-14.75	37753	a
C(OOH)H ₂ C(=O)OO• = CHOC(=O)OOH+OH	1.61E+41	-9.97	26200	a
CH ₃ C•O = CH ₂ CO+H	2.33E-23	1.64	38980	a
CH ₃ C•O = CH ₃ +CO	4.87E+06	0.33	12525	a
CH ₃ C•O = C•H ₂ CHO	7.10E-25	1.48	39974	a
C•H ₂ CHO = CH ₂ CO+H	1.43E+38	-8.75	46719	a
C•H ₂ CHO = CH ₃ C•O	5.84E+38	-9.08	46719	a
C(OO•)H ₂ CHO+NO = C(O•)H ₂ CHO+NO ₂	1.26E+12	0.0	1133	e
C(O•)H ₂ CHO = CH ₂ O+HCO	8.72E+22	-4.9	12378	a
C(O•)H ₂ CHO = CHOCHO+H	2.94E+13	-2.2	28503	a
CH ₃ +O ₂ = CH ₂ O+OH	2.61E+08	1.01	12487	f
CH ₃ +O ₂ = CH ₃ OO	1.99E+31	-6.72	4212	f
CH ₃ OO = CH ₂ O+OH	1.99E+20	-7.76	47315	a
CH ₃ +CH ₂ O = HCO+CH ₄	5.54E+03	2.81	5862	g
CH ₃ +HO ₂ = CH ₃ O+OH	1.81E+13	0.0	0	b
CH ₃ O = CH ₂ O+H	6.13E+28	-5.65	31351	f
CH ₃ O+HO ₂ = CH ₂ O+H ₂ O ₂	3.01E+11	0.0	0	g
CH ₂ O+O = OH+HCO	1.81E+13	0.0	3080	g
CH ₂ O+H = H ₂ +HCO	2.29E+10	1.05	3279	b
CH ₂ O+OH = H ₂ O+HCO	3.44E+09	1.18	-447	b
HCO+O ₂ = CO+HO ₂	6.25E+15	-1.15	2018	f
HCO+O ₂ = CO ₂ +OH	5.45E+14	-1.15	2018	f
CO+O = CO ₂	6.17E+14	0.0	3001	g

Table 4.9 Detailed Mechanism (Continued)

Reactions	A	n	<i>E_a</i>	References
CO+OH = CO ₂ +H	6.32E+06	1.5	-497	g
CO+HO ₂ = CO ₂ +OH	1.51E+14	0.0	23650	g
CO+O ₂ = CO ₂ +O	2.53E+12	0.0	47693	g
H+O ₂ +M = HO ₂ +M	1.41E+18	-0.8	0	b
H+O ₂ = OH+O	1.99E+14	0.0	16802	b
OH+OH = O+H ₂ O	1.51E+09	1.14	99	b
H ₂ +OH = H ₂ O+H	1.02E+08	1.6	3300	b
H+OH+M = H ₂ O+M	2.21E+22	-2.0	0	b
O+HO ₂ = OH+O ₂	1.75E+13	0.0	-397	h
OH+HO ₂ = H ₂ O+O ₂	1.45E+16	-1.0	0	g
H+HO ₂ = OH+OH	1.69E+14	0.0	874	g
H+HO ₂ = H ₂ +O ₂	6.62E+13	0.0	2126	g
H+HO ₂ = H ₂ O+O	3.01E+13	0.0	1721	b
H+O+M = OH+M	4.71E+18	-1.0	0	g
H ₂ O ₂ +M = OH+OH+M	1.21E+17	0.0	45507	b
H ₂ O ₂ +OH = H ₂ O+HO ₂	1.75E+12	0.0	318	h
H ₂ O ₂ +O = OH+HO ₂	9.63E+06	2.0	3974	g
H ₂ O ₂ +H = OH+H ₂ O	2.41E+13	0.0	3974	g
H ₂ O ₂ +H = HO ₂ +H ₂	4.82E+13	0.0	7949	g
CH ₄ +HO ₂ = H ₂ O ₂ +CH ₃	9.04E+12	0.0	24641	b
2HO ₂ = 2OH+O ₂	1.00E+12	0.0	11500	f
HO ₂ +HO ₂ = H ₂ O ₂ +O ₂	1.87E+12	0.0	1540	b
H+H+M = H ₂ +M	5.44E+18	-1.3	0	g
O+H ₂ = OH+H	5.12E+04	2.67	6285	b

^a From QRRK calculations (3 Torr, 298-2000K). ^b Reference 93. ^c Reference 96. ^d Estimate in this study. ^e Reference 97. ^f Reference 90. ^g Reference 98. ^h Reference 99.

The reactions of CH₃CHO + OH → CH₃C•O and → C•H₂CHO + H₂O are analyzed to model these typical low-pressure flow reactor conditions: 0 – 0.01 s, 300 K, and 3 Torr. The reaction with no O₂ added (mole fraction: CH₃CHO = 1.2 × 10⁻⁴, OH = 3.6 × 10⁻⁶) shows 99% CH₃C•O, acetyl radical, and 1% C•H₂CHO, formyl methyl radical at 0.01 s via OH abstraction paths. This is in agreement with data of Michael et al.¹³ and Slagle et al.¹⁴

Data on concentration versus time for reaction conditions similar to those above: reaction time (0 – 1.0 s), plus 3 Torr of O₂ (mole fraction: 9.1×10^{-4}) are illustrated in Figure 4.7. **Formation of CH₃C•O is not included here as we focus on C•H₂CHO** (CH₃C•O is discussed in reference 30). C(OO•)H₂CHO, CO, and CH₂O are the major products; these result from formyl methyl radical reaction with O₂. In the mechanism the diradical, CH₂O•C•O dissociates to CH₂O + CO. Under these conditions (3 Torr of O₂), we observe that 11% of the OH radical is regenerated through the formyl methyl radical with O₂ reaction.

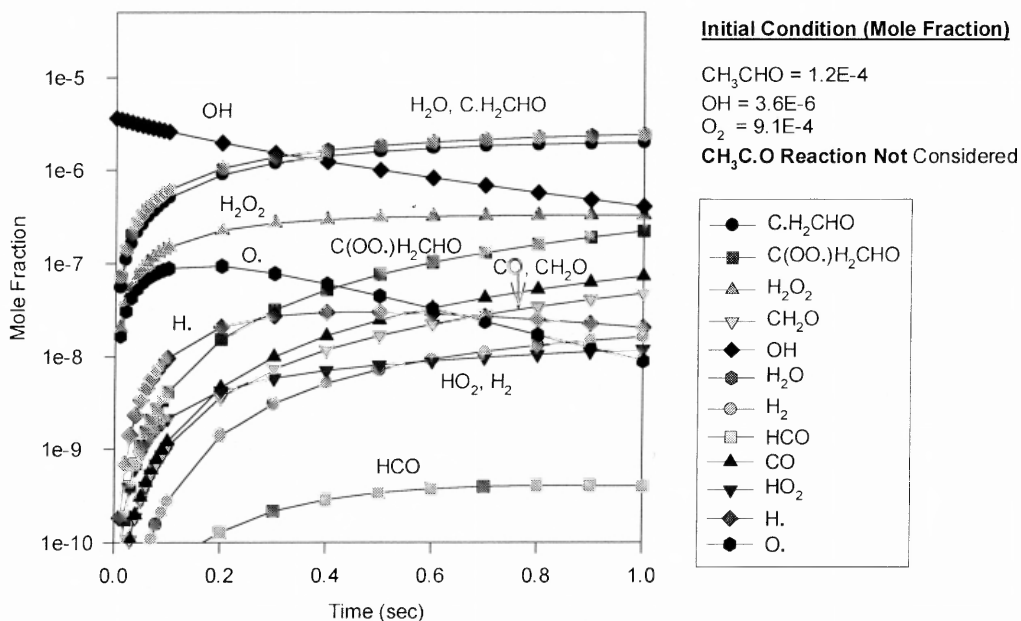


Figure 4.7 Chemkin kinetic calculation: concentration vs. time (OH abstraction of the carbonyl H atom is turned off in these model runs in order to observe the formyl methyl radical formation and its reactions).

Reaction analysis at atmospheric pressure is also modeled with reaction time (0 – 1.0 s), 300 K. (Mole fractions: $N_2 = 0.8$, $O_2 = 0.2$, $CH_3CHO = 1.0 \times 10^{-4}$, and $OH = 1.0 \times 10^{-7}$) The product ratio is determined as 34.12 % $[C(OO\bullet)H_2CHO/OH]$. The concentration of $CO + CH_2O + OH$ product set is about 10^3 times lower to $C(OO\bullet)H_2CHO$.

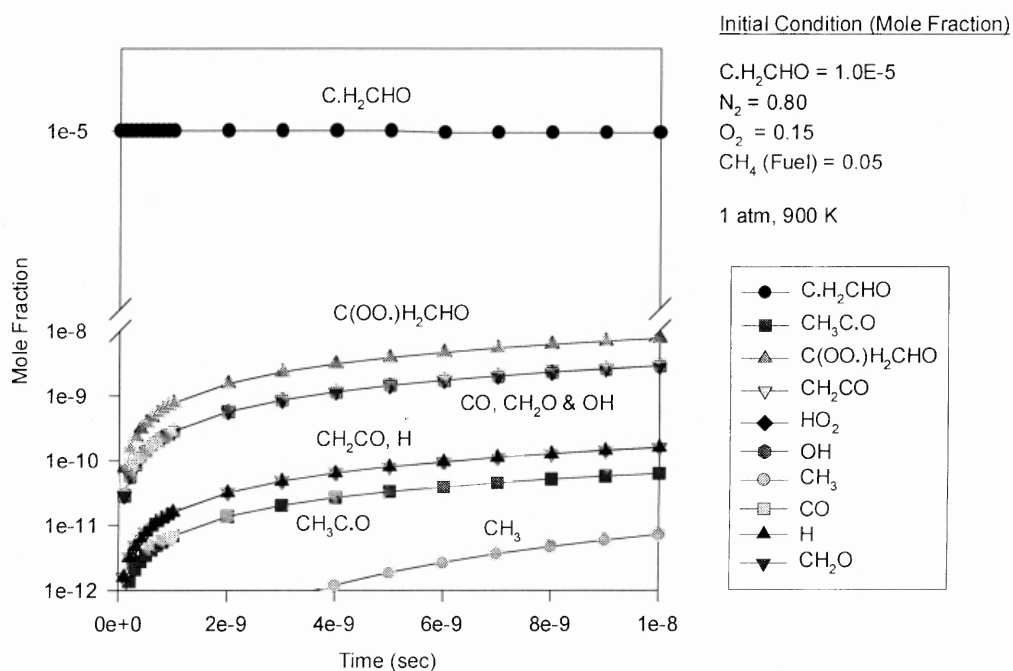


Figure 4.8 Chemkin kinetic calculation: concentration vs. time.

4.3.11 Comparison of $C\bullet H_2CHO + O_2$ with Unimolecular Dissociation of $C\bullet H_2CHO$

The competition between unimolecular dissociation of $C\bullet H_2CHO \rightarrow CH_2CO + H$ versus association of $C\bullet H_2CHO$ with O_2 as a function of reactor temperature is considered. The above mechanism is used for this evaluation because the reaction system is complex and it involves reactions of chemical activated and stabilized $C(OO\bullet)H_2CHO$.

Several reaction condition sets are evaluated, one is the low-pressure flow reactor above.⁹ (1.0 s reaction time with CH_3CHO at 1.2×10^{-4} , $OH = 3.6 \times 10^{-6}$, and $O_2 = 9.1 \times 10^{-4}$ mole fractions). The second condition set is 1 atm pressure; both conditions sets are over varied temperature. The fraction of formyl methyl that reacts with O_2 versus unimolecular dissociation is summarized in Scheme 4.5. It shows the two reaction processes, oxidation and unimolecular dissociation, are competitive around 800 K at 3 Torr. The unimolecular dissociation channel accounts for more than 80% of the reaction at 900 K at 3 Torr.

The third condition set considers the competition between oxidation and dissociation at concentrations more relative to combustion. Mole fractions: ($C\bullet H_2CHO = 1.0 \times 10^{-5}$, $O_2 = 0.15$, $N_2 = 0.80$, and $CH_4(\text{fuel}) = 0.05$). Plots of concentration versus time for 10 ns, at 900 K and 1 atm are illustrated in Figure 4.8. The $C\bullet H_2CHO$ radicals decrease slowly with time, from the oxidation with effectively no unimolecular dissociation. At 0.1 s time, the ratio of oxidation to unimolecular dissociation products, $CO + CH_2O + OH : CH_2CO + H$ is 42:1. The major products are stabilized $C(OO\bullet)H_2CHO$, CO , CH_2O and OH , which result from

formyl methyl radical reaction with O_2 . The $C(OO\bullet)H_2CHO$ has a barrier to $C\bullet H_2CHO + O_2$ of only 27.5 kcal/mol and it dissociates rapidly at this temperature. It is not a highly stable product.

Scheme 4.5 Fraction of Oxidation and Dissociation of Formyl Methyl Radical
($t = 1.0$ s, mole fraction : $CH_3CHO = 1.2 \times 10^{-4}$, $OH = 3.6 \times 10^{-6}$, and $O_2 = 9.1 \times 10^{-4}$)

T / %	Oxidation		Dissociation	
	3 Torr	1 atm	3 Torr	1 atm
600K	99.9	99.0	0.1	1.0
650K	99.2	86.7	0.8	13.3
700K	95.3	39.8	4.7	60.2
750K	81.3	8.7	18.7	91.3
800K	53.6	1.8	46.4	98.2
850K	27.0	0.5	73.0	99.5
900K	12.1	0.1	87.9	99.9
950K	5.4	0.1	94.6	99.9
1000K	2.6	0.0	97.4	100.0

Products are illustrated in Figure 4.9 for reaction at 1100 K, 1 atm, and short times to evaluate initial reactor paths. The major species are CO, CH_2O , OH, CH_2CO , H and $C(OO\bullet)H_2CHO$; these result from both formyl methyl radical reaction with O_2 and $C\bullet H_2CHO$ unimolecular dissociation to $CH_2CO + H$. Above 1200 K, the major products are ketene and H from the unimolecular dissociation. The oxidation and dissociation channels are competitive around 1100 K under these conditions. Ratios of the product sets are summarized in Scheme 4.6 at varied temperature. These data are in reasonable agreement with the relative unimolecular rate constants where $[O_2]$

was included in the bimolecular rate constant for $C\bullet H_2CHO + O_2$ association at these conditions. Similar trends are observed for longer times.

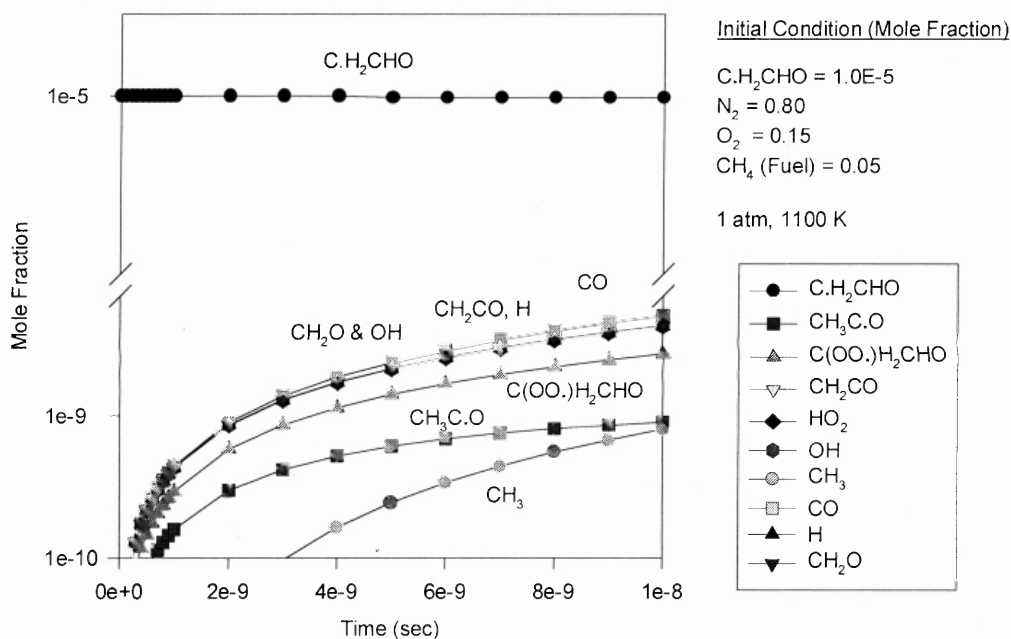


Figure 4.9 Chemkin kinetic calculation: concentration vs. time.

Scheme 4.6 Fraction of Oxidation and Dissociation of Formyl Methyl Radical
($t = 10$ ns, Pressure = 1 atm, mole fraction : $C\bullet H_2CHO = 1.0 \times 10^{-5}$, $O_2 = 0.15$, $N_2 = 0.80$, and $CH_4(\text{fuel}) = 0.05$)

T / %	Oxidation	Dissociation	Ratio
900K	94.8	5.2	0.1
1000K	78.3	21.7	0.3
1100K	50.0	50.0	1.0
1200K	26.2	73.8	2.8
1250K	18.6	81.4	4.4
1300K	13.2	86.8	6.6
1400K	7.0	93.0	13.2
1500K	4.0	96.0	23.8
1600K	2.5	97.5	39.1

(Ratio: Dissociation/Oxidation)

4.4 Summary

Thermochemical properties of stable radicals and transition states on the $C\bullet H_2CHO + O_2$ reaction system are calculated using density functional and ab initio methods. Enthalpies of formation ($\Delta H_f^\circ_{298}$) are determined using isodesmic reactions at the CBSQ level. Entropies (S°_{298}) and heat capacities ($C_p(T)$) include internal rotor contributions. The $C\bullet H_2CHO + O_2$ system is found to have a lower well depth of 27.5 kcal/mol compared to $CH_3C\bullet O + O_2$ and $C_2H_5\bullet + O_2$ as 35.5 and 35.3 kcal/mol, respectively. The H shift and the HO_2 elimination barriers are also significantly different from ethyl and acetyl radical with O_2 reactions. Reaction paths and kinetics are analyzed on $C\bullet H_2CHO + O_2$ reaction system using QRRK for $k(E)$ and master

equation of for falloff. Reaction to products is evaluated versus both pressure and temperature.

Major reaction paths at 1atm pressure are stabilization of peroxy adduct ($C(OO\bullet)H_2CHO$) below 500 K, with reverse dissociation and $CO + CH_2O + OH$ products via H shift important above 1000 K.

A detailed reaction mechanism is constructed which includes pressure dependence for the formyl methyl radical reaction with O_2 . The mechanism is also used to compare the competition between formyl methyl radical decomposition and reaction with O_2 versus temperature.

CHAPTER 5

REACTION OF H + KETENE TO FORMYL METHYL RADICAL AND ACETYL RADICALS AND REVERSE DISSOCIATIONS

5.1 Background

Ketene ($\text{CH}_2=\text{C}=\text{O}$), acetaldehyde and the corresponding formyl methyl and acetyl radicals are important intermediates in the oxidation of higher molecular weight hydrocarbons and oxy-hydrocarbons to CO and CO_2 in combustion systems. The formation of ketene can occur through the unimolecular reactions of formyl methyl and acetyl radicals. The reactions of ketene and of ketenyl radical ($\text{HC}\bullet\text{CO}$) with NO are thought to be of some importance in conversion of NO_x to HCN in fuel reburning.¹²⁰⁻¹²² Ketenyl radical is also involved in formation of polycyclic aromatic hydrocarbons^{123,124} through reactions with highly reactive $^1\text{CH}_2$ and CH radicals.

The reaction of ketenyl radicals with NO has been studied, both experimentally^{125,126} and theoretically,^{121,127} where two products sets for the reaction, (1a) and (1b) below, are identified as important. One product set, $\text{HCN} + \text{CO}_2$, does allow some NO conversion to N_2 and; is therefore indicated to have some affect in reducing NO_x via a re-burn process in thermal and combustion systems.



The formation of ketenyl radical and of ketene, $\text{C}_2\text{H}_2\text{O}$ is reported to occur in conversion acetylene by McEnally et al.,¹²⁴



Another important route to C_2H_2O is the reaction of vinyl radical with O_2 studied by Bozzelli et al.^{18,31} and by Mebel et al.,¹⁰⁰



followed by H atom dissociation (β scission) from $C\bullet H_2CHO$.¹²⁸



The kinetics and products of the reactions of the ketene ($CH_2=C=O$) with atomic hydrogen have been investigated in a number of experimental studies.¹²⁹⁻¹³² Carr et al.¹²⁹ and Slemr et al.¹³⁰ both indicated that the major reaction products are CH_3 and CO using the discharge flow-mass spectrometric studies. Thus, suggesting that the reaction can be written as



The rate constant for reaction (6) was determined by Carr et al.¹²⁹ and Slemr et al.¹³⁰ to be $7.8 \times 10^{10} \text{ cm}^3/(\text{mol}\cdot\text{s})$ and $(7.2 \pm 0.6) \times 10^{10} \text{ cm}^3/(\text{mol}\cdot\text{s})$ at room temperature, respectively. Slemr et al.¹³⁰ also measured the rate constant as function of temperature and obtained $k_6(T) = (3.6 \pm 1.3) \times 10^{12} \times e^{(-2341 \pm 199/RT)} \text{ cm}^3/(\text{mol}\cdot\text{s})$ for 218-363 K. Michael et al.¹³¹ used different techniques, flash photolysis-resonance fluorescence (FP-RF) and discharge flow-resonance fluorescence (DF-RF) to study the kinetics of this reaction system. The measured values at room temperature were $(3.73 \pm 1.01) \times 10^{10} \text{ cm}^3/(\text{mol}\cdot\text{s})$ and $(4.4 \pm 0.8) \times 10^{10} \text{ cm}^3/(\text{mol}\cdot\text{s})$, respectively. They also reported the rate constant as function of temperature which value was $k_6(T) = (1.13 \pm 0.67) \times 10^{13} \times e^{(-3428 \pm 378/RT)} \text{ cm}^3/(\text{mol}\cdot\text{s})$ over the temperature range 298 – 500 K by the FP-RF technique.

Frank et al.¹³² deduced $(1.8 \pm 0.6) \times 10^{13} \text{ cm}^3/(\text{mol}\cdot\text{s})$ for the rate constant of reaction (6) between 1650 and 1850 K from the reactions of CH_2 and ketene with CH_2 and H at elevated temperatures in the post-shock region behind reflected shocks. They used atomic and molecular resonance absorption spectrometry for recording H-atom and CO-molecule concentration profiles. Frank et al.¹³² also reported that the measurements of Michael et al.¹³¹ and their high temperature data could be satisfactorily correlated by the transition state theory expression for $k_6(T)$ and their results could be expressed by an empirical correlation curve : $k_6(T) = 4.54 \times 10^9 \times T^{1.28} \times e^{(-3159/R7)} \text{ cm}^3/(\text{mol}\cdot\text{s})$

Rate constants for unimolecular dissociation of both acetyl and formyl methyl radicals have been evaluated, both experimentally^{133,134} and theoretically.^{135,136}

Bencsura et al.¹³³ and Baldwin et al.¹³⁴ measured the rate constant of acetyl radical to methyl plus CO products, reaction (7), as function of temperature, by thermal-mass spectrometry and flash-photolysis gas chromatography, respectively. They obtained $k_7(T) = 2.5 \times 10^{13} \times e^{(-16381/R7)} \text{ s}^{-1}$ for 420-500 K and 0.9 – 6 Torr (Bencsura et al.¹³³) and $2.0 \times 10^{13} \times e^{(-17500/R7)} \text{ s}^{-1}$ for 332-391 K and 248 – 1.8×10^3 Torr (Baldwin et al.¹³⁴). Baulch et al.¹³⁵ also report an evaluated rate constant for reaction (7) of $k_{7,\infty}(T) = 2.8 \times 10^{13} \times e^{(-17148/R7)} \text{ s}^{-1}$ for 300 – 500 K with high-pressure range via literature review.



Colket et al.¹³⁶ estimated the rate constant for dissociation of formyl methyl radical by reactions (8) and (9) as $k_8(T) = 1.0 \times 10^{13} \times e^{(-46997/R7)} \text{ s}^{-1}$ and $k_9(T) = 1.58 \times$

$10^{13} \times e^{(-34997/RT)} \text{ s}^{-1}$ for the temperature range 800 – 1225 K at 760 Torr by methods of thermochemical kinetics.



This study focuses on the reaction of H + ketene ($\text{CH}_2=\text{C}=\text{O}$) to formyl methyl and acetyl radicals and reverse dissociations. Thermochemical properties are estimated for reactants, intermediates, products and transition states in the reaction path using ab initio and density functional calculations. The thermochemical parameters are used to calculate high-pressure limit rate constants using canonical Transition State Theory (TST). Rate constants as a function of temperature and pressure are estimated using a multifrequency quantum RRK analysis for $k(E)$ and the master equation for falloff. The data at relevant pressures and temperatures should be useful to both atmospheric and combustion models.

5.2 Calculation Methods

Enthalpies of formation ($\Delta H_f^\circ_{298}$) for reactants, intermediate radicals, transition states and products are calculated using CBS-QCI/APNO and CBS-Q composite methods in addition to density functionals. The initial structure of each compound or transition state is determined using ROHF or UHF/PM3 in MOPAC,⁶³ followed by optimization and vibrational frequency calculation at HF/6-311G(d,p) level of theory using GAUSSIAN 94.⁶⁴ Zero-point vibrational energies (ZPVE) are scaled by 0.9251 as recommended by Petersson et al.⁶⁷ Single point energy calculations are carried out at the B3LYP/6-31G(d'). The prime in 6-31G(d') indicates the basis set orbitals of

Petersson et al.^{65,66} The complete basis set (CBS-QCI/APNO) method of Petersson and coworkers for computing accurate energies⁶⁷ is chosen as the determining enthalpies used in this kinetic analysis.

The CBS-QCI/APNO calculation sequence is performed on a geometry determined at the QCISD/6-311G(d,p) level followed by single point calculations at the theory level of QCISD(T)/6-311++G(2df,p), MP2=Full/CBSB6 CBSExtrap=(Nmin=5,Pop), HF/CBSB5A SCF=Tight and MP2/CBSB5 CBSExtrap=(Nmin=10,Pop).

The CBS-Q calculation sequence is performed on a geometry determined at the MP2/6-31G(d') level followed by single point calculations at the theory level of QCISD(T)/6-31+G(d'), MP4(SDQ)/CBSB4 and MP2/CBSB3 CBSExtrap=(Nmin=10,Pop) including corrections for unpaired electron and spin contamination in intermediate overlap (i.e., $0 < {}^{\alpha\beta}S_{ij} < 1$) between the α - and β -spin orbitals.⁷⁰

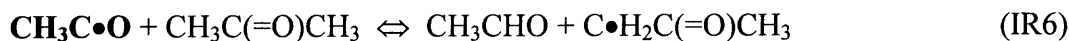
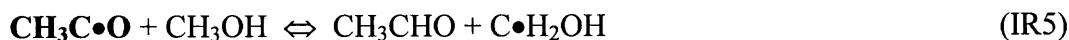
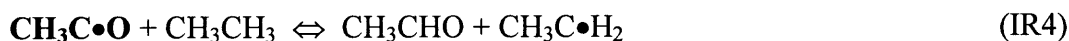
5.2.1 Determination of Enthalpy of Formation

The method of isodesmic reactions is used to determine the enthalpy of formation ($\Delta H_f^\circ_{298}$) for $\text{C}\cdot\text{H}_2\text{CHO}$ and $\text{CH}_3\text{C}\cdot\text{O}$ radical species. It provides higher accuracy for estimates of $\Delta H_f^\circ_{298}$ than heats of atomization.^{71,83,84,113,114}

The working reactions for estimation of $\Delta H_f^\circ_{298}$ on $\text{C}\cdot\text{H}_2\text{CHO}$ are



The working reactions for estimation of $\Delta H_f^\circ_{298}$ on $\text{CH}_3\text{C}\bullet\text{O}$ are



Ab initio calculations with ZPVE and thermal correction are performed on all of four compounds in the reaction. $\Delta H_f^\circ_{298}$ of three compounds in reaction, excepting the target molecule, $\text{C}\bullet\text{H}_2\text{CHO}$, have been experimentally or theoretically determined. The unknown $\Delta H_f^\circ_{298}$ of $\text{C}\bullet\text{H}_2\text{CHO}$ is obtained with the calculated $\Delta H^\circ_{\text{rxn}(298)}$ and known $\Delta H_f^\circ_{298}$ of the three reference compounds. The $\text{CH}_3\text{C}\bullet\text{O}$ is calculated in the same manner.

5.2.2 Determination of Entropy and Heat Capacity

The contributions of external rotations, translations, and vibrations to entropies and heat capacities are calculated from scaled vibration frequencies and moments of inertia for the optimized HF/6-311G(d,p) structures. The number of optical isomers and spin degeneracy of unpaired electrons are also incorporated. Contributions from hindered internal rotation for S and $C_p(T)$ are determined using direct integration over energy levels of the intramolecular rotational potential curves. A program, "ROTATOR¹³⁷", is used for calculation of the energy levels. This technique employs expansion of the hindrance potential in the Fourier series (EI), calculation of the Hamiltonian matrix on the basis of wave functions of the free internal rotor, and subsequent calculation of energy levels by direct diagonalization of the Hamiltonian

matrix.¹³⁸⁻¹⁴⁰ The torsional potential calculated at discrete torsion angles is represented by a truncated Fourier series:

$$V(\Phi) = a_0 + \sum a_i \cos(i\Phi) + \sum b_i \sin(i\Phi) \quad i = 1, 2, 3, \dots \text{ (EI)}$$

Values of the coefficients (a_0 , a_i and b_i) are calculated to provide the minimum and maximum of the torsional potentials with allowance of a shift of the theoretical extreme angular positions.¹³⁸⁻¹⁴⁰

Tunneling is included in analysis of the intramolecular hydrogen atom transfer reaction of TS3 and hydrogen atom dissociation reactions, TS1 and TS2. The tunneling corrections are determined using the Erwin-Henry computer code⁷⁴ that is based on Eckart's one-dimensional potential function.⁷⁵ The Erwin-Henry code requires input of vibrational frequencies, moments of inertia, symmetries, electronic degeneracies, and total energies at 0 K of reactants, transition states, and products; imaginary frequencies are also required. Schwartz et al.⁷⁶ note that calculated vibrational frequencies using HF/6-31G(d) level of theory need to be reduced by one-half to one-third in order for calculated transition states rate constant to match experimental data in abstraction reactions from fluorinated methane's.

5.2.3 High-Pressure Limit A Factor (A) and Rate Constant (k_∞) Determination

For the reactions where thermochemical properties of transition state are calculated by ab initio or density functional methods, k_∞ 's are fit by three parameters A, n, and Ea over temperature range from 298 to 2000K, $k_\infty = A (T)^n \exp(-Ea /RT)$. Entropy differences between reactant and transition state are used to determine the pre-exponential factor, A, via canonical Transition State Theory (TST)

$$A = (k_b T/h_p) \exp(\Delta S^\ddagger/R), \quad Ea = \Delta H^\ddagger$$

(h_p is the Planck constant and k_b is the Boltzmann constant.) Treatment of the internal rotors for S and $C_p(T)$ is important here because these internal rotors are often lost in the cyclic transition state structures.

5.2.4 Kinetic Analysis

The potential energy surface and thermochemical properties are evaluated and forward or reverse rate constants (high-pressure limit) for each, elementary reaction step are determined from the calculations and use of literature data for enthalpies of stable molecules.

Multifrequency quantum Rice-Ramsperger-Kassel (QRRK) analysis is used to calculate $k(E)$ with a master equation analysis⁴¹ for falloff. A 500 cal energy grain is used to obtain rate constants as a function of temperature and pressure, for the chemical activation and dissociation reactions. The master equation analysis⁴¹ uses an exponential-down model for the energy transfer function with $(\Delta E)^\circ_{\text{down}} = 1000$ cal/mol, which is constant with temperature. Troe et al.^{42,43} concluded that $(\Delta E)^\circ_{\text{down}}$ is independent of temperature (293 – 866 K) for the rare and diatomic bath gases and Miller et al.⁴⁴ recently determined a value of $(\Delta E)^\circ_{\text{down}} = 500 \text{ cm}^{-1}$ for matching the two-dimensional master equation solutions to the experimental falloff behavior in the $\text{C}_3\text{H}_3 + \text{O}_2$ system with N_2 bath gas. Knyazev et al.⁴⁵ reported that $(\Delta E)^\circ_{\text{down}}$ changes with temperature; they compared three models, two of which are $(\Delta E)^\circ_{\text{down}} = \alpha T$ and $(\Delta E)^\circ_{\text{down}} = \text{constant}$, in reaction of $n\text{-C}_4\text{H}_9 \rightleftharpoons \text{C}_2\text{H}_5 + \text{C}_2\text{H}_4$ with He as bath gas. The difference between the values of the energy barrier height (E) needed to fit the experimental data with these two models for $(\Delta E)^\circ_{\text{down}}$ is only 0.4 kJ/mol; but this is over a relatively narrow temperature range (560 – 620 K). A larger temperature range

(298 – 2000 K) and a constant $(\Delta E)^\circ_{\text{down}}$ (where N_2 is the third body) are used in this study.

The QRRK/master equation analysis is described by Chang et al.^{31,41} The QRRK code utilizes a reduced set of three vibration frequencies which accurately reproduce the molecules' (adduct) heat capacity; the code includes contribution from one external rotation in calculation of the ratio of the density of states to the partition coefficient $\rho(E)/Q$. Comparisons of ratios of these $\rho(E)/Q$ with direct count $\rho(E)/Q$'s are shown to be in good agreement.³⁸ Rate constant results from the quantum RRK-Master equation analysis are shown to accurately reproduce (model) experimental data on several complex systems. They also provide a reasonable method to estimate rate constants for numerical integration codes by which the effects of temperature and pressure can be evaluated in complex reaction systems.

Dissociation rate constants between QRRK-master equation analysis and ChemRate⁴⁶ (Rice-Ramsperger-Kassel-Marcus (RRKM) -master equation analysis) are compared on $C\bullet H_2CHO$ in this study.

5.3. Results and Discussion

5.3.1 Geometries of Intermediate Radicals and Transition States

Figures 5.1 to 5.4 show the QCISD/6-311G(d,p) optimized geometries of the four transition states. All bond lengths are from QCISD/6-311G(d,p) determined geometries. Values in parenthesis indicate MP2/6-31G(d') and B3LYP/6-31G(d') optimized geometry, respectively.

Bond Length (Å)		Bond Angle (deg)		Dihedral Angle (deg)
H2-C1	1.08(1.09,1.08)			
H3-C1	1.08(1.09,1.08)	H3-C1-H2	119.3(117.0,119.9)	
C4-C1	1.34(1.34,1.33)	C4-C1-H2	116.7(115.4,119.1)	C4-C1-H2-H3 -149.3(-140.7,-164.2)
H5-C1	1.89(1.70,2.16)	H5-C1-H2	92.9(94.4,88.4)	H5-C1-H2-H3 95.0(97.2,87.2)
O6-C4	1.16(1.17,1.16)	O6-C4-C1	172.1(170.8,177.1)	O6-C4-C1-H2 -105.0(-109.3,-97.8)

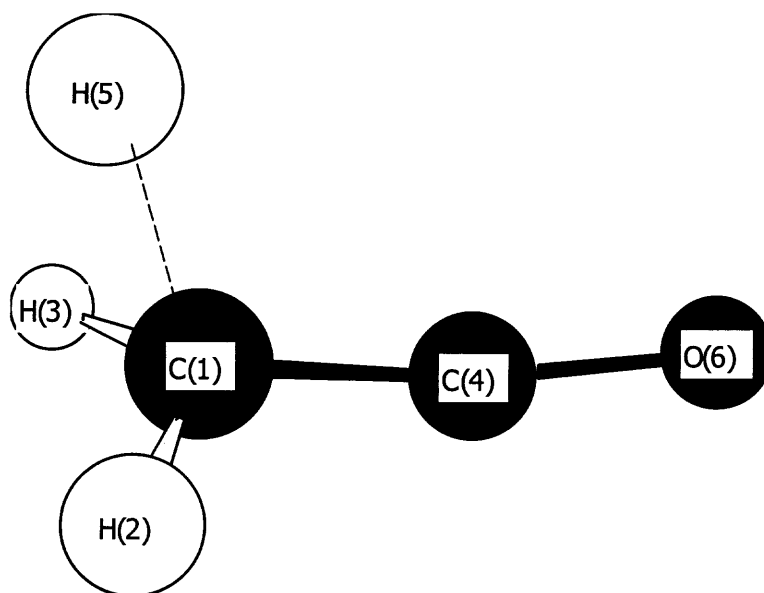


Figure 5.1 Structure for TS1 [$\text{CH}_2=\text{C}=\text{O} + \text{H} \rightarrow \text{TS1} \rightarrow \text{CH}_3\text{C}\cdot\text{O}$].

Bond Length (Å)	Bond Angle (deg)	Dihedral Angle (deg)
H2-C1 1.08(1.09,1.09)		
H3-C1 1.08(1.08,1.08)	H3-C1-H2 120.1(121.1,120.5)	
C4-C1 1.36(1.35,1.34)	C4-C1-H2 117.2(117.4,118.1)	C4-C1-H2-H3 -153.2(-168.1,-173.9)
H5-C4 1.80(1.64,1.90)	H5-C4-C1 91.4(89.5,87.7)	H5-C4-C1-H2 77.0(117.8,126.8)
O6-C4 1.16(1.17,1.17)	O6-C4-C1 162.4(161.1,166.6)	O6-C4-C1-H2 -103.0(-54.5,-44.3)

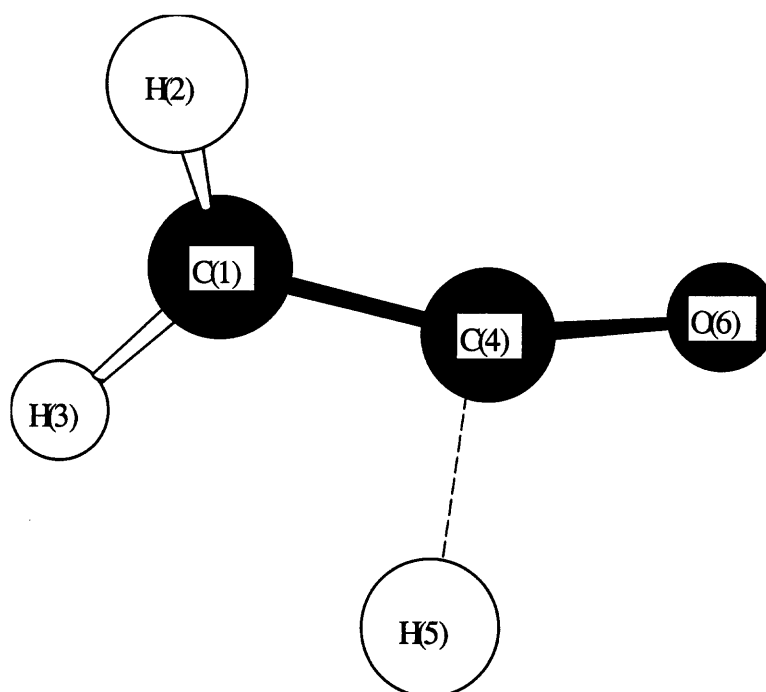


Figure 5.2 Structure for TS2 [$\text{CH}_2=\text{C}=\text{O} + \text{H} \rightarrow \text{TS2} \rightarrow \text{C}\cdot\text{H}_2\text{CHO}$].

Bond Length (Å)		Bond Angle (deg)		Dihedral Angle (deg)	
C2-C1	1.41(1.40,1.40)				
O3-C2	1.20(1.20,1.21)	O3-C2-C1	139.3(144.5,139.8)		
H4-C2	1.28(1.27,1.30)	H4-C2-C1	66.5(68.1,65.5)	H4-C2-C1-O3	122.5(127.9,120.4)
H5-C1	1.09(1.10,1.10)	H5-C1-C2	122.0(122.2,122.7)	H5-C1-C2-O3	-5.5(-7.9,-2.6)
H6-C1	1.08(1.08,1.09)	H6-C1-C2	117.8(118.0,118.2)	H6-C1-C2-O3	169.0(166.2,169.4)

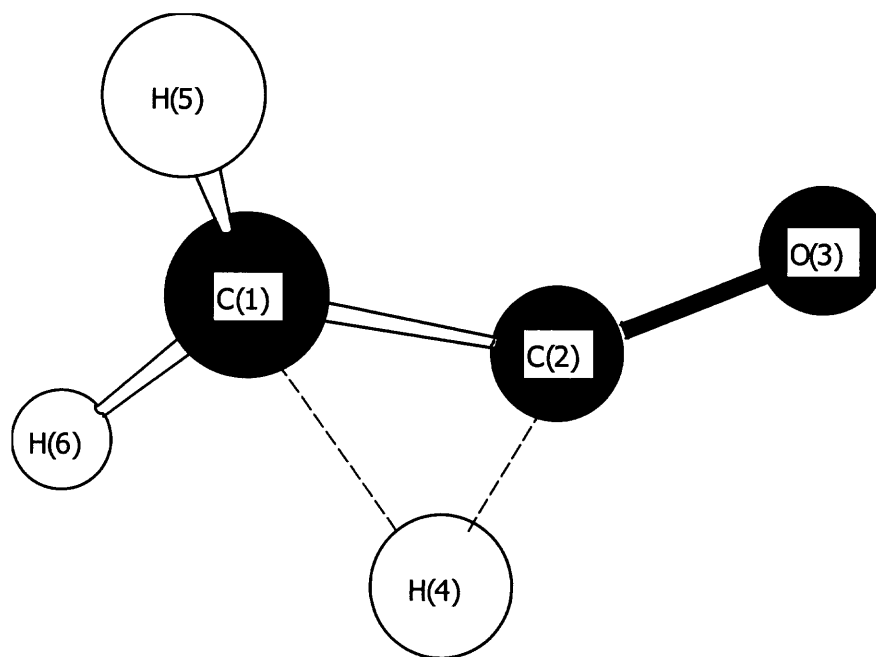


Figure 5.3 Structure for TS3 [$\text{C}\cdot\text{H}_2\text{CHO} \rightarrow \text{TS3} \rightarrow \text{CH}_3\text{C}\cdot\text{O}$].

Figure 5.1 shows the transition state (TS) structure for a hydrogen atom adding to the carbon in CH_2 - group of the ketene to form the acetyl radical: $\text{CH}_2=\text{C}=\text{O} + \text{H} \rightarrow \text{TS1} \rightarrow \text{CH}_3\text{C}\bullet\text{O}$. The C_1 - C_4 bond length in the transition state is calculated as 1.34\AA and the forming C_1 - H_5 bond is calculated as 1.89\AA . The imaginary frequency is calculated as 1110 cm^{-1} at HF/6-311G(d,p).

The TS structure for formation of the formyl methyl radical via hydrogen atom addition to the carbon of the carbonyl group, $\text{CH}_2=\text{C}=\text{O} + \text{H} \rightarrow \text{C}\bullet\text{H}_2\text{CHO}$, TS2 is illustrated in Figure 5.2. The transition state C_1 - C_4 bond length is calculated as 1.36\AA and the forming C_4 - H_5 bond is calculated as 1.80\AA .

Figure 5.3 shows the TS structure for the H shift (isomerization) reaction: $\text{C}\bullet\text{H}_2\text{CHO} \rightarrow \text{TS3} \rightarrow \text{CH}_3\text{C}\bullet\text{O}$. The H_4 atom is in a bridge structure shifting from C_2 to the radical site on C_1 . The leaving H_4 - C_2 and the forming H_4 - C_1 bonds are calculated as 1.28\AA and 1.48\AA , respectively. The calculated imaginary frequency is 2313 cm^{-1} at HF/6-311G(d,p).

The TS structure for decomposition of the acetyl radical to methyl radical + carbon monoxide, $\text{CH}_3\text{C}\bullet\text{O} \rightarrow \text{CH}_3 + \text{CO}$, TS4 is illustrated in Figure 5.4. The leaving C_1 - C_2 bond is calculated as 2.11\AA in length and the forming CO triple bond is 1.15\AA in the TS structure.

Bond Length (Å)	Bond Angle (deg)	Dihedral Angle (deg)
C2-C1 2.11(2.11,2.34)		
O3-C2 1.15(1.16,1.14)	O3-C2-C1 115.1(115.5,113.4)	
H4-C1 1.09(1.09,1.09)	H4-C1-C2 103.1(102.8,99.0)	H4-C1-C2-O3 180.0(180.0,170.0)
H5-C1 1.09(1.09,1.09)	H5-C1-C2 99.6(100.0,97.3)	H5-C1-C2-O3 59.5(59.6,49.6)
H6-C1 1.09(1.09,1.09)	H6-C1-C2 99.6(100.0,96.9)	H6-C1-C2-O3 -59.5(-59.6,-70.0)

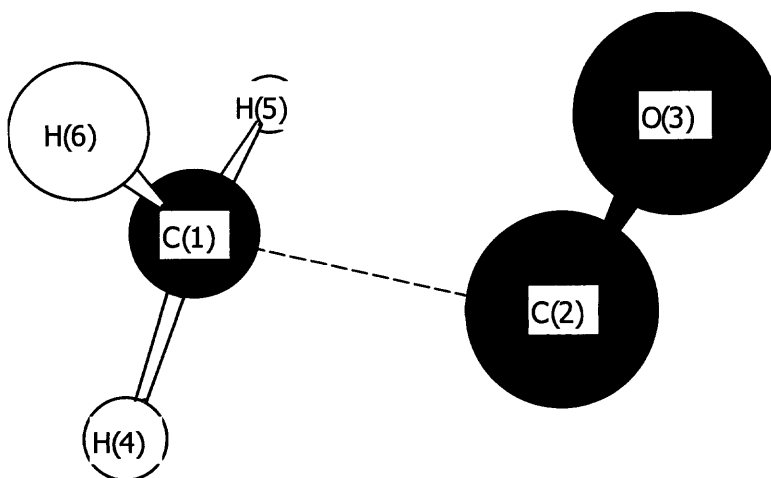


Figure 5.4 Structure for TS4 [$\text{CH}_3\text{C}\cdot\text{O} \rightarrow \text{TS4} \rightarrow \text{CH}_3 + \text{CO}$].

5.3.2 Enthalpy of Formation ($\Delta H_f^\circ_{298}$) using Calculated Total Energies and Isodesmic Reactions

Total energies at 0 K, ZPVE's, thermal corrections to 298.15 K, and total energies at 298 K are shown in Tables 5.1 and 5.2 for CBS-QCI/APNO and CBSQ calculations, respectively. The evaluated enthalpies of formation for the reference molecules and radicals in the isodesmic reactions are listed in Table 5.3. The evaluated reaction enthalpies and enthalpies of formation in the isodesmic reactions are listed in Table 5.4.

A low or zero $\Delta H^\circ_{\text{rxn},298}$ in the working reactions suggests good cancellation of errors in the reaction analysis leading to accurate $\Delta H_f^\circ_{298}$ values, and supports the hypothesis of group additivity. As an example, $\Delta H_f^\circ_{298}[\text{C}\bullet\text{H}_2\text{CHO}]$ is evaluated from

$$\begin{aligned}\Delta H_f^\circ_{\text{rxn},298} &= \Delta H_f^\circ_{298} [\text{CH}_3\text{CHO}] + \Delta H_f^\circ_{298} [\text{CH}_3\text{C}\bullet\text{H}_2] \\ &\quad - \Delta H_f^\circ_{298} [\text{C}\bullet\text{H}_2\text{CHO}] - \Delta H_f^\circ_{298} [\text{CH}_3\text{CH}_3] \\ \Delta H_f^\circ_{\text{rxn},298} &= 6.28 \text{ (CBS-QCI/APNO) and } 5.66 \text{ (CBSQ)}\end{aligned}$$

The enthalpies of formation of $\text{C}\bullet\text{H}_2\text{CHO}$ obtained are 3.04 and 3.66 kcal/mol by CBS-QCI/APNO and CBSQ, respectively.

The enthalpies of formation of $\text{C}\bullet\text{H}_2\text{CHO}$ by CBS-QCI/APNO and CBSQ are also obtained from use of isodesmic reactions (IR2) and (IR3) and values of reference species in Table 5.3. Bond dissociation energies of reference species in these reactions: $\text{H}-\text{CH}_2\text{OH}$ and $\text{CH}_3\text{C}(=\text{O})\text{CH}_2-\text{H}$ are 96.29 and 95.51 kcal/mol, respectively. The data result in enthalpy values of 3.39 and 2.83 kcal/mol by CBS-QCI/APNO and 3.82 and 3.09 kcal/mol by CBSQ in isodesmic reactions (IR2) and (IR3) for $\text{C}\bullet\text{H}_2\text{CHO}$, respectively (Table 5.4).

Table 5.1 List of Total Energy, ZPVE, and Thermal Correction of CBS-QCI/APNO Calculation^a

Species	Total Energy at 0K ^b	ZPVE ^c	Thermal Correction ^d	Total Energy at 298K ^b
CH ₃ CHO	-153.7707680	0.0591580	0.0047460	-153.7659190
CH ₃ C.O ^e	-153.1311580	0.0459650	0.0048410	-153.1262310
C.H ₂ CHO ^e	-153.1205850	0.0444940	0.0043590	-153.1161110
CH ₂ =C=O	-152.5637460	0.0338590	0.0042950	-152.5593550
TS1	-153.0529730	0.0362650	0.0047370	-153.0529730
TS2	-153.0513140	0.0352200	0.0049280	-153.0462350
TS3	-153.0567140	0.0407640	0.0042610	-153.0523600
TS4	-153.1039510	0.0413600	0.0052380	-153.0986160

^a Unit in hartree, 1 hartree = 627.51 kcal/mol.

^b Total Energy from CBS-QCI/APNO Calculation.

^c Non-scaled.

^d Non-scaled.

^e "." stands for radical site.

Table 5.2 List of Total Energy, ZPVE, and Thermal Correction of CBSQ Calculation^a

Species	Total Energy at 0K ^b	ZPVE ^c	Thermal Correction ^d	Total Energy at 298K ^b
CH ₃ CHO	-153.5808040	0.0596140	0.0047500	-153.5760540
CH ₃ C.O ^e	-152.9410302	0.0463440	0.0048310	-152.9361992
C.H ₂ CHO ^e	-152.9300441	0.0447890	0.0043670	-152.9256771
CH ₂ =C=O	-152.3751740	0.0340450	0.0043090	-152.3708650
TS1	-152.8721531	0.0364530	0.0047490	-152.8674041
TS2	-152.8677099	0.0353790	0.0049240	-152.8627859
TS3	-152.8669795	0.0410460	0.0042610	-152.8627185
TS4	-152.9149530	0.0416470	0.0052700	-152.9096830

^a Unit in hartree, 1 hartree = 627.51 kcal/mol.

^b Scaled ZPVE are included. Scaling factor is recommended as 0.91844 by Petersson et.al [67].

^c Non-scaled.

^d Non-scaled.

^e "." stands for radical site.

Table 5.3 Enthalpies of Formation for Reference Molecules in the Isodesmic Reactions

Compounds	ΔH_f° (kcal/mol)	Compounds	ΔH_f° (kcal/mol)
CH ₃ CHO	-39.72 ± 0.12 ^a [77]	CH ₃ CH ₃	-20.24 ± 0.10 ^a [80]
CH ₃ C.H ₂	28.80 ± 0.50 [81]	CH ₃ OH	-48.16 ± 0.07 [78]
C.H ₂ OH	-3.97 ± 0.22 [82]	CH ₃ C(=O)CH ₃	-51.94 ± 0.17 [78]
C.H ₂ C(=O)CH ₃	-8.53 ± 1.15 [83]		

^a The uncertainties are evaluated from ref [78].

Table 5.4 Reaction Enthalpies and Enthalpies of Formation for C•H₂CHO and CH₃C•O (Units: kcal/mol)

Working Reaction Series	$\Delta H_{\text{rxn}}^\circ$		ΔH_f° 298	
	APNO	CBSQ	APNO	CBSQ
C.H ₂ CHO + CH ₃ CH ₃ <=> CH ₃ CHO + CH ₃ C.H ₂	6.28	5.66	3.04	3.66
C.H ₂ CHO + CH ₃ OH <=> CH ₃ CHO + C.H ₂ OH	1.08	0.65	3.39	3.82
C.H ₂ CHO + CH ₃ C(=O)CH ₃ <=> CH ₃ CHO + C.H ₂ C(=O)CH ₃	0.86	0.60	2.83	3.09
Average for C.H ₂ CHO		3.08 ± 0.28	3.52 ± 0.38	
CH ₃ C.O + CH ₃ CH ₃ <=> CH ₃ CHO + CH ₃ C.H ₂	12.63	12.26	-3.31	-2.94
CH ₃ C.O + CH ₃ OH <=> CH ₃ CHO + C.H ₂ OH	7.43	7.25	-2.96	-2.78
CH ₃ C.O + CH ₃ C(=O)CH ₃ <=> CH ₃ CHO + C.H ₂ C(=O)CH ₃	7.21	7.20	-3.52	-3.51
Average for CH ₃ C.O		-3.27 ± 0.28	-3.08 ± 0.38	

The CH₃C•O radical is calculated in the same manner.

The average values of ΔH_f° from three isodesmic reactions for C•H₂CHO and CH₃C•O are 3.08 and -3.27 kcal/mol with respective bond dissociation energies, 94.90 and 88.55 kcal/mol by CBS-QCI/APNO.

The activation energies and enthalpies of transition states in CBS-QCI/APNO level are summarized in Table 5.5.

Table 5.5 Activation Energies and Enthalpies of Transition States in CBS-QCI/APNO Calculation (Units: kcal/mol)

Reactant	Transition State	Product	E_a	$\Delta H_f^\circ_{298}$ of TS
$\text{CH}_2=\text{C}=\text{O} + \text{H}$	TS1	$\text{CH}_3\text{C}.\text{O}$	2.49	42.70
$\text{CH}_2=\text{C}=\text{O} + \text{H}$	TS2	$\text{C}.\text{H}_2\text{CHO}$	6.72	46.93
$\text{C}.\text{H}_2\text{CHO}$	TS3	$\text{CH}_3\text{C}.\text{O}$	40.00	43.08
$\text{CH}_3\text{C}.\text{O}$	TS4	$\text{CH}_3 + \text{CO}$	17.33	14.06

5.3.3 Entropy ($S^\circ_{(298)}$) and Heat Capacity ($C_p(T)$)

Entropy and heat capacities are calculated based on vibration frequencies and moments of inertia of the optimized HF/6-311G(d,p) and HF/6-31G(d') structures.

The calculation results using QCISD/6-311G(d,p) and MP2/6-31G(d') determined geometries and scaled HF/6-311G(d,p) or /6-31G(d') determined frequencies are summarized in Table 5.6. TVR represents the sum of the contributions from translation, vibrations and external rotations for $S^\circ_{(298)}$ and $C_p(T)$'s. Symmetry, number of optical isomers and electronic spin are incorporated in estimation of $S^\circ_{(298)}$ as described in Table 5.6. Torsion frequencies are omitted in these calculations, instead, contributions from internal rotation for $S^\circ_{(298)}$ and $C_p(T)$'s are determined using direct integration over energy levels of the intramolecular rotational potential curves¹³⁸⁻¹⁴⁰ and noted in Table 5.6. Thermochemical properties ($50 \text{ K} \leq T \leq 5000 \text{ K}$) are summarized in Table 5.7.

Table 5.6 Ideal Gas Phase Thermochemical Properties Obtained by CBS-QCI/APNO, CBSQ Calculation and by Therm^a

Species (s, e, OI) ^g		ΔH_f° ^b	S° ^c	Cp_{300}° ^c	Cp_{400}	Cp_{500}	Cp_{600}	Cp_{800}	Cp_{1000}	Cp_{1500}
CH ₃ CHO (3,0,1)	TVR ^d		57.94 ^g	11.57	14.29	16.90	19.23	23.02	25.85	30.14
	Internal Rotor 1 ^f		5.28	1.52	1.34	1.24	1.17	1.10	1.06	1.03
	Total(CBS-APNO)		63.22	13.09	15.63	18.14	20.40	24.12	26.91	31.17
	Total(CBSQ)		63.13	13.02	15.59	18.11	20.37	24.08	26.87	31.13
	THERM	-39.18	63.13	13.22	15.71	18.22	20.47	24.22	26.97	
CH ₃ C.O (3,1/2,1)	TVR		58.79	11.12	13.26	15.27	17.05	19.94	22.10	25.42
	Internal Rotor 1		5.54	1.07	1.04	1.03	1.02	1.01	1.00	1.00
	Total(CBS-APNO)	-3.27	64.33	12.19	14.30	16.30	18.07	20.95	23.10	26.42
	Total(CBSQ)	-3.08	64.27	12.28	14.34	16.30	18.05	20.92	23.08	26.39
	THERM	-2.73	64.27	12.28	14.34	16.30	18.05	20.92	23.08	
C.H ₂ CHO (1,1/2,1)	TVR ^d		61.92	13.05	15.76	18.03	19.86	22.64	24.65	27.69
	Total(CBS-APNO)	3.08	61.92	13.05	15.76	18.03	19.86	22.64	24.65	27.69
	Total(CBSQ)	3.52	61.99	13.10	15.79	18.04	19.86	22.63	24.62	27.66
	THERM	3.62	61.99	13.10	15.79	18.04	19.86	22.63	24.62	
CH ₂ =C=O (2,0,1)	TVR		57.48	12.20	14.07	15.59	16.84	18.82	20.30	22.63
	Total(CBS-APNO)	-11.89	57.48	12.20	14.07	15.59	16.84	18.82	20.30	22.63
	Total(CBSQ)	-12.59	57.57	12.26	14.10	15.61	16.85	18.81	20.29	22.61
	THERM	-11.80	57.81	12.68	14.77	16.43	17.75	19.65	20.92	22.91
TS1 (1,1/2,1)	TVR		63.14	14.63	17.02	18.86	20.32	22.53	24.12	26.55
	Total(CBS-APNO)	42.70	63.14	14.63	17.02	18.86	20.32	22.53	24.12	26.55
	Total(CBSQ)	40.09	63.25	14.69	17.05	18.88	20.34	22.53	24.12	26.54
TS2 (1,1/2,1)	TVR		64.05	15.22	17.54	19.29	20.68	22.78	24.31	26.64
	Total(CBS-APNO)	46.93	64.05	15.22	17.54	19.29	20.68	22.78	24.31	26.64
	Total(CBSQ)	42.98	64.09	15.29	17.59	19.33	20.71	22.79	24.31	26.64
TS3 (1,1/2,1)	TVR		61.29	12.10	14.47	16.60	18.41	21.22	23.22	26.13
	Total(CBS-APNO)	43.08	61.29	12.10	14.47	16.60	18.41	21.22	23.22	26.13
	Total(CBSQ)	43.03	61.32	12.12	14.47	16.59	18.40	21.21	23.21	26.11
TS4 (3,1/2,1)	TVR		60.61	12.19	13.90	15.41	16.75	19.01	20.80	23.71
	Internal Rotor 1		5.54	1.07	1.04	1.03	1.02	1.01	1.00	1.00
	Total(CBS-APNO)	14.06	66.15	13.26	14.94	16.44	17.77	20.02	21.80	24.71
	Total(CBSQ)	13.56	66.15	13.38	15.02	16.48	17.79	20.01	21.79	24.69

a : Thermochemical properties are referred to a standard state of an ideal gas of pure enantiomer at 1 atm.

Therm values for stable species are included for comparison [refs 37, 85].

b : kcal/mol. c : cal/mol-K. d : Sum of contributions from translations, vibrations, and external rotations.

f : Contribution from internal rotation.

g : Symmetry number, optical isomer and electronic spin are taken into account, $-R\ln(s)$, $R\ln 2$, $R\ln 2$, respectively. s = number of symmetry, e = electronic spin, OI = number of optical isomer.

Table 5.7 Thermochemical Properties^a (50 K ≤ T ≤ 5000 K)

Species	Temperature (K)	50	100	200	298.15	500	1000	2000	3000	4000	5000
CH ₃ CHO	<i>C_p</i> (T)	8.74	9.77	11.06	13.05	18.14	26.91	33.27	35.07	35.73	36.00
	<i>S</i> ^o (T)	44.92	51.34	58.48	63.23	71.14	86.68	107.73	121.62	131.80	139.81
	$\Delta H^{\circ}(T) - \Delta H^{\circ}(0K)$	0.40	0.80	1.65	2.66	5.54	16.49	46.27	79.60	114.08	149.06
CH ₃ C.O	<i>C_p</i> (T)	9.40	9.46	10.37	12.16	16.30	23.11	28.06	29.47	29.99	30.19
	<i>S</i> ^o (T)	46.59	53.13	59.89	64.33	71.58	85.19	103.07	114.76	123.31	130.03
	$\Delta H^{\circ}(T) - \Delta H^{\circ}(0K)$	0.40	0.80	1.65	2.65	5.31	14.86	40.00	67.90	96.70	125.89
C.H ₂ CHO	<i>C_p</i> (T)	7.95	8.16	10.22	13.00	18.03	24.65	29.22	30.54	31.07	31.32
	<i>S</i> ^o (T)	45.64	51.18	57.36	61.93	69.87	84.68	103.48	115.61	124.48	131.44
	$\Delta H^{\circ}(T) - \Delta H^{\circ}(0K)$	0.40	0.80	1.70	2.84	6.00	16.91	44.35	74.34	105.18	136.39
CH ₂ =C=O	<i>C_p</i> (T)	7.95	8.14	9.99	12.16	15.59	20.31	23.81	24.85	25.26	25.46
	<i>S</i> ^o (T)	41.44	46.98	53.10	57.49	64.62	77.03	92.42	102.30	109.51	115.17
	$\Delta H^{\circ}(T) - \Delta H^{\circ}(0K)$	0.40	0.80	1.69	2.78	5.61	14.72	37.17	61.59	86.67	112.04
TS1	<i>C_p</i> (T)	7.96	8.60	11.64	14.58	18.86	24.13	27.76	28.82	29.23	29.43
	<i>S</i> ^o (T)	45.49	51.14	57.96	63.15	71.76	86.67	104.76	116.25	124.60	131.14
	$\Delta H^{\circ}(T) - \Delta H^{\circ}(0K)$	0.40	0.81	1.81	3.10	6.52	17.45	43.80	72.18	101.23	130.58
TS2	<i>C_p</i> (T)	8.09	9.06	12.19	15.17	19.30	24.31	27.82	28.84	29.25	29.44
	<i>S</i> ^o (T)	45.61	51.47	58.64	64.06	72.95	88.06	106.23	117.73	126.09	132.63
	$\Delta H^{\circ}(T) - \Delta H^{\circ}(0K)$	0.40	0.83	1.88	3.23	6.75	17.82	44.27	72.69	101.76	131.12
TS3	<i>C_p</i> (T)	7.95	8.17	9.81	12.06	16.60	23.22	27.53	28.71	29.17	29.40
	<i>S</i> ^o (T)	45.35	50.90	56.99	61.29	68.61	82.41	100.15	111.57	119.90	126.43
	$\Delta H^{\circ}(T) - \Delta H^{\circ}(0K)$	0.40	0.80	1.69	2.76	5.67	15.86	41.74	69.96	98.94	128.23
TS4	<i>C_p</i> (T)	9.42	9.88	11.45	13.23	16.44	21.81	26.22	27.54	28.03	28.22
	<i>S</i> ^o (T)	47.33	53.99	61.27	66.16	73.76	86.93	103.69	114.61	122.60	128.88
	$\Delta H^{\circ}(T) - \Delta H^{\circ}(0K)$	0.40	0.81	1.74	2.85	5.64	14.82	38.30	64.30	91.16	118.38

a : Thermochemical properties are referred to a standard state of an ideal gas of pure enantiomer at 1 atm.

[Units: ΔH° in kcal/mol, *S*^o and *C_p* in cal/mol-K]

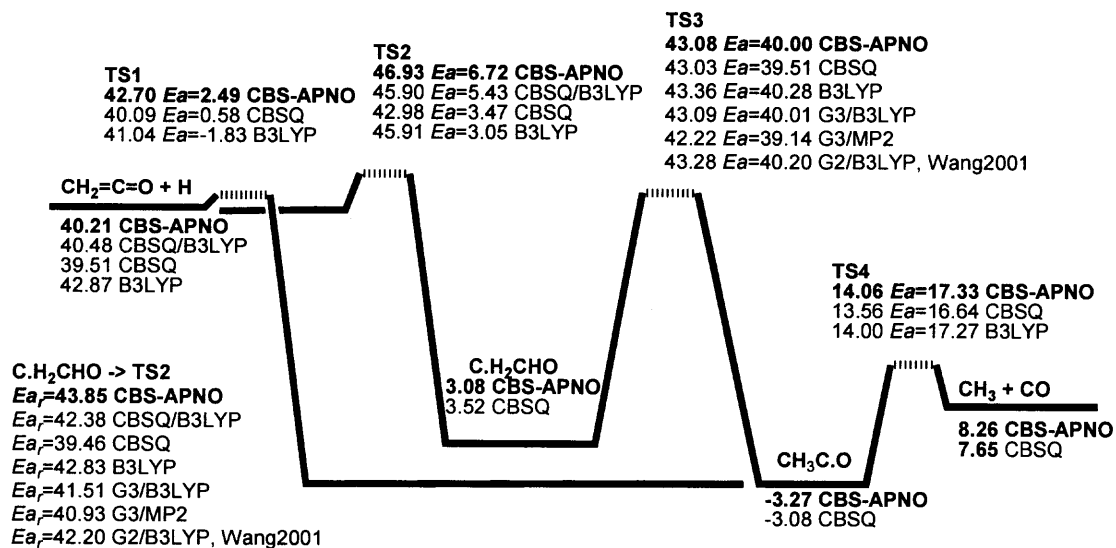


Figure 5.5 Potential energy diagram of $\text{CH}_2=\text{C}=\text{O} + \text{H}$.

5.3.4 Potential Energy Diagram for $\text{CH}_2=\text{C}=\text{O} + \text{H}$ / Formyl Methyl and Acetyl Radical System

The overall energy diagram for the $\text{CH}_2=\text{C}=\text{O} + \text{H}$ reaction to the two adducts is illustrated in Figure 5.5, where enthalpies of formation are from CBS-QCI/APNO calculations and in units of kcal/mol. Transition state enthalpies are relative to the stabilized adduct. Hydrogen atom adds to the CH_2 - carbon of the ketene to form the acetyl radical $\text{CH}_3\text{C}\cdot\text{O}$ ($E_a = 2.49$ kcal/mol, $\Delta H_f^\circ_{298} = -3.27$ kcal/mol). The acetyl radical $\text{CH}_3\text{C}\cdot\text{O}$ can undergo β scission back to reactants, $\text{CH}_2=\text{C}=\text{O} + \text{H}$ ($E_a = 45.97$), isomerize via hydrogen shift ($E_a = 46.35$) to form the slight higher energy, formyl methyl radical $\text{C}\cdot\text{H}_2\text{CHO}$ ($\Delta H_f^\circ_{298} = 3.08$), or decompose to $\text{CH}_3 + \text{CO}$ ($E_a = 17.33$).

The hydrogen atom also can add to the carbon in carbonyl group of the $\text{CH}_2=\text{C}=\text{O}$ to form $\text{C}\bullet\text{H}_2\text{CHO}$ ($E_a = 6.72$). The formyl methyl radical can undergo β -scission back to reactants, $\text{CH}_2=\text{C}=\text{O} + \text{H}$ ($E_a = 43.85$), or isomerize via hydrogen shift ($E_a = 40.00$) to form the acetyl radical isomer, $\text{CH}_3\text{C}\bullet\text{O}$ which can readily decompose to $\text{CH}_3 + \text{CO}$.

5.3.5 Analysis of Chemical Activation Reaction in $\text{CH}_2=\text{C}=\text{O} + \text{H}$ via TS1 and TS2

5.3.5.1 Input Data. The QRRK calculations for $k(E)$ and the master equation analysis for falloff are performed on this $\text{CH}_2=\text{C}=\text{O} + \text{H}$ via TS1 and TS2 to estimate rate constants as a function of temperature and pressure (Table 5.8, input data: high-pressure limit values).

Reduced sets of three vibration frequencies and their associated degeneracies are computed from fits to heat capacity data, as described by Ritter and Bozzelli et al.^{37,38} [$\text{CH}_3\text{C}\bullet\text{O}$: 574.8 cm^{-1} (3.408), 1419.3 cm^{-1} (4.867), 2820.3 cm^{-1} (3.225); $\text{C}\bullet\text{H}_2\text{CHO}$: 584.5 cm^{-1} (3.878), 1236.4 cm^{-1} (5.112), 2938.8 cm^{-1} (3.010)] Lennard-Jones parameters, σ (Å) and ϵ/k (K) are obtained from tabulations¹⁴¹ and from a calculation method based on molar volumes and compressibility.⁸⁹ [$\sigma=4.34\text{Å}$, $\epsilon/k=422.61\text{K}$] (ΔE)_{down}^o = 1000 cal/mol ⁴²⁻⁴⁴ is used for master equation analysis, N_2 is the third body. The units of A factors and rate constants k are s^{-1} for unimolecular reactions and $\text{cm}^3/(\text{mol s})$ for bimolecular reactions.

Table 5.8 Input Parameters^a and High-Pressure Limit Rate Constants (k_{∞})^b for QRRK Calculations**1) Input Data for CH₂=C=O + H via TS1**

Input parameters for QRRK calculations with master equation analysis for falloff

(#) Reaction	A	High-pressure Limit Rate Constants	
		n	k_{∞} Ea (kcal/mol)
TS1-1 CH ₂ =C=O + H => CH ₃ C•O ^c	1.42E+09	1.38	2.56
TS1- (-1) CH ₃ C•O => CH ₂ =C=O + H ^c	4.57E+07	1.85	45.45
TS1-2 CH ₃ C•O => CH ₃ + CO ^c	8.48E+11	0.63	17.78

2) Input Data for CH₂=C=O + H via TS2

Input parameters for QRRK calculations with master equation analysis for falloff

(#) Reaction	A	High-pressure Limit Rate Constants	
		n	k_{∞} Ea (kcal/mol)
TS2-1 CH ₂ =C=O + H => C•H ₂ CHO ^c	8.88E+08	1.53	6.73
TS2- (-1) C•H ₂ CHO => CH ₂ =C=O + H ^c	1.95E+10	1.21	43.77
TS2-2 C•H ₂ CHO => CH ₃ C•O ^c	2.86E+10	0.81	39.18
TS2-3 CH ₃ C•O => CH ₃ + CO ^c	8.48E+11	0.63	17.78

^aGeometric mean frequency [from CPFIT, ref 43,51; CH₃C•O: 574.8 cm⁻¹(3.408) ; 1419.3 cm⁻¹ (4.867) ; 2820.3 cm⁻¹ (3.225); C•H₂CHO: 584.5 cm⁻¹(3.878) ; 1236.4 cm⁻¹ (5.112) ; 2938.8 cm⁻¹ (3.010)], Lennard-Jones parameters: [σ =4.34Å, ϵ/k =422.61K, ref 89,141], (ΔE)^o_{down} of 1000 cal/mol [ref 42-44] is used, N₂ for bath gas.

^bThe units of A factors and rate constants k are s⁻¹ for unimolecular reactions and cm³/(mol-s) for bimolecular reactions.

^cA is calculated using TST and entropy of transition state, $\Delta S^{\ddagger}_{298}$ from HF/6-311G(d,p); Ea is from CBS-QCI/APNO calculation. All parameters A, n, Ea, are fit over the temperature range of 298-2000K.

Table 5.9 Resulting Rate Constants in QRRK Calculations^a for CH₂=C=O + H via TS1

1) Calculated Reaction Parameters at P = 0.01 atm,
 $k = A \times (T)^n \times \exp(-Ea/RT)$ (298 ≤ T/K ≤ 2000)

(#) Reaction	A	n	Ea (kcal/mol)	k ₂₉₈
TS1-1 CH ₂ =C=O + H => CH ₃ C•O	2.66E+15	-6.70	6.18	2.07E-06
TS1-3 CH ₂ =C=O + H => CH ₃ + CO	1.50E+09	1.38	2.57	5.12E+10
TS1-2 CH ₃ C•O => CH ₃ + CO	1.08E+09	-0.18	13.71	3.42E-02

^aThe units of A factors and rate constants k are s⁻¹ for unimolecular reactions and cm³/(mol-s) for bimolecular reactions.

2) Calculated Reaction Parameters at P = 0.1 atm,

(#) Reaction	A	n	Ea (kcal/mol)	k ₂₉₈
TS1-1 CH ₂ =C=O + H => CH ₃ C•O	1.31E+16	-6.62	5.82	2.93E-05
TS1-3 CH ₂ =C=O + H => CH ₃ + CO	1.50E+09	1.38	2.57	5.12E+10
TS1-2 CH ₃ C•O => CH ₃ + CO	5.85E+09	-0.10	13.68	3.06E-01

3) Calculated Reaction Parameters at P = 1 atm,

(#) Reaction	A	n	Ea (kcal/mol)	k ₂₉₈
TS1-1 CH ₂ =C=O + H => CH ₃ C•O	5.69E+16	-6.54	4.26	2.80E-03
TS1-3 CH ₂ =C=O + H => CH ₃ + CO	1.50E+09	1.38	2.57	5.12E+10
TS1-2 CH ₃ C•O => CH ₃ + CO	3.25E-09	5.98	7.87	3.41E+00

4) Calculated Reaction Parameters at P = 10 atm,

(#) Reaction	A	n	Ea (kcal/mol)	k ₂₉₈
TS1-1 CH ₂ =C=O + H => CH ₃ C•O	3.61E+22	-7.91	2.04	3.09E+01
TS1-3 CH ₂ =C=O + H => CH ₃ + CO	1.50E+09	1.38	2.57	5.12E+10
TS1-2 CH ₃ C•O => CH ₃ + CO	8.24E+13	-0.70	15.74	4.33E+00

Table 5.10 Comparison of Rate Constants with Experimental Data

Reference	Method	$k_6(298\text{K})$	Arrhenius Expression	T range (K)
Carr et al.[129]	A	7.8×10^{10}	-	-
Slemr et al.[130]	A	$(7.2 \pm 0.6) \times 10^{10}$	$(3.6 \pm 1.3) \times 10^{12} \times \exp(-2341 \pm 199/RT)$	218 - 363
Michael et al.[131]	B	$(3.73 \pm 1.01) \times 10^{10}$	$(1.13 \pm 0.67) \times 10^{13} \times \exp(-3428 \pm 378/RT)$	298 - 500
	C	$(4.4 \pm 0.8) \times 10^{10}$	-	-
Frank et al.[132]	D	$(1.8 \pm 0.6) \times 10^{13}$	$4.54 \times 10^9 \times T^{1.28} \times \exp(-3159/RT)$	298 - 2000
This study		5.12×10^{10}	$1.50 \times 10^9 \times T^{1.38} \times \exp(-2565/RT)$	298 - 2000

A : Discharge flow-mass spectrometric technique

B : Flash Photolysis Resonance Fluorescence (FP-RF)

C : Discharge Flow-Resonance Fluorescence (DF-RF)

D : Deduced Value (T range : 1650 - 1850 K)

5.3.5.2 Results of Chemical Activation Reaction in $\text{CH}_2=\text{C}=\text{O} + \text{H}$ via TS1.

Resulting calculated data versus temperature and pressure in $\text{CH}_2=\text{C}=\text{O} + \text{H}$ via TS1 are illustrated in Table 5.9.



The rate constant for reaction (6) was calculated to be $5.12 \times 10^{10} \text{ cm}^3/(\text{mol}\cdot\text{s})$ at room temperature and is represented as function of temperature by the Arrhenius expression: $k_6(T) = 1.50 \times 10^9 \times T^{1.38} \times e^{(-2565/RT)} \text{ cm}^3/(\text{mol}\cdot\text{s})$ in 298-2000 K, and over the pressure range (0.01 – 10 atm).

The rate constant at room temperature and the Arrhenius expression for reaction (6) from previous experimental studies and the calculation results in this study are summarized in Table 5.10. An Arrhenius plot of the rate constants versus $1000/T$ along with data of previous studies is illustrated in Figure 5.6, where no adjustment has been made in any of this calculated parameters. The rate constants of

Carr et al.¹²⁹ and Slemr et al.¹³⁰ are about two times higher than data of Michael et al.¹³¹ at room temperature; our value is in between. The rate constants of our study are about 1.5 times higher than those of Michael et al.¹³¹ at 298 – 500K. The rate constants of our study and Frank et al.¹³² show agreement above 500K.

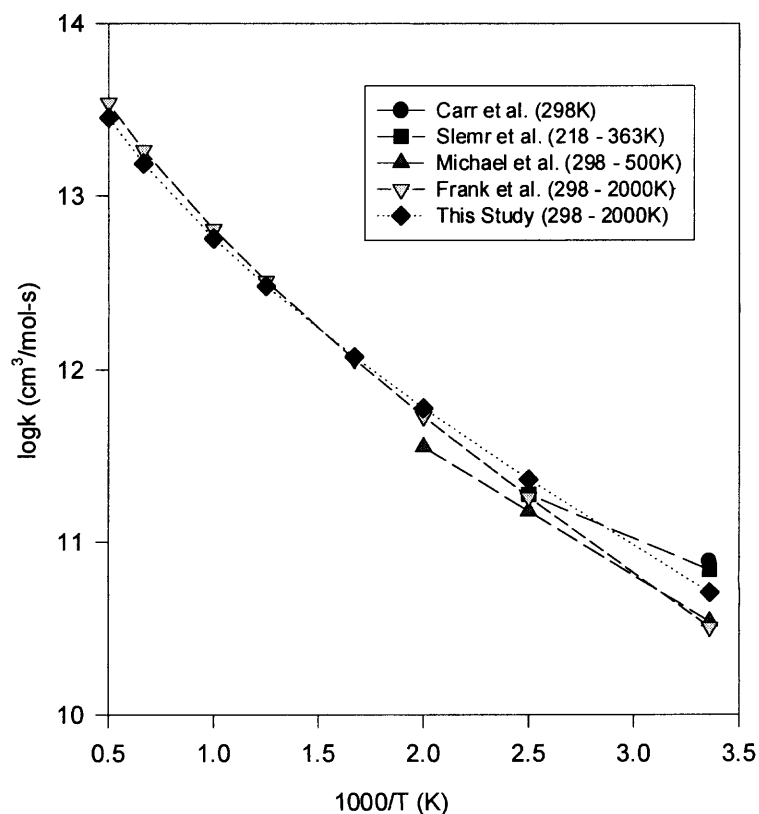


Figure 5.6 Arrhenius plot for the reaction $\text{CH}_2=\text{C}=\text{O} + \text{H} \rightarrow \text{CH}_3 + \text{CO}$.

Table 5.11 Resulting Rate Constants in QRRK Calculations^a for CH₂=C=O + H via TS2

1) Calculated Reaction Parameters at P = 0.01 atm,

$$k = A \times (T)^n \times \exp(-Ea/RT) \quad (298 \leq T/K \leq 2000)$$

(#) Reaction	A	n	Ea (kcal/mol)	k ₂₉₈
TS2-1 CH ₂ =C=O + H => C•H ₂ CHO	1.07E+42	-10.22	12.96	1.74E+07
TS2-4 CH ₂ =C=O + H => CH ₃ + CO	1.54E+14	-0.23	8.23	3.83E+07
TS2-5 CH ₂ =C=O + H => CH ₃ C•O	2.40E+09	-5.29	8.59	9.85E-11
TS2-2 C•H ₂ CHO => CH ₃ C•O	2.21E+39	-8.87	46.51	1.92E-17
TS2-3 CH ₃ C•O => CH ₃ + CO	1.08E+09	-0.18	13.71	3.42E-02

^aThe units of A factors and rate constants *k* are s⁻¹ for unimolecular reactions and cm³/(mol-s) for bimolecular reactions.

2) Calculated Reaction Parameters at P = 0.1 atm,

(#) Reaction	A	n	Ea (kcal/mol)	k ₂₉₈
TS2-1 CH ₂ =C=O + H => C•H ₂ CHO	8.66E+42	-9.89	14.75	4.45E+07
TS2-4 CH ₂ =C=O + H => CH ₃ + CO	8.16E+16	-0.99	10.20	9.51E+06
TS2-5 CH ₂ =C=O + H => CH ₃ C•O	1.58E+16	-6.92	11.70	3.13E-10
TS2-2 C•H ₂ CHO => CH ₃ C•O	3.39E+37	-8.02	46.85	2.10E-17
TS2-3 CH ₃ C•O => CH ₃ + CO	5.85E+09	-0.10	13.68	3.06E-01

3) Calculated Reaction Parameters at P = 1 atm,

(#) Reaction	A	n	Ea (kcal/mol)	k ₂₉₈
TS2-1 CH ₂ =C=O + H => C•H ₂ CHO	7.68E+38	-8.25	14.75	4.52E+07
TS2-4 CH ₂ =C=O + H => CH ₃ + CO	1.76E+17	-1.03	11.89	9.44E+05
TS2-5 CH ₂ =C=O + H => CH ₃ C•O	7.50E+14	-6.18	11.05	3.00E-09
TS2-2 C•H ₂ CHO => CH ₃ C•O	1.50E+33	-6.47	46.17	2.02E-17
TS2-3 CH ₃ C•O => CH ₃ + CO	3.25E-09	5.98	7.87	3.41E+00

Table 5.11 Resulting Rate Constants in QRRK Calculations^a for $\text{CH}_2=\text{C}=\text{O} + \text{H}$ via TS2 (Continued)

4) Calculated Reaction Parameters at $P = 10$ atm,

(#) Reaction	A	n	E_a (kcal/mol)	k_{298}
TS2-1 $\text{CH}_2=\text{C}=\text{O} + \text{H} \Rightarrow \text{C}\bullet\text{H}_2\text{CHO}$	1.46E+32	-5.93	13.42	4.43E+07
TS2-4 $\text{CH}_2=\text{C}=\text{O} + \text{H} \Rightarrow \text{CH}_3 + \text{CO}$	5.50E+12	0.37	11.90	8.44E+04
TS2-5 $\text{CH}_2=\text{C}=\text{O} + \text{H} \Rightarrow \text{CH}_3\text{C}\bullet\text{O}$	2.13E+15	-6.00	8.14	3.26E-06
TS2-2 $\text{C}\bullet\text{H}_2\text{CHO} \Rightarrow \text{CH}_3\text{C}\bullet\text{O}$	4.17E+27	-4.62	44.83	2.05E-17
TS2-3 $\text{CH}_3\text{C}\bullet\text{O} \Rightarrow \text{CH}_3 + \text{CO}$	8.24E+13	-0.70	15.74	4.33E+00

5.3.5.3 Results of Chemical Activation Reaction in $\text{CH}_2=\text{C}=\text{O} + \text{H}$ via TS2.

Resulting calculated data versus temperature and pressure in $\text{CH}_2=\text{C}=\text{O} + \text{H}$ via TS2 are illustrated in Table 5.11.

Rate constants at 1atm versus $1000/T$ are also illustrated in Figure 5.7. Stabilization ($\text{C}\bullet\text{H}_2\text{CHO}$) is important below 600 K, with reverse reaction and $\text{CH}_3 + \text{CO}$ products via H shift both important above 1000 K.

Plots of rate constants at 298 K versus pressure are illustrated in Figure 5.8. Stabilization is the dominant path at pressures above 0.1 atm. $\text{CH}_3 + \text{CO}$ via H shift and reverse dissociation are most important below 0.001 atm.

Rate constants at 1000 K as a function of pressure are illustrated in Figure 5.9. Reverse dissociation and $\text{CH}_3 + \text{CO}$ products via H shift are most important at both high and low pressures. Stabilization is also important above 10 atm and increases as pressure is increased.

5.3.5.4 Overall Results. At room temperature, the rate constant for $\text{CH}_2=\text{C}=\text{O} + \text{H} \rightarrow \text{Products}$ via TS1 channel is about 10^3 times higher than that of $\text{CH}_2=\text{C}=\text{O} + \text{H} \rightarrow \text{Products}$ via TS2. The $\text{CH}_2=\text{C}=\text{O} + \text{H} \rightarrow \text{Products}$ via TS1 channel exhibit no pressure dependence over the range 10^{-4} to 10 atm, which is in agreement with Michael et al.¹³¹ The $\text{CH}_2=\text{C}=\text{O} + \text{H} \rightarrow \text{Products}$ via TS2 increase slowly with increasing pressure (ca. 20% increase from 10^{-4} to 10 atm), but do not contribute a significant fraction to the overall reaction.

5.3.6 Abstraction of Hydrogen Atom in $\text{CH}_2=\text{C}=\text{O}$ by H

A transition state for direct abstraction of hydrogen atom on $\text{CH}_2=\text{C}=\text{O}$ by H to form, ketyl radical plus H_2 is identified with a barrier of 12.27 and 12.16 kcal/mol, at the CBS-QCI/APNO and the CBSQ levels, respectively.



($\Delta H_f^\circ_{\text{rxn},298} = 1.77$ kcal/mol, at CBS-QCI/APNO)

This abstraction channel to form $\text{HC}\cdot\text{CO} + \text{H}_2$ is not competitive with the chemical activation $\text{CH}_2=\text{C}=\text{O}$ by H (addition) via TS1 and TS2 paths below 1500 K at 1 atm.

The enthalpy of formation ($\Delta H_f^\circ_{298}$) of $\text{HC}\cdot\text{CO}$ and the C—H bond dissociation energy of the $\text{CH}_2=\text{C}=\text{O}$ values are 41.98 and 105.97 kcal/mol by CBS-QCI/APNO, respectively.

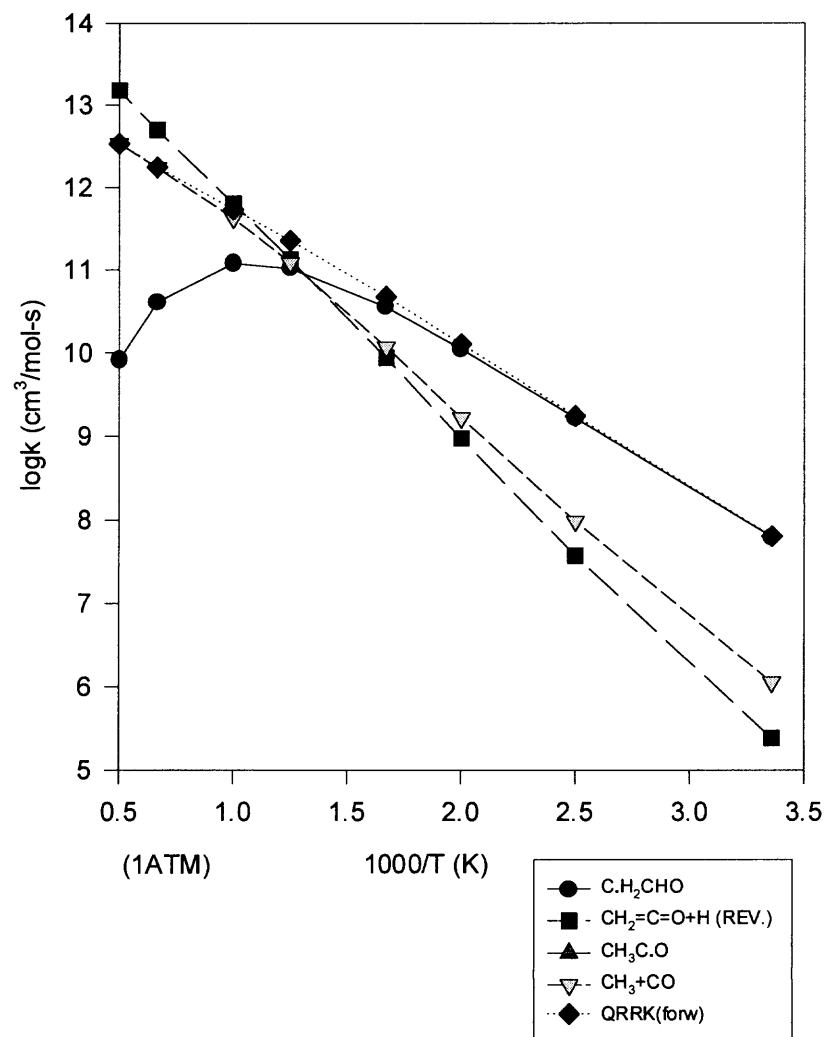


Figure 5.7 $\text{CH}_2=\text{C}=\text{O} + \text{H} \rightarrow \text{products}$ (via TS2) k vs. $1000/T$ at 1 atm.

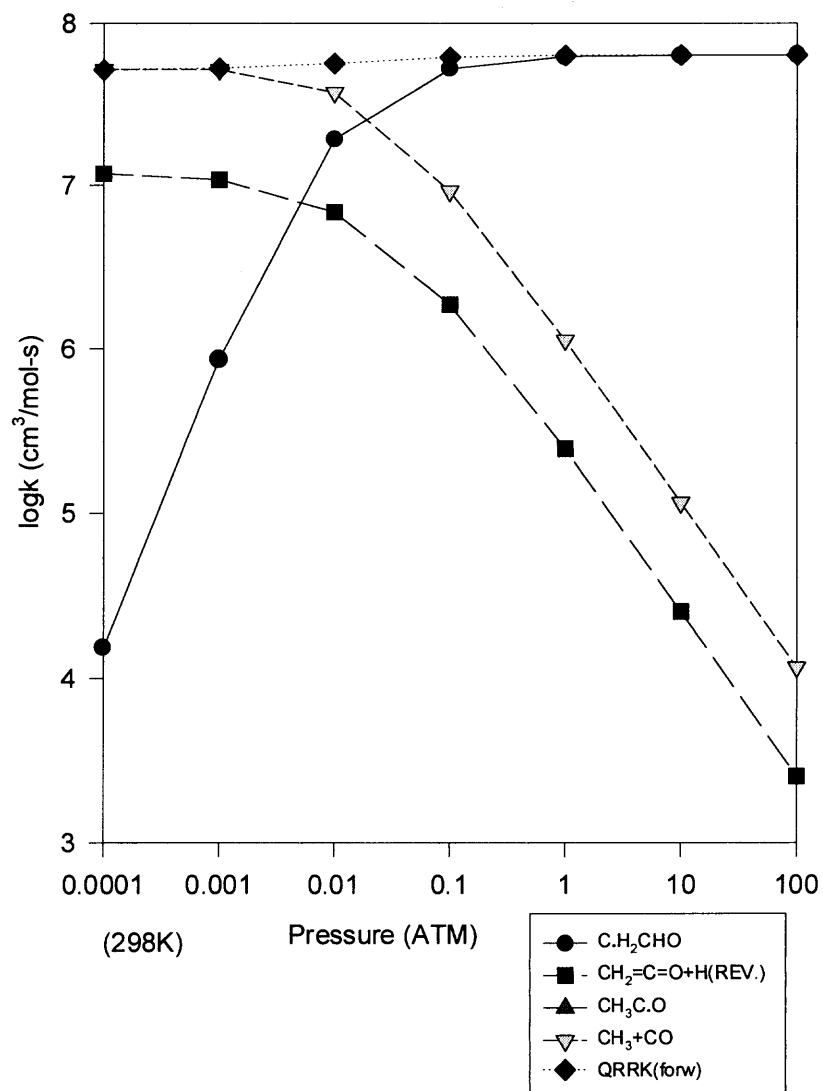


Figure 5.8 $\text{CH}_2=\text{C}=\text{O} + \text{H} \rightarrow \text{products}$ (via TS2) k vs. pressure at 298 K.

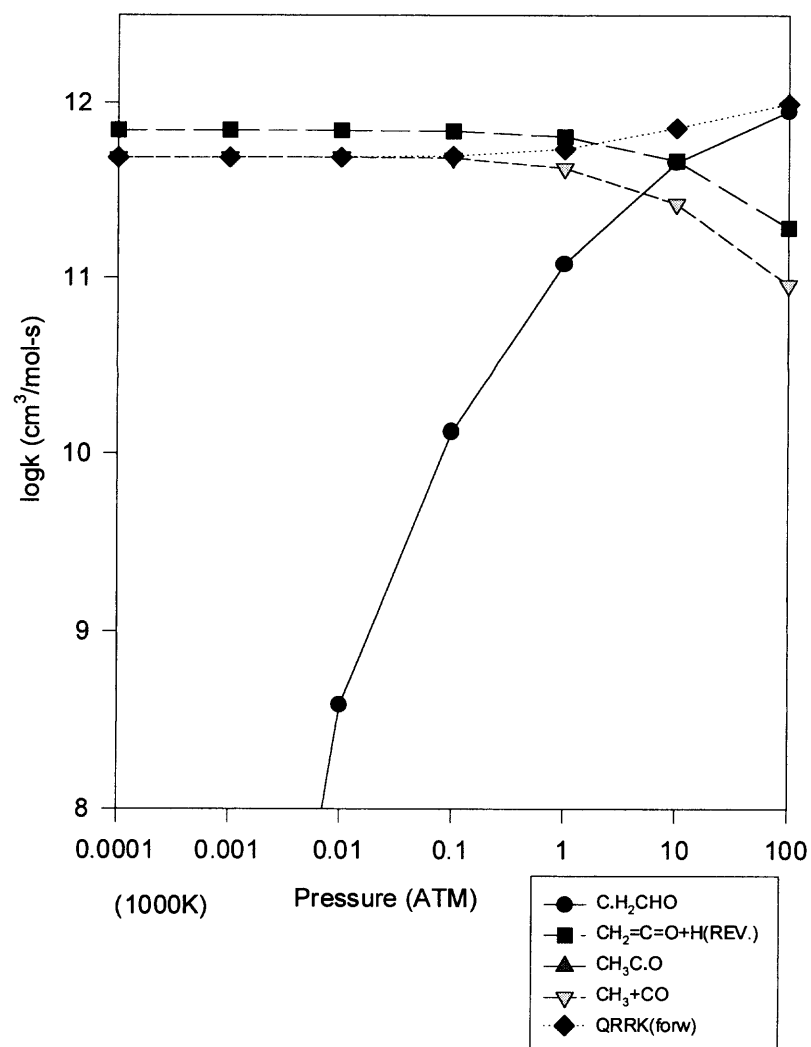


Figure 5.9 $\text{CH}_2=\text{C}=\text{O} + \text{H} \rightarrow \text{products}$ (via TS2) k vs. pressure at 1000 K.

5.3.7 Radical Dissociations

Stabilization of the adducts is observed to be important at lower temperature and moderate pressure conditions. Important products of the dissociation reactions of the stabilized adducts and the rate constants are, therefore, of value.

1) C•H₂CHO Dissociation. Plots of dissociation rate constants at 1 atm pressure versus 1000/T for C•H₂CHO are illustrated in Figure 5.10. CH₃ + CO resulting from a unimolecular H atom shift reaction and the ketene + H products are important and competitive above 500 K.

The rate constants for C•H₂CHO dissociation at 1000 K versus pressure are illustrated in Figure 5.11. The CH₃ + CO product set is the dominant path at both high and low pressures, with ketene + H also important above 10 atm. Any C•H₂CHO formed will dissociate rapidly.

Barriers for C•H₂CHO isomerization to CH₃C•O (8) and dissociation to H + CH₂=C=O (9) in our calculation are 39.1 and 44.4 kcal/mol at 1000 K and 760 Torr, respectively, which are somewhat different from those reported by Colket et al.,¹³⁶ $k_8(T) = 1.0 \times 10^{13} \times e^{(-46997/RT)} \text{ s}^{-1}$ and $k_9(T) = 1.58 \times 10^{13} \times e^{(-34997/RT)} \text{ s}^{-1}$ for the temperature range 800 – 1225 K at 760 Torr.



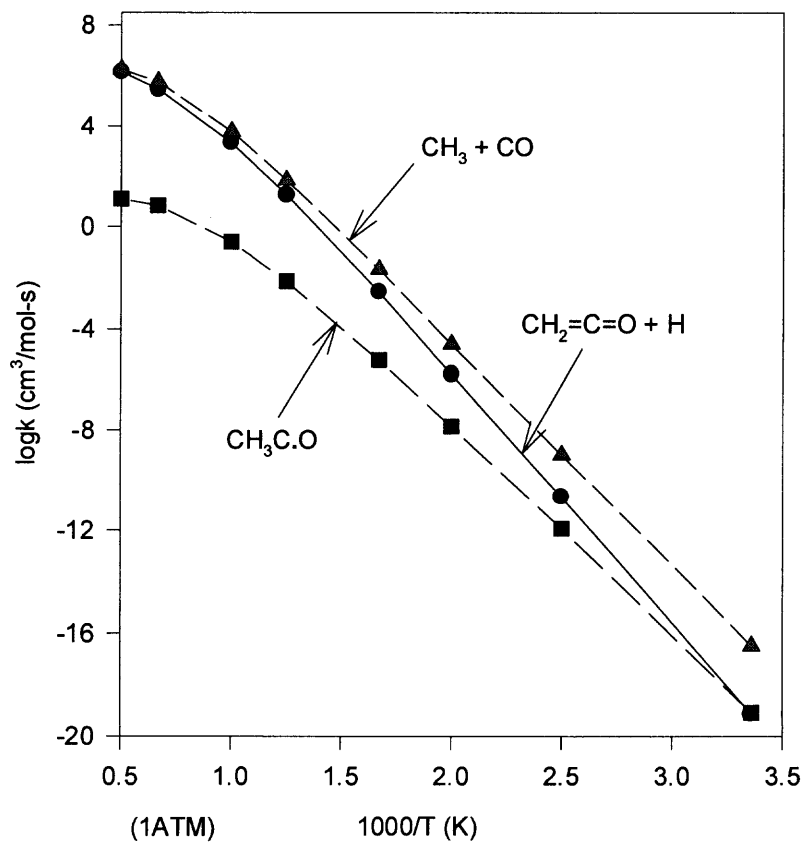


Figure 5.10 $\text{C}\cdot\text{H}_2\text{CHO}$ dissociation k vs. $1000/T$ at 1 atm.

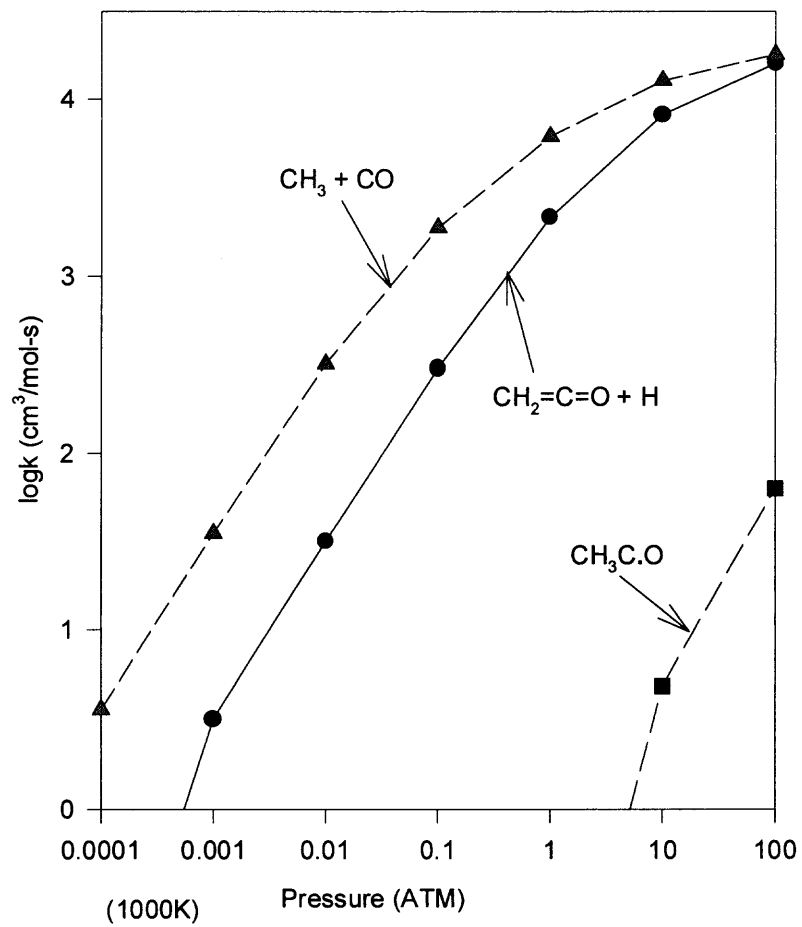


Figure 5.11 $\text{C}\bullet\text{H}_2\text{CHO}$ dissociation k vs. pressure at 1000 K.

2) Comparison of Rate Constants between QRRK with Master Equation and ChemRate (RRKM with Master Equation) on C•H₂CHO Dissociation.

The C•H₂CHO dissociation rate constants at 600 and 1000 K versus pressure from our QRRK- master equation analysis are compared to those of ChemRate⁴⁶ (Rice-Ramsperger-Kassel-Marcus (RRKM)- master equation analysis) in Figures 5.12 and 5.13, respectively. Both QRRK with master equation and ChemRate use harmonic oscillator data only (i.e. no internal rotors).

Dissociation rate constants at 600 K versus pressure for C•H₂CHO are compared in Figure 5.12. The rate constants to CH₃ + CO products via H shift show agreement above 0.01 atm pressures. The rate constants from QRRK with the master equation are, however, 1.1 – 1.3 times higher than those calculated with ChemRate for the CH₂=C=O + H channel at pressures higher than 0.1 atm.

The C•H₂CHO dissociation at 1000 K versus pressure are compared in Figure 5.13. CH₃ + CO products via H shift show agreement over all pressures (0.001 to 100 atm) and the CH₂=C=O + H channel shows agreement above 0.1 atm pressures. Overall the agreement between the two codes is quite good. One possible reason for this agreement is that there is no low barrier internal rotor in the C•H₂CHO because of resonance; hence there are no different treatments of the internal rotation contribution.

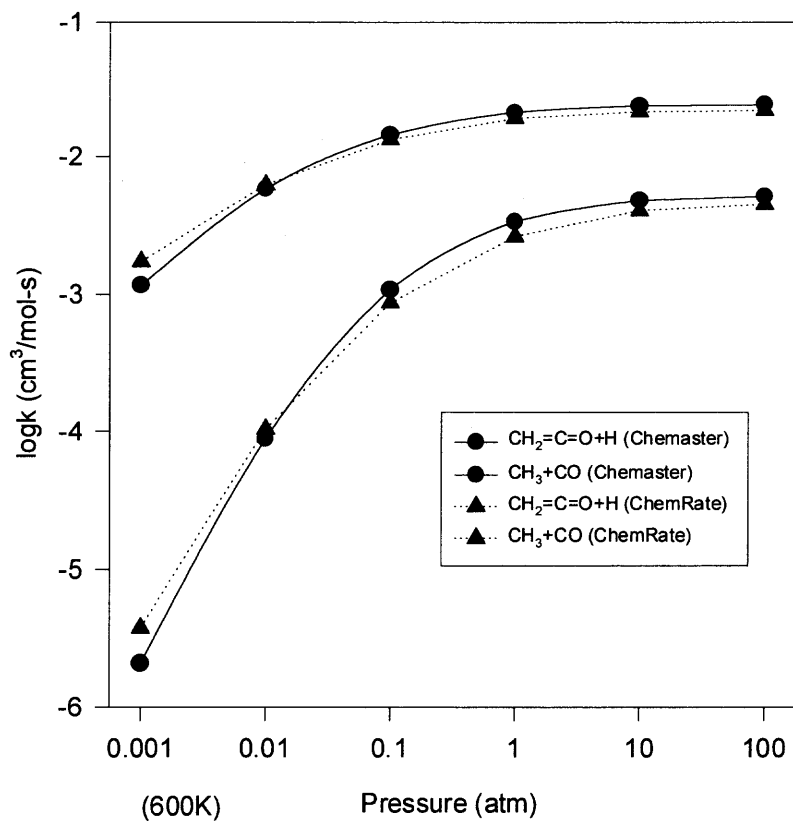


Figure 5.12 Comparison of rate constants between Chemaster and ChemRate with pressure in 600 K with C•H₂CHO dissociation.

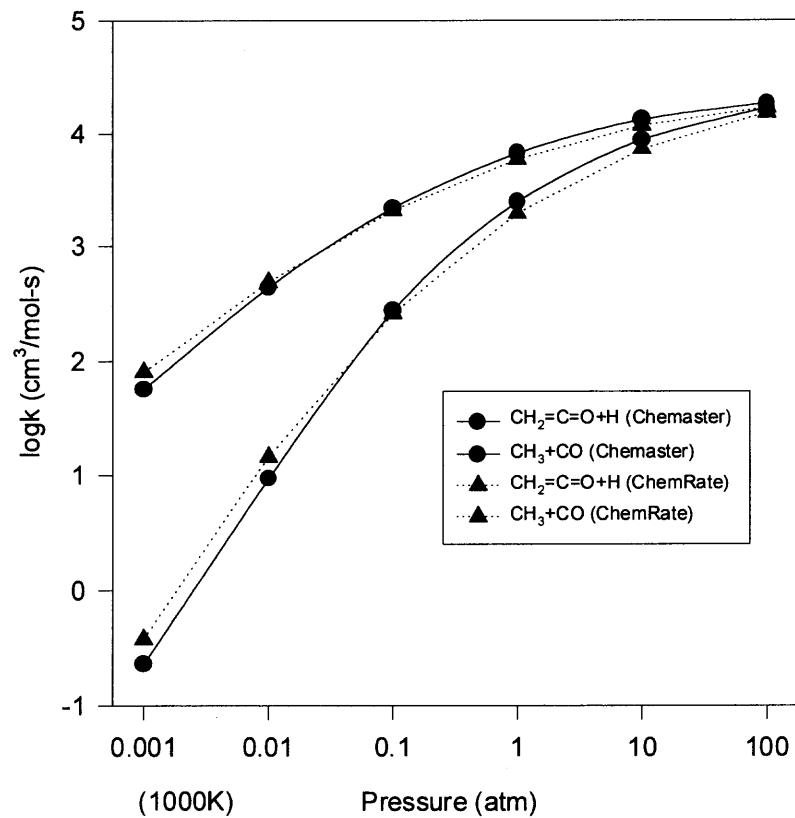


Figure 5.13 Comparison of rate constants between Chemaster and ChemRate with pressure in 1000 K with C•H₂CHO dissociation.

5.4 Summary

Thermochemical properties of stable radicals and transition states on the $\text{CH}_2=\text{C}=\text{O} + \text{H}$ reaction system are calculated using density functional and ab initio methods. Enthalpies of formation ($\Delta H_f^\circ_{298}$) are determined using the CBS-QCI/APNO and the CBSQ level in addition to density functional calculations with isodesmic reactions. Entropies (S°_{298}) and heat capacities ($C_p(T)$) are also determined, with inclusion of internal rotor contributions.

Reaction pathways and kinetics are analyzed on the $\text{CH}_2=\text{C}=\text{O} + \text{H}$ reaction system using QRRK for $k(E)$ and the master equation for falloff. Reaction to products is evaluated versus both pressure and temperature. $\text{CH}_3 + \text{CO}$ is observed to be the major product set at all temperatures (298 K to 2000 K) and pressures (10^{-4} to 100 atm).

The calculated reaction pathways, barriers, and kinetics for the $\text{CH}_2=\text{C}=\text{O} + \text{H}$ reaction system are in a good agreement with experimental data.

The $\text{CH}_2=\text{C}=\text{O} + \text{H} \rightarrow \text{Products}$ via TS1 channel exhibits no pressure dependence over the range 10^{-4} to 10 atm, which is in agreement with Michael et al.,¹³¹ whereas the $\text{CH}_2=\text{C}=\text{O} + \text{H} \rightarrow \text{Products}$ via TS2 show a small pressure dependence, but do not contribute a significant fraction to the overall reaction. Simple QRRK analysis for $k(E)$ with the master equation analysis for falloff and thermochemical properties determined by the CBS-QCI/APNO and the CBSQ methods with working reactions appear to yield accurate results.

CHAPTER 6

THERMOCHEMICAL PROPERTIES, REACTION PATHWAYS AND KINETICS OF THE ALLYL RADICAL WITH O₂ REACTION SYSTEM

6.1 Background

Olefins (Alkenes) are major initial products from pyrolysis, oxidation or photochemical reactions of alkanes and ethers. The double bond in alkenes provides both an unsaturated site for addition reactions and an allylic site for facile abstractions, where the corresponding activation energy is lowered due to electron delocalization on the radical formed. The stability and low reactivity of these alkenyl radicals have been connected to the antiknock effect of fuel additives such as ethyl tert-butyl ether (ETBE).¹⁴² The relatively high octane ratings for olefin blending suggest that olefins play an important role in pre-ignition chemistry related to engine knock. It is valuable to understand the fundamental chemical reaction pathways and kinetics of olefin oxidation in moderate to low temperature combustion chemistry for model development. The oxidation reactions of olefins are also important in the atmospheric photochemistry of hydrocarbons, biochemical synthesis and metabolism.^{143,144}

Ruiz et al.,¹⁴⁵ Morgan et al.,¹⁴⁶ and Slagle et al.^{147,148} have reported the R—O₂ bond energy (17.2, 18.2, 18.4 kcal/mol, respectively) for the allyl (CH₂CHCH₂) radical. Walker and co-workers^{149,150} had studied at a total pressure of 60 Torr between 400 and 520 °C, where the equilibrium in the R + O₂ ⇌ RO₂ addition reaction is shifted to left, the rate constants of the CH₂CHCH₂• + O₂ → products reaction are significantly lower than those observed in the case of alkyl radicals.

Baldwin et al.¹⁵¹ and Lodhi and Walker¹⁴⁹ reported similarly low rate constants for the substituted allyl radicals, $\text{CH}_3\text{CH}_2\text{CHCH}_2\bullet$ and $\text{CH}_3\text{CHCHCH}_2\bullet$ reactions with O_2 . Knyazev and Slagle¹⁴⁸ also studied the kinetics of the reaction $\text{CH}_3\text{CHCHCH}_2\bullet + \text{O}_2 \rightleftharpoons \text{CH}_3\text{CHCHCH}_2\text{O}_2\bullet$ using laser photolysis/photoionization mass spectrometry. Room temperature decay constants of the $\text{CH}_3\text{CHCHCH}_2\bullet$ radical were determined in time-resolved experiments as a function of bath gas density ($[\text{He}] = (3\text{-}24) \times 10^{16} \text{ molecule cm}^{-3}$) and the rate constant at 297 K is $k = (6.42 \pm 0.54) \times 10^{-13} \text{ cm}^3 / (\text{molecule s})$. At high temperatures (600K – 700K), no reaction of $\text{CH}_3\text{CHCHCH}_2\bullet$ with O_2 could be observed and upper limits to the rate constants were determined ($1 \times 10^{-16} \text{ cm}^3 / (\text{molecule s})$ at 600 K and $2 \times 10^{-16} \text{ cm}^3 / (\text{molecule s})$ at 700 K).

Chen et al.¹¹³ studied allylic isobutenyl radical with O_2 . They reported the forward and reverse rate constants for initiation reaction, $\text{CH}_2\text{C}(\text{CH}_3)_2\text{H} + \text{O}_2 \rightleftharpoons \text{CH}_2\text{C}(\text{CH}_3)_2\bullet + \text{HO}_2$ to be $1.86 \times 10^9 \times T^{1.301} \times \exp(-40939 \text{ cal/RT}) \text{ cm}^3 / (\text{mol s})$ and $6.39 \times 10^8 \times T^{0.944} \times \exp(-123.14 \text{ cal/RT}) \text{ cm}^3 / (\text{mol s})$, respectively. They also proposed an important new reaction path, $\text{CH}_2\text{C}(\text{CH}_2\bullet)\text{COOH} \rightleftharpoons \text{CH}_2\text{C}(\text{CH}_2\bullet)\text{CO}\bullet + \text{OH} \rightleftharpoons \text{CH}_2\text{Y}(\text{CCOC}) + \text{OH}$, for methylene oxirane formation.

Olivella et al.¹⁵² recently studied the 1,3-migration of the peroxy group in allylic peroxy radicals. They indicate the chemistry of allylic peroxy radicals involved in the spontaneous autoxidation of unsaturated lipids in biological systems is important in several biological processes: peroxidative destruction of cell membranes, DNA and protein modification, radiation damage, and tumor initiation.^{153,154} In non symmetric allylic radicals, the shift creates a different isomer

and thus a structure than may have a different biochemical function. They reported the well depth is 18.0 kcal/mol at RCCSD(T)/6-311+G(3df,2p) level for $\text{CH}_2=\text{CHC}\bullet\text{H}_2$ addition to O_2 to form the $\text{CH}_2=\text{CHCH}_2\text{OO}\bullet$ peroxy radical with optimized geometry at UMP2/6-311+G(3df,2p) level. They also studied the transition state (TS) structure for cyclization to form a stable five member cyclic peroxide-alkyl radical from the peroxy radical, $\text{CH}_2=\text{CHCH}_2\text{OO}\bullet \rightarrow \text{TS} \rightarrow \text{YCC}\bullet\text{COO}$ (Y represents cyclic) with a barrier of 33.9 kcal/mol. Olivella et al. find transition state (TS1) for adduct formation at 3.7 kcal/mol above the allyl + O_2 reactants (21.7 kcal/mol above the adduct); and while this TS1 transition state can react to the peroxy adduct, it can connect through a weakly bound, symmetric, O_2 – allyl Π adduct (CX), which resides 4.7 kcal/mol below the adduct formation TS structures. They indicate that ‘adduct \rightarrow TS1 \rightarrow CX \rightarrow TS1’ \rightarrow adduct’ is the major path for the 1,3- peroxy migration in biochemical processes. A third highly non symmetric, TS structure (TS2 in Olivella et al), is reported for direct 1,3 peroxy migration at 23.6 kcal/mol above the stabilized peroxy adduct.

This study focuses on the reaction mechanism of the allyl radical association with O_2 . Thermochemical properties are estimated for reactants, intermediates, products and transition states in the reaction paths using ab initio and density functional calculations. The thermochemical parameters are used to calculate high-pressure limit rate constants using canonical Transition State Theory (TST). Rate constants as a function of temperature and pressure are estimated using a multifrequency quantum RRK analysis for $k(E)$ and master equation for falloff. The

data at relevant pressures and temperatures should be useful to both atmospheric and combustion models.

6.2 Calculation Methods

Enthalpies of formation ($\Delta H_f^\circ_{298}$) for reactants, intermediate radicals, transition states and products are calculated using the CBS-Q//B3LYP/6-31G(d,p) composite method and density functionals. The initial structure of each compound or transition state is determined using ROHF or UHF/PM3 in MOPAC,⁶³ followed by optimization and vibrational frequency calculation at B3LYP/6-31G(d,p) level of theory using GAUSSIAN 94.⁶⁴ Transition state geometries are identified by the existence of only one imaginary frequency, structure information and the TST reaction coordinate vibration information. Zero-point vibrational energies (ZPVE) are scaled by 0.9806 as recommended by Scott and Radom.¹⁵⁵ Single point energy calculations are carried out at the B3LYP/6-31G(d,p), /6-311+G(d,p), or /6-311++G(d,p). The CBS-Q method of Petersson and co-workers for computing accurate energies^{68,69} is chosen as the determining enthalpies used in our kinetic analysis.

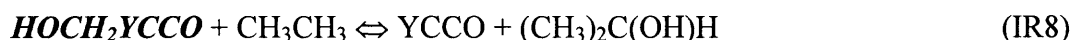
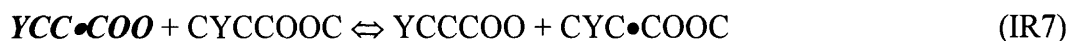
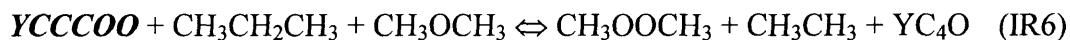
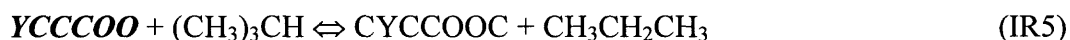
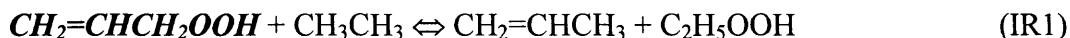
The CBS-Q//B3LYP/6-31G(d,p) calculation sequence is illustrated in Scheme 6.1 [Corrections for unpaired electron and spin contamination in intermediate overlap (i.e., $0 < \alpha\beta S_{ij} < 1$) between the α - and β -spin orbitals⁷⁰ are included].

Scheme 6.1 CBS-Q//B3LYP/6-31G(d,p) Calculation Sequence

	Level of Theory
Optimized Geometry	B3LYP/6-31G(d,p)
Single Point Calculation	QCISD(T)/6-31+G(d')
	MP4(SDQ)/CBSB4
	MP2/CBSB3 CBSExtrap = (Nmin=10,Pop)

6.2.1 Determination of Enthalpy of Formation

The method of isodesmic reactions (IR1 – IR9, *target species* are bold and italicized) is used to determine the enthalpy of formation ($\Delta H_f^\circ_{298}$) for parent and radical species. It provides higher accuracy for estimates of $\Delta H_f^\circ_{298}$ than heats of atomization does.^{71,83,84,113,114}



Ab initio calculations for ZPVE and thermal correction energy are performed on all of four compounds in the reaction. The three reference compounds in the working reaction (IR1), excepting the target molecule, CH₂=CHCH₂OOH in (IR1), have experimental or theoretical determined values of $\Delta H_f^\circ_{298}$. The unknown $\Delta H_f^\circ_{298}$ of CH₂=CHCH₂OOH is obtained with the calculated $\Delta H^\circ_{\text{rxn}(298)}$ and known $\Delta H_f^\circ_{298}$ of the three reference compounds. The other parent and radical species are calculated in the same manner.

6.2.2 Determination of Entropy and Heat Capacity

The contributions of external rotations, translations, and vibrations to entropies and heat capacities are calculated from scaled vibration frequencies and moments of inertia for the optimized B3LYP/6-31G(d,p) structures. The number of optical isomers and spin degeneracy of unpaired electrons are also incorporated. Contributions from hindered internal rotation for S and $C_p(T)$ are determined using direct integration over energy levels of the intramolecular rotational potential curves. A program, “ROTATOR¹³⁷”, is used for calculation of the energy levels. This technique employs expansion of the hindrance potential in the Fourier series (EI), calculation of the Hamiltonian matrix on the basis of wave functions of the free internal rotor, and subsequent calculation of energy levels by direct diagonalization of the Hamiltonian matrix.¹³⁸⁻¹⁴⁰ The torsional potential calculated at discrete torsion angles is represented by a truncated Fourier series:

$$V(\Phi) = a_0 + \sum a_i \cos(i\Phi) + \sum b_i \sin(i\Phi) \quad i = 1, 2, 3, \dots \text{ (EI)}$$

Values of the coefficients (a_0 , a_i and b_i) are calculated to provide the minimum and maximum of the torsional potentials with allowance of a shift of the theoretical extreme angular positions.¹³⁸⁻¹⁴⁰

6.2.3 High-Pressure Limit A Factor (A) and Rate Constant (k_∞) Determination

For the reactions where thermochemical properties of transition state are calculated by ab initio or density functional methods, k_∞ 's are fit by three parameters A, n, and Ea over temperature range from 298 to 2000K, $k_\infty = A (T)^n \exp(-Ea /RT)$. Entropy differences between reactant and transition state are used to determine the pre-exponential factor, A, via canonical Transition State Theory (TST)

$$A = (k_b T/h_p) \exp(\Delta S^\ddagger/R), \quad Ea = \Delta H^\ddagger$$

(h_p is the Planck constant and k_b is the Boltzmann constant.) Treatment of the internal rotors for S and $C_p(T)$ is important here because these internal rotors are often lost in the cyclic transition state structures.

6.2.4 Kinetic Analysis

Thermochemical properties for each species on the potential energy surface for the reaction system are evaluated. Forward or reverse rate constants (high-pressure limit) for each, elementary reaction step are determined from the calculations and use of literature data for enthalpies of stable molecules. Reverse rate constants are calculated from microscopic reversibility.

Multifrequency quantum Rice-Ramsperger-Kassel (QRRK) analysis is used to calculate $k(E)$ with a master equation analysis⁴¹ for falloff in order to obtain rate constants as a function of temperature and pressure. This kinetic analysis is for the

chemical activation and the dissociation reaction systems. The master equation analysis⁴¹ uses an exponential-down model for the energy transfer function with $(\Delta E)^\circ_{\text{down}} = 1000 \text{ cal/mol}$,^{42,45} for N_2 as the third body and a 500 cal energy grain is used.

The QRRK/master equation analysis is described by Chang et al.^{38,41} The QRRK code utilizes a reduced set of three vibration frequencies which accurately reproduce the molecules' heat capacity; the code includes contribution from one external rotation in calculation of the ratio of the density of states to the partition coefficient $\rho(E)/Q$. Comparisons of ratios of these $\rho(E)/Q$ with direct count $\rho(E)/Q$'s have been shown to result in good agreement.³¹ Rate constant results from the quantum RRK-Master equation analysis are shown to accurately reproduce (model) experimental data on several complex systems. They also provide a reasonable method to estimate rate constants for numerical integration codes by which the effects of temperature and pressure can be evaluated in complex reaction systems.

6.3 Results and Discussion

6.3.1 Geometries

Structure parameters for reactant, intermediates and transition states calculated at B3LYP/6-31G(d,p) level are listed in Appendix C (Table C.1). Vibrational frequencies and moments of inertia determined at the same level are listed in Appendix C (Table C.2).

Energies of activation (E_a) reported below are at CBS-Q level and relative to the corresponding stabilized adduct and 298K.

The transition state (TS) structure, TC=CC-O₂, represents CH₂=CHC•H₂ addition to O₂ to form the CH₂=CHCH₂OO• peroxy radical. There is a small barrier to reaction, 0.99 kcal/mol, and the well depth is 19.04 kcal/mol. The CH₂=CHC•H₂ structure is planar with the O₂ group perpendicular to the plane; the forming O₄-C₃ bond length is calculated as 2.17Å. The imaginary frequency is 269 cm⁻¹.

The isomerization: CH₂=CHCH₂OO• → C•H=CHCH₂OOH, is denoted by TC•=CCOOHS (S represents H atom shift). The H₆ atom is in a bridge structure shifting from the C₁ carbon to the radical site O₁₀. The leaving H₆-C₁ bond is 1.49Å and the forming H₆-O₁₀ bond is 1.10Å. The imaginary frequency is 1178 cm⁻¹ and the *Ea* is 28.88 kcal/mol.

The TS structure for β scission of C•H=CHCH₂OOH to products, (C₂H₂ + {C•H₂OOH} → C₂H₂ + CH₂O + OH) is TC•=CCOOH. The cleaving C₂-C₃ bond is 2.28Å and in the transition state the C₃-O₄ is in process of moving to a double bond at 1.36Å; the *Ea* is 28.69 kcal/mol and the imaginary frequency is 486 cm⁻¹. The intermediate C•H₂OOH is not formed, it dissociates to lower energy CH₂O + OH products with little or no barrier.

The TS structure, TALLYL-OHSQ, involves a hydrogen transfer from the ipso carbon to the peroxy radical site forming the unstable intermediate {CH₂=CHC•HOOH}, which immediately dissociates to more stable products, 2-propenal, CH₂=CHC(=O)H + OH. The leaving O₉-O₅ and H₁₀-C₃ bonds are 1.49 and 1.30Å, respectively. The imaginary frequency is 1757 cm⁻¹ and the *Ea* is 37.73 kcal/mol.

The H shift reaction (isomerization) from the secondary sp^2 carbon to the peroxy radical, $\text{CH}_2=\text{CHCH}_2\text{OO}\bullet \rightarrow \text{CH}_2=\text{C}\bullet\text{CH}_2\text{OOH}$, is identified as $\text{TC}=\text{C}\bullet\text{COOHS}$. The H_4 atom is in a bridge structure shifting from C_2 to the radical site O_8 . The leaving $\text{H}_4\text{-C}_2$ bond is 1.41\AA and the forming $\text{H}_4\text{-O}_8$ bond is 1.17\AA . The imaginary frequency is 2060 cm^{-1} and the E_a is 37.97 kcal/mol . This intermediate, $\text{CH}_2=\text{C}\bullet\text{CH}_2\text{OOH}$, will undergo β scission to, $\text{CH}_2=\text{C}=\text{CH}_2 + \text{HO}_2$ through transition state $\text{TC}=\text{C}\bullet\text{COOH}$. The cleaving $\text{O}_4\text{-C}_3$ bond is 1.87\AA and the $\text{C}_2\text{-C}_3$ bond shortens from 1.48 to 1.36\AA . The imaginary frequency is 553 cm^{-1} and the E_a is 15.47 kcal/mol .

The $\text{CH}_2=\text{C}\bullet\text{CH}_2\text{OOH}$ and $\text{C}\bullet\text{H}=\text{CHCH}_2\text{OOH}$ intermediates can also undergo a ring closure reactions.

The $\text{CH}_2=\text{C}\bullet\text{CH}_2\text{OOH}$ will form methylene oxirane (methylene epoxide) plus OH radical via $\text{TC}=\text{YCOC-OH}$ (Y represents cyclic). The radical site on the secondary vinyl carbon attacks the oxygen bonded to the carbon in the peroxy group, with an E_a of 18.17 kcal/mol and a ΔH_{rxn} of -19.54 kcal/mol . The carbon–oxygen bond being formed in the TS is 1.93 \AA in length.

The $\text{C}\bullet\text{H}=\text{CHCH}_2\text{OOH}$ will form an unsaturated oxirane ring (unsaturated cyclic ether), with a very weak (ca. 55 kcal/mol) oxygen – methylene carbon bond. The cyclic ether will undergo a facile ring opening reaction to form the stable 2-propenal, $\text{CH}_2=\text{CHC}(=\text{O})\text{H}$.

The HO_2 molecular elimination: The TS structure for direct HO_2 elimination from the peroxy adduct is $\text{TC}=\text{C}=\text{C-OOHE}$: $\text{CH}_2=\text{CHCH}_2\text{OO}\bullet \rightarrow \text{CH}_2=\text{C}=\text{CH}_2 + \text{HO}_2$. The $\text{O}_9\text{-O}_{10}$ bond shortens from 1.31 to 1.27\AA while the cleaving $\text{O}_9\text{-C}_6$ and $\text{H}_5\text{-}$

C₂ bonds lengthen to 2.27 and 1.37Å, respectively. The imaginary frequency is 1053 cm⁻¹ and the *Ea* is 36.61 kcal/mol. the carbons in C-CH₂OOH are planar with the HO₂ leaving group perpendicular to the plane and parallel with one of the hydrogens on the CH₂=C group.

6.3.1.1 Intramolecular Peroxy Radical Addition to sp² Hybridized Carbons - Cyclization Reaction Paths.

The transition state structure, TYCC•COO, represents cyclization to form a stable five member cyclic peroxide-alkyl radical, YCC•COO, with the reaction from the peroxy radical being near thermo-neutral (only 1.84 kcal/mol exothermic). The peroxy radical undergoes addition to the C=C π bond: CH₂=CHCH₂OO• → [TYCC•COO] → YCC•COO. The forming O₅-C₁ bond is 1.97Å. The imaginary frequency is 695 cm⁻¹ and the *Ea* is 25.07 kcal/mol. Olivella et al.¹⁵² reported the forming O₅-C₁ bond is calculated as 1.98Å at UMP2/6-311+G(3df,2p) level and the *Ea* is 33.9 kcal/mol at RCCSD(T)/6-311+G(3df,2p) level. Boyd et al.¹⁵⁶ have earlier reported an *Ea* of 41 kcal/mol at MP2/6-31G(d,p)//UHF/6-31G(d) level. Chen et al.¹¹³ studied this cyclization path in the allylic isobutenylperoxy radical, CH₂=C(CH₃)CH₂OO• → TS → YCC•(CH₃)COO in the reaction of allylic isobutenyl radical with O₂. They report a barrier to this reaction as 28.17 kcal/mol at CBS-q//MP2/6-31G(d) level. Comparison of activation energies in six different calculation levels is given in Scheme 6.2. Comparison of bond lengths (Å) for the TS structure in four different calculation levels is also given in Scheme 6.3.

Scheme 6.2 Comparison of Activation Energies

Calculation level (Units: kcal/mol)	<i>E_a</i>	Reference
CBS-Q//B3LYP/6-31G(d,p)	25.07	this study
B3LYP/6-31G(d,p)	25.33	this study
CBS-q//MP2/6-31G(d)	28.17	113
B3LYP/6-31G(3df,2p)//B3LYP/6-31G(d)	24.98	113
RCCSD(T)/6-311+G(3df,2p)//UMP2/6-311+G(3df,2p)	33.9	152 (TS3)
MP2/6-31G(d,p)//UHF/6-31G(d)	41	156

Scheme 6.3 Comparison of Bond Lengths in TS Structure

Calculation level (Unit: Å)	C ₁ -C ₂	C ₂ -C ₃	C ₃ -O ₄	O ₄ -O ₅	C ₁ -O ₅
B3LYP/6-31G(d,p) [this study]	1.388	1.511	1.431	1.413	1.968
UMP2/6-311+G(3df,2p) [ref. 152] (TS3)	1.351	1.503	1.426	1.398	1.976
MP2/6-31G(d) [ref. 113]	1.391	1.517	1.428	1.418	1.967
B3LYP/6-31G(d) [ref. 113]	1.358	1.510	1.429	1.409	1.963

The TS structure for $\text{YCC}\bullet\text{COO} \rightarrow \text{O}\bullet\text{CH}_2\text{YCCO}$ is $\text{TO}\bullet\text{CH}_2\text{YCCO}$. The radical site in the carbon of $\text{YCC}\bullet\text{COO}$ attacks one of the oxygen's in the five member cyclic structure to open the five member ring (cleaving the weak O—O bond, 44 kcal/mol) and form a three member oxirane ring bonded to an alkoxy radical, $\text{O}\bullet\text{CH}_2\text{--YCCO}$. The cleaving O₅-O₄ bond is 1.99Å and the O₅-C₂ bond shortens from 2.30 to 2.15Å in the TS structure. The imaginary frequency is 651 cm⁻¹ and the *E_a* is 40.19 kcal/mol.

The $\text{O}\bullet\text{CH}_2\text{YCCO}$ intermediate will undergo β scission to products, $\text{C}\bullet\text{H}_2\text{CHO} + \text{CH}_2\text{O}$ via $\text{TYCCO}-\text{CH}_2\text{O}$. The cleaving C_2-C_3 bond is 2.28\AA and the transition state C_3-O_4 is forming a double bond at 1.23\AA . The E_a is 16.31 kcal/mol .

The TS structure, $\text{TC}\bullet\text{YCCOO}$, represents cyclization to form the four member cyclic peroxide-alkyl radical, $\text{C}\bullet\text{H}_2\text{YCCOO}$. The allyl-peroxy radical undergoes intramolecular addition of the peroxy oxygen radical to the secondary carbon of the $\text{CH}_2=\text{CHCH}_2\text{OO}\bullet$ π bond: $\text{CH}_2=\text{CHCH}_2\text{OO}\bullet \rightarrow \text{C}\bullet\text{H}_2\text{YCCOO}$ through a four member transition state structure. The forming O_8-C_2 bond is 1.84\AA . The imaginary frequency is 717 cm^{-1} and the E_a is 29.71 kcal/mol .

The TS structure for β scission of this 4 member ring peroxide, $\text{C}\bullet\text{H}_2\text{YCCOO}$, to products, $\text{C}\bullet\text{H}_2\text{CHO} + \text{CH}_2\text{O}$ is $\text{TC}=\text{COOC}\bullet$. The cleaving C_3-C_2 and O_7-O_8 bonds are 1.95 and 1.53\AA , respectively, and the C_3-O_7 bond is moving to a double bond at 1.38\AA . The E_a is 13.91 kcal/mol .

The TS structure for four member cyclic peroxide-alkyl radical to form three member alkoxy radical: $\text{C}\bullet\text{H}_2\text{YCCOO} \rightarrow \text{O}\bullet\text{CH}_2\text{YCCO}$ is labeled TYCOCYCO . The radical on the terminal carbon attacks an oxygen in the 4 member ring peroxide $\{-\text{YCCOO}\}$ to form three member alkoxy radical again cleaving the weak $\text{O}-\text{O}$ bond in the peroxide, $\text{O}\bullet\text{CH}_2\text{YCCO}$. The cleaving O_8-O_7 bond is 1.78\AA and the O_8-C_1 bond is 2.08\AA . The imaginary frequency is 793 cm^{-1} and the E_a is 21.61 kcal/mol .

6.3.1.2 Comparison to recent work of Olivella et al.¹⁵² Olivella et al.¹⁵² have recently studied the 1,3-migration of the peroxy group in the allylperoxy radical, which is an important, but small part of this allyl + O_2 system. They reported the well depth is 18.0 kcal/mol at $\text{RCCSD(T)/6-311+G(3df,2p)}$ level for $\text{CH}_2=\text{CHC}\bullet\text{H}_2$

addition to O_2 to form the $CH_2=CHCH_2OO\bullet$ peroxy radical. Overall Olivella et al. found three transition states, two stabilized peroxy radical adducts - 'adduct' and 'adduct'' and one loosely bound complex CX, where these structures relate to peroxy radical formation, and are also reported to be part of one 1,3 peroxy migrations path. They do not relate to further reaction or oxidation of the allyl peroxy radical. TS1 and TS1' are identical in structure for allyl; but have the oxygen on the opposite end carbons, the 'adduct' and 'adduct'' structures are similarly identical. TS1 and TS1' are calculated to be 3.7 kcal/mol above the allyl + O_2 reactants and represent transition states for peroxy radical adduct formation from the allyl + 3O_2 reactants, and one path for 1,3 peroxy migration. CX resides 4.7 kcal/mol below TS1.

A highly non-symmetric, TS structure, TS2 is reported for direct 1,3 peroxy migration at 23.6 kcal/mol above the stabilized peroxy adduct.

Olivella et al. also reported a second higher energy 1,3 peroxy migration path for allylperoxy radical, 'adduct \rightarrow TS3 \rightarrow a five member cyclic peroxide-alkyl adduct \rightarrow TS3' \rightarrow adduct''. TS3 and TS3' are both 33.9 kcal/mol above allylperoxy radical and represent the transition states for a stable five member cyclic peroxide-alkyl adduct formation from allylperoxy radical, and the transition state for 1,3 peroxy migration. This TS3 structure and the reaction path, 'adduct (1A) \rightarrow TS3 \rightarrow a five member cyclic peroxide-alkyl adduct (2)' are similar/ corresponding to the TYCC \bullet COO structure and ' $CH_2=CHCH_2OO\bullet \rightarrow [TYCC\bullet COO] \rightarrow YCC\bullet COO$ ' reaction path in this allyl + O_2 reaction system. Comparisons of barrier and the geometry of the TS structure are discussed in Cyclization Reaction Path, TYCC \bullet COO discussion.

Comparison of bond lengths (Å) and dihedral angle (degree) for the allylperoxy radical in four different calculation levels is given in Scheme 6.4. The transition state structure for TC=CC-O₂ in the CH₂=CHC•H₂ addition to O₂ to form the CH₂=CHCH₂OO• peroxy radical, is different from all the transition states (TS1, TS2, and CX) in Olivella et al. Comparison of bond lengths (Å) and dihedral angle (degree) for the TS structures is given in Scheme 6.5.

Scheme 6.4 Comparison of Bond Lengths in Allylperoxy Radical

Calculation level	C ₁ -C ₂	C ₂ -C ₃	C ₃ -O ₄	O ₄ -O ₅	∠ (O ₅ -O ₄ -C ₃ -C ₂)
B3LYP/6-31G(d,p) [this study]	1.332	1.495	1.470	1.322	74.97
UMP2/6-311+G(3df,2p) [ref. 152] (1A)	1.329	1.488	1.459	1.290	80.02
MP2/6-31G(d) [ref. 113] ^a	1.324	1.496	1.467	1.315	288.85
B3LYP/6-31G(d) [ref. 113] ^a	1.336	1.504	1.472	1.322	284.56

^a allylic isobutenylperoxy radical (CH₂=C(CH₃)CH₂OO•)

Scheme 6.5 Comparison of Bond Lengths (Å) and Dihedral Angle (degree) in TS Structures

Reference	C ₁ -C ₂	C ₂ -C ₃	C ₃ -O ₄	O ₄ -O ₅	C ₁ -O ₅	∠ (O ₅ -O ₄ -C ₃ -C ₂)
TC=CC-O ₂ [this study] ^a	1.372	1.393	2.290	1.237	2.619	-28.6
TS1 [ref. 152] ^b	1.328	1.426	1.959	1.203	4.539	165.4
CX [ref. 152] ^b	1.372	1.372	3.218	1.220	3.218	-151.6
TS2 [ref. 152] ^b	1.360	1.402	1.777	1.250	2.048	-152.1

^a B3LYP/6-31G(d,p) optimized geometry

^b UMP2/6-311+G(3df,2p) optimized geometry

The conclusions for comparison to Olivella et al. are summarized in Scheme 6.6.

Scheme 6.6 Conclusions for comparison to Olivella et al.¹⁵²

Name in Ref. 152	TS assignment in Ref. 152	IRC assignment ^a (Ref. 157)
TS1	CH ₂ =CHCH ₂ OO• = Complex (CX)	CH ₂ =CHC•H ₂ + O ₂ = CH ₂ =CHCH ₂ OO•
TS2	CH ₂ =CHCH ₂ OO• = CH ₂ =CHCH ₂ OO•(self)	TS not found at MPW1K or B3LYP, but is found at MP2, with correct reactants and products. ^b
TS3	CH ₂ =CHCH ₂ OO• = YCC•COO	Correct, but lower energy, "TS3B" exists.
TS3B	N/A	CH ₂ =CHCH ₂ OO• = YCC•COO lower than TS3
TS4	N/A	CH ₂ =CHCH ₂ OO• = Complex (CX), Real TS, not what they had.

^a Intrinsic reaction coordinate (IRC) calculation with MPW1K method for verifying the reaction path

^b 6-31G(d,p) basis set

6.3.2 Enthalpy of Formation ($\Delta H_f^\circ_{298}$)

The evaluated enthalpies of formation for the reference molecules and radicals in the isodesmic reactions are listed in Table 6.1. The evaluated reaction enthalpies and enthalpies of formation in the isodesmic reactions are listed in Table 6.2.

A low or zero $\Delta H^\circ_{\text{rxn},298}$ in the working reactions where the central atom environments are similar on both sides, suggests good cancellation of errors in the reaction analysis leading to accurate $\Delta H_f^\circ_{298}$ values. This also supports the hypothesis of group additivity. As an example, $\Delta H_f^\circ_{298}[\text{CH}_2=\text{CHCH}_2\text{OOH}]$ is evaluated from

$$\Delta H_f^\circ_{\text{rxn},298} = \Delta H_f^\circ_{298} [\text{CH}_2=\text{CHCH}_3] + \Delta H_f^\circ_{298} [\text{C}_2\text{H}_5\text{OOH}]$$

$$-\Delta H_f^\circ{}_{298} [\text{CH}_2=\text{CHCH}_2\text{OOH}] - \Delta H_f^\circ{}_{298} [\text{CH}_3\text{CH}_3]$$

$$\Delta H_f^\circ{}_{\text{rxn},298} = -1.05 \text{ (B3LYP/6-31G(d,p)) and } -1.09 \text{ (CBSQ//B3LYP/6-31G(d,p))}$$

Table 6.1 Enthalpies of Formation for Reference Molecules in the Isodesmic Reactions

Compounds	$\Delta H_f^\circ{}_{298}$ (kcal/mol)	Compounds	$\Delta H_f^\circ{}_{298}$ (kcal/mol)
CH ₃ CH ₃	-20.24 ± 0.10 ^a [80]	CH ₂ =CHCH ₃	4.88 ± 0.19 ^a [80]
C ₂ H ₅ OOH	-39.70 ± 0.3 [61]	C ₂ H ₅ OH	-56.23 ± 0.12 [158]
CH ₂ =CHCH ₂ OH	-29.55 ± 0.35 [159]	C ₂ H ₅ OO.	-6.80 ± 2.3 [88]
(CH ₃) ₃ CH	-32.07 ± 0.17 [78]	CYCCOOC	-34.31 [113]
CH ₃ CH ₂ CH ₃	-25.02 ± 0.12 [78]	CH ₃ OCH ₃	-44.00 ± 0.12 [78]
CH ₃ OOCH ₃	-31.00 [84]	YC ₄ O	-46.87 [160]
CYC.COOC	12.66 [113]	YCCO	-12.58 ± 0.15 [48]
(CH ₃) ₂ C(OH)H	-65.18 [77]	CH ₃ OH	-48.08 ± 0.05 [81]
CH ₃ O.	4.10 ± 1.00 [109]		

^a The uncertainties are evaluated from ref [78].

Table 6.2 Reaction Enthalpies and Enthalpies of Formation in the Isodesmic Reactions

Working Reaction Series (Units in kcal/mol)	$\Delta H_{\text{rxn},298}^{\circ}$			$\Delta H_{\text{f},298}^{\circ}$			CBSQ	
	B3LYP		CBSQ	B3LYP		CBSQ		
	a	b	c	a	b			c
$\text{CH}_2=\text{CHCH}_2\text{OOH} + \text{CH}_3\text{CH}_3 \rightleftharpoons \text{CH}_2=\text{CHCH}_3 + \text{C}_2\text{H}_5\text{OOH}$	-1.05	-1.71	-1.71	-1.09	-13.53	-12.87	-12.87	-13.49
$\text{CH}_2=\text{CHCH}_2\text{OO} + \text{C}_2\text{H}_5\text{OH} \rightleftharpoons \text{CH}_2=\text{CHCH}_2\text{OH} + \text{C}_2\text{H}_5\text{OO}.$	-1.59	-1.30	-1.32	-1.14	21.47	21.18	21.20	21.02
$\text{C.H}=\text{CHCH}_2\text{OOH} + \text{C}_2\text{H}_4 \rightleftharpoons \text{CH}_2=\text{CHCH}_2\text{OOH} + \text{C}_2\text{H}_3$	-0.89	-0.87	-0.88	-1.16	46.46	47.10	47.11	46.77
$\text{CH}_2=\text{C}.\text{CH}_2\text{OOH} + \text{CH}_2=\text{CHCH}_3 \rightleftharpoons \text{CH}_2=\text{CHCH}_2\text{OOH} + \text{CH}_2=\text{C}.\text{CH}_3$	-1.47	-1.70	-1.72	-1.18	44.84	45.73	45.75	44.58
$\text{YCCCOO} + (\text{CH}_3)_3\text{CH} \rightleftharpoons \text{CYCCOOC} + \text{CH}_3\text{CH}_2\text{CH}_3$	-0.25	-0.12	-0.16	-0.23	-27.01	-27.14	-27.10	-27.03
$\text{YCCCOO} + \text{CH}_3\text{CH}_2\text{CH}_3 + \text{CH}_3\text{OCH}_3 \rightleftharpoons \text{CH}_3\text{OOCH}_3 + \text{CH}_3\text{CH}_3 + \text{YC}_4\text{O}$	-0.78	-1.47	-1.43	-0.54	-28.31	-27.62	-27.66	-28.55
$\text{YCC}.\text{COO} + \text{CYCCOOC} \rightleftharpoons \text{YCCCOO} + \text{CYC}.\text{COOC}$	-0.01	-0.01	-0.01	0.00	19.32	19.60	19.59	19.18
$\text{HOCH}_2\text{YCCO} + \text{CH}_3\text{CH}_3 \rightleftharpoons \text{YCCO} + (\text{CH}_3)_2\text{C}(\text{OH})\text{H}$	3.48	1.88	1.91	1.72	-61.00	-59.40	-59.43	-59.24
$\text{O}.\text{CH}_2\text{YCCO} + \text{CH}_3\text{OH} \rightleftharpoons \text{HOCH}_2\text{YCCO} + \text{CH}_3\text{O}.$	-3.18	-2.28	-2.29	-3.02	-5.75	-5.04	-5.06	-4.14

a: 6-31G(d,p), b: 6-311+G(d,p), c: 6-311++G(d,p) basis set

The enthalpies of formation for $\text{CH}_2=\text{CHCH}_2\text{OOH}$ are -13.53 and -13.49 kcal/mol by B3LYP/6-31G(d,p) and CBSQ//B3LYP/6-31G(d,p), respectively. The enthalpy of formation for the parent hydroperoxide is important because it allows the evaluation of peroxy radicals. Other parents and radical species are calculated in the same manner.

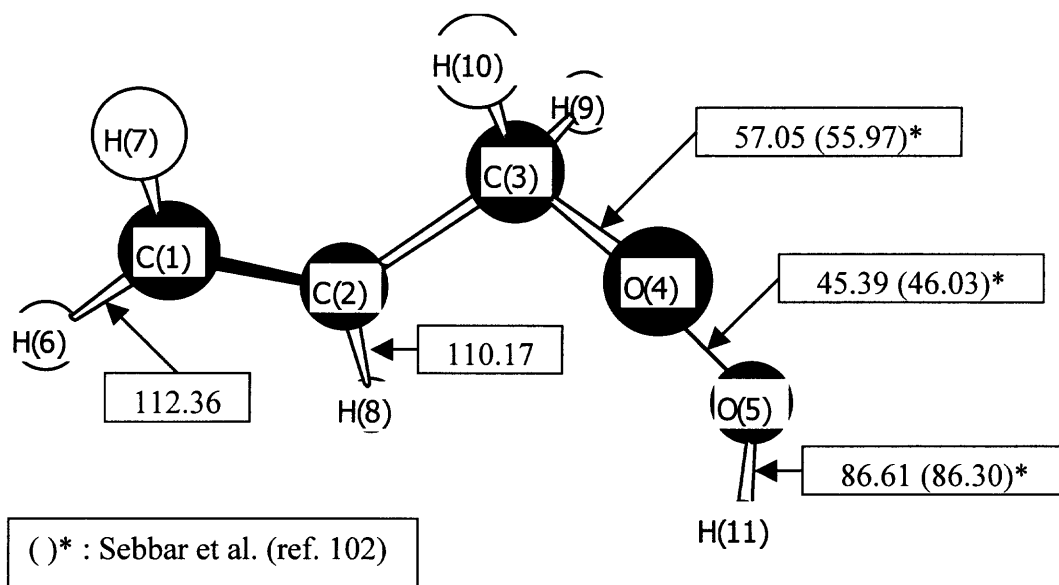


Figure 6.1 Bond dissociation energy of $\text{CH}_2=\text{CHCH}_2\text{OOH}$ (Units : kcal/mol).

The bond energies of $\text{CH}_2=\text{CHCH}_2\text{OOH}$ (Figure 6.1), $\text{C}(\text{OOH})\text{H}_2\text{CHO}$, $\text{C}_2\text{H}_5\text{OOH}$ and $\text{CH}_3\text{C}(=\text{O})\text{OOH}$ are compared in Table 6.3. The R–OOH bond energy in $\text{CH}_2=\text{CHCH}_2\text{OOH}$ is 14 kcal/mol lower than that of $\text{C}_2\text{H}_5\text{OOH}$, because the radical site is resonantly stabilized. The RO–OH and ROO–H bonds in $\text{CH}_2=\text{CHCH}_2\text{OOH}$ are 45.4 and 86.6 kcal/mol, similar to those in $\text{C}_2\text{H}_5\text{OOH}$, 45.1 and 85.3 kcal/mol, respectively.

Table 6.3 Comparison of Bond Energies between $\text{CH}_2=\text{CHCH}_2\text{OOH}$, $\text{C}(\text{OOH})\text{H}_2\text{C}(=\text{O})\text{H}$, $\text{C}_2\text{H}_5\text{OOH}$, and $\text{CH}_3\text{C}(=\text{O})\text{OOH}$

(units in kcal/mol)	$\text{C}(\text{OOH})\text{H}_2\text{CHO}$	$\text{C}_2\text{H}_5\text{OOH}$	$\text{CH}_3\text{C}(=\text{O})\text{OOH}$	$\text{CH}_2=\text{CHCH}_2\text{OOH}$
ROO--H	87.28	85.27	98.33	86.61
RO--OH	45.13	45.12	50.95	45.39
R--OOH	63.21	71.35	85.22	57.05
H--CH=CHCH₂OOH				112.36
CH₂=C(--H)CH₂OOH				110.17
$\text{C}(\text{OOH})\text{H}_2\text{C}(=\text{O})\text{--H}$,	88.65	-	-	-
H--CH ₂ CH ₂ OOH,	-	103.21	-	-
H--CH ₂ C(=O)OOH	-	-	103.95	-
$\text{CH}_3\text{CH}_2\text{O--H}$,	-	104.7 ± 0.8	-	-
$\text{CH}_3\text{C}(=\text{O})\text{O--H}$	-	-	112.32	-

6.3.3 Entropy ($S^{\circ}_{(298)}$) and Heat Capacity ($C_p(T)$, $300 \leq T/K \leq 1500$)

Entropy and heat capacities are calculated based on vibration frequencies and moments of inertia of the optimized B3LYP/6-31G(d,p) structures. The calculation results using B3LYP/6-31G(d,p) determined geometries and scaled frequencies are summarized in Table 6.4. TVR represents the sum of the contributions from translation, vibrations and external rotations for $S^{\circ}_{(298)}$ and $C_p(T)$'s. Symmetry, number of optical isomers and electronic spin are incorporated in estimation of $S^{\circ}_{(298)}$ as described in Table 6.4. Torsion frequencies are omitted in these calculations, instead, contributions from internal rotation for $S^{\circ}_{(298)}$ and $C_p(T)$'s are determined, using direct integration over energy levels of the intramolecular rotational potential curves¹³⁸⁻¹⁴⁰ and noted in Table 6.4.

Table 6.4 Ideal Gas Phase Thermodynamic Properties Obtained by CBSQ Calculation^a

Species (s, e, OI) ^b		ΔH_f° ₂₉₈ ^b	S° ₂₉₈ ^c	Cp_{300} ^c	Cp_{400}	Cp_{500}	Cp_{600}	Cp_{800}	Cp_{1000}	Cp_{1500}
CH ₂ =CHCH ₂ .	TVR ^d		62.94 ^e	14.81	18.61	21.84	24.49	28.56	31.59	36.47
(1,1/2,1)	Total	40.06	62.94	14.81	18.61	21.84	24.49	28.56	31.59	36.47
CH ₂ =CHCH ₂ OOH	TVR		69.81	16.71	21.71	26.17	29.89	35.60	39.75	46.23
(CH ₂ =CH-CH ₂ OOH)	I. R. 1 ^f		6.26	2.63	2.22	1.90	1.66	1.30	1.04	0.63
(CH ₂ =CHCH ₂ -OOH)	I. R. 2		5.66	3.32	2.80	2.38	2.05	1.56	1.20	0.70
(CH ₂ =CHCH ₂ O-OH)	I. R. 3		3.42	1.92	1.73	1.64	1.58	1.50	1.43	1.29
(1,0,2)	Total	-13.49	85.15	24.58	28.46	32.09	35.18	39.96	43.42	48.85
CH ₂ =CHCH ₂ OO.	TVR		69.63	16.50	21.21	25.39	28.86	34.13	37.91	43.66
(CH ₂ =CH-CH ₂ OO.)	I. R. 1		6.31	2.61	2.19	1.87	1.62	1.27	1.01	0.62
(CH ₂ =CHCH ₂ -OO.)	I. R. 2		6.98	1.79	1.56	1.39	1.26	1.02	0.83	0.51
(1,1/2,1)	Total	21.02	82.92	20.90	24.96	28.65	31.74	36.42	39.75	44.79
C.H=CHCH ₂ OOH	TVR		71.08	16.73	21.26	25.14	28.31	33.08	36.52	41.88
(C.H=CH-CH ₂ OOH)	I. R. 1		6.70	1.80	1.59	1.44	1.32	1.14	0.98	0.68
(C.H=CHCH ₂ -OOH)	I. R. 2		5.86	2.97	2.56	2.22	1.94	1.50	1.18	0.70
(C.H=CH-CH ₂ O-OH)	I. R. 3		3.51	1.82	1.67	1.59	1.55	1.47	1.40	1.26
(1,1/2,2)	Total	46.77	87.15	23.32	27.08	30.39	33.12	37.19	40.08	44.52
CH ₂ =C.CH ₂ OOH	TVR		71.61	16.82	21.18	24.99	28.15	32.97	36.46	41.88
(CH ₂ =C.-CH ₂ OOH)	I. R. 1		6.81	1.49	1.31	1.21	1.14	1.05	0.97	0.75
(CH ₂ =C.CH ₂ -OOH)	I. R. 2		4.90	4.12	3.77	3.17	2.63	1.85	1.35	0.71
(CH ₂ =C.H ₂ O-OH)	I. R. 3		2.79	2.60	2.30	2.07	1.92	1.73	1.60	1.40
(1,1/2,2)	Total	44.58	86.11	25.03	28.56	31.44	33.84	37.60	40.38	44.74
O.CH ₂ YCCO	TVR		69.96	17.24	22.40	26.94	30.66	36.22	40.12	45.91
(O.CH ₂ -YCCO)	I. R. 1		6.20	2.29	2.03	1.83	1.67	1.39	1.16	0.74
(1,1/2,1)	Total	-4.14	76.16	19.53	24.43	28.77	32.33	37.61	41.28	46.65
C.H ₂ YCCOO	TVR		71.15	18.42	23.48	27.82	31.35	36.59	40.30	45.91
(C.H ₂ -YCCOO)	I. R. 1		4.05	2.04	1.98	1.84	1.71	1.49	1.35	1.17
(1,1/2,1)	Total	40.18	75.20	20.46	25.46	29.66	33.06	38.08	41.65	47.08
CH ₂ =CHC(=O)H	TVR		64.07	13.92	17.38	20.54	23.23	27.44	30.51	35.23
(CH ₂ =CH-C(=O)H)	I. R. 1		3.58	2.96	2.97	2.85	2.73	2.53	2.34	1.83
(1,1/2,1)	Total	-16.08	67.65	16.88	20.35	23.39	25.96	29.97	32.85	37.06
YCC.CO	TVR		72.80	19.09	24.35	28.95	32.69	38.25	42.14	47.91
(1,1/2,1)	Total	19.18	72.80	19.09	24.35	28.95	32.69	38.25	42.14	47.91
TC=CC-O ₂	TVR		71.96	17.61	21.88	25.57	28.62	33.27	36.67	41.99
(TC=C-COO)	I. R. 1		6.07	2.31	2.23	2.06	1.89	1.61	1.43	1.21
(TC=CC-OO)	I. R. 2		7.43	1.06	1.03	1.02	1.01	1.00	1.00	1.00
(1,1/2,1)	Total	41.05	85.46	20.98	25.14	28.65	31.52	35.88	39.10	44.20
TC.=CCOOHS	TVR		71.33	19.48	24.74	29.14	32.69	37.89	41.48	46.72
(1,1/2,1)	Total	49.90	71.33	19.48	24.74	29.14	32.69	37.89	41.48	46.72
TC.=CCOOH	TVR		74.98	19.80	23.72	26.77	29.17	32.80	35.55	40.18
(TC.=C-COOH)	I. R. 1		6.75	1.83	1.57	1.40	1.30	1.17	1.11	1.05
(TC.=CC-OOH)	I. R. 2		5.72	2.13	2.24	2.31	2.33	2.21	2.02	1.63
(TC.=CCO-OH)	I. R. 3		2.74	2.18	2.29	2.27	2.17	1.93	1.71	1.38
(1,1/2,2)	Total	75.47	90.19	25.94	29.82	32.75	34.97	38.11	40.39	44.24

Table 6.4 Ideal Gas Phase Thermodynamic Properties Obtained by CBSQ Calculation^a (Continued)

Species (s, e, OI) ^g		ΔH_f° ₂₉₈ ^b	S° ₂₉₈ ^c	Cp ₃₀₀ ^c	Cp ₄₀₀	Cp ₅₀₀	Cp ₆₀₀	Cp ₈₀₀	Cp ₁₀₀₀	Cp ₁₅₀₀
TALLYL-OHSQ	TVR		71.37	18.12	23.01	27.21	30.62	35.70	39.25	44.52
(TC=C-YCOOH)	I. R. 1		4.81	2.29	2.21	2.04	1.87	1.60	1.42	1.21
(1,1/2,1)	Total	58.74	76.18	20.41	25.22	29.25	32.49	37.30	40.67	45.73
TC=C.COOS	TVR		73.64	20.25	25.22	29.42	32.83	37.92	41.47	46.71
(1,1/2,1)	Total	58.99	73.64	20.25	25.22	29.42	32.83	37.92	41.47	46.71
TC=C.COOH	TVR		72.26	17.15	21.20	24.63	27.43	31.73	34.91	40.02
(TC=C.-COOH)	I. R. 1		4.29	1.80	1.63	1.48	1.37	1.23	1.15	1.07
(TC=C.C-OOH)	I. R. 2		6.96	2.13	1.86	1.65	1.49	1.31	1.20	1.09
(TC=C.CO-OH)	I. R. 3		3.24	2.27	2.16	1.97	1.79	1.54	1.38	1.18
(1,1/2,2)	Total	60.05	86.75	23.35	26.85	29.73	32.08	35.81	38.64	43.36
TC=C=C-OOHE	TVR		75.47	21.58	26.25	30.17	33.37	38.17	41.57	46.67
(1,1/2,1)	Total	57.28	75.47	21.58	26.25	30.17	33.37	38.17	41.57	46.67
TYCC.CO	TVR		70.21	18.17	23.39	27.81	31.36	36.61	40.31	45.91
(1,1/2,1)	Total	46.09	70.21	18.17	23.39	27.81	31.36	36.61	40.31	45.91
TO.CH ₂ YCCO	TVR		70.99	18.34	23.35	27.74	31.34	36.73	40.53	46.17
(1,1/2,1)	Total	59.37	70.99	18.34	23.35	27.74	31.34	36.73	40.53	46.17
TYCCO-CH ₂ O	TVR		73.48	18.09	22.40	26.31	29.61	37.40	38.39	43.99
(TCH ₂ O.-YCCO)	I. R. 1		6.98	1.74	1.49	1.34	1.25	1.14	1.09	1.04
(1,1/2,1)	Total	12.17	80.46	19.83	23.89	27.65	30.86	38.54	39.48	45.03
TC.YCCOO	TVR		72.65	19.07	23.95	28.14	31.56	36.68	40.33	45.89
(1,1/2,1)	Total	50.73	72.65	19.07	23.95	28.14	31.56	36.68	40.33	45.89
TC=COOC.	TVR		72.44	20.42	25.37	29.42	32.65	37.43	40.85	46.13
(1,1/2,1)	Total	54.09	72.44	20.42	25.37	29.42	32.65	37.43	40.85	46.13
TYCOCYCO	TVR		71.80	19.00	23.90	28.12	31.56	36.72	40.39	45.96
(1,1/2,1)	Total	61.79	71.80	19.00	23.90	28.12	31.56	36.72	40.39	45.96
TC=YCOC-OH	TVR		76.91	21.32	25.30	28.69	31.49	35.81	39.01	44.11
(TC=YCOC-OH)	I. R. 1		2.79	2.60	2.30	2.07	1.92	1.73	1.60	1.40
(1,1/2,1)	Total	62.75	79.70	23.92	27.60	30.76	33.41	37.54	40.61	45.51

a : Thermodynamic properties are referred to a standard state of an ideal gas of pure enantiomer at 1 atm.

b : Units in kcal/mol c : Units in cal/mol-K

d : Sum of contributions from translations, vibrations, and external rotations.

f : Contribution from internal rotation

g : Symmetry number, optical isomer and electronic spin are taken into account, -Rln(s), Rln2, Rln2, respectively.

s = number of symmetry, e = electronic spin, OI = number of optical isomer

6.3.4 Potential Energy Diagram for $\text{CH}_2=\text{CHCH}_2\bullet + \text{O}_2$ Reaction System

The energy diagram for the allyl ($\text{CH}_2=\text{CHCH}_2\bullet$) + O_2 reaction is illustrated in two Figures 6.2A and 6.2B. The reactions involving intramolecular hydrogen transfer and direct HO_2 elimination are illustrated in Figure 6.2A. Reactions involving peroxy radical addition to each of the π bond carbons, ring formation, and subsequent reactions of the two cyclic peroxide alkyl radicals are illustrated in Figure 6.2B. 15 reaction paths, 6 reaction intermediates, and 15 transition states are illustrated. Enthalpies of formation are from CBSQ// B3LYP/6-31G(d,p) calculations and in units of kcal/mol. Transition state enthalpies are relative to the corresponding stabilized adduct.

The allyl radical adds to O_2 ($E_a = 0.99$) to form an energized peroxy adduct $[\text{CH}_2=\text{CHCH}_2\text{OO}\bullet]^*$ with a shallow well (ca. 19 kcal/mol); which predominantly dissociates back to reactants under combustion conditions. The reaction channels of the $[\text{CH}_2=\text{CHCH}_2\text{OO}\bullet]^*$ adduct include reverse reaction to reactants, stabilization to $\text{CH}_2=\text{CHCH}_2\text{OO}\bullet$ radical ($\Delta H_f^\circ_{298} = 21.02$), decomposition to products, $\text{CH}_2=\text{C}=\text{CH}_2 + \text{HO}_2$ via direct HO_2 elimination with a barrier ($E_a = 36.61$), isomerizations via hydrogen shifts to form $\text{C}\bullet\text{H}=\text{CHCH}_2\text{OOH}$ or $\text{CH}_2=\text{C}\bullet\text{CH}_2\text{OOH}$ isomers ($\Delta H_f^\circ_{298} = 46.77$ or 44.58 , respectively) with barriers ($E_a = 28.88$ or 37.97 , respectively), or a hydrogen transfer ($E_a = 37.73$) from the ipso carbon to the peroxy radical to form the unstable intermediate $\{\text{CH}_2=\text{CHC}\bullet\text{HOOH}\}$, which immediately dissociates to more stable products, 2-propenal plus OH.

The $\text{C}\bullet\text{H}=\text{CHCH}_2\text{OOH}$ isomer can undergo β scission to products, ($\text{C}_2\text{H}_2 + \{\text{C}\bullet\text{H}_2\text{OOH}\} \rightarrow \text{C}_2\text{H}_2 + \text{CH}_2\text{O} + \text{OH}$) ($E_a = 37.73$), a ring closure to form the

unstable intermediate $\{YC=CCO\}$ plus OH, (Y = cyclic) which rapidly dissociates to more stable products, 2-propenal plus OH, or isomerize via a hydrogen shift ($E_a = 3.13$) to form a $CH_2=CHCH_2OO\bullet$ isomer.

The $CH_2=C\bullet CH_2OOH$ isomer can undergo β scission to products, $CH_2=C=CH_2 + HO_2$ ($E_a = 15.47$), a ring closure to form methylene oxirane plus OH radical ($E_a = 18.17$), or isomerize via a hydrogen shift ($E_a = 14.41$) to form a $CH_2=CHCH_2OO\bullet$ isomer.

6.3.4.1 Intramolecular Peroxy Radical Addition to sp^2 Hybridized Carbons - Cyclization Reaction Paths. The $[CH_2=CHCH_2OO\bullet]^*$ adduct can also cyclize to four- or five-member cyclic peroxide-alkyl radicals, $C\bullet H_2 YCCOO$ and $YCC\bullet COO$ ($\Delta H_f^\circ_{298} = 40.18$ and 19.18 , respectively). $CH_2=CHCH_2OO\bullet$ cyclization to four- or five-member cyclic peroxides require barriers, $E_a = 29.71$ and 25.07 , respectively), these are higher than reverse reaction ($E_a = 20.03$).

The $C\bullet H_2 YCCOO$ adduct can undergo β scission to products, $C\bullet H_2 CHO + CH_2O$ ($E_a = 13.91$), form three member alkoxy radical, $O\bullet CH_2 YCCO$ ($\Delta H_f^\circ_{298} = -4.14$) via $TYCOCYCO$ ($E_a = 21.61$), or undergo ring open to form $CH_2=CHCH_2OO\bullet$ adduct ($E_a = 10.55$). The $O\bullet CH_2 YCCO$ intermediate will undergo β scission to products, $C\bullet H_2 CHO + CH_2O$ via $TYCCO-CH_2O$ ($E_a = 16.31$).

The $YCC\bullet COO$ adduct can also form three member alkoxy radical, $O\bullet CH_2 YCCO$ via $TO\bullet CH_2 YCCO$ ($E_a = 40.19$), or undergo ring open to form $CH_2=CHCH_2OO\bullet$ adduct ($E_a = 26.91$).

All the product formation pathways of allyl radical with O_2 involve barriers that are above the energy of the initial reactants.

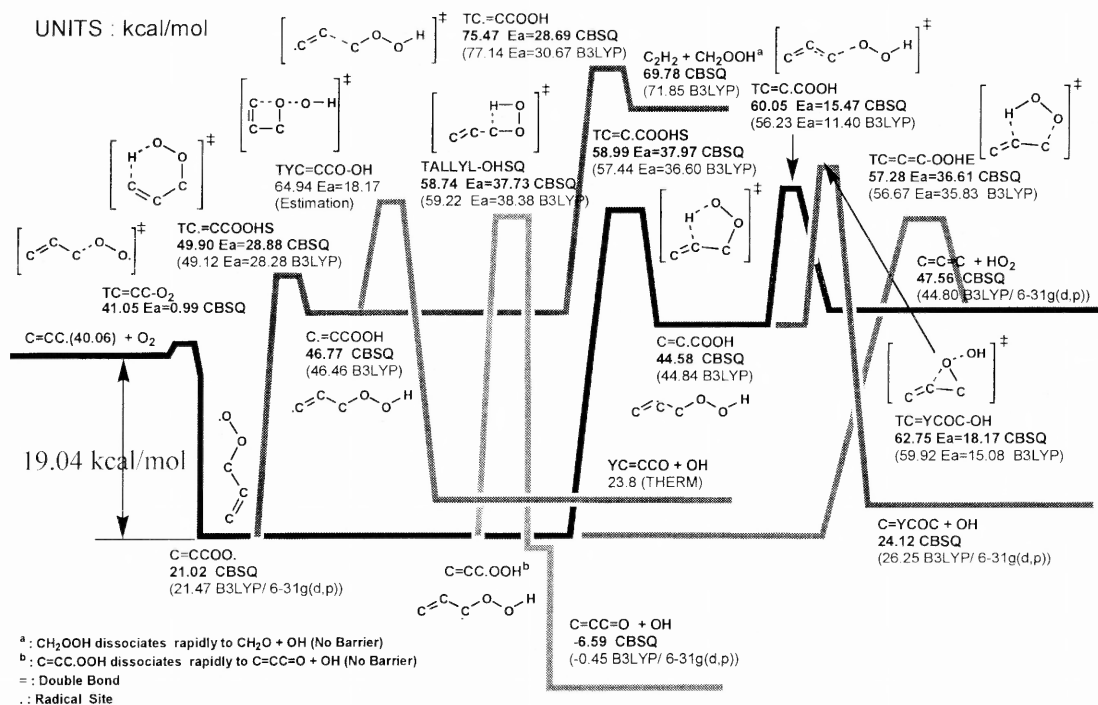


Figure 6.2A Potential energy diagram for allyl + O₂
 (a) isomerizations via H shifts.

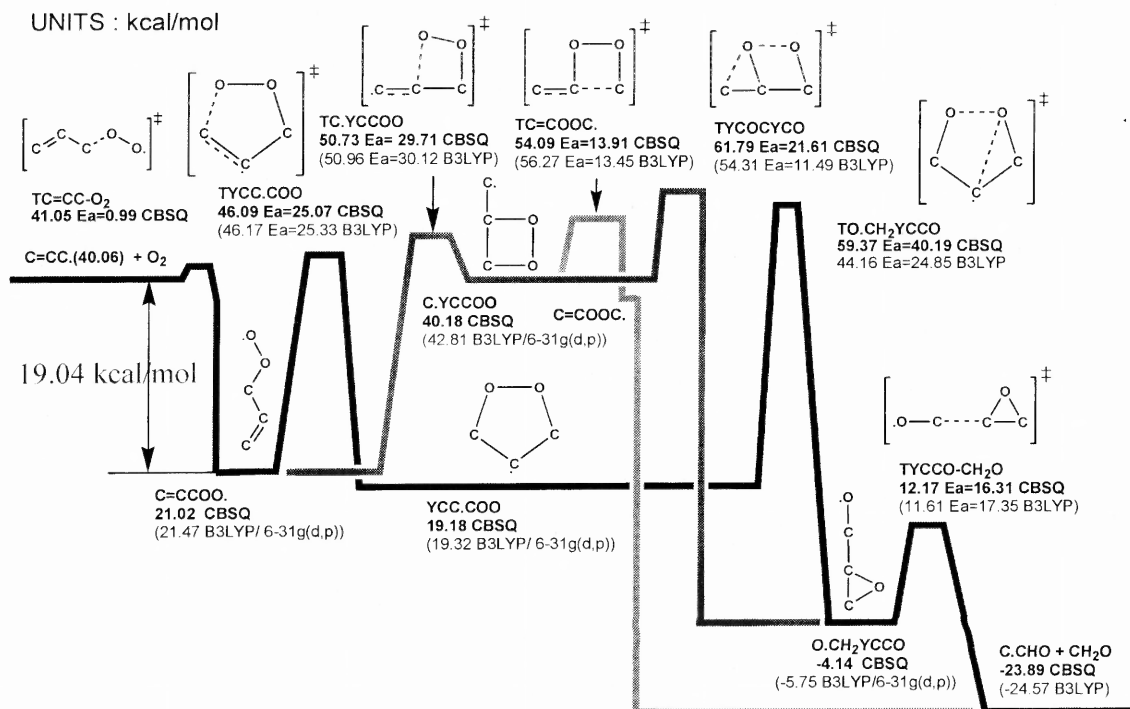


Figure 6.2B Potential energy diagram for allyl + O₂
(a) cyclization pathways to form cyclic adducts and further reactions.

6.3.5 Comparison of $\text{CH}_2=\text{CHC}\cdot\text{H}_2 + \text{O}_2$, $\text{C}\cdot\text{H}_2\text{CHO} + \text{O}_2$, $\text{CH}_3\text{C}\cdot\text{O} + \text{O}_2$ and $\text{C}_2\text{H}_5 + \text{O}_2$

The $\text{CH}_2=\text{CHC}\cdot\text{H}_2 + \text{O}_2$, $\text{C}\cdot\text{H}_2\text{CHO} + \text{O}_2$, $\text{CH}_3\text{C}\cdot\text{O} + \text{O}_2$, and $\text{C}_2\text{H}_5 + \text{O}_2$ ⁴¹ reaction systems have significant differences. The $\text{CH}_2=\text{CHC}\cdot\text{H}_2 + \text{O}_2$ reaction system of this study has a lower well depth of 19.04 kcal/mol compared to $\text{C}\cdot\text{H}_2\text{CHO} + \text{O}_2$, $\text{CH}_3\text{C}\cdot\text{O} + \text{O}_2$ and $\text{C}_2\text{H}_5 + \text{O}_2$, which have well depths of 27.5, 35.5 and 35.3 kcal/mol, respectively.

The H shift barriers in the $\text{CH}_2=\text{CHCH}_2\text{OO}\cdot$, $\text{C}(\text{OO}\cdot)\text{H}_2\text{CHO}$ and $\text{CH}_3\text{C}(=\text{O})\text{OO}\cdot$ peroxy radicals are lower than those of concerted HO_2 elimination, whereas in $\text{C}_2\text{H}_5\text{OO}\cdot$, direct HO_2 elimination has a lower barrier than the H shift.

The well depth and barriers of H shift and HO_2 elimination in the $\text{CH}_2=\text{CHC}\cdot\text{H}_2$, $\text{C}\cdot\text{H}_2\text{CHO}$, $\text{CH}_3\text{C}\cdot\text{O}$ and $\text{C}_2\text{H}_5\cdot$ with O_2 reaction systems are compared in Table 6.5.

Table 6.5 Comparison of $\text{CH}_2=\text{CHC}\cdot\text{H}_2$, $\text{C}\cdot\text{H}_2\text{CHO}$, $\text{CH}_3\text{C}\cdot(=\text{O})$, and C_2H_5 with O_2

(units in kcal/mol)	$\text{C}\cdot\text{H}_2\text{CHO} + \text{O}_2$	$\text{CH}_3\text{C}\cdot(=\text{O}) + \text{O}_2$	$\text{C}_2\text{H}_5 + \text{O}_2$	$\text{CH}_2=\text{CHC}\cdot\text{H}_2 + \text{O}_2$
Well Depth	27.5	35.5	35.3	19.04
Barrier in				
1) H Shift ^a	20.25	26.42	36.36	28.88
2) HO_2 Elimination ^a	48.31	34.58	30.48	36.61

^a H shift and HO_2 elimination for the $\text{C}(\text{OO}\cdot)\text{H}_2\text{CHO}$, $\text{CH}_3\text{C}(=\text{O})\text{OO}\cdot$, $\text{C}_2\text{H}_5\text{OO}\cdot$, and $\text{CH}_2=\text{CHCH}_2\text{OO}\cdot$.

Table 6.6 Input Parameters^a and High-Pressure Limit Rate Constants (k_{∞})^b for QRRK Calculations^c

Input Parameters for QRRK Calculations with Master Equation Analysis for Falloff			
Reaction	High-Pressure Limit Rate Constants		
	A	n	E_a (kcal/mol)
1 $\text{CH}_2=\text{CHC}\cdot\text{H}_2 + \text{O}_2 \Rightarrow \text{CH}_2=\text{CHCH}_2\text{OO}\cdot^{\text{d}}$	5.78E+07	1.59	1.08
-1 $\text{CH}_2=\text{CHCH}_2\text{OO}\cdot \Rightarrow \text{CH}_2=\text{CHC}\cdot\text{H}_2 + \text{O}_2^{\text{d}}$	1.02E+11	0.86	20.05
2 $\text{CH}_2=\text{CHCH}_2\text{OO}\cdot \Rightarrow \text{C}\cdot\text{H}=\text{CHCH}_2\text{OOH}^{\text{d}}$	5.17E+05	1.65	28.25
3 $\text{CH}_2=\text{CHCH}_2\text{OO}\cdot \Rightarrow \text{CH}_2=\text{C}\cdot\text{CH}_2\text{OOH}^{\text{d}}$	1.83E+06	1.66	37.41
4 $\text{CH}_2=\text{CHCH}_2\text{OO}\cdot \Rightarrow \text{YCC}\cdot\text{COO}^{\text{d}}$	1.92E+08	0.71	25.09
5 $\text{CH}_2=\text{CHCH}_2\text{OO}\cdot \Rightarrow \text{C}\cdot\text{H}_2\text{YCCOO}^{\text{d}}$	4.57E+07	1.10	29.45
6 $\text{CH}_2=\text{CHCH}_2\text{OO}\cdot \Rightarrow \text{CH}_2=\text{CHC}(=\text{O})\text{H} + \text{OH}^{\text{d}}$	2.24E+07	1.49	37.32
7 $\text{CH}_2=\text{CHCH}_2\text{OO}\cdot \Rightarrow \text{CH}_2=\text{C}=\text{CH}_2 + \text{HO}_2^{\text{d}}$	1.06E+06	1.90	35.65
8 $\text{C}\cdot\text{H}=\text{CHCH}_2\text{OOH} \Rightarrow \text{CH}_2=\text{CHCH}_2\text{OO}\cdot^{\text{d}}$	9.16E+04	1.55	23.63
9 $\text{C}\cdot\text{H}=\text{CHCH}_2\text{OOH} \Rightarrow \text{C}_2\text{H}_2 + \text{CH}_2\text{O} + \text{OH}^{\text{d}}$	4.31E+09	1.55	28.75
10 $\text{C}\cdot\text{H}=\text{CHCH}_2\text{OOH} \Rightarrow \text{YC}=\text{CCO} + \text{OH}^{\text{e}}$	2.17E+10	0.48	18.34
11 $\text{CH}_2=\text{C}\cdot\text{CH}_2\text{OOH} \Rightarrow \text{CH}_2=\text{CHCH}_2\text{OO}\cdot^{\text{d}}$	1.18E+08	0.72	14.08
12 $\text{CH}_2=\text{C}\cdot\text{CH}_2\text{OOH} \Rightarrow \text{CH}_2=\text{C}=\text{CH}_2 + \text{HO}_2^{\text{d}}$	1.68E+14	-0.30	16.23
13 $\text{CH}_2=\text{C}\cdot\text{CH}_2\text{OOH} \Rightarrow \text{C}=\text{YCOC} + \text{OH}^{\text{d}}$	2.17E+10	0.48	18.34
14 $\text{YCC}\cdot\text{COO} \Rightarrow \text{CH}_2=\text{CHCH}_2\text{OO}\cdot^{\text{d}}$	1.09E+12	0.23	27.45
15 $\text{YCC}\cdot\text{COO} \Rightarrow \text{O}\cdot\text{CH}_2\text{YCCO}^{\text{d}}$	2.79E+08	0.48	40.50
16 $\text{C}\cdot\text{H}_2\text{YCCOO} \Rightarrow \text{CH}_2=\text{CHCH}_2\text{OO}\cdot^{\text{d}}$	5.21E+10	0.64	10.63
17 $\text{C}\cdot\text{H}_2\text{YCCOO} \Rightarrow \text{O}\cdot\text{CH}_2\text{YCCO}^{\text{d}}$	3.89E+10	0.62	21.70
18 $\text{C}\cdot\text{H}_2\text{YCCOO} \Rightarrow \text{C}\cdot\text{H}_2\text{CHO} + \text{CH}_2\text{O}^{\text{d}}$	2.25E+09	1.11	13.80
19 $\text{O}\cdot\text{CH}_2\text{YCCO} \Rightarrow \text{YCC}\cdot\text{COO}^{\text{d}}$	5.06E+09	0.79	63.51
20 $\text{O}\cdot\text{CH}_2\text{YCCO} \Rightarrow \text{C}\cdot\text{H}_2\text{YCCOO}^{\text{d}}$	3.53E+09	0.92	65.90
21 $\text{O}\cdot\text{CH}_2\text{YCCO} \Rightarrow \text{C}\cdot\text{H}_2\text{CHO} + \text{CH}_2\text{O}^{\text{d}}$	3.35E+12	0.58	16.63

^aGeometric mean frequency (from CPFIT, ref 41) [$\text{CH}_2=\text{CHCH}_2\text{OO}\cdot$: 399.1 cm^{-1} (8.290); 1537.0 cm^{-1} (12.192); 4000.0 cm^{-1} (2.518), $\text{C}\cdot\text{H}=\text{CHCH}_2\text{OOH}$: 388.5 cm^{-1} (9.084); 1468.0 cm^{-1} (10.279); 3999.6 cm^{-1} (3.136), $\text{CH}_2=\text{C}\cdot\text{CH}_2\text{OOH}$: 338.8 cm^{-1} (10.359); 1497.5 cm^{-1} (9.625); 3999.3 cm^{-1} (2.516), $\text{YCC}\cdot\text{COO}$: 486.8 cm^{-1} (6.886); 1232.6 cm^{-1} (12.105); 3037.6 cm^{-1} (5.009), $\text{C}\cdot\text{H}_2\text{YCCOO}$: 455.9 cm^{-1} (7.682); 1220.8 cm^{-1} (10.767); 3111.7 cm^{-1} (5.051), $\text{O}\cdot\text{CH}_2\text{YCCO}$: 520.2 cm^{-1} (8.565); 1405.9 cm^{-1} (11.224); 3698.6 cm^{-1} (3.711), Lennard-Jones parameters: $\sigma_{ij}=5.19\text{\AA}$, $\epsilon/k=533.08\text{K}$, ref 89]

^bThe units of A factors and rate constants k are s^{-1} for unimolecular reactions and $\text{cm}^3/(\text{mol s})$ for bimolecular reactions.

^c ΔE down of 1000 cal/mol is used, N_2 for bath gas. [Units] k_1 : $\text{cm}^3/(\text{mol s})$, $k_1 \rightarrow k_5$: s^{-1}

^dA is calculated using TST and entropy of transition state, $\Delta S_{298}^{\ddagger}$ from B3LYP/6-31G(d,p); E_a is from CBSQ calculation (see Table 6.3). All parameters A, n, E_a , are fit over the temperature range of 298-2000K.

^eA, n and E_a are estimated from $\text{CH}_2=\text{C}\cdot\text{CH}_2\text{OOH} \Rightarrow \text{C}=\text{YCOC} + \text{OH}$.

Table 6.7 Resulting Rate Constants in QRRK Calculations^a

1) Calculated Reaction Parameters at P = 0.01 atm,

$$k = A(T/K)^n \exp(-Ea/RT) \quad (298 \leq T/K \leq 2000)$$

Reactions	A	n	Ea (kcal/mol)	k ₂₉₈
CH ₂ =CHC•H ₂ + O ₂ => CH ₂ =CHCH ₂ OO•	1.13E+37	-8.99	5.43	6.74E+10
CH ₂ =CHC•H ₂ + O ₂ => CH ₂ =CHC(=O)H + OH	2.15E+04	2.15	18.48	1.25E-04
CH ₂ =CHC•H ₂ + O ₂ => CH ₂ =C=CH ₂ + HO ₂	6.25E+02	2.62	16.69	1.09E-03
CH ₂ =CHC•H ₂ + O ₂ => C•H=CHCH ₂ OOH	5.88E+35	-9.15	15.96	2.65E+01
CH ₂ =CHC•H ₂ + O ₂ => C ₂ H ₂ + CH ₂ O + OH	2.60E+11	-0.02	18.50	6.29E-03
CH ₂ =CHC•H ₂ + O ₂ => YC=CCO + OH	3.57E+21	-3.66	15.75	8.77E+00
CH ₂ =CHC•H ₂ + O ₂ => YCC•COO	8.62E+40	-10.46	15.08	9.96E+03
CH ₂ =CHC•H ₂ + O ₂ => C•H ₂ YCCOO	1.10E+17	-3.79	9.96	2.30E+00
CH ₂ =CHC•H ₂ + O ₂ => C•H ₂ CHO + CH ₂ O	1.17E+04	1.91	13.65	6.11E-02

^aThe units of A factors and rate constants *k* are cm³/(mol s) for bimolecular reactions.

2) Calculated Reaction Parameters at P = 0.1 atm,

$$k = A(T/K)^n \exp(-Ea/RT) \quad (298 \leq T/K \leq 2000)$$

Reactions	A	n	Ea (kcal/mol)	k ₂₉₈
CH ₂ =CHC•H ₂ + O ₂ => CH ₂ =CHCH ₂ OO•	5.33E+39	-9.43	7.45	8.58E+10
CH ₂ =CHC•H ₂ + O ₂ => CH ₂ =CHC(=O)H + OH	2.95E+04	2.11	18.56	1.20E-04
CH ₂ =CHC•H ₂ + O ₂ => CH ₂ =C=CH ₂ + HO ₂	9.65E+02	2.57	16.80	1.05E-03
CH ₂ =CHC•H ₂ + O ₂ => C•H=CHCH ₂ OOH	7.26E+38	-9.69	18.41	2.43E+01
CH ₂ =CHC•H ₂ + O ₂ => C ₂ H ₂ + CH ₂ O + OH	5.68E+14	-0.97	20.67	1.57E-03
CH ₂ =CHC•H ₂ + O ₂ => YC=CCO + OH	1.10E+25	-4.62	18.59	9.49E-01
CH ₂ =CHC•H ₂ + O ₂ => YCC•COO	1.48E+38	-9.28	15.69	5.00E+03
CH ₂ =CHC•H ₂ + O ₂ => C•H ₂ YCCOO	4.51E+20	-4.53	11.56	9.29E+00
CH ₂ =CHC•H ₂ + O ₂ => C•H ₂ CHO + CH ₂ O	1.05E+05	1.64	14.19	4.67E-02

Table 6.7 Resulting Rate Constants in QRRK Calculations^a (Continued)

3) Calculated Reaction Parameters at P = 1 atm,

$$k = A(T/K)^n \exp(-Ea/RT) \quad (298 \leq T/K \leq 2000)$$

Reactions	A	n	Ea (kcal/mol)	k ₂₉₈
CH ₂ =CHC•H ₂ + O ₂ => CH ₂ =CHCH ₂ OO•	2.43E+39	-8.96	8.62	7.85E+10
CH ₂ =CHC•H ₂ + O ₂ => CH ₂ =CHC(=O)H + OH	3.36E+05	1.81	19.19	8.55E-05
CH ₂ =CHC•H ₂ + O ₂ => CH ₂ =C=CH ₂ + HO ₂	2.06E+04	2.19	17.59	6.75E-04
CH ₂ =CHC•H ₂ + O ₂ => C•H=CHCH ₂ OOH	9.17E+38	-9.34	20.53	6.25E+00
CH ₂ =CHC•H ₂ + O ₂ => C ₂ H ₂ + CH ₂ O + OH	1.41E+18	-1.88	23.83	1.04E-04
CH ₂ =CHC•H ₂ + O ₂ => YC=CCO + OH	3.55E+26	-4.96	21.55	2.98E-02
CH ₂ =CHC•H ₂ + O ₂ => YCC•COO	1.95E+34	-7.77	16.49	9.38E+02
CH ₂ =CHC•H ₂ + O ₂ => C•H ₂ YCCOO	5.90E+26	-5.96	15.36	5.78E+00
CH ₂ =CHC•H ₂ + O ₂ => C•H ₂ CHO + CH ₂ O	3.08E+09	0.37	16.91	1.00E-02

4) Calculated Reaction Parameters at P = 10 atm,

$$k = A(T/K)^n \exp(-Ea/RT) \quad (298 \leq T/K \leq 2000)$$

Reactions	A	n	Ea (kcal/mol)	k ₂₉₈
CH ₂ =CHC•H ₂ + O ₂ => CH ₂ =CHCH ₂ OO•	1.32E+35	-7.34	8.36	6.76E+10
CH ₂ =CHC•H ₂ + O ₂ => CH ₂ =CHC(=O)H + OH	3.58E+08	0.96	21.27	2.13E-05
CH ₂ =CHC•H ₂ + O ₂ => CH ₂ =C=CH ₂ + HO ₂	2.90E+07	1.30	19.83	1.36E-04
CH ₂ =CHC•H ₂ + O ₂ => C•H=CHCH ₂ OOH	2.96E+34	-7.63	21.49	6.77E-01
CH ₂ =CHC•H ₂ + O ₂ => C ₂ H ₂ + CH ₂ O + OH	5.35E+18	-1.93	26.91	1.65E-06
CH ₂ =CHC•H ₂ + O ₂ => YC=CCO + OH	6.84E+23	-4.04	23.64	3.14E-04
CH ₂ =CHC•H ₂ + O ₂ => YCC•COO	6.50E+26	-5.21	16.29	9.43E+01
CH ₂ =CHC•H ₂ + O ₂ => C•H ₂ YCCOO	2.07E+29	-6.29	19.01	6.56E-01
CH ₂ =CHC•H ₂ + O ₂ => C•H ₂ CHO + CH ₂ O	7.60E+15	-1.41	21.85	2.34E-04

6.3.6 Analysis of Chemical Activation Reaction in Allyl + O₂

The QRRK calculations for $k(E)$ and master equation analysis for falloff are performed on this allyl ($\text{CH}_2=\text{CHCH}_2\bullet$) + O₂ reaction system to estimate rate constants and to determine important reaction paths as a function of temperature and pressure. Table 6.6 presents high-pressure-limit kinetic parameters used as input data, and Table 6.7 presents results versus temperature and pressure.

Rate constants at 1 atm pressure versus $1000/T$ are illustrated in Figure 6.3. Stabilization $\text{CH}_2=\text{CHCH}_2\text{OO}\bullet$ is important below 600 K, with reverse dissociation above 800 K. $\text{CH}_2=\text{CHCH}_2\text{OO}\bullet$ adduct, cyclic isomers, and H-shift isomers exhibit significant falloff at higher temperatures (above 800 K). Allene + HO₂ products via a HO₂ molecular elimination path, YCC•COO via cyclization, and H transfer from primary vinyl group to peroxy radical; then β -scission reaction leading to C₂H₂ + CH₂O + OH are major product channels at higher temperatures (above 800 K).

Plots of calculated rate constants for $\text{CH}_2=\text{CHCH}_2\bullet + \text{O}_2$ at 298 K versus pressure are illustrated in Figure 6.4. Stabilization is the dominant path above 0.01 atm, whereas reverse dissociation and stabilization are important below 0.01 atm.

Rate constants at 1000 K versus pressure are illustrated in Figure 6.5. Reverse dissociation is the dominant path below 10 atm whereas stabilization is important above 10 atm. Stabilization decreases as pressure is decreased (as expected).

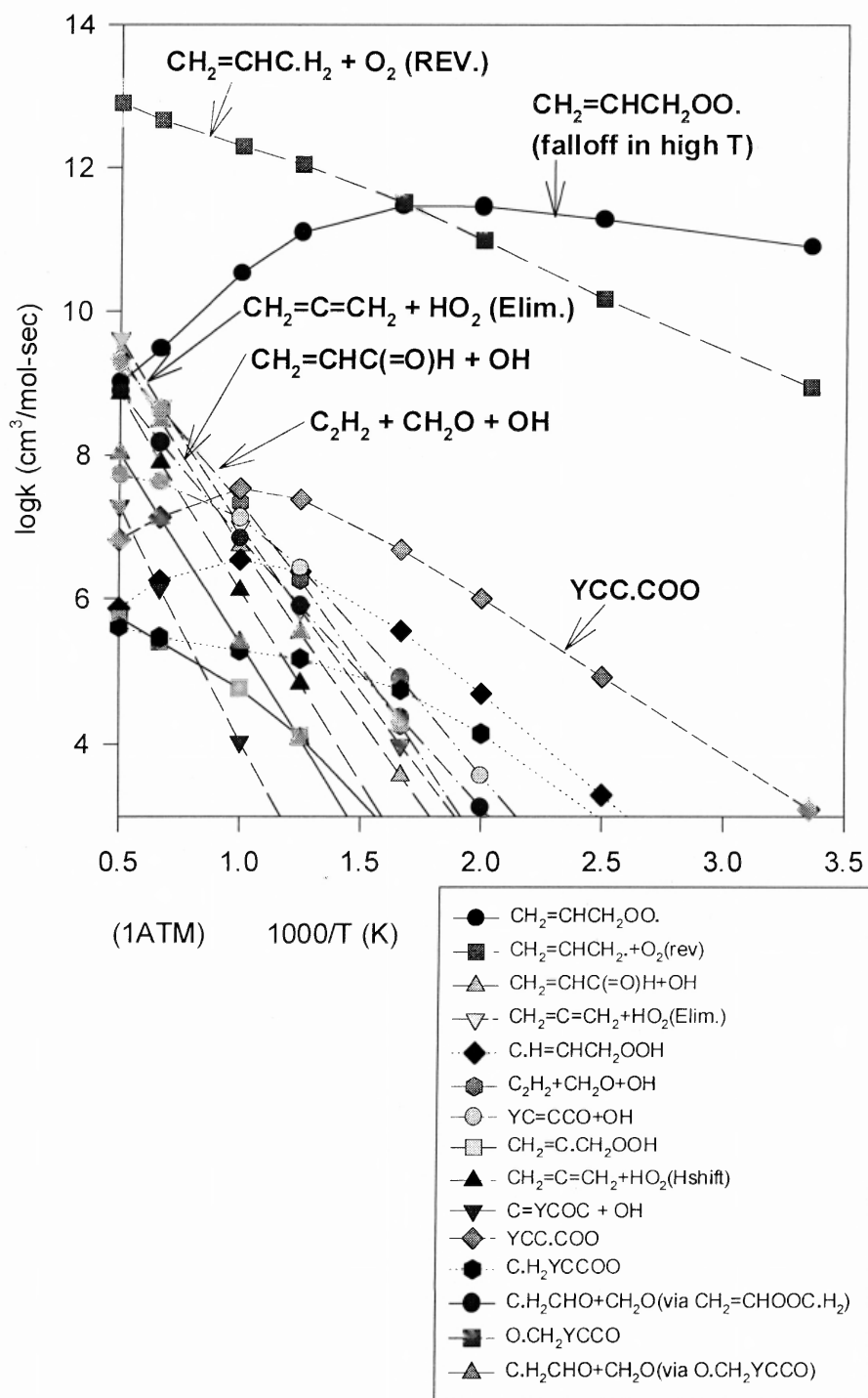


Figure 6.3 $\text{CH}_2=\text{CHC}\cdot\text{H}_2 + \text{O}_2 \rightarrow \text{products}$ k vs. $1000/T$ at 1 atm.

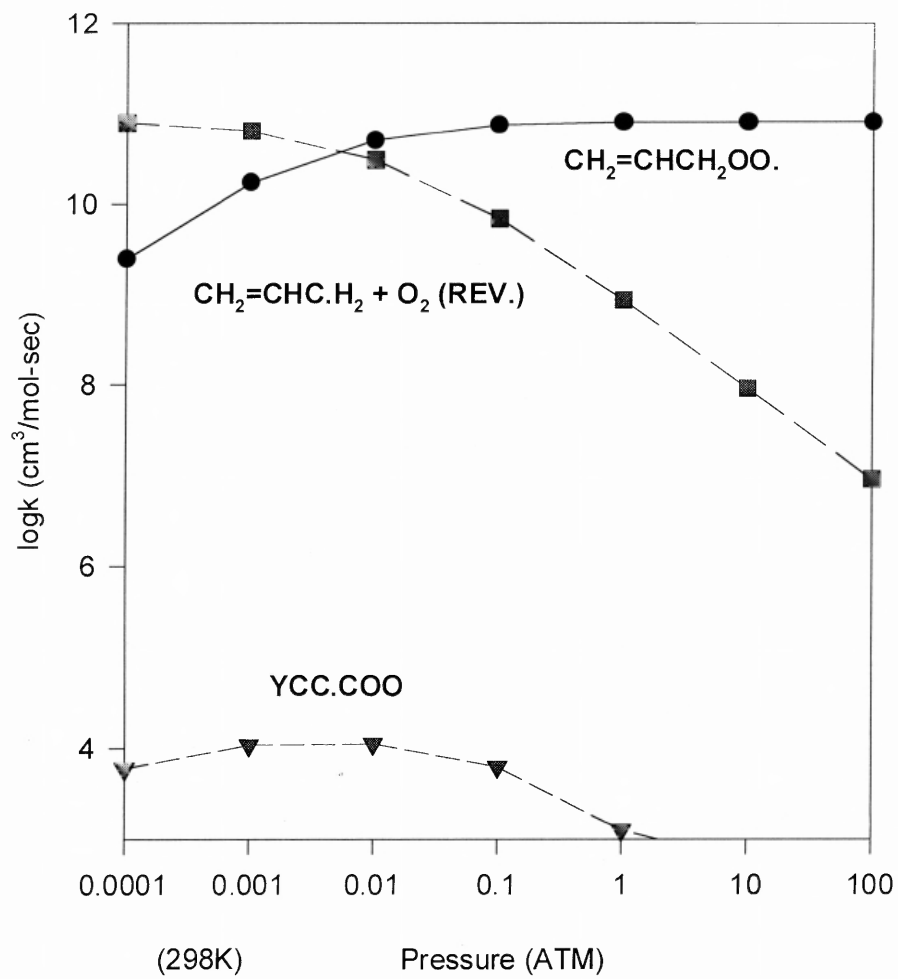


Figure 6.4 $\text{CH}_2=\text{CHC}\cdot\text{H}_2 + \text{O}_2 \rightarrow \text{products}$ k vs. pressure at 298K.

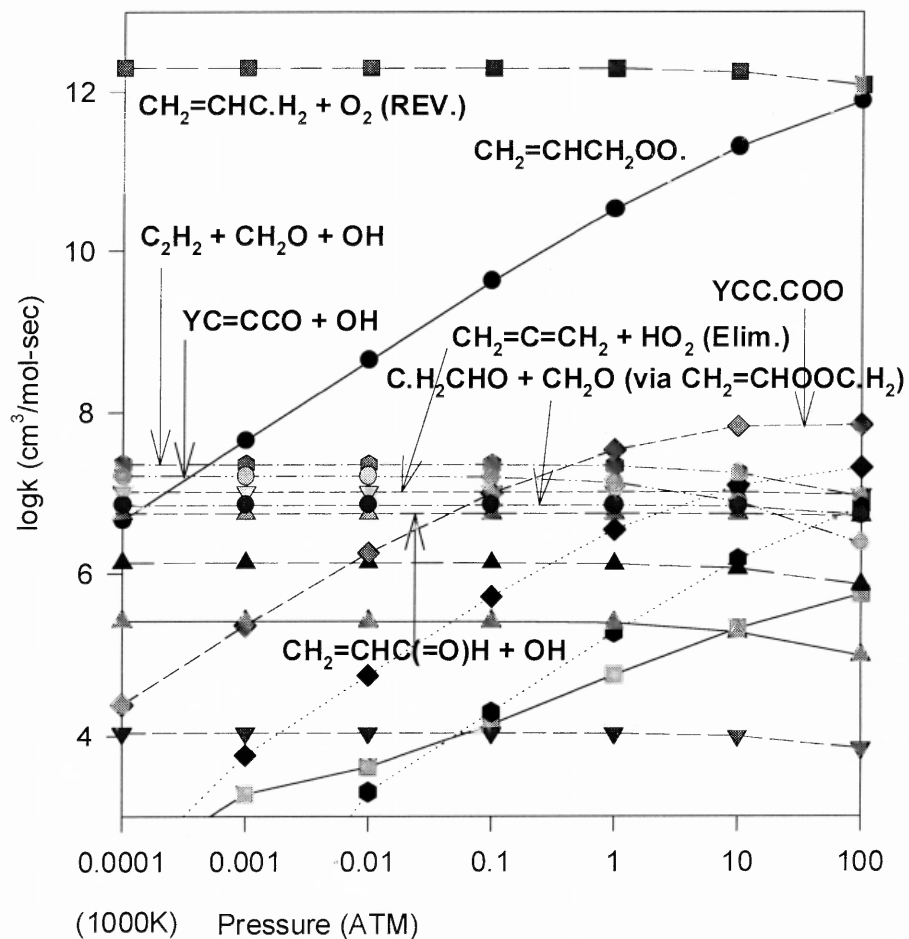


Figure 6.5 $\text{CH}_2=\text{CHC}\cdot\text{H}_2 + \text{O}_2 \rightarrow$ products k vs. pressure at 1000K.

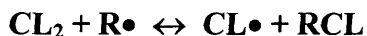
6.4 Summary

The allyl radical ($\text{CH}_2=\text{CHCH}_2\bullet$) + O_2 reaction system is analyzed with density functional and *ab initio* calculations, to evaluate thermochemical properties, reaction paths and kinetics in oxidation. Enthalpies of formation (ΔH_f°) are determined using isodesmic reaction analysis at the CBSQ//B3LYP/6-31G(d,p) composite and density functional levels. Entropies (S°) and heat capacities ($C_p^\circ(T)$) are determined using geometric parameters and vibrational frequencies obtained at the B3LYP/6-31G(d,p) level of theory. Internal rotor contributions are included in S and $C_p(T)$ values.

Rate constants are estimated as a function of pressure and temperature using quantum Rice-Ramsperger-Kassel (QRRK) analysis for $k(E)$ and master equation for falloff. $\text{CH}_2=\text{CHCH}_2\text{OO}\bullet$ adduct, cyclic isomers, and H-shift isomers exhibit significant falloff at higher temperatures. Important reactions are stabilization of $\text{CH}_2=\text{CHCH}_2\text{OO}\bullet$ adduct at low temperature and allene + HO_2 products via a HO_2 molecular elimination path, $\text{YCC}\bullet\text{COO}$ via cyclization, and H transfer from primary vinyl group to peroxy radical; then β -scission reaction leading to $\text{C}_2\text{H}_2 + \text{CH}_2\text{O} + \text{OH}$ and a ring closure to $\text{YC}=\text{CCO} + \text{OH}$ at higher temperature.

CHAPTER 7

***AB INITIO* CALCULATIONS AND THERMOCHEMICAL ANALYSIS ON CL ATOM ABSTRACTIONS OF CHLORINE FROM CHLOROCARBONS AND THE REVERSE ALKYL ABSTRACTIONS:**



7.1 Overview

Thermodynamic properties ($\Delta H_{f(298)}^{\circ}$, $S_{(298)}^{\circ}$ and $C_p(T)$ from 300 to 1500 K) for reactants, adducts, transition states, and products in reactions of CH_3 and C_2H_5 with Cl_2 are calculated using CBSQ//MP2/6-311G(d,p). Molecular structures and vibration frequencies are determined at the MP2/6-311G(d,p), with single point calculations for energy at QCISD(T)/6-311+G(d,p), MP4(SDQ)/CbsB4 and MP2/CBSB3 levels of calculation with scaled vibration frequencies. Contributions of rotational frequencies for $S_{(298)}^{\circ}$ and $C_p(T)$'s are calculated based on rotational barrier heights and moments of inertia using the method of Pitzer and Gwinn.⁷²

Thermodynamic Parameters, $\Delta H_{f(298)}^{\circ}$, $S_{(298)}^{\circ}$ and $C_p(T)$ are evaluated for C_1 and C_2 chlorocarbon molecules and radicals. These thermodynamic properties are used in evaluation and comparison of $\text{Cl}_2 + \text{R}\bullet \Rightarrow \text{Cl}\bullet + \text{RCl}$ (defined forward direction) reaction rate constants from the kinetics literature for comparison with the calculations. Data from some 20 reactions in the literature show linearity on a plot of $E_{a\text{fwd}}$ vs. $\Delta H_{\text{rxn,fwd}}$, yielding a slope of (0.38 ± 0.04) and intercept of (10.12 ± 0.81) kcal/mol. A correlation of average Arrhenius pre-exponential factor for $\text{Cl}\bullet + \text{RCl} \Rightarrow \text{Cl}_2 + \text{R}$. (reverse rxn) of $(4.44 \pm 1.58) \times 10^{13}$ cm³/mol-sec on a per chlorine basis is obtained with $E_{a\text{Rev}} = (0.64 \pm 0.04) \times \Delta H_{\text{rxn,Rev}} + (9.72 \pm 0.83)$ kcal/mol, where $E_{a\text{Rev}}$ is 0.0 if $\Delta H_{\text{rxn,Rev}}$ is more than 15.2

kcal/mol exothermic. Kinetic evaluations of literature data are also performed for classes of reactions.

$E_{a_{fwd}} = (0.39 \pm 0.11) \times \Delta H_{rxn,fwd} + (10.49 \pm 2.21)$ kcal/mol and average $A_{fwd} = (5.89 \pm 2.48) \times 10^{12}$ cm³/mol-sec for hydrocarbons: $E_{a_{fwd}} = (0.40 \pm 0.07) \times \Delta H_{rxn,fwd} + (10.32 \pm 1.31)$ kcal/mol and average $A_{fwd} = (6.89 \pm 2.15) \times 10^{11}$ cm³/mol-sec for C₁ chlorocarbons: $E_{a_{fwd}} = (0.33 \pm 0.08) \times \Delta H_{rxn,fwd} + (9.46 \pm 1.35)$ kcal/mol and average $A_{fwd} = (4.64 \pm 2.10) \times 10^{11}$ cm³/mol-sec for C₂ chlorocarbons:

Calculation results on the methyl and ethyl reactions with Cl₂ show agreement with the experimental data after an adjustment of + 2.3 kcal/mol is made in the calculated negative Ea's.

7.2 Background

High chlorinated solvents such as CH₂Cl₂, CHCl₃, CCl₄, C₂Cl₄, C₂HCl₃, C₂H₃Cl₃'s and fluoro chloro-carbon solvents or chemicals are in widespread use in the chemical, pharmaceutical and cleaning industries. The monomers are also present in a number of valuable and versatile polymers. The combustion, incineration or high temperature pyrolysis of these chlorocarbons includes reactions at or near surfaces and in liquids or polymers where oxygen is not present or is low in concentration. Chlorine atom abstraction of chlorine from the chlorocarbon is often the important chain propagation process in these systems; yet there is limited or almost no direct experimental kinetic information on these chlorine atom abstraction reactions. This is due to the Cl abstraction of Cl from R-Cl being endothermic, as the Cl-Cl bond is 57.8 kcal/mol, while a typical R-Cl bond energy ranges from 71 kcal/mol in CCl₄ to 95 or 98 in vinyl chloride

and chlorobenzene, respectively. Most chlorocarbons also have a hydrogen which is readily abstracted by Cl atoms, where the rate constants have high Arrhenius pre-exponential factors ($> 10^{13}$) and little or no energies of activation. (ca 1.0 kcal/mol if thermo neutral or exothermic) Cl abstraction of halogens is also important in designed pyrolysis and oxidation experiments, where hydrogen is limited or not present. This chlorocarbon oxidation or pyrolysis with no hydrogen source is not practical for incineration; but does have value in modeling because the presence of hydrogen adds an order of magnitude complexity to the models (number of species, and reaction product permutations). Pyrolysis of trichloroethylene, for example, shows extensive molecular weight growth products such as hexachloro-benzene, pentachloro-butadiene, etc which likely result from radical processes.¹⁶¹ The radical intermediates present in oxidation and pyrolysis of high chlorine to hydrogen ratio thermal processes result from Cl atom elimination, beta scission and from Cl atom abstraction of Cl reactions.

Seetula et. al¹⁶²⁻¹⁶⁵ studied the reaction kinetics of several halogenated methyl radicals with molecular chlorine. Halogen substitution in alkyl radicals was shown to have an important effect on the reactivity of these species.^{162,166} He showed that increased halogen substitution results in increased reaction barrier. Thermodynamic analysis also illustrates that increased halogen substitution reduces the reaction exothermicity. Seetula also investigated the transition states of the reactions of CH₃, C₂H₅ plus several halogenated methyl radicals with Cl₂ using *ab initio* MP2(FC)/6-31G(d,p) level of theory.¹⁶³

Thermodynamic properties ($\Delta H_{f(298)}^{\circ}$, $S_{(298)}^{\circ}$ and Cp(T) from 300 to 1500 K) for reactants, adducts, transition states, and products in reactions of CH₃ and C₂H₅ with Cl₂,

are determined using CBSQ//MP2/6-311G(d,p) *ab initio* calculations and kinetic predictions compared with evaluated data.

The kinetic data for these $\text{Cl}\bullet + \text{RCl} \Rightarrow \text{Cl}_2 + \text{R}\bullet$ reactions are estimated in this study by assembling and evaluating thermodynamic property data : $\Delta H_{f(298)}^\circ$, $S_{(298)}^\circ$, and $C_p(T)$ on chlorocarbon and several fluoro chlorocarbon molecules and radicals. We use the thermochemical properties with available literature data on the abstractions of Cl from Cl_2 by alkyl radicals and microscopic reversibility to evaluate trends in the forward and reverse rate constants.

7.3 Method

7.3.1 *Ab initio* Calculations on CH_3 and C_2H_5 Plus Cl_2 Reaction Systems

Thermodynamic properties ($\Delta H_{f(298)}^\circ$, $S_{(298)}^\circ$ and $C_p(T)$ from 300 to 1500 K) for reactants, adduct intermediates, transition states, and products in reactions of CH_3 and C_2H_5 with Cl_2 are calculated using the established CBSQ//MP2/6-311G(d,p) composite method of Petersson's research group.^{70,111,167} The CBSQ calculation sequence is performed on the MP2/6-311G(d,p) geometry and followed by single point calculations at the theory level of QCISD(T)/6-311+G(d,p), MP4(SDQ)/CbsB4 and MP2/CBSB3 CBSExtrap=(Nmin=10,Pop).

7.3.2 Determination of Enthalpies of Formation

$\Delta H_{f(298)}^\circ$ for reactants and products in reactions of CH_3 and C_2H_5 with Cl_2 are from literature data (see Table 7.1). $\Delta H_{f(298)}^\circ$ for transition states and adducts in reactions of CH_3 and C_2H_5 with Cl_2 are calculated using total energies obtained by CBSQ//MP2/6-311G(d,p) and MP2/6-311G(d,p) level. Total energies are corrected by zero point

vibrational energies (ZPVE) which are scaled by 0.9748 as recommended by Scott et al.¹⁵⁷ Thermal correction, 0 to 298.15 K, is calculated to estimate $\Delta H_{f(298)}^{\circ}$ at 298.15 K.⁷¹

7.3.3 Determination of Entropy and Heat Capacity

Entropy and heat capacities for reactants and products in reactions of CH_3 and C_2H_5 with Cl_2 are from literature data (see Table 7.1). Entropy and heat capacities for transition states and adducts in reactions of CH_3 and C_2H_5 with Cl_2 are calculated based on vibration frequencies and moments of inertia of the optimized MP2/6-311G(d,p) structures using statistical mechanics.¹⁵⁷ Contributions of internal rotation for $S_{(298)}^{\circ}$ and $C_p(T)$'s are calculated based on rotational barrier heights, moments of inertia of the rotors, and Pitzer and Gwinn's⁷² general treatment.

7.3.4 Thermodynamic Properties

Evaluated thermodynamic parameters: $\Delta H_{f(298)}^{\circ}$, $S_{(298)}^{\circ}$, and $C_p(300)$ to $C_p(1500)$ for species in the reaction schemes are listed in Table 7.1 along with literature references. Enthalpies of chlorocarbon (C_1 and C_2) radicals are from literature data and some from calculations in this study using isodesmic reactions: for example $\text{C}\bullet\text{H}_2\text{CH}_2\text{Cl}$ is from a calculated ΔH_{rxn} for $(\text{CH}_3\text{CH}_3 + \text{C}\bullet\text{H}_2\text{CH}_2\text{Cl} \rightleftharpoons \text{CH}_3\text{CH}_2\text{Cl} + \text{C}\bullet\text{H}_2\text{CH}_3)$ and the known $\Delta H_{f(298)}^{\circ}$ for ethane, chloroethane and ethyl radical. Entropies and $C_p(T)$ values of C_2H_3 , C_2H_5 are from use of Hydrogen Bond Increment(HBI) method.¹⁶⁸ The HBI group technique is based on known thermodynamic properties of the parent molecule and calculated changes that occur upon formation of a radical via loss of a H atom. The HBI incorporates changes in radical formation, that result from loss or changes in vibrational frequencies, internal rotations, spin degeneracy and mass.

Table 7.1 Evaluated Thermodynamic Property Data

SPECIES	H _f (298)	S(298)	Cp300	Cp400	Cp500	Cp600	Cp800	Cp1000	Cp1500	REF(a)
CH3	34.82	46.38	9.26	10.05	10.82	11.54	12.89	14.09	16.29	JANAF(79)
TSCH3XC12	32.10	74.11	15.86	17.27	18.43	19.42	21.06	22.41	24.82	CBSQ(in this study)
CH3CI	-19.60	56.00	9.77	11.51	13.19	14.66	17.05	18.87	21.76	TRC(77)
C2H5	29.30	57.42	11.89	14.57	16.95	19.09	22.76	25.66		LAY/BOZ95(168)
TSC2H5XC12	24.20	84.10	19.94	22.96	25.60	27.84	31.46	34.25	38.82	CBSQ(in this study)
C2H5CI	-26.80	66.01	15.03	18.57	21.61	24.22	28.37	31.44	36.16	JANAF(79)
i-C3H7	21.02	70.39	16.58	20.27	24.03	27.49	33.13	37.52	44.37	LAY/BOZ95(168)
i-C3H7CI	-34.70	73.41	20.85	25.88	30.48	34.34	40.33	44.92		WONG/BOZ(170)
t-C4H9	11.90	75.67	22.33	27.04	31.82	36.27	43.62	49.34	58.53	LAY/BOZ95(168)
t-C4H9CI	-44.13	76.42	26.66	33.67	39.89	45.02	52.53	57.84		WONG/BOZ(170)
C2H3	71.64	53.79	10.10	11.93	13.57	14.97	17.22	18.95		LAY/BOZ95(168)
CH2CHCI	5.00	63.08	12.89	15.56	17.80	19.61	22.35	24.35		ZHU/BOZ95(171)
C3H5	40.75	62.05	14.87	18.66	21.88	24.63	28.95	32.10	36.78	LAY/BOZ95(168)
C3H5CI	-0.46	73.31	18.14	22.12	25.51	28.40	32.94	36.28	41.45	SWS(80)
C3H3	81.58	59.57	13.76	16.10	18.10	19.80	22.48	24.43	27.31	LAY/BOZ95(168)
C3H3CI	39.17	68.78	17.26	20.10	22.45	24.39	27.33	29.42	32.62	TRC(77)
CH2CI	27.99	58.61	10.08	11.45	12.53	13.38	14.66	15.64	17.30	TAY/DEL91(172)
CH2CI2	-22.83	64.57	12.20	14.24	15.93	17.30	19.32	20.76	22.91	JANAF(79)
CHCI2	23.50	68.10	12.90	14.16	15.09	15.79	16.76	17.44	18.46	KAFAFI89(freq.)(173)
CHCI3	-24.20	70.66	15.76	17.83	19.34	20.44	21.91	22.86		SWS(80)
CCI3	19.00	70.92	15.25	16.66	17.56	18.16	18.83	19.18	19.56	JANAF(79)
CCI4	-22.94	74.02	19.98	21.92	23.09	23.82	24.64	25.05	25.47	JANAF(79)
CF3	-113.01	63.42	11.93	13.68	15.05	16.09	17.46	18.22	19.07	JANAF(79)
CF3CI	-169.20	68.17	16.04	18.53	20.32	21.59	23.16	24.02	24.98	JANAF(79)
CF2CI	-66.02	67.72	13.17	14.73	15.93	16.83	17.98	18.59	19.25	RAYEZ94(174)
CF2CI2	-117.50	71.91	17.36	19.68	21.28	22.37	23.68	24.39	25.16	JANAF(79)
CFCI2	-21.60	69.17	14.02	15.42	16.49	17.28	18.26	18.77	19.34	RAYEZ94(174)
CFCI3	-67.70	74.07	18.71	20.84	22.22	23.13	24.19	24.74	25.33	TRC(77)
C2CI5	9.06	95.68	28.56	31.13	32.72	33.75	34.93	35.54	36.20	TRC(77)
C2CI6	-33.80	94.77	32.67	36.11	38.29	39.69	41.29	42.11		SWS(80)
CHCI2CHCI	11.53	84.51	21.49	24.59	26.84	28.49	30.64	32.05	34.08	TRC(77)
C2H2CI4	-36.00	84.86	23.74	27.67	30.65	32.89	35.99	38.01	40.66	TRC(77)
CH2CICCI2	7.65	84.56	21.39	24.09	26.15	27.70	29.95	31.50	33.77	TRC(77)
CH2CICCI3	-35.71	85.07	24.67	28.36	31.16	33.28	36.24	38.17	40.70	TRC(77)
CH2CICHCI	14.65	78.56	18.33	21.15	23.40	25.19	27.82	29.73	32.70	TRC(77)
CH2CICHCI2	-34.80	79.71	20.40	24.47	27.74	30.29	33.85	36.15	39.29	TRC(77)
CHCI2CH2	20.31	74.64	18.95	21.99	24.28	26.05	28.54	30.31	33.01	TRC(77)
CCI3CHCI	11.28	88.26	25.57	28.51	30.38	31.62	33.13	34.03	35.25	TRC(77)
CHCI2CCI3	-34.80	91.18	28.30	31.96	34.52	36.34	38.64	40.17	41.99	TRC(77)
CHCI2CCI2	6.55	90.65	23.88	26.74	28.78	30.23	32.15	33.32	34.89	TRC(77)

UNITS : H_f(kcal/mol), S(cal/K-mol), Cp(cal/K-mol) (a) : reference for Cp(T) and S only

Table 7.2 Cl₂ + Radicals -----> Products + Cl

REACTIONS	A _{fwd} *	Ea _{fwd} *	A _{rev} **	A _{rev} /Cl#	Ea _{rev} **	ΔH ^o _{rxn,fwd} **	P(torr)	T (K)	Reference*	
<HYDROCARBONS>										
1. Cl ₂ + CH ₃ -----> CH ₃ Cl + Cl	3.02E+12	0.53	2.99E+13	2.99E+13	26.10	-25.50	1.9-2.8	296-712	175	
2. Cl ₂ + C ₂ H ₅ -----> C ₂ H ₅ Cl + Cl	7.59E+12	-0.30	8.51E+13	8.51E+13	26.66	-27.18	1.7-2.2	295-498	175	
3. Cl ₂ + i-C ₃ H ₇ *** -----> i-C ₃ H ₇ Cl + Cl	1.51E+13	-0.48	1.03E+15	1.03E+15	25.82	-26.80	1.4-1.9	295-498	175	
4. Cl ₂ + t-C ₄ H ₉ *** -----> t-C ₄ H ₉ Cl + Cl	2.40E+13	-0.01	4.04E+15	4.04E+15	26.37	-27.11	1.4-1.8	295-498	175	
5. Cl ₂ + C ₂ H ₃ -----> CH ₂ CHCl + Cl	5.25E+12	-0.48	4.49E+13	4.49E+13	37.10	-37.72	1.4-1.7	298-435	169	
6. Cl ₂ + C ₃ H ₅ -----> C ₃ H ₅ Cl + Cl	4.67E+12	4.30	1.58E+13	1.58E+13	16.52	-12.29	2.0-3.6	487-693	169	
7. Cl ₂ + C ₃ H ₃ -----> C ₃ H ₃ Cl + Cl	8.30E+12	6.70	7.00E+13	7.00E+13	20.01	-13.49	2.6-4.1	525-693	169	
	(Avg.) 9.70E+12			7.59E+14	(not recommended)					
If i-C ₃ H ₇ , t-C ₄ H ₉ , C ₂ H ₃ are excluded, (Avg.) (5.89 +/- 2.48)E+12				(5.02 +/- 3.27)E+13						
<C₁ CHLOROCARBONS>										
8. Cl ₂ + CH ₂ Cl -----> CH ₂ Cl ₂ + Cl	9.10E+11	0.98	4.83E+13	2.42E+13	22.87	-21.90	1.7-4.3	295-719	162	
9. Cl ₂ + CHCl ₂ -----> CHCl ₃ + Cl	5.18E+11	2.46	1.30E+14	4.34E+13	21.09	-18.78	1.8-4.6	357-719	162	
10. Cl ₂ + CCl ₃ -----> CCl ₄ + Cl	4.08E+11	5.26	6.00E+13	1.50E+13	17.91	-13.02	3.1	690-700	166	
11. Cl ₂ + CF ₃ -----> CF ₃ Cl + Cl	2.69E+12	3.58	1.83E+14	1.83E+14	30.53	-27.27	2.3-2.6	487-693	166	
12. Cl ₂ + CF ₂ Cl -----> CF ₂ Cl ₂ + Cl	7.76E+11	1.91	6.89E+13	3.44E+13	24.13	-22.56	1.8-2.9	376-626	166	
13. Cl ₂ + CFCl ₂ -----> CFCl ₃ + Cl	8.32E+11	3.35	4.74E+13	1.58E+13	20.12	-17.18	1.5-2.6	435-693	166	
	(Avg.) 1.02E+12			5.26E+13	(not recommended)					
If CF ₃ is excluded, (Avg.) (6.89 +/- 2.15)E+11				(2.66 +/- 1.22)E+13						
<C₂ CHLOROCARBONS>										
14. Cl ₂ + C ₂ Cl ₅ -----> C ₂ Cl ₆ + Cl	2.00E+11	5.50	2.17E+14	3.61E+13	19.04	-13.94	50	298-423	176	
15. Cl ₂ + CHCl ₂ CHCl -----> (CHCl ₂) ₂ + Cl	6.31E+11	2.70	4.92E+14	1.23E+14	21.17	-18.61	50	298-423	176	
16. Cl ₂ + CH ₂ CICCl ₂ -----> CH ₂ CICCl ₃ + Cl	6.92E+11	4.10	4.29E+14	1.07E+14	18.27	-14.44	50-300	298-321	177	
17. Cl ₂ + CH ₂ CICHCl -----> CH ₂ CICHCl ₂ + Cl	2.00E+12	2.00	1.05E+15	3.49E+14	22.39	-20.53	80-280	298-328	178	
18. Cl ₂ + CHCl ₂ CH ₂ -----> CH ₂ CICHCl ₂ + Cl	6.31E+11	0.90	5.37E+13	1.79E+13	27.09	-26.19	50	298-423	176	
19. Cl ₂ + CCl ₃ CHCl -----> CHCl ₂ CCl ₃ + Cl	3.16E+11	5.10	7.96E+13	1.59E+13	22.30	-17.16	50	298-423	176	
20. Cl ₂ + CHCl ₂ CCl ₂ -----> CHCl ₂ CCl ₃ + Cl	3.16E+11	5.10	1.96E+14	3.91E+13	17.30	-12.43	50	298-423	176	
	(Avg.) 6.84E+11			9.83E+13	(not recommended)					
If CH ₂ CICHCl is excluded, (Avg.) (4.64 +/- 2.10)E+11				(5.65 +/- 4.65)E+13						
TOTALS	(TOTAL Avg.) 3.80E+12			3.03E+14	(not recommended)					
If i-C ₃ H ₇ , t-C ₄ H ₉ , C ₂ H ₃ , CF ₃ , CH ₂ CICHCl are excluded, (2.35 +/- 3.07)E+12				(4.44 +/- 1.58)E+13						

 UNITS :: A_{fwd} and A_{rev} : cm³/(mol-sec), Ea and ΔH^o_{rxn,fwd} : kcal/mol

 A_{fwd} = (2.35 +/- 3.07)*10¹² cm³/(mol-sec)

 A_{rev}(avg)/cl = (4.44 +/- 1.58)*10¹³ cm³/(mol-sec)

 (i-C₃H₇, t-C₄H₉, C₂H₃, CF₃, CH₂CICHCl are excluded in calc. of A_{fwd} and A_{rev}(avg)/cl.)

 * : references for A_{fwd} and Ea_{fwd}

** : calculated from Thermodynamic Properties of reactants and products

- microscopic reversibility -

 *** : i-C₃H₇, t-C₄H₉ Symmetries = 162 & 18 respectively

7.3.5 Thermodynamic Analysis for the Reactions

Arrhenius pre exponential factors on a per chlorine basis, energies of activation and enthalpies of reaction, A_{Rev} , $A_{\text{Rev}}/\text{Cl}\#$, $E_{a\text{Rev}}$ and $\Delta H^{\circ}_{\text{rxn,fwd}}$ are calculated using literature reference data on the forward reactions A_{fwd} and $E_{a\text{fwd}}$, the evaluated thermodynamic properties of reactants and products, and microscopic reversibility. The forward reaction direction is defined as $\text{Cl}_2 + \text{R}\bullet \Rightarrow \text{Cl}\bullet + \text{RCl}$. Allyl radical C_3H_5 and propargyl radical C_3H_3 have resonant structures each having two radical sites with near equal population at temperature of the experimental data, 500-700K. (Ref.169 in Table 7.2) These radical reactions with Cl_2 are assessed as occurring via both radical sites, and estimated similar rates for each site. The experimental rate constant for the forward direction is multiplied by 0.5 to obtain the forward rate constant on a per radical site basis.

7.4 Results and Discussion

7.4.1 *Ab initio* Calculations of Thermodynamic Properties in Reactions of CH_3 and C_2H_5 with Cl_2

$\text{CH}_3 + \text{Cl}_2 \rightarrow \text{CH}_3\text{Cl} + \text{Cl}$. Reaction Path Energies. The $\text{CH}_3 + \text{Cl}_2$ form an initial $\text{CH}_3\text{-ClCl}$ adduct which has a shallow well 1.45 kcal/mol below that of the reactants (CBSQ//MP2/6-311G(d,p) level) with C-Cl bond length of 3.10Å and Cl-Cl bond length of 2.04Å. The Cl-Cl bond in this adduct is 0.01Å longer than calculated for Cl_2 . This $\text{CH}_3\text{-ClCl}$ adduct reacts to the Transition State (TS) which is 4 kcal/mol above the adduct at the MP2/6-311G(d,p) level, but not higher in energy at the CBSQ level of calculation. (see Figure 7.1) The C-Cl bond length is 0.77Å shorter and the Cl-Cl bond is 0.06Å longer in the TS than in the $\text{CH}_3\text{-ClCl}$ adduct, where the carbon-Cl bond is forming and the Cl-Cl bond is breaking. The TS has a 9.12 cal/mol-K lower $S^{\circ}_{(298)}$ than the $\text{CH}_3\text{-ClCl}$

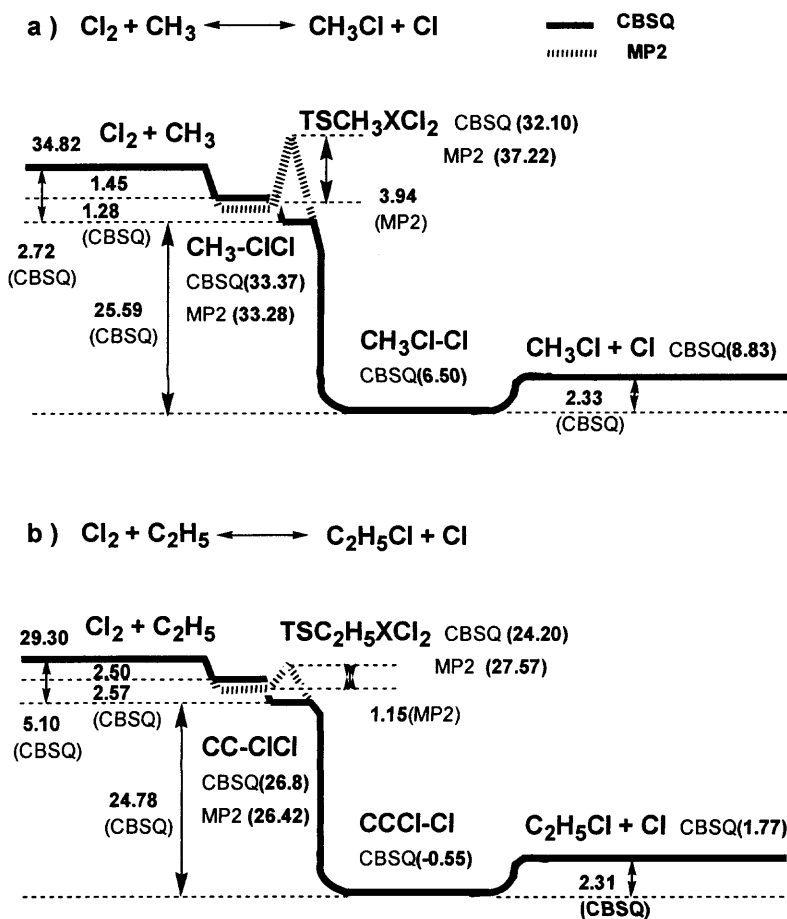


Figure 7.1 Reaction path diagrams in CH_3 with Cl_2 and C_2H_5 with Cl_2 .

adduct. The TS then goes to a $\text{CH}_3\text{Cl-Cl}$ adduct which has a 25.59 kcal/mol well (CBSQ) with the C-Cl bond length 0.55 Å shorter and the Cl-Cl bond length 1.20 Å longer than in the TS. The $\text{CH}_3\text{Cl-Cl}$ adduct has a 6.34 cal/mol-K higher $S^0_{(298)}$ than the TS structure. The $\text{CH}_3\text{Cl-Cl}$ adduct dissociates to $\text{CH}_3\text{Cl} + \text{Cl}$ with a low barrier of 2.33 kcal/mol.

$\text{C}_2\text{H}_5 + \text{Cl}_2 \rightarrow \text{C}_2\text{H}_5\text{Cl} + \text{Cl}$. Reaction Path Energies. The $\text{C}_2\text{H}_5 + \text{Cl}_2$ form an initial adduct CC-ClCl which also has a shallow well, about 2.5 kcal/mol below that of the reactants at the CBSQ//MP2/6-311G(d,p) level, with C-Cl bond length of 2.85 Å and Cl-Cl bond length of 2.04 Å. The Cl-Cl bond in this adduct is 0.01 Å longer than

calculated for Cl_2 . This CC-ClCl adduct reacts to the TS which is 1.15 kcal/mol higher in energy at the MP2/6-311G(d,p) level, but not higher in energy at the CBSQ level of calculation. (see Figure 7.1) The C-Cl bond length is 0.45Å shorter and the Cl-Cl bond is 0.04Å longer in the TS than in the CC-ClCl adduct. The TS has a 3.37 cal/mol-K lower $S^\circ_{(298)}$ than the $\text{CH}_3\text{-ClCl}$ adduct. The TS goes to the CCCI-Cl which has a well of 24.78 kcal/mole at the CBSQ level where the C-Cl bond length is 0.61Å shorter and the Cl-Cl bond is 1.17Å longer than in the TS. The CCCI-Cl adduct has a 2.06 cal/mol-K higher $S^\circ_{(298)}$ than the TS structure. The CCCI-Cl adduct dissociates to products of $\text{C}_2\text{H}_5\text{Cl} + \text{Cl}$ with low barrier of 2.31 kcal/mol.

7.4.2 Estimation of Entropy and Heat Capacity for Transition States and Adducts

Entropy and heat capacities are calculated based on vibration frequencies and moments of inertia of the optimized MP2/6-311G(d,p) structures. The calculation results using MP2/6-311G(d,p) determined geometries and frequencies are summarized in Table 7.3. TVR represents the sum of the contributions from translations, vibrations and external rotations to $S^\circ_{(298)}$ and $\text{Cp}(T)$'s. Symmetry is incorporated in estimation of $S^\circ_{(298)}$ as described in Table 7.3. Contributions of internal rotation for $S^\circ_{(298)}$ and $\text{Cp}(T)$'s are calculated based on rotational barrier heights, moments of inertia of the rotors using the method of Pitzer and Gwinn's.⁷²

Entropy differences between reactant and TS are used to determine the pre-exponential factor, A, via canonical transition state theory:

$$A = (k_b T/h_p) \exp(\Delta S^\ddagger/R), E_a = \Delta H^\ddagger$$

(h_p is Plank's constant and k_b is the Boltzman constant.)

Table 7.3 Ideal Gas Phase Thermodynamic Properties^a : $\Delta H_f^{\circ}_{298}$: CBSQ//MP2/6-311G(d,p), S°_{298} and $C_p(T)$: MP2/6-311G(d,p)

Species and Symmetry #		$\Delta H_f^{\circ}_{298}$	S°_{298} ^b	C_{p300} ^b	C_{p400}	C_{p500}	C_{p600}	C_{p800}	C_{p1000}	C_{p1500}
ch3-clcl (3)	TVR ^c		83.23	20.23	21.32	22.23	23.03	24.43	25.64	27.91
	Total ^f	33.37	83.23 ^e	20.23	21.32	22.23	23.03	24.43	25.64	27.91
tsch3xcl2 (3)	TVR		68.68	14.39	15.96	17.22	18.27	19.97	21.36	23.80
	Internal Rotor 1 ^d		5.42	1.48	1.31	1.21	1.15	1.08	1.05	1.02
	Total ^f	32.10	74.11 ^e	15.86	17.27	18.43	19.42	21.06	22.41	24.82
ch3cl-cl (3)	TVR		74.70	13.48	15.15	16.79	18.25	20.62	22.44	25.40
	Internal Rotor 1		5.75	0.99	0.99	0.99	0.99	0.99	0.99	0.99
	Total ^f	6.23	80.45 ^e	14.47	16.14	17.79	19.24	21.61	23.43	26.39
cc-clcl (3)	TVR		83.09	21.39	24.37	27.05	29.35	33.06	35.92	40.63
	Internal Rotor 1		4.38	1.63	1.76	1.76	1.70	1.58	1.47	1.27
	Total ^f	26.8	87.47 ^e	23.02	26.13	28.81	31.05	34.64	37.39	41.90
tsc2h5xcl2 (3)	TVR		72.22	16.70	19.84	22.65	25.05	28.87	31.80	36.58
	Internal Rotor 1,2		11.89	3.24	3.11	2.95	2.79	2.59	2.44	2.24
	Total ^f	24.2	84.10 ^e	19.94	22.96	25.60	27.84	31.46	34.25	38.82
cccl-cl (3)	TVR		74.31	16.16	19.48	22.62	25.35	29.72	33.00	38.20
	Internal Rotor 1,2		11.85	3.46	3.33	3.16	2.99	2.76	2.58	2.32
	Total ^f	-1.19	86.16 ^e	19.62	22.81	25.78	28.35	32.47	35.58	40.52

^a Thermodynamic properties are referred to a standard state of an ideal gas of pure enantiomer at 1 atm. ^b In cal/mol-K. ^c The sum of contributions from translations, external rotations, and vibrations. ^d Contribution from internal rotation.

^e Symmetry number is taken into account ($-R * \ln(\text{number of symmetry})$)

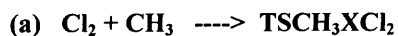
^f Spin degeneracy contribution for entropy = $1.987 * \ln(2)$ (cal/mol-K) is taken into account.

7.4.3 Calculated Enthalpies of Formation

Enthalpies for reactants, adducts, transition states, and products in reactions of CH_3 and C_2H_5 with Cl_2 are calculated using CBSQ//MP2/6-311G(d,p) and MP2/6-311G(d,p). The activation energies of $\text{TSCH}_3\text{XCl}_2$ are estimated by taking the difference of total energy between reactants and $\text{TSCH}_3\text{XCl}_2$ resulting in -2.73 and 2.4 kcal/mol for CBSQ//MP2/6-311G(d,p) and MP2/6-311G(d,p). $\Delta H_{f(298)}^0$ of the $\text{CH}_3\text{-ClCl}$ intermediate adduct is calculated as 33.37 and 33.28 kcal/mol, which is 1.45 and 1.54 kcal/mol below that of the reactants, respectively. Activation energies of $\text{TSC}_2\text{H}_5\text{XCl}_2$ are estimated by taking the difference of total energy between reactants and $\text{TSC}_2\text{H}_5\text{XCl}_2$ resulting in -5.07 and -1.73 kcal/mol for CBSQ//MP2/6-311G(d,p) and MP2/6-311G(d,p). $\Delta H_{f(298)}^0$ of CC-ClCl is calculated as 26.80 and 26.42 kcal/mol, respectively, which is below that of the reactants by 2.5 and 2.88 kcal/mol. The overall energy diagram is illustrated in Figure 7.1.

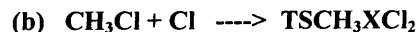
7.4.4 Thermodynamic Analysis for Reactions of CH_3 and C_2H_5 with Cl_2

The enthalpy of reaction, internal energy of reaction and the Arrhenius pre-exponential factor are calculated using thermodynamic properties of the respective reactants, products and transition state structures on each system for temperature from 300K to 2000K with results listed in Table 7.4. The reported experimental A_{fwd} of 3.02×10^{12} for $\text{Cl}_2 + \text{CH}_3 \Rightarrow \text{CH}_3\text{Cl} + \text{Cl}$ (Timonen/Gutman1986 [175]) reaction in Table 7.2, corresponds to the calculated A_{fwd} value near 700K as listed in Table 7.4 (a). The A_{Rev} of 2.99×10^{13} in $\text{CH}_3\text{Cl} + \text{Cl} \Rightarrow \text{Cl}_2 + \text{CH}_3$ reported in this study from microscopic reversibility, Table 7.2, corresponds to the calculated A_{Rev} near 500K in Table 7.4 (b).

Table 7.4 Thermodynamic and Kinetic Analysis for Reactions of CH₃ and C₂H₅ with Cl₂ Comparing with Experiment Data^a

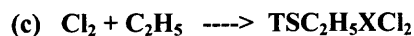
T(K)	ΔH ^a rxn	ΔU ^a rxn	Af ^a
300	-0.423	0.173	1.08E+12
400	-0.563	0.232	1.57E+12
500	-0.675	0.318	2.15E+12
600	-0.768	0.424	2.85E+12
800	-0.918	0.672	4.54E+12
1000	-1.044	0.943	6.61E+12
1200	-1.164	1.220	9.00E+12
1500	-1.339	1.641	1.32E+13
2000	-1.568	2.406	2.19E+13

P(torr)	T(K)		Af ^a
1.9 - 2.8	296-712	Expt.*	3.02E+12



T(K)	ΔHrxn	ΔUrxn	Af
300	25.08	25.68	9.04E+12
400	25.14	25.93	1.74E+13
500	25.14	26.14	2.75E+13
600	25.10	26.30	3.82E+13
800	24.91	26.50	5.93E+13
1000	24.60	26.59	7.78E+13
1200	24.21	26.59	9.37E+13
1500	23.55	26.53	1.14E+14
2000	22.41	26.38	1.46E+14

P(torr)	T(K)		Af
1.9 - 2.8	296-712	Expt.*	2.99E+13



T(K)	ΔHrxn	ΔUrxn	Af
300	-2.800	-2.204	6.39E+11
400	-2.810	-2.015	1.12E+12
500	-2.808	-1.814	1.75E+12
600	-2.803	-1.611	2.54E+12
800	-2.812	-1.223	4.48E+12
1000	-2.865	-0.878	6.80E+12
1200	-2.959	-0.575	9.38E+12
1500	-3.139	-0.158	1.37E+13
2000	-3.400	0.574	2.26E+13

P(torr)	T(K)		Af
1.7 - 2.2	295-498	Expt.*	7.59E+12



T(K)	ΔHrxn	ΔUrxn	Af
300	24.38	24.98	9.98E+12
400	24.37	25.17	1.75E+13
500	24.33	25.32	2.60E+13
600	24.25	25.44	3.49E+13
800	24.01	25.60	5.25E+13
1000	23.70	25.68	6.87E+13
1200	23.33	25.71	8.36E+13
1500	22.73	25.71	1.05E+14
2000	21.73	25.70	1.39E+14

P(torr)	T(K)		Af
1.7 - 2.2	295-498	Expt.*	8.51E+13

^aUnits ; ΔH and ΔU : kcal/mol, Af : cm³/mol-sec

The reported experimental A_{fwd} of 7.59×10^{12} for $\text{Cl}_2 + \text{C}_2\text{H}_5 \Rightarrow \text{C}_2\text{H}_5\text{Cl} + \text{Cl}$ (Timonen/Gutman1986 [175]) reaction in Table 7.2, corresponds to the calculated A_{fwd} near 1100K in Table 7.4 (c). The A_{Rev} of 8.51×10^{13} for $\text{C}_2\text{H}_5\text{Cl} + \text{Cl} \Rightarrow \text{Cl}_2 + \text{C}_2\text{H}_5$ reaction from microscopic reversibility, Table 7.2, corresponds to the calculated A_{Rev} near 1200K in Table 7.4 (d).

The calculated rate constants, triangles in Figures 7.2 and 7.3, versus temperature are higher than the measured values (squares), when the calculated negative $\Delta H_{\text{f}(298)}^{0\dagger}$ for TS's for the forward reactions are used. The profiles of calculated k vs $1000/T$ both show negative temperature coefficients at temperatures below 600 K, where the ethyl system, which is more exothermic, has a more pronounced effect. Only the Ethyl + Cl_2 show negative temperature data in the experiment. This negative coefficient is attributed to the high negative, calculation value of the $\Delta H_{\text{f}(298)}^{0\dagger}$ (-5.10) relative to the $\Delta H_{\text{f}(298)}^0$ of the reactants.

The E_a 's ($\Delta H_{\text{f}(298)}^{0\dagger}$ for TS's) upward is adjusted, for each reaction, the adjusted values are constant at 2.3 kcal/mol higher than the calculated CBSQ values. For each reactions, this places the $\Delta H_{\text{f}(298)}^{0\dagger}$ for the TS of $\text{Cl} + \text{CH}_3\text{Cl}$ at 0.4 kcal/mol below the $\Delta H_{\text{rxn}(298)}^0$ and 2.8 kcal/mol for $\text{Cl} + \text{C}_2\text{H}_5\text{Cl}$, not constant differences $\Delta H_{\text{rxn}(298)}^0$ and the TS enthalpy. The profiles with the adjusted $\Delta H_{\text{f}(298)}^{0\dagger}$ (TS) now show acceptable relative rate agreement with the experiments (circles), and the negative curvature at lower temperatures only remains for the more exothermic ethyl system. This trend is also observed in the experimental values. The rate constant trend turns upward above 600 K, which is outside the temperature range of the experiments. This is attributed to the T^n term and our method of determining the A factor (see results and discussion section). The

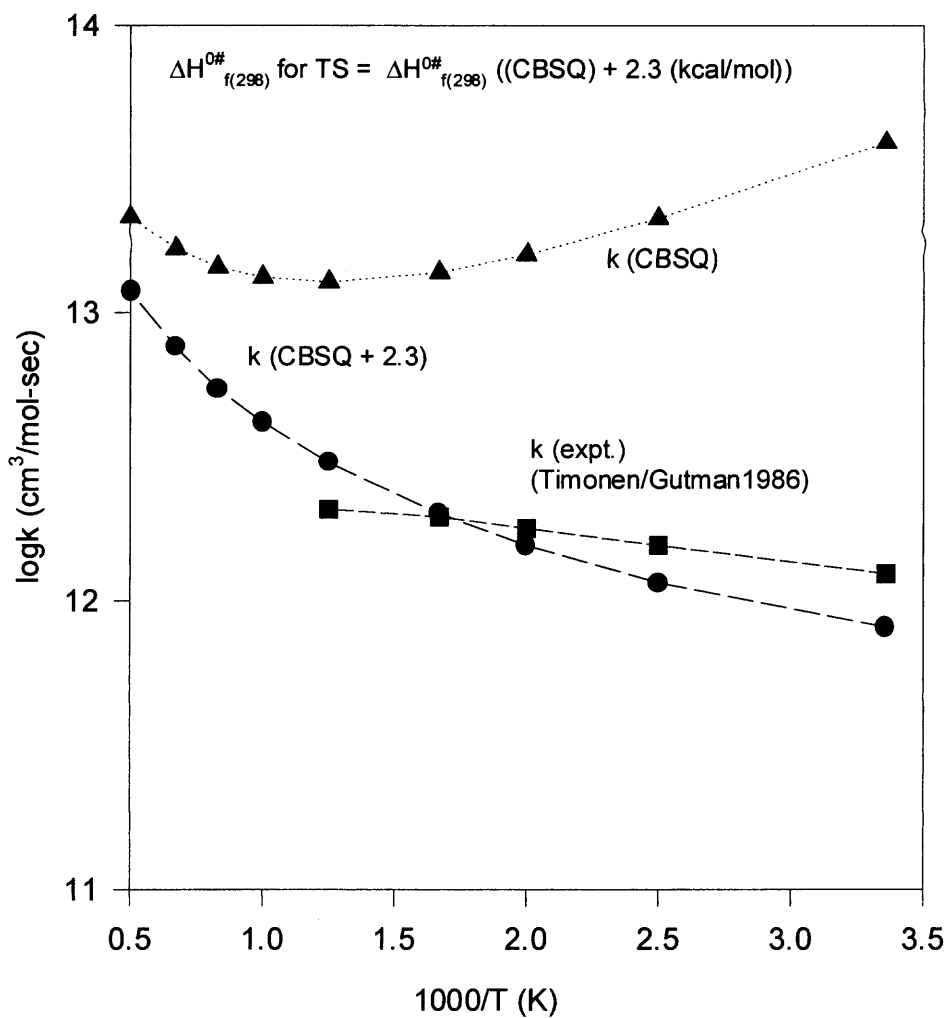


Figure 7.2 $\log k$ vs. $1000/T$ on $\text{CH}_3 + \text{Cl}_2 \rightarrow \text{CH}_3\text{Cl} + \text{Cl}\cdot$.

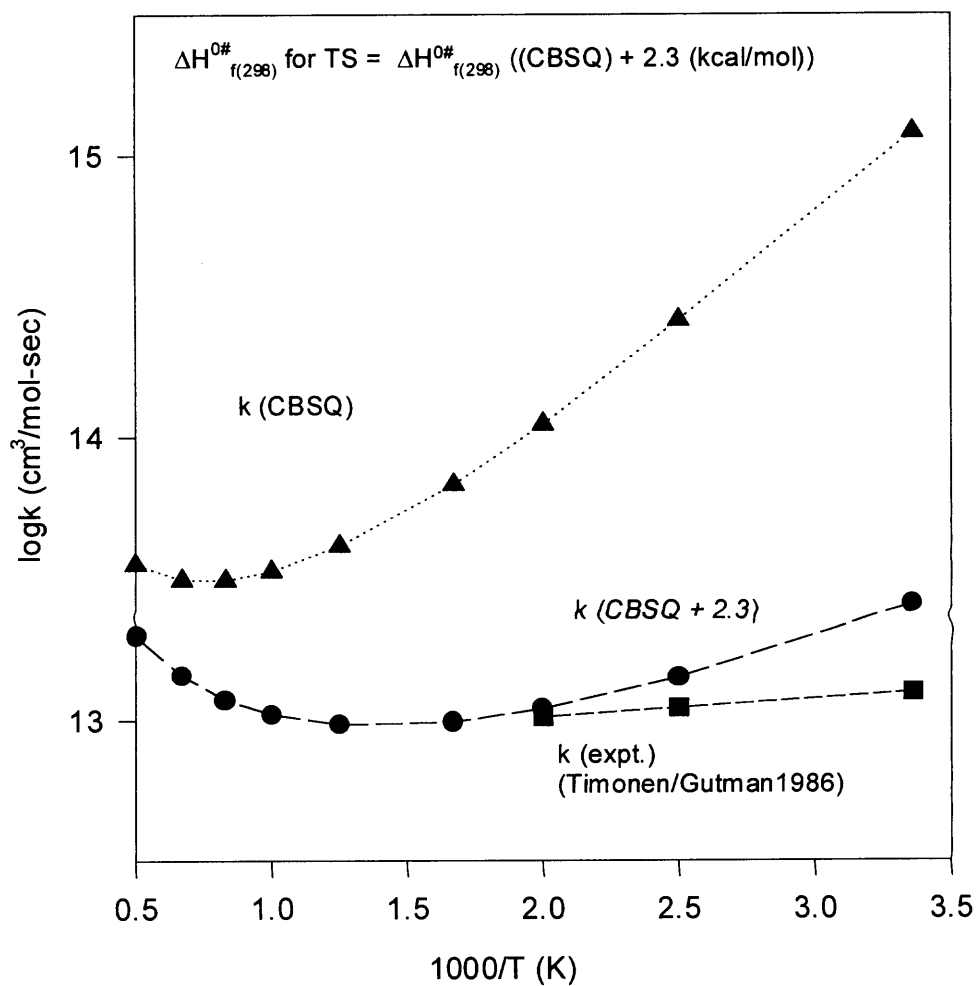


Figure 7.3 log k vs. 1000/T on $C_2H_5 + Cl_2 \rightarrow C_2H_5Cl + Cl\bullet$.

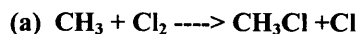
identical adjustment in each of these hydrocarbon systems suggests use of these adjusted transition state enthalpies as the calculated rate constants for the methyl and ethyl reactions with Cl₂ are reasonable. The equation below is cautiously recommended, for use of CBSQ values in these alkyl hydrocarbon(R) + Cl₂ reactions, until further calculation trends can be evaluated.

$$\Delta H_{f(298)}^{0\ddagger} \text{ for TS} = \Delta H_{f(298)}^{0\ddagger} (\text{CBSQ calculated TS} + 2.3 \text{ kcal/mol})$$

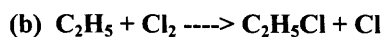
7.4.5 Atomic Charges in Reactants, Adducts, Transition States, and Products CH₃ + Cl₂ → CH₃Cl + Cl and C₂H₅ + Cl₂ → C₂H₅Cl + Cl Reactions

Table 7.5 illustrates Mulliken Atomic Charges on the H, C, and Cl atoms in the CH₃ + Cl₂ and C₂H₅ + Cl₂ reaction systems as obtained in the Gaussian 94 MP2/6-311G(d,p) calculations.⁶⁴ Calculated charges on the H atoms remain positive throughout the reaction process at ca. 0.1. Charges on the carbon bonding to Cl are negative 0.34 in CH₃ with a progressive decrease in negative charge (increase in overall charge) to -0.26 in the CH₃Cl molecule.

The corresponding carbon in the C₂H₅ reaction experiences a decrease from -0.25 to -0.31 when C₂H₅ + Cl₂ react to the TSC₂H₅XCl₂ and then increases to -0.21 in C₂H₅Cl. The Cl atom bonding to the carbon has no charge in Cl₂, positive 0.01 and 0.02 charges in the TSCH₃XCl₂ and the TSC₂H₅XCl₂, respectively, then decreases to -0.16 in the Cl atom of the products (both CH₃Cl and C₂H₅Cl). The leaving Cl has no charge in Cl₂, negative 0.13 charge in both the TSCH₃XCl₂ and the TSC₂H₅XCl₂, then increases near zero (-0.01) in both the CH₃Cl-Cl adduct and the CCl₂-Cl adduct.

Table 7.5 Calculated Atomic Charges, Bond Lengths(Å) and Bond Angles(deg) MP2/6-311G(d,p)Expt. $E_a = 0.53$ kcal/mol

	CH_3	$\text{Cl}_1\text{-Cl}_2$	$\text{CH}_3\text{-Cl}_1\text{Cl}_2$	$\text{TSC}_2\text{H}_5\text{XCl}_2$	$\text{CH}_3\text{Cl-Cl}$	CH_3Cl
Charges						
H	0.11		0.12	0.16	0.145	0.14
C	-0.34		-0.36	-0.35	-0.264	-0.26
Cl_1		0	0.02	0.01	-0.161	-0.159
Cl_2		0	-0.04	-0.13	-0.011	
Bond Length						
C-Cl			3.10	2.33	1.78	1.78
Cl-Cl		2.03	2.04	2.10	3.30	
Bond Angle						
C-Cl-Cl			180.0	180.0	89.1	

Expt. $E_a = -0.30$ kcal/mol

	C_2H_5	$\text{Cl}_5\text{-Cl}_6$	$\text{C}_3\text{C}_4\text{-Cl}_5\text{Cl}_6$	$\text{TSC}_2\text{H}_5\text{XCl}_2$	CCCl-Cl	$\text{C}_2\text{H}_5\text{Cl}$
Charges						
H_1	0.095		0.105	0.12	0.11	0.1
H_2	0.11		0.13	0.153	0.147	0.11
C_3	-0.25		-0.24	-0.23	-0.234	-0.24
C_4	-0.25		-0.29	-0.31	-0.22	-0.21
Cl_5		0	0.03	0.02	-0.161	-0.16
Cl_6		0	-0.06	-0.13	-0.01	
Bond Length						
C-Cl			2.85	2.40	1.79	1.79
Cl-Cl		2.03	2.04	2.08	3.25	
Bond Angle						
C-Cl-Cl			176.3	177.3	89.6	

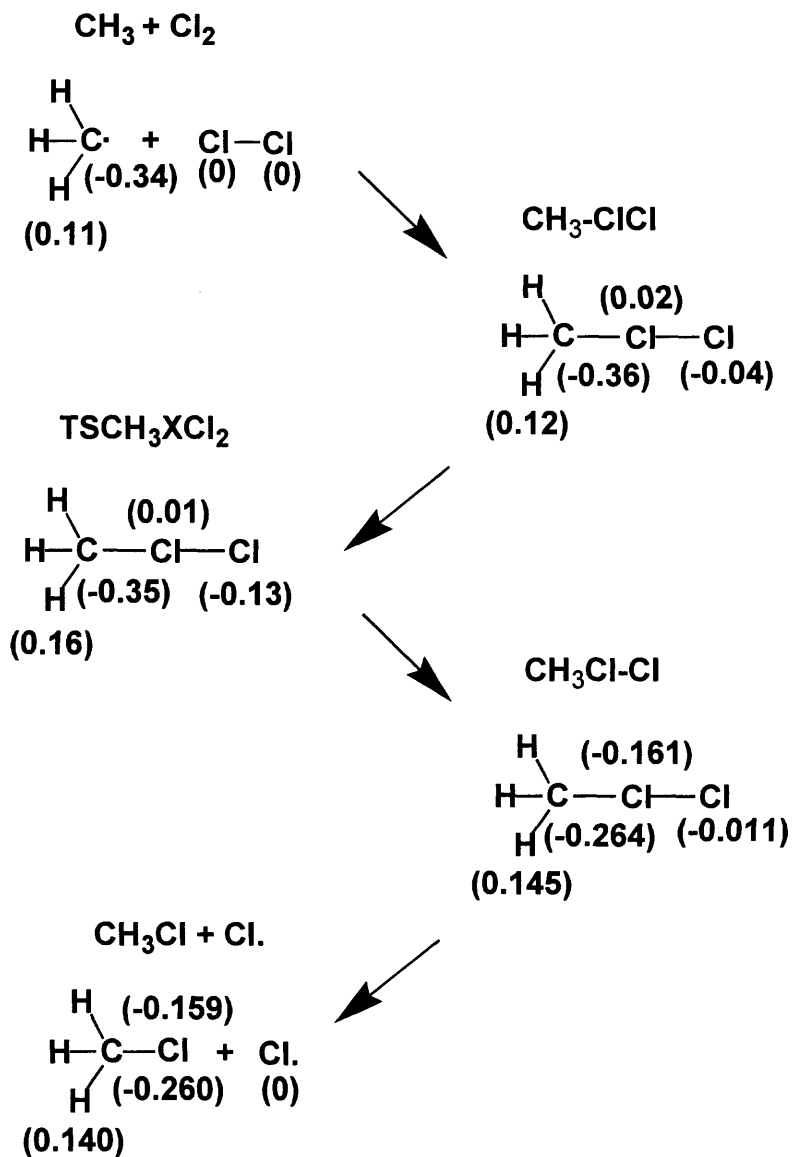
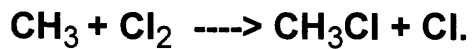


Figure 7.4A Calculated atomic charges at MP2/6-311G(d,p) $\text{CH}_3 + \text{Cl}_2 \longrightarrow \text{CH}_3\text{Cl} + \text{Cl}.$

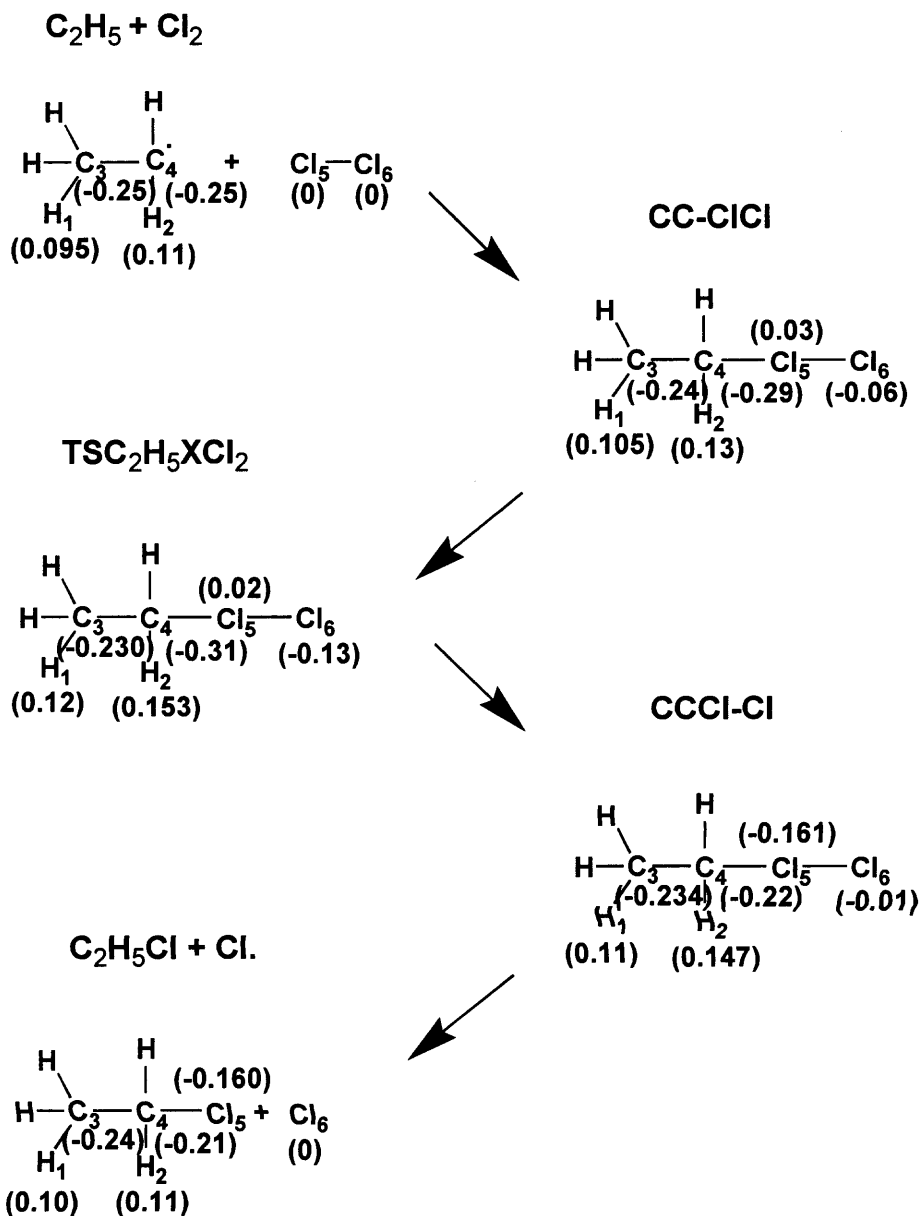
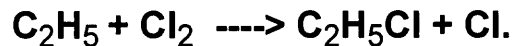


Figure 7.4B Calculated atomic charges at MP2/6-311G(d,p) $\text{C}_2\text{H}_5 + \text{Cl}_2 \longrightarrow \text{C}_2\text{H}_5\text{Cl} + \text{Cl}$.

Figure 7.4 and the above description of charges show that H atoms donate e^- to the carbon radical center and to chlorine in R-Cl. Replacement of the H's with electronegative halogens or other electronegative species must reduce the available e^- density to/at the carbon site. This likely reduces bond energy of additional R-Cl bonds being formed. Repulsive effects may also be important in the reduced bond energies.

Seetula also reported computational results for the transition states of the reactions of CH_3 , C_2H_5 and several halogenated methyl radicals with Cl_2 using *ab initio* methods.¹⁶³ Structures of species needed for transition state calculations were fully optimized at the MP2(full) level of theory using a 6-31G(d,p) basis set. His calculation results are in good agreement with MP2/6-311G(d,p) level calculations (Table 7.6) in this study with exception of $\Delta S_{298,\text{calc}}^\ddagger$ for $\text{C}_2\text{H}_5 + \text{Cl}_2$. The bond lengths of $\text{CH}_3\text{---Cl}_2$ and $\text{C}_2\text{H}_5\text{---Cl}_2$ in the transition state structures are 2.319Å and 2.383Å, respectively, in his calculation and 2.330Å and 2.402Å, respectively, in this study. The C-Cl-Cl angles in $\text{TSCH}_3\text{XCl}_2$ and $\text{TSC}_2\text{H}_5\text{XCl}_2$ are 180.0° and 178.4°, respectively, in his work and 180.0° and 177.3°, respectively, in this study. The activation energies to $\text{TSCH}_3\text{XCl}_2$ and $\text{TSC}_2\text{H}_5\text{XCl}_2$ in the reactants and the transition states of the reactions are 0.72 and -0.24 kcal/mol, respectively, in his MP2/6-31G(d,p) and CBSQ// MP2/6-311G(d,p) values in this study are -2.73 and -5.07 kcal/mol and MP2/6-311G(d,p) values are 2.4 and -1.73 kcal/mol in this study. $\Delta S_{298,\text{calc}}^\ddagger$ in the reactants and the transition states of the reactions are -25.57 cal/mol-K and -31.79 cal/mol-K, respectively, in his calculation and -25.56 and -26.61 cal/mol-K, respectively, in this study. Plausible reasons for different $\Delta S_{298,\text{calc}}^\ddagger$ values are: this treatment of internal rotors and/or his inclusion of a steric factor term. Vibration frequencies were not provided by Seetula for comparison: but are judged

similar due to near identical structures. ΔG^\ddagger to $\text{TSCH}_3\text{XCl}_2$ and $\text{TSC}_2\text{H}_5\text{XCl}_2$ in the reactants and the transition states of the reactions of Seetula (MP2/6-31G(d,p)) are 8.75 and 6.93 kcal/mol, respectively; while CBSQ//MP2/6-311G(d,p) results show 4.90 and 2.83 kcal/mol and MP2/6-311G(d,p) values are 10.02 and 6.20 kcal/mol, respectively, in this study.

Table 7.6 Comparison of Calculated Structures and Thermodynamic Parameters: Methyl and Ethyl Radical + Cl_2

(a) $\text{CH}_3 + \text{Cl}_2 \rightarrow \text{CH}_3\text{Cl} + \text{Cl}$

	Seetula(31) MP2/6-31G(d,p)	This Study	
		MP2/6-311G(d,p)	CBSQ//MP2/6-311G(d,p)
Bond Length(A)			
C-Cl	2.319	2.330	-
Cl-Cl	2.098	2.097	-
Bond Angle(degree)			
C-Cl-Cl	180.0	180.0	-
$\Delta S_{298,\text{calc}}^\#$ (cal/mol*K)	-25.57	-25.56	-
$\Delta G_{298}^\#$ (kcal/mol)	8.75	10.02	4.90
$\Delta H_{298}^\#$ (kcal/mol)	1.13	2.40	-2.72

(b) $\text{C}_2\text{H}_5 + \text{Cl}_2 \rightarrow \text{C}_2\text{H}_5\text{Cl} + \text{Cl}$

	Seetula(31) MP2/6-31G(d,p)	This Study	
		MP2/6-311G(d,p)	CBSQ//MP2/6-311G(d,p)
Bond Length(A)			
C-Cl	2.383	2.402	-
Cl-Cl	2.084	2.083	-
Bond Angle(degree)			
C-Cl-Cl	178.4	177.3	-
$\Delta S_{298,\text{calc}}^\#$ (cal/mol*K)	-31.79	-26.61	-
$\Delta G_{298}^\#$ (kcal/mol)	6.93	6.20	2.83
$\Delta H_{298}^\#$ (kcal/mol)	-2.54	-1.73	-5.10

7.4.6 Thermodynamics of Literature Data and Comparison

Overall Thermochemical and kinetic data for the $\text{Cl}_2 + \text{R}\bullet$ reactions for the 20 reference reactions are listed in Table 7.2. The average A_{fwd} for reaction $\text{Cl}_2 + \text{R}\bullet \Rightarrow \text{Cl}\bullet + \text{RCl}$ (defined forward direction) is

$$A_{\text{fwd}} = (2.35 \pm 3.07) \times 10^{12} \text{ cm}^3/\text{mol}\cdot\text{sec} \text{ and}$$

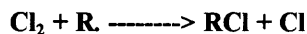
$$E_{a_{\text{fwd}}} = (0.38 \pm 0.04) \times \Delta H_{\text{rxn},\text{fwd}} + (10.12 \pm 0.81) \text{ kcal/mol.}$$

Figure 7.5 shows the correlation of $E_{a_{\text{fwd}}}$ vs. $\Delta H_{\text{rxn},\text{fwd}}$ with several exclusions noted. A correlation for the average Arrhenius pre-exponential factor for $\text{Cl}\bullet + \text{RCl} \Rightarrow \text{Cl}_2 + \text{R}\bullet$ (reverse rxn) of $A_{\text{rev}} = (4.44 \pm 1.58) \times 10^{13} \text{ cm}^3/\text{mol}\cdot\text{sec}$ on a per chlorine basis is obtained with $E_{a_{\text{Rev}}} = (0.64 \pm 0.04) \times \Delta H_{\text{rxn},\text{Rev}} + (9.72 \pm 0.83) \text{ kcal/mol}$, where $E_{a_{\text{Rev}}}$ is 0.0 if $\Delta H_{\text{rxn},\text{Rev}}$ is more than 15.2 kcal/mol exothermic.

Hydrocarbons Thermochemical and kinetic data for separate classes of reaction R equals Hydrocarbons are listed in Table 7.2 and plots of $E_{a_{\text{fwd}}}$ vs. $\Delta H_{\text{rxn},\text{fwd}}$ for Hydrocarbons are shown in Figure 7.6. Data for CH_3 , C_2H_5 , C_3H_5 and C_3H_3 show a slope leading to $E_{a_{\text{fwd}}} = (0.39 \pm 0.11) \times \Delta H_{\text{rxn},\text{fwd}} + (10.49 \pm 2.21) \text{ kcal/mol}$ and Average $A_{\text{fwd}} = (5.89 \pm 2.48) \times 10^{12} \text{ cm}^3/\text{mol}\cdot\text{sec}$, where Isopropyl, tertiary butyl and C_2H_3 radicals are excluded.

Tertiary butyl, isopropyl and ethyl radicals show slightly negative E_a 's for the forward reactions. This may suggest adduct formation occurs before further reaction to $\text{Cl}\bullet + \text{RCl}$ products.

The tertiary butyl and isopropyl radical reactions with Cl_2 result in unexpected high reverse Arrhenius pre-exponential factors. As can be noted in Table 7.1, the literature values of Arrhenius pre-exponential factor show a forward value of 1.5 and 2.4



	R.	$\Delta H_{\text{rxn,fwd}}^\circ$	$E_{\text{a,fwd}}$	Reference
1	CH ₃	-25.50	0.53	JANAF(79)
2	C ₂ H ₅	-27.18	-0.30	CIO/LIU97(179)
3	i-C ₃ H ₇	-26.80	-0.48	LAY/BOZ95(168)
4	t-C ₄ H ₉	-27.11	-0.01	LAY/BOZ95(168)
5	C ₂ H ₃	-37.32	-0.48	LAY/BOZ95(168)
6	C ₃ H ₅	-12.29	4.30	LAY/BOZ95(168)
7	C ₃ H ₃	-13.49	6.70	LAY/BOZ95(168)
8	CH ₂ Cl	-21.90	0.98	Seet98(180)
9	CHCl ₂	-18.78	2.46	ROUX/PAD87(181)
10	CCl ₃	-13.02	5.26	JANAF(79)
11	CF ₃	-27.27	3.60	JANAF(79)
12	CF ₂ Cl	-22.56	1.91	RAYEZ94(174)
13	CFCl ₂	-17.18	3.35	RAYEZ94(174)
14	C ₂ Cl ₅	-13.94	5.50	CIO/LIU97(179)
15	CHCl ₂ CHCl	-18.83	2.70	CIO/LIU97(179)
16	CH ₂ ClCCl ₂	-14.66	4.10	CIO/LIU97(179)
17	CH ₂ ClCHCl	-20.61	2.00	CIO/LIU97(179)
18	CHCl ₂ CH ₂	-26.19	0.90	CIO/LIU97(179)
19	CCl ₃ CHCl	-16.47	5.10	CIO/LIU97(179)
20	CHCl ₂ CCl ₂	-12.01	5.10	CIO/LIU97(179)

$$E_{\text{a,fwd}}(\text{R} + \text{Cl}_2 \rightarrow \text{RCl} + \text{Cl}) = (0.38 \pm 0.04) \Delta H_{\text{rxn,fwd}}^\circ + (10.12 \pm 0.81)$$

$$E_{\text{a,rev}}(\text{RCl} + \text{Cl} \rightarrow \text{R} + \text{Cl}_2) = (0.64 \pm 0.04) \Delta H_{\text{rxn,rev}}^\circ + (9.72 \pm 0.83)$$

$$\text{if } \Delta H_{\text{rxn,rev}}^\circ \leq -15.19 \quad E_{\text{a,rev}} = 0.0$$

(* : i-C₃H₇, t-C₄H₉, C₂H₃, CF₃, CH₂ClCHCl are excluded.)

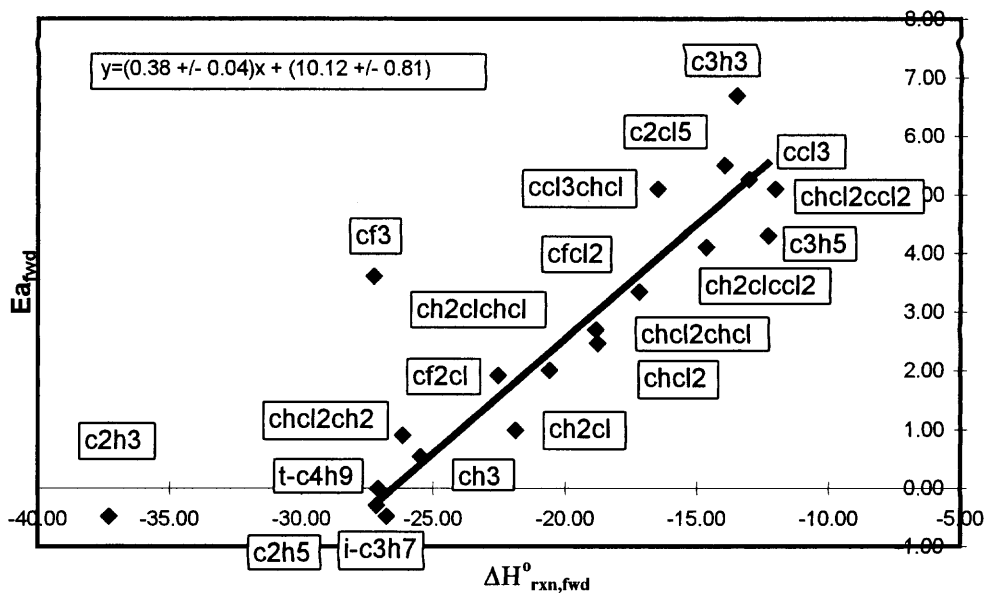


Figure 7.5 $E_{\text{a,fwd}}$ vs. $\Delta H_{\text{rxn,fwd}}^\circ$.

R.	$\Delta H^{\circ}_{\text{rxn,fwd}}$	$E_{\text{a,fwd}}$			
1	CH3	-25.50	0.53		
2	C2H5	-27.18	-0.30		
				3	i-C3H7
					-26.80
				4	t-C4H9
					-27.11
				5	C2H3
					-37.32
6	C3H5	-12.29	4.30		
7	C3H3	-13.49	6.70		

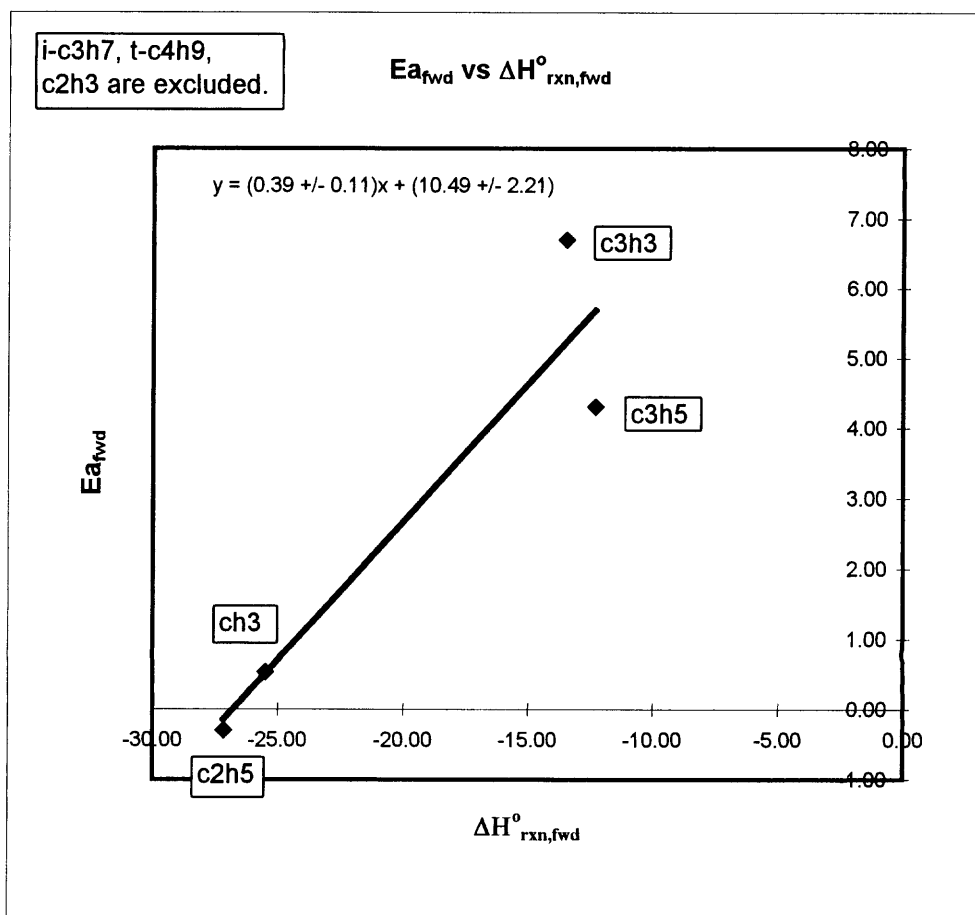


Figure 7.6 Hydrocarbons.

$\times 10^{13}$ cm³/mol-sec respectively. Thermodynamic analysis of the reaction systems lead to calculated pre-exponential factors for reverse reaction of 1×10^{15} and 4×10^{15} cm³/mol-sec respectively; Approximately 2.5 to 10 times higher than the estimated collision rate at 300K. The thermodynamic properties of species have been re-evaluated in these reactions and errors are not found in entropy terms that can account for the unreasonably large, reverse rate constants that are calculated. The kinetic data on these reactions are omitted from this analysis.

C₁ Chlorocarbons Thermochemical and kinetic data for C₁ Chlorocarbons are listed in Table 7.2 and plots of $E_{a\text{fwd}}$ vs. $\Delta H_{\text{rxn,fwd}}$ for the C₁ Chlorocarbons are shown in Figure 7.7. Data for CH₂Cl, CHCl₂, CCl₃, CF₂Cl and CFCl₂ yield a slope leading to $E_{a\text{fwd}} = (0.40 \pm 0.07) \times \Delta H_{\text{rxn,fwd}} + (10.32 \pm 1.31)$ kcal/mol and Average $A_{\text{fwd}} = (6.89 \pm 2.15) \times 10^{11}$ cm³/mol-sec. The experimental value for CF₃ is $k = 2.69 \times 10^{12} \exp(-3.58/RT)$ while an estimated k_{est} is $6.89 \times 10^{11} \exp(+0.59/RT)$.

C₂ Chlorocarbons Thermochemical and kinetic data for C₂ Chlorocarbons are listed in Table 7.2 and plots of $E_{a\text{fwd}}$ vs. $\Delta H_{\text{rxn,fwd}}$ for the C₂ Chlorocarbons are shown in Figure 7.8. Data for C₂Cl₅, CHCl₂CHCl, CH₂ClCCl₂, CHCl₂CH₂, CCl₃CHCl and CHCl₂CCl₂ show a correlation resulting in $E_{a\text{fwd}} = (0.33 \pm 0.08) \times \Delta H_{\text{rxn,fwd}} + (9.46 \pm 1.35)$ kcal/mol and Average $A_{\text{fwd}} = (4.64 \pm 2.10) \times 10^{11}$ cm³/mol-sec. The experimental value for CH₂ClCHCl is $k = 2.00 \times 10^{12} \exp(-2.00/RT)$ while an estimated k_{est} is $4.64 \times 10^{11} \exp(-2.69/RT)$.

A trend in E_a 's for these reactions are determined by thermochemical analysis of experimental and theoretical data in the literature references. (see Table 7.2)

R.	$\Delta H^{\circ}_{\text{rxn,fwd}}$	$E_{\text{a,fwd}}$
8 CH ₂ Cl	-21.90	0.98
9 CHCl ₂	-18.78	2.46
10 CCl ₃	-13.02	5.26
11 CF ₃	-27.27	3.58
12 CF ₂ Cl	-22.56	1.91
13 CFCl ₂	-17.18	3.35

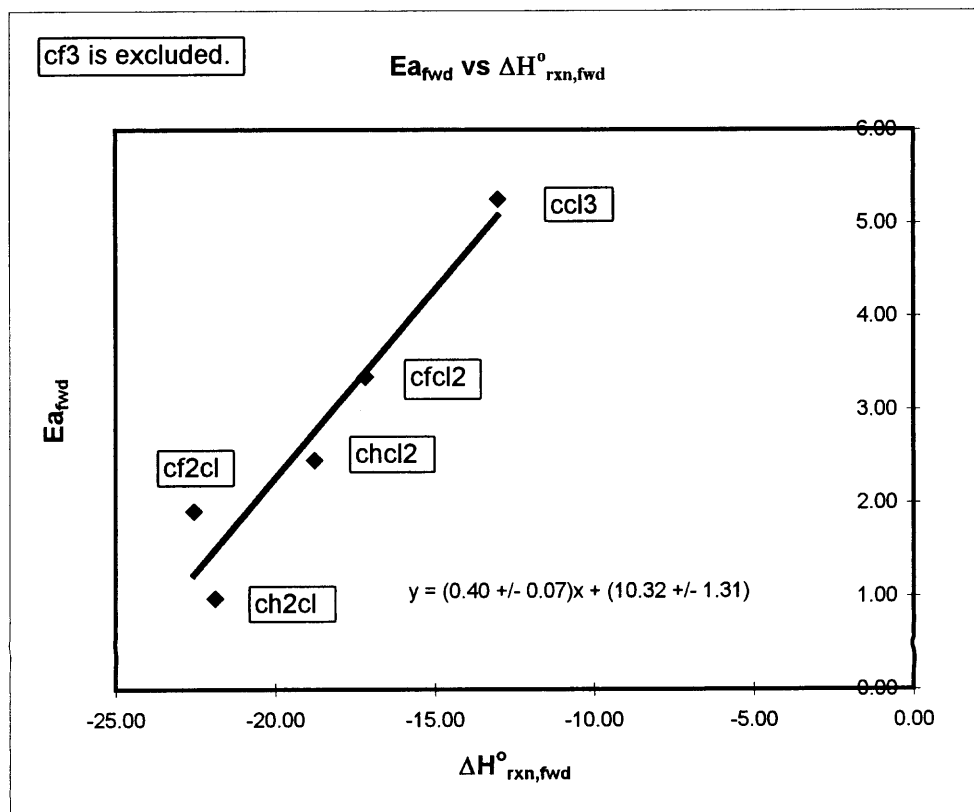


Figure 7.7 C₁ chlorocarbons.

R.	$\Delta H^{\circ}_{\text{rxn,fwd}}$	$E_{\text{a,fwd}}$
14 C2Cl5	-13.94	5.50
15 CHCl2CHCl	-18.83	2.70
16 CH2ClCCl2	-14.66	4.10
17 CH2ClCHCl	-20.61	2.00
18 CHCl2CH2	-26.19	0.90
19 CCl3CHCl	-16.47	5.10
20 CHCl2CCl2	-12.01	5.10

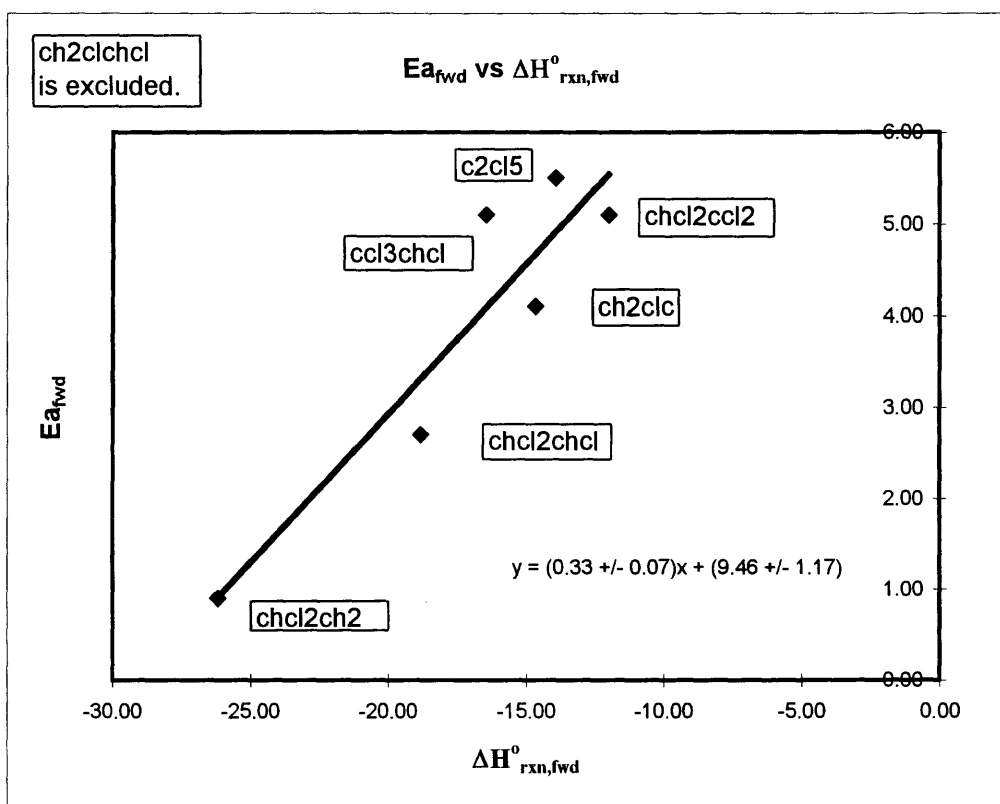
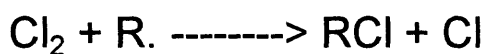


Figure 7.8 C₂ chlorocarbons.

The more exothermic $\text{Cl}_2 + \text{R}\bullet$ reactions ($\Delta H^\circ_{\text{rxn,fwd}} < -20$ kcal/mol) are those which involve hydrocarbon free radicals; these are shown to have small activation energies (less than 1 kcal/mol) in Table 7.2. The calculated transition states in CH_3 and C_2H_5 reaction with Cl_2 in Table 7.2, have enthalpy values which are -2.7 and -5.1 kcal/mol relative to the reactants (at the CBSQ composite level), respectively, in the exothermic $\text{Cl}_2 + \text{R}\bullet$ reaction direction (Figure 7.1).

Timonen et al.¹⁶⁹ studied the kinetics of the reactions of unsaturated hydrocarbon free radicals (vinyl, allyl, and propargyl) with molecular chlorine. They report the reactivities of C_3H_3 and C_3H_5 are significantly reduced below that of the vinyl radical in these Cl atom transfer reactions, and suggest the reduction is due entirely to the presence of energy barriers in reactions C_3H_3 and C_3H_5 . The Arrhenius pre-exponential factors of reactions C_2H_3 , C_3H_3 and C_3H_5 are all similar.¹⁶⁹ They indicate that the relatively low exothermicities of reactions C_3H_3 and C_3H_5 ($\Delta H^\circ_{\text{rxn,fwd}} = -14.8$ kcal/mol and -11.7 kcal/mol, respectively) could account for the existence of the observed 4.3 kcal/mol to 6.7 kcal/mol activation energies.

Seetula¹⁶³ shows a linear correlation in a plot of the rate constants for $\text{Cl}_2 + \text{R}\bullet$ reactions at 500K vs. Δ electronegativity of the radical species R. He suggests this results from a polar transition state, which involves intramolecular electronic repulsion or attraction forces of the R group and that these forces determine properties such as stability, which are driving forces behind reactivity of the radical. He suggests that an electronegative substituent at the radical site improves thermal stability of the radical and makes it less reactive by inductive effects.^{164,165} He also suggests that similar intramolecular electron delocalization forces are effective in the transition state

formation. Seetula concludes the trend in reactivity among $\text{Cl}_2 + \text{R}\bullet$ reactions is due primarily to changes in the activation energies for these reactions. This $E_{a,\text{fwd}}$ vs $\Delta H_{\text{rxn},\text{fwd}}$ trend is illustrated and supported by data in Figures 7.5 to 7.8. Table 7.7 shows the presence of Cl on the carbon of the radical site reduces bond energy of new R-Cl bonds being formed. The data show no significant barrier other than ΔH_{rxn} for the endothermic $\text{Cl}\bullet + \text{RCl} \Rightarrow \text{Cl}_2 + \text{R}\bullet$ (rxn) where $\text{Cl}_2 + \text{R}\bullet \Rightarrow \text{Cl}\bullet + \text{RCl}$ is highly exothermic (ca. 26 kcal/mol or 27 kcal/mol) like CH_3 or C_2H_5 with Cl_2 .

Table 7.7 $\text{Cl}_2 + \text{Radicals} \text{-----} \rightarrow \text{Products} + \text{Cl}$ (C-Cl Bnd Energy)

REACTIONS	ΔH_f^{298}	C--Cl bond energy
1. $\text{Cl}_2 + \text{CH}_3 \text{-----} \rightarrow \text{CH}_3\text{Cl} + \text{Cl}$	-25.50	83.34
8. $\text{Cl}_2 + \text{CH}_2\text{Cl} \text{-----} \rightarrow \text{CH}_2\text{Cl}_2 + \text{Cl}$	-21.90	79.74
9. $\text{Cl}_2 + \text{CHCl}_2 \text{-----} \rightarrow \text{CHCl}_3 + \text{Cl}$	-18.78	76.62
10. $\text{Cl}_2 + \text{CCl}_3 \text{-----} \rightarrow \text{CCl}_4 + \text{Cl}$	-13.02	70.86
11. $\text{Cl}_2 + \text{CF}_3 \text{-----} \rightarrow \text{CF}_3\text{Cl} + \text{Cl}$	-27.27	85.11
12. $\text{Cl}_2 + \text{CF}_2\text{Cl} \text{-----} \rightarrow \text{CF}_2\text{Cl}_2 + \text{Cl}$	-22.56	80.40
13. $\text{Cl}_2 + \text{CFCl}_2 \text{-----} \rightarrow \text{CFCl}_3 + \text{Cl}$	-17.18	75.02

UNITS :: ΔH_f^{298} and bond energy : kcal/mol

7.5 Summary

Thermodynamic Parameters, ΔH_f^0 , S^0 and $C_p(T)$ are evaluated for reactants and products in $\text{R}\bullet + \text{Cl}_2 \rightleftharpoons \text{RCl} + \text{Cl}\bullet$ reactions. The forward rate constants are evaluated from the literature. The reverse rate constants are calculated from evaluated thermodynamic properties of reactants and products and microscopic reversibility. The

trends of $E_{a_{\text{fwd}}}$ vs $\Delta H_{\text{rxn,fwd}}$ and Arrhenius pre-exponential factor for overall, hydrocarbons, C_1 chlorocarbons, and C_2 chlorocarbons are evaluated.

Rate expressions of average $A_{\text{fwd}} = (2.35 \pm 3.07) \times 10^{12} \text{ cm}^3/\text{mol}\cdot\text{sec}$ and $E_{a_{\text{fwd}}} = (0.38 \pm 0.04) \times \Delta H_{\text{rxn,fwd}} + (10.12 \pm 0.81) \text{ kcal/mol}$ for overall, average $A_{\text{fwd}} = (5.89 \pm 2.48) \times 10^{12} \text{ cm}^3/\text{mol}\cdot\text{sec}$ and $E_{a_{\text{fwd}}} = (0.39 \pm 0.11) \times \Delta H_{\text{rxn,fwd}} + (10.49 \pm 2.21) \text{ kcal/mol}$ for hydrocarbons, average A_{fwd} of $(6.89 \pm 2.15) \times 10^{11} \text{ cm}^3/\text{mol}\cdot\text{sec}$ and $E_{a_{\text{fwd}}} = (0.40 \pm 0.07) \times \Delta H_{\text{rxn,fwd}} + (10.32 \pm 1.31) \text{ kcal/mol}$ for C_1 chlorocarbons, and average A_{fwd} of $(4.64 \pm 2.10) \times 10^{11} \text{ cm}^3/\text{mol}\cdot\text{sec}$ and $E_{a_{\text{fwd}}} = (0.33 \pm 0.08) \times \Delta H_{\text{rxn,fwd}} + (9.46 \pm 1.35) \text{ kcal/mol}$ for C_2 chlorocarbons are recommended.

Ab initio calculation has been performed on $\text{CH}_3 + \text{Cl}_2 \rightleftharpoons \text{CH}_3\text{Cl} + \text{Cl}$ and $\text{C}_2\text{H}_5 + \text{Cl}_2 \rightleftharpoons \text{C}_2\text{H}_5\text{Cl} + \text{Cl}$ reaction. The canonical transition state calculations show some agreement with experimental data for these two, low $E_{a_{\text{fwd}}}$, reaction systems at temperatures below 1200K. The carbon atom which undergoes bonding to the Cl has a negative charge of -0.34 and -0.25 in CH_3 and C_2H_5 , respectively, which becomes more negative, -0.35 and -0.31 in $\text{TSCH}_3\text{XCl}_2$ and $\text{TSC}_2\text{H}_5\text{XCl}_2$, respectively, then the charge increases, becomes less negative, -0.26 and -0.21 in CH_3Cl and $\text{C}_2\text{H}_5\text{Cl}$, respectively.

CHAPTER 8

INTERNAL ROTOR ANALYSIS, THERMODYNAMIC PROPERTIES, BOND ENERGIES, DISSOCIATION PATHS AND KINETICS ON DIETHYL AND CHLORODIETHYL SULFIDES: CH₃CH₂SCH₂CH₃, CH₃CH₂SCH₂CH₂CL, and CH₂CLCH₂SCH₂CH₂CL

8.1 Overview

The use of Density Functional Theory, B3LYP/6-31g(d,p), with isodesmic working reactions for enthalpy of formation of sulfur hydrocarbons is tested using a set of known sulfur hydrocarbons. Thermodynamic properties for reactants, transition states and products for unimolecular dissociation of CH₃CH₂SCH₂CH₃, CH₃CH₂SCH₂CH₂Cl, and CH₂ClCH₂SCH₂CH₂Cl are then analyzed.

Standard enthalpy, $\Delta H_f^\circ_{298}$, are determined using isodesmic reaction analysis at the B3LYP/6-31G(d,p) level, with S°_{298} and $C_p(T)$ determined using geometric parameters and vibrational frequencies obtained at this same level of theory. Potential barriers for the internal rotor potentials are also calculated at the B3LYP/6-31G(d,p) level, and the hindered rotation contributions to S°_{298} and $C_p(T)$ are calculated. A more limited number of studies, specifically for transition states are also performed at KMLYP/6-311G(d,p), CBS-Q, and CBS-QB3 levels of theory, with the CBS-QB3 barriers recommended.

Hydrogen bond dissociation energies of CH₃SH, CH₃CH₂SH, CH₃SCH₃, CH₃CH₂SCH₂CH₃, and CH₃CH₂SCH₂CH₂Cl are calculated and compared with literature values where available.

Four center (Retro-ene like) reactions and C—S bond dissociations are important initial decomposition channels in the hydrocarbon – sulfur moieties. In the chlorine

systems HCl molecular elimination is the most important decomposition channel at lower temperatures. Carbon–sulfur and carbon–chlorine bond cleavage reactions, which have higher Arrhenius pre-exponential factors become important at higher temperatures.

8.2 Background

Sulfur species are present in many of the fuels that are used in combustion; these fuels include coals, heating, aircraft and diesel as well as automotive liquids. H₂S also has a significant presence in unrefined natural gas.^{182,183} In all these cases the source is contact of the elemental forms of sulfur with the natural underground deposits, where it becomes incorporated into the gas and crude oil stocks. A significant fraction of the sulfur in these liquid fuels is removed prior to use (combustion) in order to prevent pollution of the air, formation of SO₂ and subsequent formation of acid rain. It is more difficult to remove the sulfur from coals; but this is performed in many cases as well. Sulfur does persist in these cleaned fuels and oils that are treated for its removal to some extent and the sulfur species are subsequently combusted in their use.

In plants and animals, sulfur occurs in various proteins, and it is one of the 10 most abundant elements in the human body.¹⁸² Sulfur compounds are present and of interest in biological systems, in atmospheric chemistry, and in environmental science. The known involvement of sulfur centered radicals in these biological systems suggests that knowledge on the fundamental thermodynamic properties of the sulfur moieties would be valuable in understanding its affects on these systems.¹⁸⁴ Chlorinated sulfur compounds are also a major component of some biological agents used in chemical warfare.

The knowledge and understanding the oxidation and thermal reactivity of these sulfur species requires their thermodynamic properties, bond energies and kinetic parameters for unimolecular reactions.

8.3 Calculation Methods

8.3.1 Geometries and Vibration Frequencies

The initial structures of reactants, transition states and products are determined using ROHF or UHF/PM3 in MOPAC,⁶³ followed by optimization and vibrational frequency calculation at B3LYP/6-31G(d,p) level using GAUSSIAN 98.¹⁸⁵ Transition state geometries are identified by the existence of only one imaginary frequency, structure information and the transition state theory reaction coordinate vibration information. Zero-point vibrational energies (ZPVE) are scaled by 0.9806 as recommended by Scott and Radom.¹⁵⁷ Geometries of transition states optimized at B3LYP/6-31G(d,p) are shown in Table 8.1.

Table 8.1 Geometries of Transition States Optimized at B3LYP/6-31G(d,p)

Species Name & Structure	Bond Length (Å)		Bond Angle (Degree)		Dihedral Angle (Degree)	
[a] TS1	r21	1.53				
	r32	1.84	∠321	114.9		
	r43	2.69	∠432	166.9	∠4321	96.0
	r54	1.40	∠543	78.1	∠5431	-104.3
	r65	1.28	∠654	100.8	∠6543	0.4
	r75	1.09	∠754	117.1	∠7543	-108.7
	r85	1.09	∠854	117.1	∠8543	109.2
	r94	1.08	∠943	96.6	∠9436	-121.3
	r104	1.08	∠1043	96.9	∠10436	120.5
	r112	1.10	∠1121	111.3	∠11213	-122.3
	r122	1.10	∠1221	111.0	∠12213	120.0
	r131	1.10	∠1312	111.0	∠13123	-179.0
	r141	1.09	∠1412	111.0	∠14123	60.7
	r151	1.09	∠1412	111.0	∠14123	-60.0
				∠1512	∠15123	
	[b] TS2A	r21	1.53			
	r32	1.85	∠321	109.4		
	r43	1.80	∠432	100.6	∠4321	176.0
	r54	1.40	∠543	119.8	∠5432	134.1
	r65	2.61	∠654	90.7	∠6543	-106.5
	r75	1.08	∠754	121.1	∠7543	161.8
	r85	1.08	∠854	121.3	∠8543	-16.7
	r94	1.25	∠943	109.2	∠9432	45.3
	r104	1.09	∠1043	117.0	∠10432	-74.5
	r112	1.09	∠1121	111.3	∠11213	-119.5
	r122	1.09	∠1221	110.9	∠12213	119.4
	r131	1.09	∠1312	109.6	∠13123	179.6
	r141	1.09	∠1412	111.4	∠14123	60.3
	r151	1.09	∠1412	111.5	∠14123	-60.8
				∠1512	∠15123	
	[c] TS2B	r21	1.53			
	r32	1.84	∠321	114.9		
	r43	2.64	∠432	165.4	∠4321	95.9
	r54	1.40	∠543	78.4	∠5431	-108.9
	r65	1.29	∠654	100.4	∠6543	1.9
	r75	1.79	∠754	118.1	∠7543	-110.5
	r85	1.09	∠854	118.1	∠8543	111.1
	r94	1.08	∠943	99.9	∠9436	-122.4
	r104	1.08	∠1043	94.4	∠10436	117.8
	r112	1.10	∠1121	111.6	∠11213	-122.0
	r122	1.10	∠1221	111.2	∠12213	119.8
	r131	1.10	∠1312	110.7	∠13123	-179.4
	r141	1.09	∠1412	111.0	∠14123	60.7
	r151	1.09	∠1412	111.0	∠14123	-59.2
				∠1512	∠15123	

Table 8.1 Geometries of Transition States Optimized at B3LYP/6-31G(d,p) (continued)

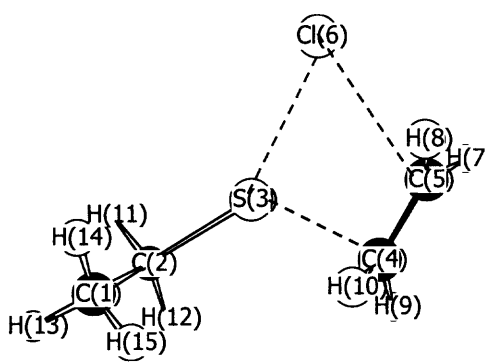
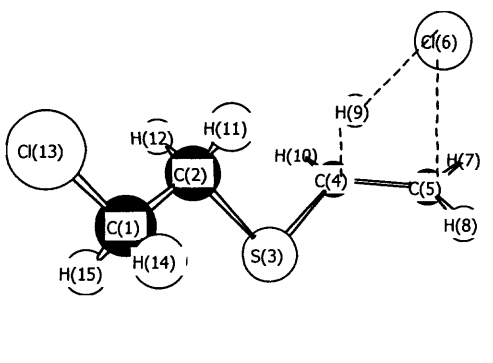
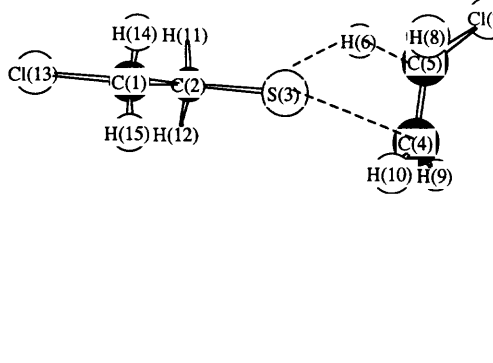
Species Name & Structure	Bond Length (Å)		Bond Angle (Degree)		Dihedral Angle (Degree)	
[d] TS2C						
	r21	1.53				
	r32	1.84	∠321	116.2		
	r43	2.30	∠432	125.3	∠4321	73.2
	r54	1.38	∠543	95.3	∠5431	179.9
	r63	2.66	∠632	141.2	∠6321	-107.0
	r75	1.08	∠754	121.4	∠7543	-91.1
	r85	1.08	∠854	121.4	∠8543	91.3
	r94	1.09	∠943	97.8	∠9432	59.1
	r104	1.09	∠1043	98.0	∠10432	-59.4
	r112	1.10	∠1121	111.1	∠11213	-115.4
	r122	1.10	∠1121	112.7	∠11213	126.8
	r131	1.10	∠1221	110.7	∠12213	175.6
	r141	1.09	∠1312	111.0	∠13123	55.3
	r151	1.09	∠1412	111.2	∠14123	-64.8
			∠1512		∠15123	
[e] TS3A						
	r21	1.52				
	r32	1.85	∠321	108.2		
	r43	1.80	∠432	99.9	∠4321	175.2
	r54	1.41	∠543	119.4	∠5432	134.6
	r65	2.60	∠654	90.4	∠6543	-106.3
	r75	1.08	∠754	120.9	∠7543	161.7
	r85	1.08	∠854	121.4	∠8543	-16.5
	r94	1.26	∠943	109.3	∠9432	45.4
	r104	1.09	∠1043	116.8	∠10432	-74.7
	r112	1.09	∠1121	110.9	∠11213	-119.6
	r122	1.09	∠1121	110.4	∠11213	119.2
	r131	1.81	∠1221	110.2	∠12213	-179.1
	r141	1.09	∠1312	111.8	∠13123	62.5
	r151	1.09	∠1412	111.8	∠14123	-60.5
			∠1512		∠15123	
[f] TS3B						
	r21	1.52				
	r32	1.84	∠321	111.7		
	r43	2.65	∠432	166.1	∠4321	94.0
	r54	1.40	∠543	78.4	∠5431	-112.0
	r65	1.29	∠654	100.3	∠6543	2.0
	r75	1.78	∠754	118.2	∠7543	-110.3
	r85	1.09	∠854	118.0	∠8543	111.0
	r94	1.08	∠943	99.9	∠9436	-122.6
	r104	1.08	∠1043	94.1	∠10436	117.7
	r112	1.09	∠1121	111.3	∠11213	-120.9
	r122	1.09	∠1121	111.1	∠11213	119.9
	r131	1.83	∠1221	111.1	∠12213	-179.7
	r141	1.09	∠1312	111.7	∠13123	61.7
	r151	1.09	∠1412	111.7	∠14123	-61.0
			∠1512		∠15123	

Table 8.1 Geometries of Transition States Optimized at B3LYP/6-31G(d,p) (continued)

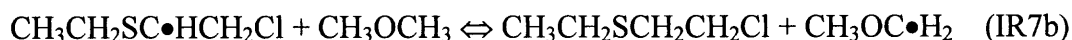
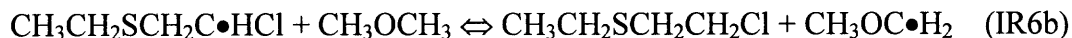
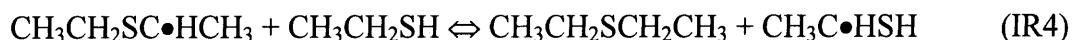
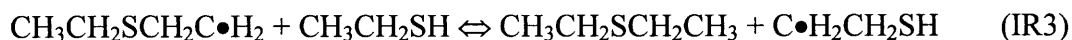
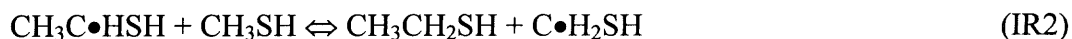
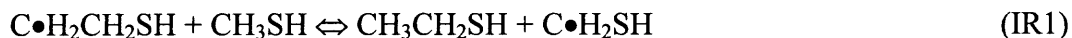
Species Name & Structure	Bond Length (Å)		Bond Angle (Degree)		Dihedral Angle (Degree)	
[g] TS3C	r21	1.52				
	r32	1.85	∠321	115.9		
	r43	2.28	∠432	124.5	∠4321	73.1
	r54	1.39	∠543	95.3	∠5431	-179.0
	r63	2.64	∠632	140.5	∠6321	-106.5
	r75	1.08	∠754	121.5	∠7543	-91.9
	r85	1.08	∠854	121.4	∠8543	89.9
	r94	1.09	∠943	98.4	∠9432	60.3
	r104	1.09	∠1043	97.1	∠10432	-58.0
	r112	1.10	∠1121	109.0	∠11213	-114.9
	r122	1.09	∠1221	111.9	∠12213	127.7
	r131	1.09	∠1312	111.5	∠13123	173.1
	r141	1.09	∠1412	111.6	∠14123	49.8
	r151	1.82	∠1412	111.3	∠14123	-68.9
				∠1512	∠15123	

8.3.2 Enthalpies of Formation

Enthalpies of formation ($\Delta H_f^\circ_{298}$) at B3LYP/6-31G(d,p) level on several sulfur hydrocarbons and corresponding radicals with a method of isodesmic reaction are evaluated and shown that the B3LYP/6-31G(d,p) values are in agreement with accepted literature values in Table 8.2. The evaluated $\Delta H_f^\circ_{298}$ for the reference molecules and radicals in the isodesmic reactions are given in Table 8.3.

Enthalpies of formation for reactants and products are calculated at B3LYP/6-31G(d,p) level. The method of isodesmic reactions for $C\bullet H_2CH_2SH$, $CH_3C\bullet HSH$, $CH_3CH_2SCH_2C\bullet H_2$, $CH_3CH_2SC\bullet HCH_3$, $CH_3CH_2SCH_2CH_2Cl$, $CH_3CH_2SCH_2C\bullet HCl$, and $CH_3CH_2SC\bullet HCH_2Cl$ is used to determine for accurate enthalpies of formation at B3LYP/6-31G(d,p) and recently published KMLYP density functional method with the

/6-311G(d,p) basis set.¹¹⁶ The evaluated reaction enthalpies and enthalpies of formation in the isodesmic reactions are listed in Table 8.4.



8.3.2.1 Enthalpies of formation for transition states. Although B3LYP has achieved good success in predicting thermochemistry of molecules, several studies report that B3LYP is less accurate for predicting barriers and has a tendency to underestimate barriers.¹¹⁶⁻¹¹⁹ Further calculations are performed for barriers with four different methods (B3LYP/6-31G(d,p), KMLYP/6-311G(d,p),¹¹⁶ CBS-Q,^{66,67,112} and CBS-QB3^{193,194}). Comparison of barriers is given in Table 8.5. The barrier is calculated relative to the reactants. The complete basis set (CBS-QB3) method of Petersson and co-workers for computing accurate energies^{193,194} is chosen as the determining activation energies used in this kinetic analysis.

Table 8.2 Comparison of Enthalpies of Formation at B3LYP/6-31G(d,p) with Literature Value

Working Reactions (Units: kcal/mol)	B3LYP/6-31G(d,p)			ΔH_f° ₂₉₈
	$\Delta H_{\text{rxn},298}^\circ$	ΔH_f° ₂₉₈	Avg. (B3LYP) ^a	Literature
CH₃SH + CH₄ <=> CH₃CH₃ + H₂S	-1.26	-5.99	-6.22 ± 0.68	-5.47 ± 0.14[186]
CH₃SH + CH₃OH <=> CH₃CH₂OH + H₂S	-6.47	-6.44		
CH₃CH₂SH + CH₄ <=> CH₃SH + CH₃CH₃	2.52	-10.34	-10.82 ± 2.93	-11.07 ± 0.14[186]
CH₃CH₂SH + CH₃OH <=> CH₃SH + CH₃CH₂OH	-2.69	-10.79		
CH₃CH₂SH + CH₃CH₂OH <=> CH₃SH + (CH₃)₂CHOH	-3.17	-11.32		
CH₃SCH₃ + CH₄ <=> CH₃SH + CH₃CH₃	0.87	-8.69	-9.17 ± 2.93	-8.96 ± 0.12[186]
CH₃SCH₃ + CH₃OH <=> CH₃SH + CH₃CH₂OH	-4.33	-9.15		
CH₃SCH₃ + CH₃CH₂OH <=> CH₃SH + (CH₃)₂CHOH	-4.82	-9.67		
C.H₂SH + CH₃OH <=> CH₃SH + C.H₂OH	-1.13	39.85	38.72 ± 2.12	36.36 ± 2.00[188]
C.H₂SH + CH₄ <=> C.H₂CH₃ + H₂S	3.43	38.36		
C.H₂SH + CH₃OH <=> C.H₂CH₂OH + H₂S	-0.38	37.94		
CH₃S. + CH₃CH₂OH <=> CH₃SH + CH₃CH₂O.	15.97	30.83	31.39 ± 2.29	30.83 ± 1.90[189]
CH₃S. + CH₃OH <=> CH₃SH + CH₃O.	14.85	31.94		
CH₃CH₂S. + CH₃CH₂OH <=> CH₃CH₂SH + CH₃CH₂O.	15.73	25.47	25.93 ± 2.09	24.14 ± 0.96[184]
CH₃CH₂S. + CH₃OH <=> CH₃SH + CH₃CH₂O.	13.05	25.74		
CH₃CH₂S. + CH₃OH <=> CH₃CH₂SH + CH₃O.	14.62	26.57		
C.H₂CH₂SH + CH₃SH <=> CH₃CH₂SH + C.H₂SH	-3.57	34.33	35.60 ± 4.06	
C.H₂CH₂SH + CH₃CH₃ <=> CH₃CH₂SH + C.H₂CH₃	1.11	36.86		
CH₃C.HSH + CH₃SH <=> CH₃CH₂SH + C.H₂SH	2.67	28.09	29.35 ± 4.06	
CH₃C.HSH + CH₃CH₃ <=> CH₃CH₂SH + C.H₂CH₃	7.36	30.61		
C.H₂SCH₃ + CH₃OCH₃ <=> CH₃SCH₃ + CH₃OC.H₂	0.68	34.45	34.33 ± 1.23	32.27 ± 0.72
C.H₂SCH₃ + CH₃CH₂OH <=> CH₃SCH₃ + C.H₂CH₂OH	7.30	34.21		[190,191]

^a Uncertainties are sum of the standard deviation for B3LYP/6-31G(d,p) level of theory

and maximum cumulative uncertainties from reference species.

Table 8.3 Enthalpies of Formation for Reference Molecules in the Isodesmic Reactions

Compounds	ΔH_f° (kcal/mol)	Compounds	ΔH_f° (kcal/mol)
CH ₃ SH	-5.47 ± 0.14 [186]	CH ₄	-17.89 ± 0.07 ^a [79]
CH ₃ CH ₃	-20.24 ± 0.10 ^a [80]	H ₂ S	-4.90 ± 0.19 [48]
CH ₃ CH ₂ SH	-11.07 ± 0.14 [186]	CH ₃ OH	-48.16 ± 0.07 [55]
CH ₃ CH ₂ OH	-56.17 ± 0.10 ^a [77]	(CH ₃) ₂ CHOH	-65.19 ± 2.2 [187]
CH ₃ SCH ₃	-8.96 ± 0.12 [186]	C.H ₂ SH	36.36 ± 2.0 [188]
C.H ₂ OH	-3.97 ± 0.22 [114]	C.H ₂ CH ₃	28.80 ± 0.50 [81]
C.H ₂ CH ₂ OH	-5.70 ± 0.85 [106]	CH ₃ S.	30.83 ± 1.90 [189]
CH ₃ CH ₂ O.	-3.90 ± 1.27 [114]	CH ₃ O.	4.10 ± 1.0 [109]
CH ₃ CH ₂ S.	24.14 ± 0.96 [184]	C.H ₂ SCH ₃	32.27 ± 0.72 [190,191]
CH ₃ CH ₂ SCH ₂ CH ₃	-20.08 ± 0.24 [186]	CH ₃ CH ₂ Cl	-26.80 ± 0.26 ^a [79]
CH ₂ ClCH ₂ Cl	-30.33 ± 0.67 [55]	CH ₃ OCH ₃	-43.99 ± 0.12 [55]
CH ₃ OC.H ₂	0.1 [192]	CH ₃ C.HOH	-13.34 ± 0.84 [114]

^a The uncertainties are evaluated from reference [55].

Table 8.4 Reaction Enthalpies and Enthalpies of Formation in the Isodesmic Reactions

Working Reactions (Units: kcal/mol)	$\Delta H_{\text{rxn},298}^{\circ}$		$\Delta H_f^{\circ}_{298}$	
	B3LYP	KMLYP	B3LYP	KMLYP
$\text{C.H}_2\text{CH}_2\text{SH} + \text{CH}_3\text{SH} \rightleftharpoons \text{CH}_3\text{CH}_2\text{SH} + \text{C.H}_2\text{SH}$	-3.57	-4.45	34.33	35.21
$\text{CH}_3\text{C.HSH} + \text{CH}_3\text{SH} \rightleftharpoons \text{CH}_3\text{CH}_2\text{SH} + \text{C.H}_2\text{SH}$	2.67	1.82	28.09	28.94
$\text{CH}_3\text{CH}_2\text{SCH}_2\text{C.H}_2 + \text{CH}_3\text{CH}_2\text{SH} \rightleftharpoons \text{CH}_3\text{CH}_2\text{SCH}_2\text{CH}_3 + \text{C.H}_2\text{CH}_2\text{SH}$	-0.72	-0.49	26.04	26.69
$\text{CH}_3\text{CH}_2\text{SC.HCH}_3 + \text{CH}_3\text{CH}_2\text{SH} \rightleftharpoons \text{CH}_3\text{CH}_2\text{SCH}_2\text{CH}_3 + \text{CH}_3\text{C.HSH}$	1.36	1.21	17.72	18.72
$\text{CH}_3\text{CH}_2\text{SCH}_2\text{CH}_2\text{Cl} + \text{CH}_3\text{CH}_3 \rightleftharpoons \text{CH}_3\text{CH}_2\text{SCH}_2\text{CH}_3 + \text{CH}_3\text{CH}_2\text{Cl}$	-0.19	-0.23	-26.45	-26.41
$\text{CH}_2\text{ClCH}_2\text{SCH}_2\text{CH}_2\text{Cl} + \text{CH}_3\text{CH}_3 \rightleftharpoons \text{CH}_3\text{CH}_2\text{SCH}_2\text{CH}_3 + \text{CH}_2\text{ClCH}_2\text{Cl}$	0.95	1.18	-31.12	-31.35
$\text{CH}_3\text{CH}_2\text{SCH}_2\text{C.HCl} + \text{CH}_3\text{CH}_2\text{OH} \rightleftharpoons \text{CH}_3\text{CH}_2\text{SCH}_2\text{CH}_2\text{Cl} + \text{C.H}_2\text{CH}_2\text{OH}$	5.71	4.70	18.32	19.36
$\text{CH}_3\text{CH}_2\text{SCH}_2\text{C.HCl} + \text{CH}_3\text{OCH}_3 \rightleftharpoons \text{CH}_3\text{CH}_2\text{SCH}_2\text{CH}_2\text{Cl} + \text{CH}_3\text{OC.H}_2$	-0.91	-1.69	18.55	19.38
				18.43 ± 1.71 (B3LYP)
Average ^a for $\text{CH}_3\text{CH}_2\text{SCH}_2\text{C.HCl}$				19.37 ± 1.56 (KMLYP)
$\text{CH}_3\text{CH}_2\text{SC.HCH}_2\text{Cl} + \text{CH}_3\text{CH}_2\text{OH} \rightleftharpoons \text{CH}_3\text{CH}_2\text{SCH}_2\text{CH}_2\text{Cl} + \text{CH}_3\text{C.HOH}$	2.80	0.99	13.58	15.43
$\text{CH}_3\text{CH}_2\text{SC.HCH}_2\text{Cl} + \text{CH}_3\text{OCH}_3 \rightleftharpoons \text{CH}_3\text{CH}_2\text{SCH}_2\text{CH}_2\text{Cl} + \text{CH}_3\text{OC.H}_2$	5.70	3.06	11.95	14.62
				12.76 ± 2.69 (B3LYP)
Average ^a for $\text{CH}_3\text{CH}_2\text{SC.HCH}_2\text{Cl}^b$				15.03 ± 2.11 (KMLYP)

^a Uncertainties are sum of the standard deviation for each calculation level of theory

and maximum cumulative uncertainties from reference species.

^b The values between B3LYP and KMLYP have 2.3 kcal/mol difference, so further calculations were performed. 12.71 ± 2.18 (B3LYP/6-311G(d,p)) and 12.85 ± 1.65 (CBSQ), so B3LYP value is recommended.

8.3.3 Entropy and Heat Capacity

The contributions of external rotations, translations, and vibrations to entropies and heat capacities are calculated from scaled vibration frequencies and moments of inertia for the optimized B3LYP/6-31G(d,p) structures. The number of optical isomers and spin degeneracy of unpaired electrons are also incorporated.

Contributions from hindered internal rotation for S and $C_p(T)$ are determined using direct integration over energy levels of the intramolecular rotational potential curves. A program, "ROTATOR¹³⁷", is used for calculation of the energy levels. This technique employs expansion of the hindrance potential in the Fourier series (E1), calculation of the Hamiltonian matrix on the basis of wave functions of the free internal rotor, and subsequent calculation of energy levels by direct diagonalization of the Hamiltonian matrix.¹³⁸⁻¹⁴⁰ The torsional potential calculated at discrete torsion angles is represented by a truncated Fourier series:

$$V(\Phi) = a_0 + \sum a_i \cos(i\Phi) + \sum b_i \sin(i\Phi) \quad i = 1, 2, 3, \dots \quad (E1)$$

Values of the coefficients (a_0 , a_i and b_i) are calculated to provide the minimum and maximum of the torsional potentials with allowance of a shift of the theoretical extreme angular positions.¹³⁸⁻¹⁴⁰ The energy levels are used to determine partition coefficients and their contributions to S and $C_p(T)$ through relationships from statistical mechanics.

8.3.4 High-Pressure Limit A Factors (A) and Rate Constants (k_∞) Determination

For the reactions where thermochemical properties of transition states are calculated by *ab initio* or density functional methods, k_∞ 's are fit by three parameters A, n, and Ea over temperature range from 298 to 2000K, $k_\infty = A (T)^n \exp(-Ea /RT)$. Entropy differences

between reactant and transition state are used to determine the pre-exponential factor, A , via canonical Transition State Theory (TST)

$$A = (k_b T/h_p) \exp(\Delta S^\ddagger/R), \quad E_a = \Delta H^\ddagger$$

where h_p is the Planck constant and k_b is the Boltzmann constant. Treatment of the internal rotors for S and $C_p(T)$ is important here because these internal rotors are often lost in the cyclic transition state structures.

Table 8.5 Comparison of Activation Energies (Units in kcal/mol)

	B3LYP/6-31G(d,p)	KMLYP/6-311G(d,p)	CBS-Q	CBS-QB3
<H Shift>				
TS1	61.51	73.42	65.46	64.41
TS2B	65.62	78.08	68.62	67.77
TS3B	64.15	76.93	66.81	66.99
<Cl Shift>				
TS2C	73.54	95.29	80.89	78.61
TS3C	73.31	94.80	79.57	77.64
<HCl Elimination>				
TS2A	52.25	59.04	58.06	57.27
TS3A	54.27	61.42	60.08	59.11

8.4 Results and Discussion

8.4.1 Rotational Barriers

Potential barriers for internal rotations of $\text{CH}_3\text{CH}_2\text{SCH}_2\text{CH}_2\text{Cl}$ and $\text{CH}_2\text{ClCH}_2\text{SCH}_2\text{CH}_2\text{Cl}$ are calculated in the B3LYP/6-31G(d,p) level and shown in Figures 8.1 and 8.2, respectively. The potential energies are calculated as a function of the dihedral angle by varying the torsion angle in 30° intervals and allowing other parameters to be optimized. The barriers for internal rotations are calculated from the differences between the total energy of each conformation and that of the most stable conformer at 0 K, where the zero point vibrational energy (ZPVE) and thermal correction to 298 K are not included. Total energies at 0 K and calculated internal rotation barriers versus the dihedral angle are presented in the Appendix D (Table D.1). The coefficients of the Fourier expansion components, a_i , and b_i in eq. (E1) are listed in the Appendix D (Table D.2).

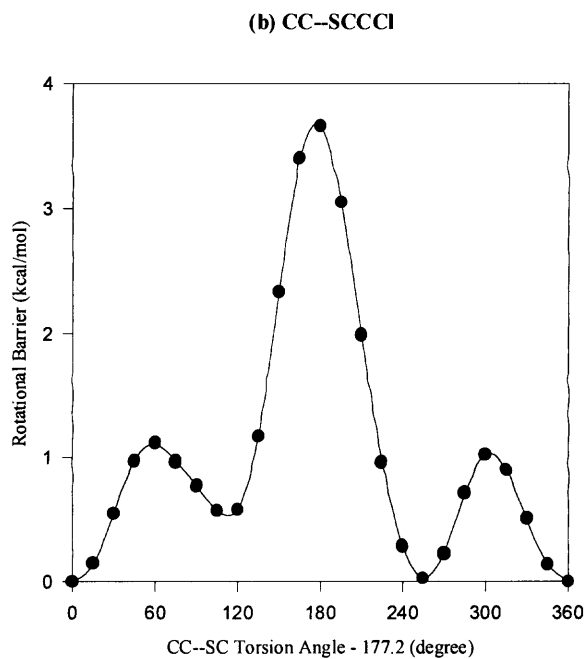
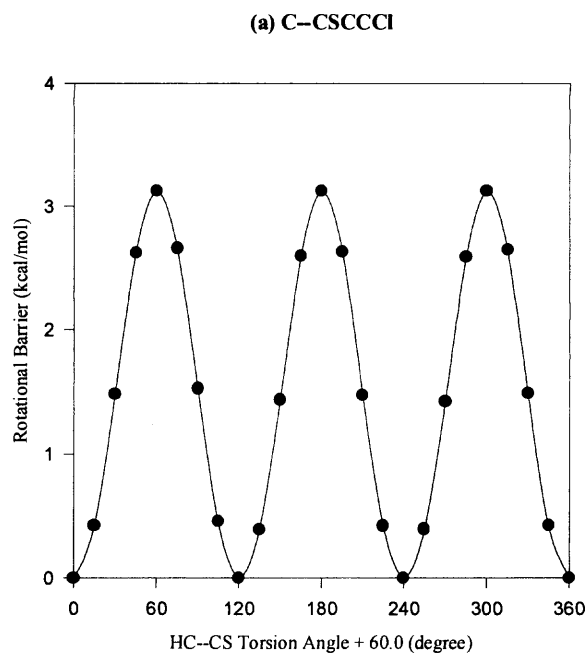
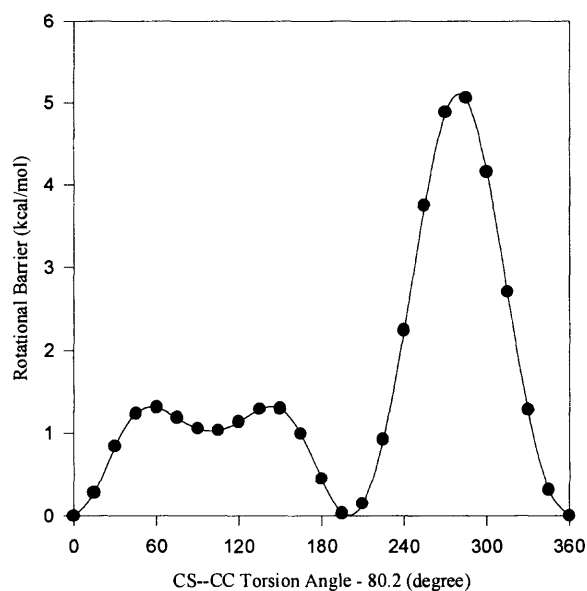


Figure 8.1 Potential barriers for four internal rotations about $\text{CH}_3\text{CH}_2\text{SCH}_2\text{CH}_2\text{Cl}$ [Points are calculated values at the B3LYP/6-31G(d,p) level. Lines are Fourier expansion with the coefficients listed in the Appendix D (Table D.2)].

(c) CCS--CCCI



(d) CCSC--CCI

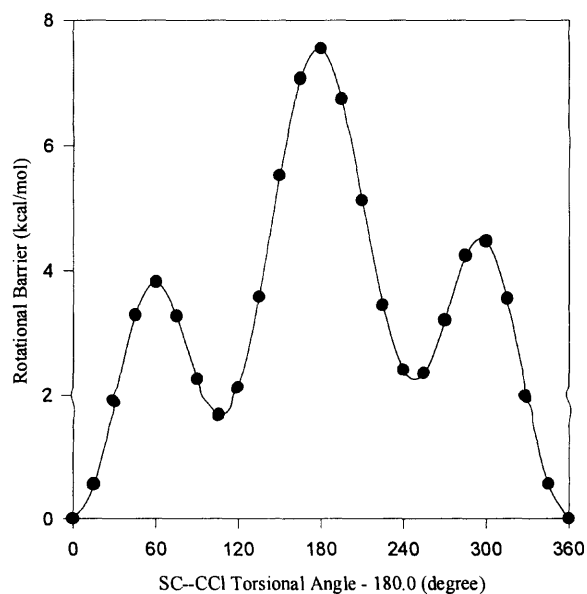


Figure 8.1 Potential barriers for four internal rotations about $\text{CH}_3\text{CH}_2\text{SCH}_2\text{CH}_2\text{Cl}$ [Points are calculated values at the B3LYP/6-31G(d,p) level. Lines are Fourier expansion with the coefficients listed in the Appendix D (Table D.2)] (Continued).

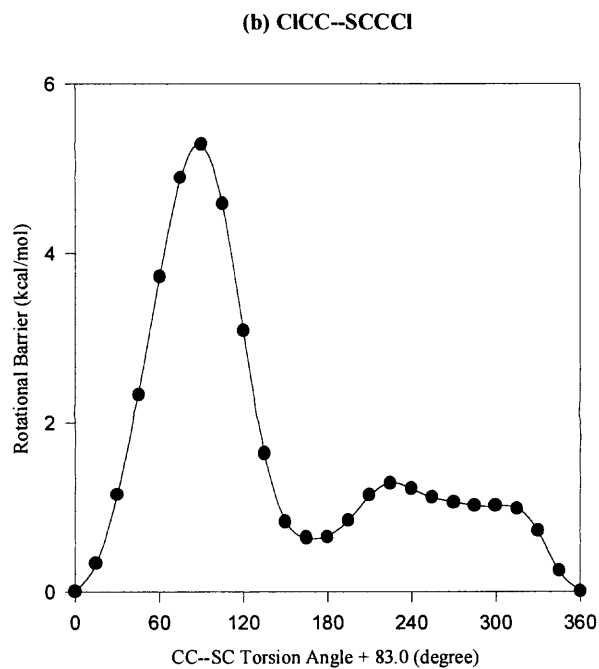
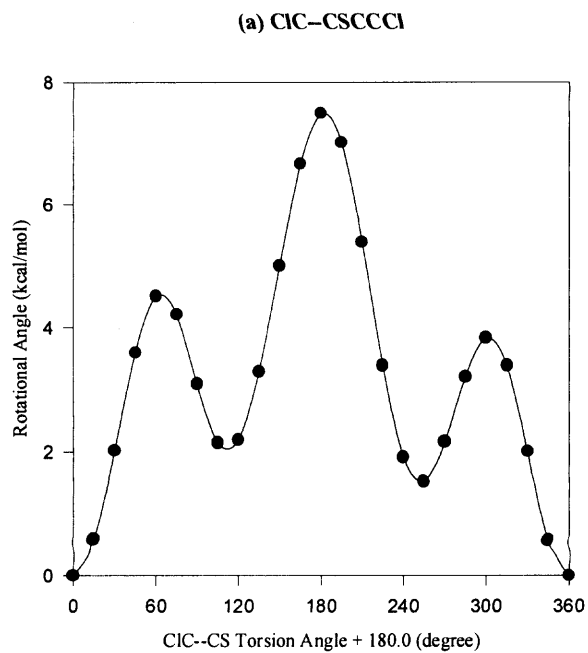


Figure 8.2 Potential barriers for two internal rotations about $\text{CH}_2\text{ClCH}_2\text{SCH}_2\text{CH}_2\text{Cl}$ [Points are calculated values at the B3LYP/6-31G(d,p) level. Lines are Fourier expansion with the coefficients listed in the Appendix D (Table D.2)].

8.4.2 Entropy (S°_{298}) and Heat Capacity ($C_p(T)$)

Entropy and heat capacities are calculated based on scaled vibration frequencies and moments of inertia of the optimized B3LYP/6-31G(d,p) structures (Appendix D, Table D.3). The calculation results are summarized in Table 8.6. The TVR represents the sum of the contributions from translation, vibrations and external rotations for S°_{298} and $C_p(T)$'s. Symmetry, number of optical isomers and electronic spin are incorporated in estimation of S°_{298} as described in Table 8.6. Torsion frequencies are omitted in these calculations, instead, contributions from internal rotation for S°_{298} and $C_p(T)$'s are determined using direct integration over energy levels of the intramolecular rotational potential curves¹³⁸⁻¹⁴⁰ and noted in Table 8.6.

Table 8.6 Ideal Gas Phase Thermodynamic Properties Obtained by B3LYP/6-31G(d,p) Calculation^a

Species (s, e, OI) ^g		$\Delta H_f^{\circ}_{298}$ ^b	S°_{298} ^c	C_{p300} ^c	C_{p400}	C_{p500}	C_{p600}	C_{p800}	C_{p1000}	C_{p1500}
REACTANTS										
CH₃CH₂SCH₂CH₃	TVR ^d		66.19	19.36	25.96	32.18	37.59	46.23	52.73	62.98
(C-CSCC)	I. R. ^f		4.40	2.11	2.12	2.02	1.88	1.63	1.46	1.23
(CC-SCC)	I. R.		7.49	1.72	1.57	1.48	1.41	1.31	1.24	1.13
(CCS-CC)	I. R.		7.49	1.72	1.57	1.48	1.41	1.31	1.24	1.13
(CCSC-C)	I. R.		4.40	2.11	2.12	2.02	1.88	1.63	1.46	1.23
(18,0,1)	Total	-20.08	89.97	27.02	33.34	39.18	44.17	52.11	58.13	67.70
CH₃CH₂SCH₂CH₂Cl	TVR ^d		75.47	22.00	28.87	35.10	40.38	48.62	54.70	64.16
(C-CSCCCI)	I. R. ^f		4.40	2.11	2.12	2.02	1.88	1.63	1.46	1.23
(CC-SCCCCI)	I. R.		7.49	1.72	1.57	1.48	1.41	1.31	1.24	1.13
(CCS-CCCCI)	I. R.		7.44	2.27	1.92	1.73	1.61	1.47	1.37	1.23
(CCSC-CCI)	I. R.		5.73	3.67	3.77	3.49	3.12	2.51	2.11	1.59
(3,0,1)	Total	-26.45	100.53	31.77	38.25	43.82	48.40	55.54	60.88	69.34
CH₂ClCH₂SCH₂CH₂Cl	TVR ^d		82.45	24.60	31.74	38.00	43.16	51.01	56.66	65.34
(ClC-CSCCCI)	I. R. ^f		5.95	3.75	3.71	3.38	3.01	2.43	2.06	1.57
(ClCC-SCCCCI)	I. R.		7.86	2.14	1.77	1.61	1.52	1.42	1.35	1.22
(ClCCS-CCCCI)	I. R.		7.86	2.14	1.77	1.61	1.52	1.42	1.35	1.22
(ClCCSC-CCI)	I. R.		5.95	3.75	3.71	3.38	3.01	2.43	2.06	1.57
(1,0,1)	Total	-31.12	110.07	36.38	42.70	47.98	52.22	58.71	63.48	70.92

Table 8.6 Ideal Gas Phase Thermodynamic Properties Obtained by B3LYP/6-31G(d,p) Calculation^a (Continued)

Species (s, e, OI) ^g		ΔH_f° ^b	S° ^c	Cp_{300}°	Cp_{400}	Cp_{500}	Cp_{600}	Cp_{800}	Cp_{1000}	Cp_{1500}
TRANSITION STATES										
TS1	TVR ^d		74.88	24.34	31.13	37.25	42.45	50.59	56.62	66.06
(C-CSCC)	I. R. ^f		4.40	2.11	2.12	2.02	1.88	1.63	1.46	1.23
(CC-SCC)	I. R.		7.49	1.72	1.57	1.48	1.41	1.31	1.24	1.13
(3,0,1)	Total	44.33	86.77	28.17	34.82	40.75	45.74	53.53	59.32	68.42
TS2A	TVR ^d		78.71	25.12	31.93	37.96	43.01	50.79	56.45	65.20
(C-CSCCCI)	I. R. ^f		4.40	2.11	2.12	2.02	1.88	1.63	1.46	1.23
(CC-SCCCI)	I. R.		7.49	1.72	1.57	1.48	1.41	1.31	1.24	1.13
(CCS-CCCI)	I. R.		7.44	2.27	1.92	1.73	1.61	1.47	1.37	1.23
(3,0,1)	Total	30.82	98.04	31.22	37.54	43.19	47.91	55.20	60.52	68.79
TS2B	TVR ^d		81.67	27.31	34.28	40.34	45.37	53.08	58.68	67.33
(C-CSCCCI)	I. R. ^f		4.40	2.11	2.12	2.02	1.88	1.63	1.46	1.23
(CC-SCCCI)	I. R.		7.49	1.72	1.57	1.48	1.41	1.31	1.24	1.13
(3,0,1)	Total	41.32	93.56	31.14	37.97	43.84	48.66	56.02	61.38	69.69
TS2C	TVR ^d		85.11	27.96	34.32	39.94	44.67	52.09	57.66	66.55
(C-CSCCCI)	I. R. ^f		4.40	2.11	2.12	2.02	1.88	1.63	1.46	1.23
(CC-SCCCI)	I. R.		7.49	1.72	1.57	1.48	1.41	1.31	1.24	1.13
(3,0,1)	Total	52.16	97.00	31.79	38.01	43.44	47.96	55.03	60.36	68.91
TS3A	TVR ^d		87.38	27.74	34.77	40.82	45.77	53.16	58.42	66.40
(CIC-CSCCCI)	I. R. ^f		5.95	3.75	3.71	3.38	3.01	2.43	2.06	1.57
(CICC-SCCCI)	I. R.		7.86	2.14	1.77	1.61	1.52	1.42	1.35	1.22
(CICCS-CCCI)	I. R.		7.86	2.14	1.77	1.61	1.52	1.42	1.35	1.22
(1,0,1)	Total	27.99	109.05	35.77	42.02	47.42	51.82	58.43	63.18	70.41
TS3B	TVR ^d		90.45	29.93	37.10	43.17	48.09	55.42	60.61	68.49
(CIC-CSCCCI)	I. R. ^f		5.95	3.75	3.71	3.38	3.01	2.43	2.06	1.57
(CICC-SCCCI)	I. R.		7.86	2.14	1.77	1.61	1.52	1.42	1.35	1.22
(1,0,1)	Total	35.87	104.26	35.82	42.58	48.16	52.62	59.27	64.02	71.28
TS3C	TVR ^d		92.58	30.43	37.08	42.74	47.38	54.44	59.61	67.74
(CIC-CSCCCI)	I. R. ^f		5.95	3.75	3.71	3.38	3.01	2.43	2.06	1.57
(CICC-SCCCI)	I. R.		7.86	2.14	1.77	1.61	1.52	1.42	1.35	1.22
(1,0,1)	Total	46.52	106.39	36.32	42.56	47.73	51.91	58.29	63.02	70.53
PRODUCTS										
CH₃CH₂SCH₂C.H₂	TVR ^d		71.66	20.15	26.31	31.88	36.61	44.09	49.72	58.66
(C-CSCC)	I. R. ^f		4.40	2.11	2.12	2.02	1.88	1.63	1.46	1.23
(CC-SCC)	I. R.		7.49	1.72	1.57	1.48	1.41	1.31	1.24	1.13
(CCS-CC)	I. R.		7.49	1.72	1.57	1.48	1.41	1.31	1.24	1.13
(CCSC-C)	I. R.		4.40	2.11	2.12	2.02	1.88	1.63	1.46	1.23
(3,1/2,1)	Total	26.04	95.44	27.81	33.69	38.88	43.19	49.97	55.12	63.38
CH₃CH₂SC.HCH₃	TVR ^d		69.19	19.66	25.69	31.27	36.08	43.74	49.50	58.60
(C-CSCC)	I. R. ^f		4.40	2.11	2.12	2.02	1.88	1.63	1.46	1.23
(CC-SCC)	I. R.		7.49	1.72	1.57	1.48	1.41	1.31	1.24	1.13
(CCS-CC)	I. R.		7.49	1.72	1.57	1.48	1.41	1.31	1.24	1.13
(CCSC-C)	I. R.		4.40	2.11	2.12	2.02	1.88	1.63	1.46	1.23
(9,1/2,1)	Total	17.72	92.97	27.32	33.07	38.27	42.66	49.62	54.90	63.32

Table 8.6 Ideal Gas Phase Thermodynamic Properties Obtained by B3LYP/6-31G(d,p) Calculation^a (Continued)

Species (s, e, OI) ^g		ΔH_f° ₂₉₈ ^b	S° ₂₉₈ ^c	Cp ₃₀₀ ^c	Cp ₄₀₀	Cp ₅₀₀	Cp ₆₀₀	Cp ₈₀₀	Cp ₁₀₀₀	Cp ₁₅₀₀
CH₃CH₂SCH₂CH₂Cl	TVR ^d		77.13	22.39	28.71	34.29	38.96	46.20	51.53	59.83
(C-CSCCCI)	I. R. ^f		4.40	2.11	2.12	2.02	1.88	1.63	1.46	1.23
(CC-SCCCCI)	I. R.		7.49	1.72	1.57	1.48	1.41	1.31	1.24	1.13
(CCS-CCCI)	I. R.		7.44	2.27	1.92	1.73	1.61	1.47	1.37	1.23
(CCSC-CCI)	I. R.		5.73	3.67	3.77	3.49	3.12	2.51	2.11	1.59
(3,1/2,1)	Total	18.43	102.19	32.16	38.09	43.01	46.98	53.12	57.71	65.01
CH₃CH₂SC.HCH₂Cl	TVR ^d		76.51	22.33	28.62	34.18	38.84	46.07	51.39	59.71
(C-CSCCCI)	I. R. ^f		4.40	2.11	2.12	2.02	1.88	1.63	1.46	1.23
(CC-SCCCCI)	I. R.		7.49	1.72	1.57	1.48	1.41	1.31	1.24	1.13
(CCS-CCCI)	I. R.		7.44	2.27	1.92	1.73	1.61	1.47	1.37	1.23
(CCSC-CCI)	I. R.		5.73	3.67	3.77	3.49	3.12	2.51	2.11	1.59
(3,1/2,1)	Total	12.76	101.57	32.10	38.00	42.90	46.86	52.99	57.57	64.89
CH₃CH₂SH	TVR ^d		62.12	13.43	17.03	20.40	23.34	28.11	31.74	37.51
(C-CSH)	I. R. ^f		4.27	2.10	2.16	2.09	1.96	1.71	1.53	1.27
(CC-SH)	I. R.		4.57	1.94	1.64	1.44	1.32	1.19	1.12	1.05
(3,0,1)	Total	-10.82	70.96	17.47	20.83	23.93	26.62	31.01	34.39	39.83
CH₃CH₂S.	TVR ^d		63.58	13.65	16.85	19.82	22.39	26.53	29.67	34.64
(C-CS)	I. R. ^f		4.50	2.09	2.06	1.94	1.79	1.55	1.40	1.20
(3,1/2,1)	Total	25.93	68.08	15.74	18.91	21.76	24.18	28.08	31.07	35.84
CH₃CH₂SCl	TVR ^d		68.19	15.91	19.55	22.82	25.61	30.00	33.28	38.42
(C-CSCl)	I. R. ^f		4.40	2.11	2.13	2.03	1.89	1.64	1.46	1.23
(CC-SCl)	I. R.		6.69	2.21	2.07	1.92	1.78	1.56	1.42	1.22
(3,0,1)	Total	-12.95	79.28	20.23	23.75	26.77	29.28	33.20	36.16	40.87
CH₃CH₂SCHCH₂	TVR ^d		69.15	19.38	25.37	30.70	35.20	42.23	47.47	55.73
(C-CSC=C)	I. R. ^f		4.48	2.14	2.11	1.97	1.82	1.57	1.40	1.20
(CC-SC=C)	I. R.		6.85	2.13	1.90	1.75	1.65	1.49	1.38	1.22
(CCS-C=C)	I. R.		6.17	2.24	2.09	1.93	1.78	1.55	1.40	1.20
(3,0,1)	Total	10.59	86.65	25.89	31.47	36.35	40.45	46.84	51.65	59.35
CH₂ClCH₂SCl	TVR ^d		76.25	18.46	22.34	25.63	28.31	32.34	35.21	39.60
(ClC-CSCl)	I. R. ^f		5.72	3.26	3.38	3.30	3.10	2.65	2.27	1.72
(ClCC-SCl)	I. R.		6.89	2.39	2.43	2.31	2.14	1.83	1.61	1.32
(1,0,1)	Total	-16.75	88.86	24.11	28.15	31.24	33.55	36.82	39.09	42.64

a : Thermodynamic properties are referred to a standard state of an ideal gas of pure enantiomer at 1 atm.

b : Units in kcal/mol c : Units in cal/mol-K

d : Sum of contributions from translations, vibrations, and external rotations.

f : I. R. represents contribution from internal rotation

g : Symmetry number, optical isomer and electronic spin are taken into account,
-Rln(s), Rln2, Rln2, respectively.

s = number of symmetry, e = electronic spin, OI = number of optical isomer

8.4.3 Hydrogen Bond Dissociation Energies (BDEs) in CH₃SH, CH₃CH₂SH, CH₃SCH₃, CH₃CH₂SCH₂CH₃, and CH₃CH₂SCH₂CH₂Cl

Hydrogen BDEs for the C—H and S—H bonds in CH₃SH, CH₃CH₂SH, CH₃SCH₃, CH₃CH₂SCH₂CH₃, and CH₃CH₂SCH₂CH₂Cl are presented in Table 8.7. Calculation results at B3LYP/6-31G(d,p) level of theory in this study are compared with literature values available. If not, the values of KMLYP density functional method with the /6-311G(d,p) basis set are compared.

For alkyl RSH species Lias et al.¹⁸⁶ and Griller et al.¹⁸⁹ agreed that BDE (S—H) was effectively independent of the structure of the R group. This was based on values of BDE derived from the electron affinities of the RS radicals and the $\Delta H_{\text{acid}}^{\circ}$ values of the molecules. They recommended a value of 87.00 ± 2.15 [186] and 88.43 ± 1.91 [189] kcal/mol, respectively, for BDE (S—H). Armstrong³ also reported BDE (S—H) value for all the RSH species is 87.47 ± 0.96 kcal/mol. Calculation values in this study are ~ 89 kcal/mol for CH₃S—H and CH₃CH₂S—H.

The BDEs of H—CH₂SH (96.3) and H—CH₂SCH₃ (95.4) are determined ~ 2 kcal/mol higher than literature values, 93.9 and 93.3 kcal/mol, respectively.^{186,188,190,191}

The corresponding hydrogen BDEs for CH₃CH₂SH, CH₃CH₂SCH₂CH₃, and CH₃CH₂SCH₂CH₂Cl are reported in Table 8.7.

Table 8.7 Bond Energies at 298K

Reaction Series (Units: kcal/mol)	Bond Energies		
	B3LYP ^a	KMLYP ^b	Literature ^c
CH ₃ SH => CH ₃ S. + H.	88.96 ± 2.43	-	88.40 ± 2.04[186,189]
CH ₃ SH => C.H ₂ SH + H.	96.29 ± 2.26	-	93.93 ± 2.14[186,188]
CH ₃ CH ₂ SH => CH ₃ CH ₂ S. + H.	89.10 ± 2.23	-	87.31 ± 1.10[186,184]
CH ₃ CH ₂ SH => C.H ₂ CH ₂ SH + H.	98.77 ± 4.20	98.38 ± 4.20	n/a
CH ₃ CH ₂ SH => CH ₃ C.HSH + H.	92.52 ± 4.20	92.11 ± 4.20	n/a
CH ₃ SCH ₃ => C.H ₂ SCH ₃ + H.	95.39 ± 1.35	-	93.33 ± 0.84[186,190,191]
CH ₃ CH ₂ SCH ₂ CH ₃ =>CH ₃ CH ₂ SCH ₂ C.H ₂ + H.	98.22 ± 2.90	98.87 ± 2.90	n/a
CH ₃ CH ₂ SCH ₂ CH ₃ =>CH ₃ CH ₂ SC.HCH ₃ + H.	89.90 ± 2.90	90.90 ± 2.90	n/a
CH ₃ CH ₂ SCH ₂ CH ₂ Cl => CH ₃ CH ₂ SCH ₂ C.HCl + H.	96.98 ± 1.71	97.88 ± 1.56	n/a
CH ₃ CH ₂ SCH ₂ CH ₂ Cl => CH ₃ CH ₂ SC.HCH ₂ Cl + H.	91.31 ± 2.69	93.53 ± 2.11	n/a

^a Uncertainties are sum of the standard deviation for B3LYP/6-31G(d,p) level of theory and maximum cumulative uncertainties from reference species.

^b Uncertainties are sum of the standard deviation for KMLYP/6-311G(d,p) level of theory and maximum cumulative uncertainties from reference species.

^c Uncertainties are sum of maximum cumulative uncertainties from reference species.

8.4.4 Unimolecular Dissociation Reactions on $\text{CH}_3\text{CH}_2\text{SCH}_2\text{CH}_3$, $\text{CH}_3\text{CH}_2\text{SCH}_2\text{CH}_2\text{Cl}$, and $\text{CH}_2\text{ClCH}_2\text{SCH}_2\text{CH}_2\text{Cl}$

Potential energy diagrams for unimolecular dissociations of $\text{CH}_3\text{CH}_2\text{SCH}_2\text{CH}_3$, $\text{CH}_3\text{CH}_2\text{SCH}_2\text{CH}_2\text{Cl}$, and $\text{CH}_2\text{ClCH}_2\text{SCH}_2\text{CH}_2\text{Cl}$ are illustrated in Figure 8.3.

8.4.4.1 Retro-ene Reaction. The $\text{CH}_3\text{CH}_2\text{SCH}_2\text{CH}_3$ can dissociate to $\text{CH}_3\text{CH}_2\text{SH} + \text{C}_2\text{H}_4$ via a four center hydrogen shift transition state (TS1). This reaction, when involving a 6-member ring, is often termed a retro-ene reaction and we use this terminology through the rest of this manuscript. TS1 structure is illustrated in Table 8.1(a). The H6 atom is in a bridge structure shifting from C5 to S3. The cleaving C5-H6 bond is 1.28Å and the forming S3-H6 bond is 1.75Å. The cleaving S3-C4 bond is 2.69Å. All structures are from B3LYP/6-31G(d,p) determined geometries. The barrier is 64.41 kcal/mol is some 20 kcal/mol higher than a conventional six center retro-ene reaction due to strain in the four center ring strain of the transition state.

The $\text{CH}_3\text{CH}_2\text{SCH}_2\text{CH}_2\text{Cl}$ can dissociate to $\text{CH}_3\text{CH}_2\text{SH} + \text{CH}_2\text{CHCl}$ or $\text{CH}_3\text{CH}_2\text{SCl} + \text{C}_2\text{H}_4$ via a hydrogen or a chlorine atom shift (TS2B or TS2C), where transition state structures are illustrated in Table 8.1(c) and 8.1(d), respectively. The latter reaction (TS2C) with a chlorine shift has an ~11 kcal/mol higher barrier than TS2B which has a hydrogen shift. (78.61 and 67.77 kcal/mol barriers for TS2C and TS2B, respectively.) This is a result of the weak S—Cl bond being formed, relative to the S—H bond.

The $\text{CH}_2\text{ClCH}_2\text{SCH}_2\text{CH}_2\text{Cl}$ also can undergo a dissociation to $\text{CH}_2\text{ClCH}_2\text{SH} + \text{CH}_2\text{CHCl}$ or $\text{CH}_2\text{ClCH}_2\text{SCl} + \text{C}_2\text{H}_4$ via a hydrogen or a chlorine shift (TS3B or TS3C), where Table 8.1(f) and 8.1(g) show transition state structures, respectively. The optimized geometries of TS3B and TS3C and barriers of 66.99 and 77.64 kcal/mol in

these reactions are very similar to the optimized geometries of the respective reactions of TS2B and TS2C and 67.77 and 78.61 kcal/mol barriers for the $\text{CH}_3\text{CH}_2\text{SCH}_2\text{CH}_2\text{Cl}$.

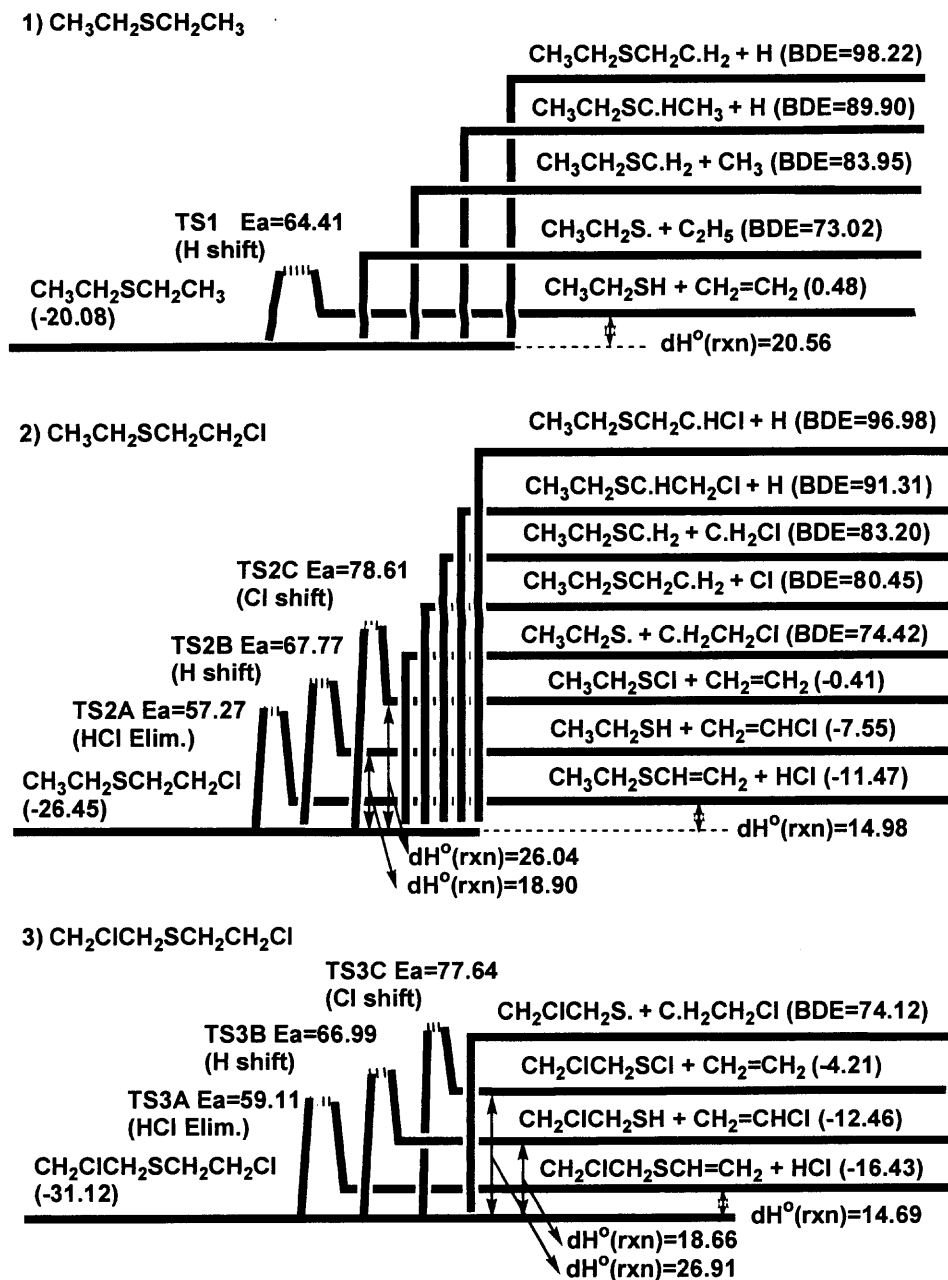


Figure 8.3 Potential energy diagram (units in kcal/mol).

8.4.4.2 HCl Elimination. The $\text{CH}_3\text{CH}_2\text{SCH}_2\text{CH}_2\text{Cl}$ can dissociate to $\text{CH}_3\text{CH}_2\text{SCH}=\text{CH}_2 + \text{HCl}$ via HCl elimination (TS2A) with a 57.27 kcal/mol barrier, which is ~ 10 and 21 kcal/mol lower than the 4 center hydrogen and chlorine shift reactions (TS2B or TS2C), respectively. The TS2A structure is illustrated in Table 8.1(b). The leaving C4-H9 and C5-Cl6 bonds are 1.25 and 2.61 Å, respectively.

The $\text{CH}_2\text{ClCH}_2\text{SCH}_2\text{CH}_2\text{Cl}$ also can undergo dissociation to $\text{CH}_2\text{ClCH}_2\text{SCH}=\text{CH}_2 + \text{HCl}$ via HCl elimination (TS3A). The optimized geometry of TS3A and a barrier of 59.11 kcal/mol in this reaction are very similar to the optimized geometry of TS2A and 57.27 kcal/mol barrier in $\text{CH}_3\text{CH}_2\text{SCH}_2\text{CH}_2\text{Cl}$ reaction with only one Cl in the dithiol molecule. Table 8.1(e) shows transition state structure. The leaving C4-H9 and C5-Cl6 bonds are 1.26 and 2.60 Å, respectively.

8.4.4.3 Bond Cleavage Reaction. Bond dissociation energies of $\text{CH}_3\text{CH}_2\text{SCH}_2\text{CH}_3$ and $\text{CH}_3\text{CH}_2\text{SCH}_2\text{CH}_2\text{Cl}$ are illustrated in Figure 8.4. $\text{CH}_3\text{CH}_2\text{SCH}_2\text{CH}_3$ can undergo bond cleavage reactions to $\text{CH}_3\text{CH}_2\text{S}\bullet + \text{C}_2\text{H}_5$ or $\text{CH}_3\text{CH}_2\text{SCH}_2\bullet + \text{CH}_3$ with barriers of 73.02 or 83.95 kcal/mol, respectively.

The $\text{CH}_3\text{CH}_2\text{SCH}_2\text{CH}_2\text{Cl}$ can undergo similar bond cleavage reactions to $\text{CH}_3\text{CH}_2\text{S}\bullet + \text{C}\bullet\text{H}_2\text{CH}_2\text{Cl}$ or $\text{CH}_3\text{CH}_2\text{SCH}_2\bullet + \text{CH}_2\text{Cl}$ with 74.42 or 83.20 kcal/mol barriers, respectively. $\text{CH}_3\text{CH}_2\text{SCH}_2\text{CH}_2\text{Cl}$ also can undergo dissociation to $\text{CH}_3\text{CH}_2\text{SCH}_2\text{CH}_2\bullet + \text{Cl}$ with a barrier of 80.45 kcal/mol.

Hydrogen bond dissociation energies (BDEs) for $\text{CH}_3\text{CH}_2\text{SCH}_2\text{CH}_3$ and $\text{CH}_3\text{CH}_2\text{SCH}_2\text{CH}_2\text{Cl}$ are discussed in Section 8.4.3.

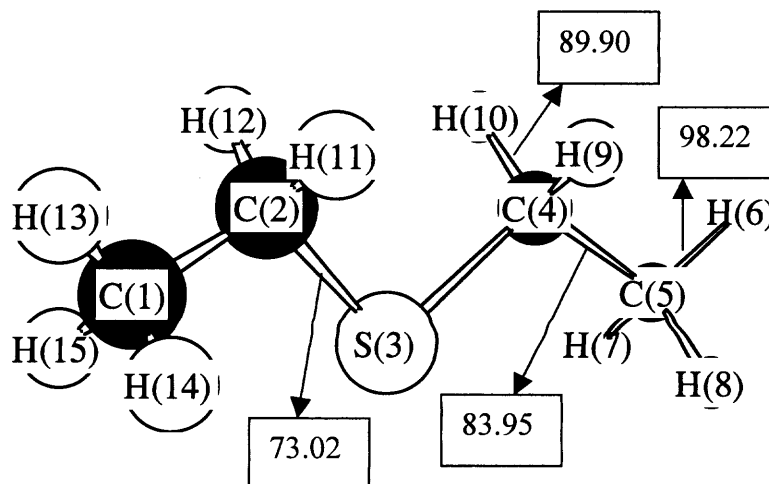
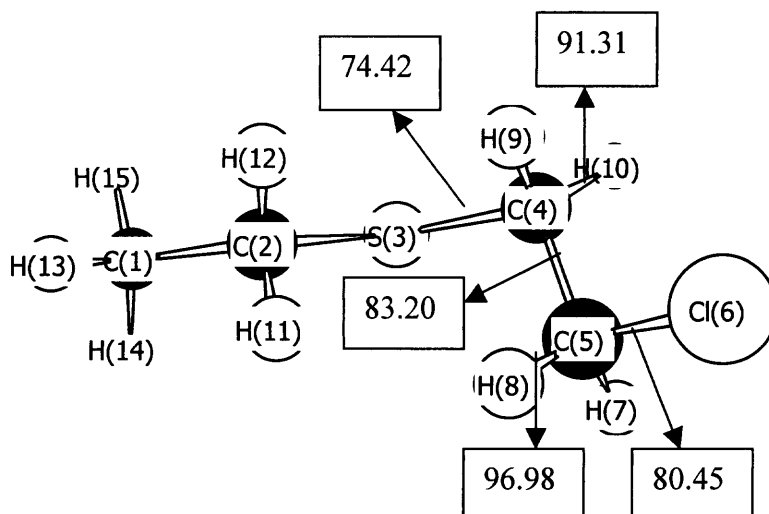
(a) $\text{CH}_3\text{CH}_2\text{SCH}_2\text{CH}_3$ (b) $\text{CH}_3\text{CH}_2\text{SCH}_2\text{CH}_2\text{Cl}$ 

Figure 8.4 Bond dissociation energies^a (kcal/mol) of $\text{CH}_3\text{CH}_2\text{SCH}_2\text{CH}_3$ ^b and $\text{CH}_3\text{CH}_2\text{SCH}_2\text{CH}_2\text{Cl}$ ^c.

^a Bond energies are calculated in this work. (Table 8.6)

^b $\text{CH}_3\text{CH}_2\text{SCH}_2\text{—CH}_3$: $\Delta_f H^\circ_{298}$ of $[\text{C}_2\text{H}_5\text{SCH}_3] = -14.24 \pm 0.26$ (ref. 186), $[\text{CH}_3] = 34.82 \pm 0.2$ (ref. 79) and BDE of $[\text{CH}_3\text{SCH}_2\text{—H}] = 95.39$ (in this study) are used.

^c $\text{CH}_3\text{CH}_2\text{S—CH}_2\text{CH}_2\text{Cl}$: $\Delta_f H^\circ_{298}$ of $[\text{C}\cdot\text{H}_2\text{CH}_2\text{Cl}] = 23.83$ (ref. 195) is used.

^c $\text{CH}_3\text{CH}_2\text{SCH}_2\text{—CH}_2\text{Cl}$: $\Delta_f H^\circ_{298}$ of $[\text{C}\cdot\text{H}_2\text{Cl}] = 27.7 \pm 2.0$ (ref. 196) is used.

8.4.4.4 Thermodynamic and Kinetic Analysis of Retro-ene and HCl Elimination

Reactions. Thermodynamic and kinetic analysis on the unimolecular dissociation of $\text{CH}_3\text{CH}_2\text{SCH}_2\text{CH}_3$, $\text{CH}_3\text{CH}_2\text{SCH}_2\text{CH}_2\text{Cl}$, and $\text{CH}_2\text{ClCH}_2\text{SCH}_2\text{CH}_2\text{Cl}$ are shown in the Appendix D (Table D.4 and D.5). The pre-exponential A factor and activation energy (E_a) are $1.25\text{E}+12 \text{ s}^{-1}$ and 64.41 kcal/mol at 300 K for the unimolecular dissociation of $\text{CH}_3\text{CH}_2\text{SCH}_2\text{CH}_3$ to products, $\text{CH}_3\text{CH}_2\text{SH} + \text{C}_2\text{H}_4$ via TS1.

For the unimolecular dissociations of $\text{CH}_3\text{CH}_2\text{SCH}_2\text{CH}_2\text{Cl}$ and $\text{CH}_2\text{ClCH}_2\text{SCH}_2\text{CH}_2\text{Cl}$, HCl eliminations (TS2A or TS3A) are the most important channel because of \sim one order of magnitude higher A factor and $\sim 10 \text{ kcal/mol}$ lower E_a compared to hydrogen shift reactions (TS2B or TS3B) at temperature from 300 to 2000 K . Chlorine shift unimolecular dissociation of $\text{CH}_3\text{CH}_2\text{SCH}_2\text{CH}_2\text{Cl}$ and $\text{CH}_2\text{ClCH}_2\text{SCH}_2\text{CH}_2\text{Cl}$ have similar A factors and E_a with temperature, but not important channel because of higher E_a compared to HCl elimination and H shift.

8.4.4.5 Overall Kinetic Analysis of Unimolecular Dissociation Reactions.

Multifrequency quantum Rice-Ramsperger-Kassel (QRRK) calculations^{31,41} for $k(E)$ and modified strong collision analysis of Gilbert et al.³⁴⁻³⁶ for falloff are performed on this reaction system to estimate rate constants and to determine important reaction paths as a function of temperature. All dissociation paths are pressure-independent above 0.01 atm . Plots of rate constants at 1 atm versus $1000/T$ for unimolecular dissociations of $\text{CH}_3\text{CH}_2\text{SCH}_2\text{CH}_3$, $\text{CH}_3\text{CH}_2\text{SCH}_2\text{CH}_2\text{Cl}$, and $\text{CH}_2\text{ClCH}_2\text{SCH}_2\text{CH}_2\text{Cl}$ are illustrated in Figure 8.5, 8.6 and 8.7, respectively.

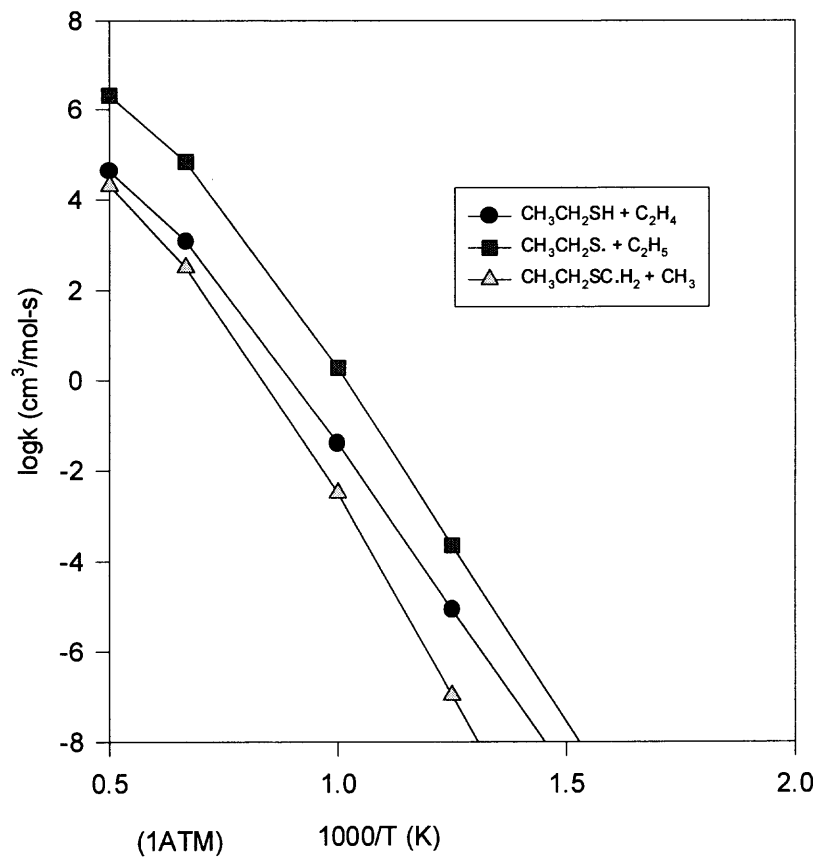


Figure 8.5 $\text{CH}_3\text{CH}_2\text{SCH}_2\text{CH}_3$ dissociation k vs. $1000/T$ at 1 atm.

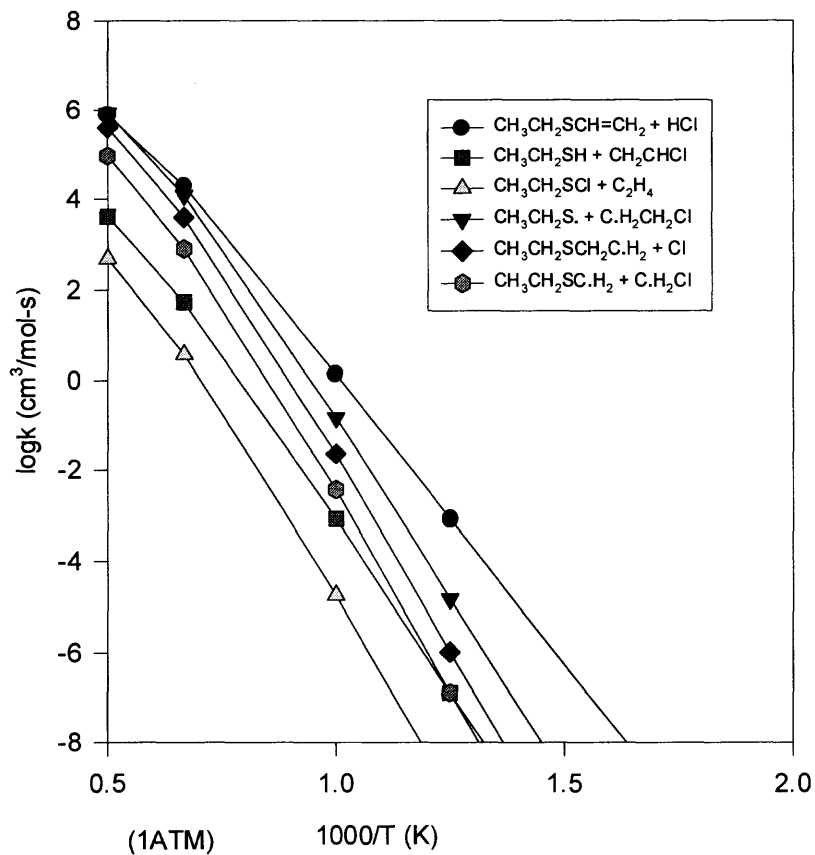


Figure 8.6 $\text{CH}_3\text{CH}_2\text{SCH}_2\text{CH}_2\text{Cl}$ dissociation k vs. $1000/T$ at 1 atm.

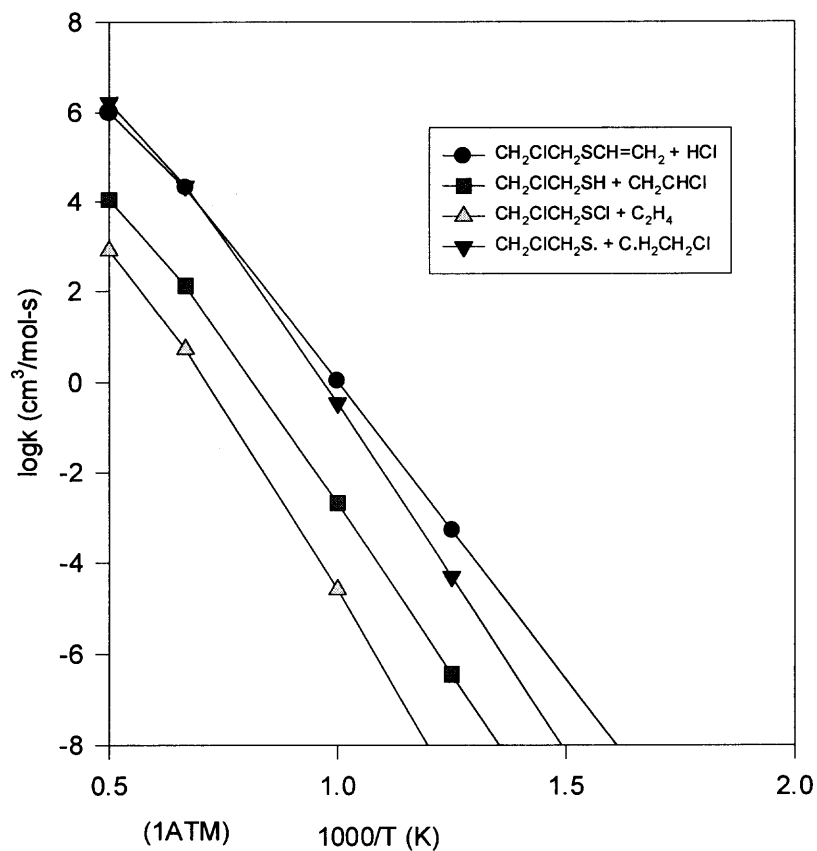


Figure 8.7 $\text{CH}_2\text{ClCH}_2\text{SCH}_2\text{CH}_2\text{Cl}$ dissociation k vs. $1000/T$ at 1 atm.

For $\text{CH}_3\text{CH}_2\text{SCH}_2\text{CH}_3$ dissociation, bond cleavage reactions to $\text{CH}_3\text{CH}_2\text{S}\bullet + \text{C}_2\text{H}_5$ is most important above 800 K. $\text{CH}_3\text{CH}_2\text{SH} + \text{C}_2\text{H}_4$ via TS1 and $\text{CH}_3\text{CH}_2\text{SCH}_2\bullet + \text{CH}_3$ products have 2 orders of magnitude lower rate constants than C—S bond cleavage reaction above 1500 K.

For the unimolecular dissociations of $\text{CH}_3\text{CH}_2\text{SCH}_2\text{CH}_2\text{Cl}$ and $\text{CH}_2\text{ClCH}_2\text{SCH}_2\text{CH}_2\text{Cl}$, HCl eliminations (TS2A or TS3A) are most important channel at high and low temperatures. Carbon–sulfur and carbon–chlorine bond cleavage reactions become important at higher temperatures (above 1000 K), because of higher Arrhenius pre-exponential factors.

8.5. Summary

Thermodynamic properties for reactants, transition states and products for the unimolecular dissociation of $\text{CH}_3\text{CH}_2\text{SCH}_2\text{CH}_3$, $\text{CH}_3\text{CH}_2\text{SCH}_2\text{CH}_2\text{Cl}$, and $\text{CH}_2\text{ClCH}_2\text{SCH}_2\text{CH}_2\text{Cl}$ are calculated at the B3LYP/6-31G(d,p) level. $\Delta H_f^\circ_{298}$ values are determined with isodesmic reactions. Entropy and heat capacities are determined using geometric parameters and vibrational frequencies obtained at the B3LYP/6-31G(d,p). The hindered rotational contributions to S°_{298} and $C_p(T)$ are calculated by intramolecular torsion potential curves. Hydrogen bond dissociation energies of CH_3SH , $\text{CH}_3\text{CH}_2\text{SH}$, CH_3SCH_3 , $\text{CH}_3\text{CH}_2\text{SCH}_2\text{CH}_3$, and $\text{CH}_3\text{CH}_2\text{SCH}_2\text{CH}_2\text{Cl}$ are calculated at the B3LYP/6-31G(d,p). For $\text{CH}_3\text{CH}_2\text{SCH}_2\text{CH}_3$ dissociation, bond cleavage reactions to $\text{CH}_3\text{CH}_2\text{S}\bullet + \text{C}_2\text{H}_5$ is most important at higher temperature (above 800 K). For the unimolecular dissociations of $\text{CH}_3\text{CH}_2\text{SCH}_2\text{CH}_2\text{Cl}$ and $\text{CH}_2\text{ClCH}_2\text{SCH}_2\text{CH}_2\text{Cl}$, HCl eliminations via TS2A and TS3A, respectively, are most important channel at high and low temperatures.

APPENDIX A

CH₃C(=O)OO• AND C•H₂C(=O)OOH DISSOCIATIONS

This appendix illustrates plots of rate constants for CH₃C(=O)OO• and C•H₂C(=O)OOH dissociations versus temperature and pressure and potential barriers for internal rotation in CH₃C(=O)OONO₂ and C₂H₅OONO₂ as discussed in Chapter 3.

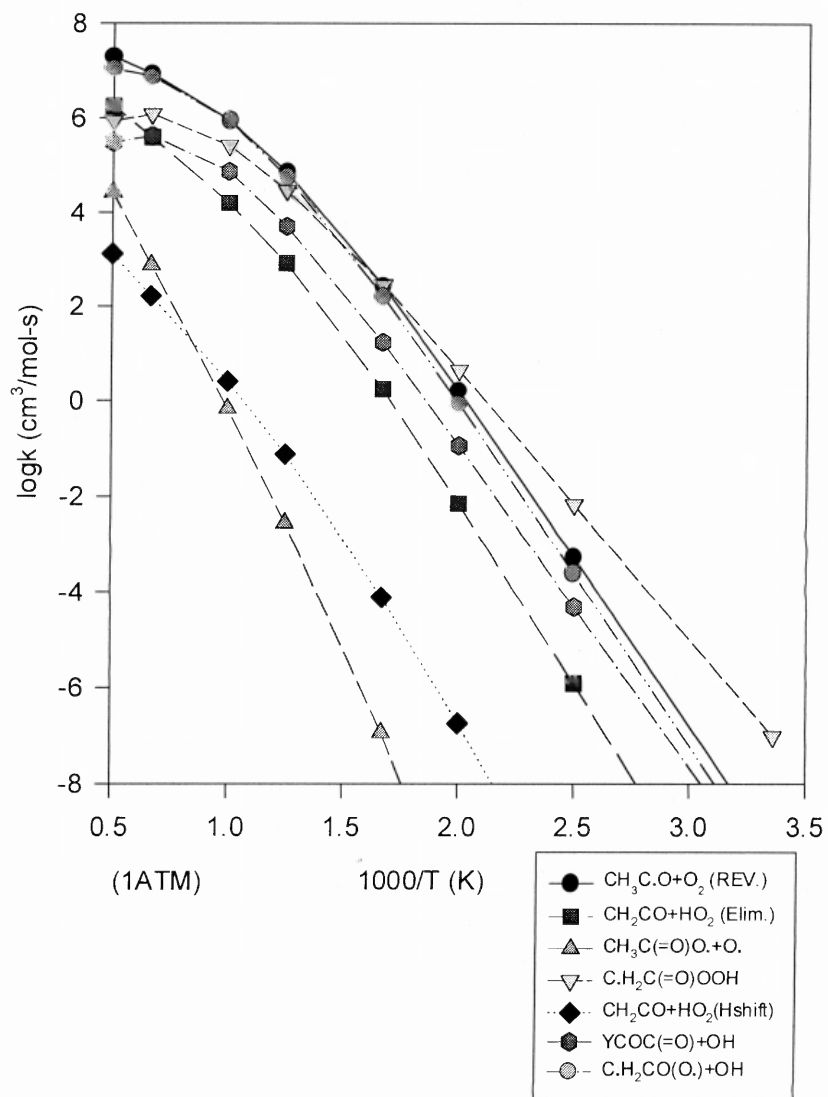


Figure A.1 $\text{CH}_3\text{C}(=\text{O})\text{OO}\cdot$ dissociation k vs. $1000/T$ at 1 atm.

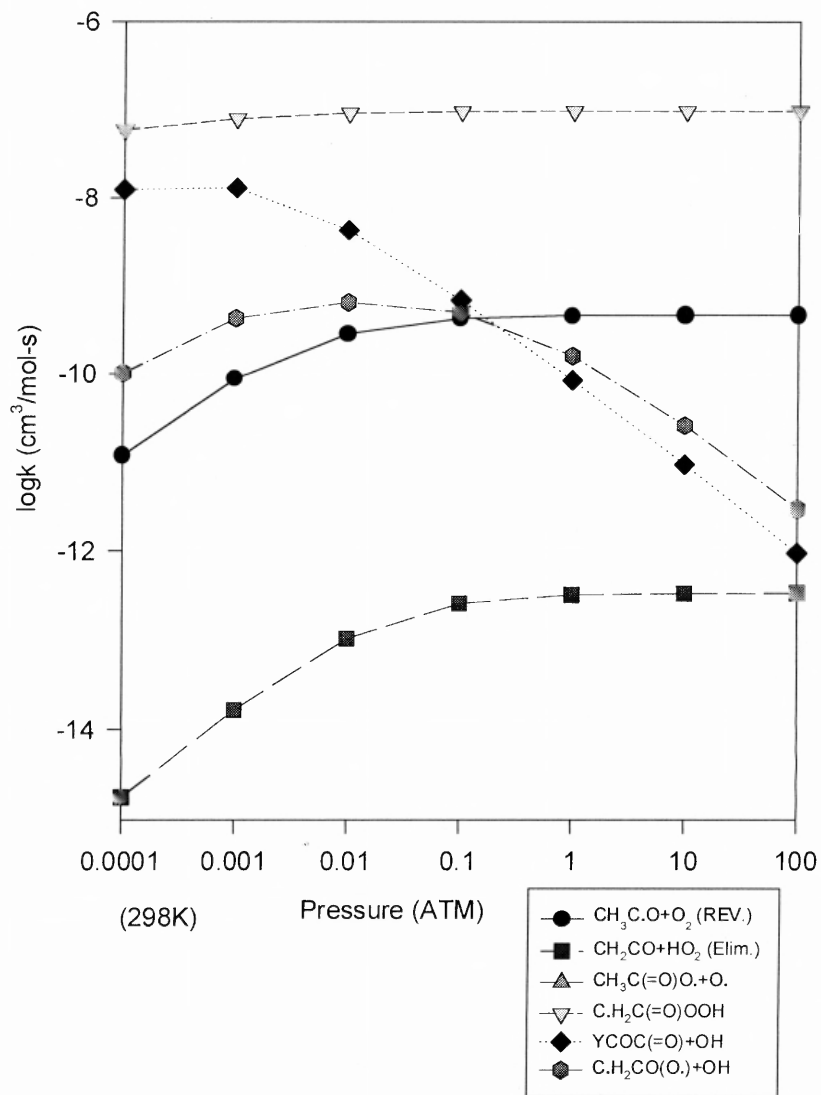


Figure A.2 $\text{CH}_3\text{C}(\text{=O})\text{OO}\cdot$ dissociation k vs. pressure at 298K.

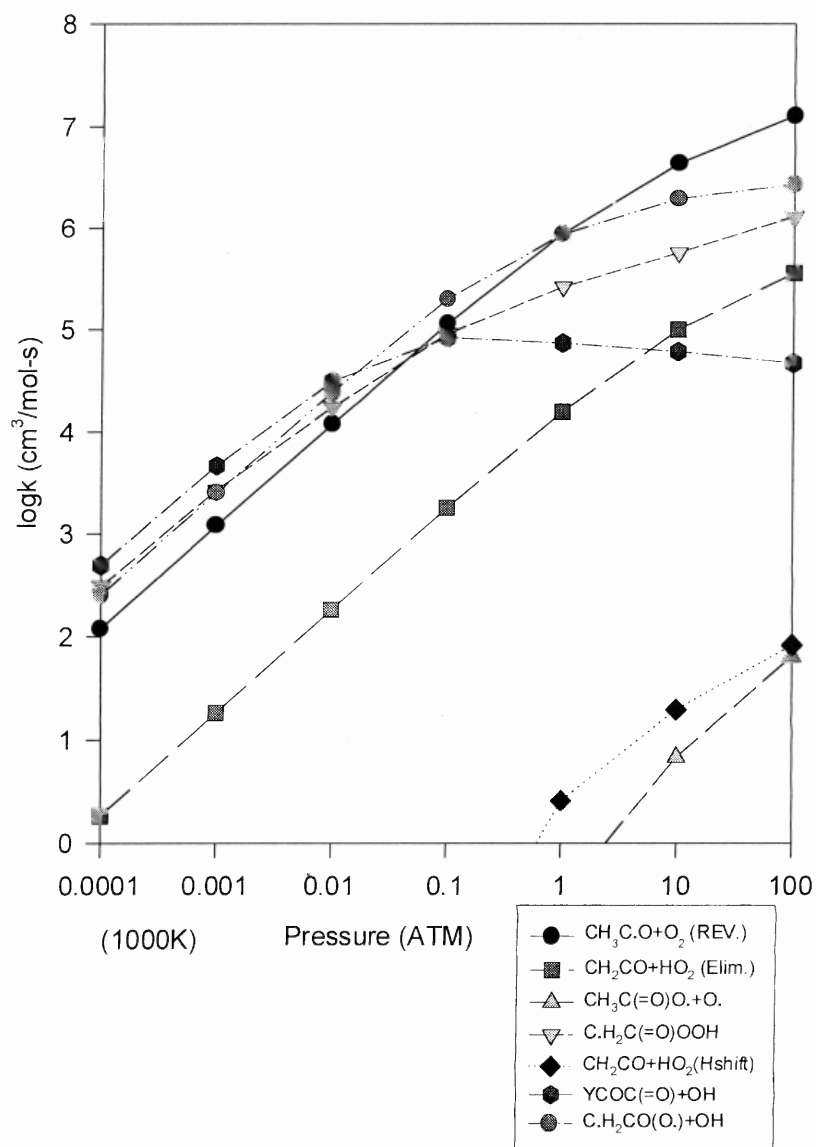


Figure A.3 $\text{CH}_3\text{C(=O)OO}\cdot$ dissociation k vs. pressure at 1000K.

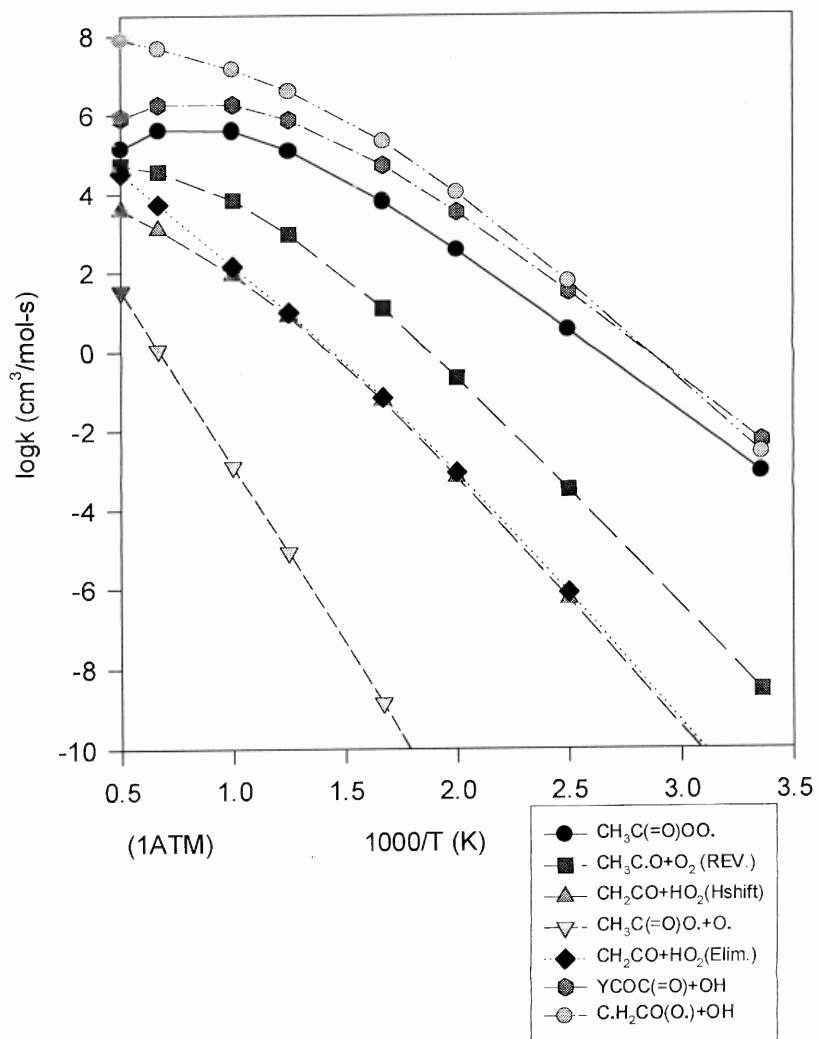


Figure A.4 $\text{C}\cdot\text{H}_2\text{C}(=\text{O})\text{OOH}$ dissociation k vs. $1000/T$ at 1atm.

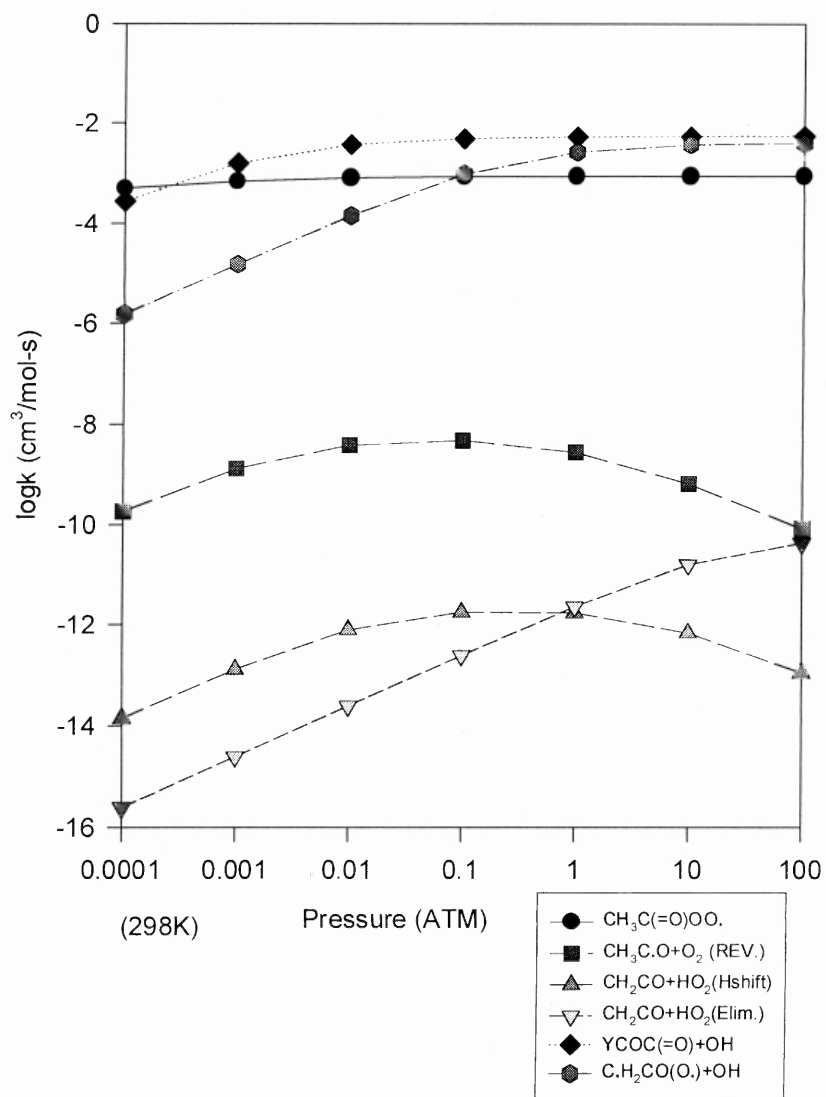


Figure A.5 $\text{C}\cdot\text{H}_2\text{C}(=\text{O})\text{OOH}$ dissociation k vs. pressure at 298K.

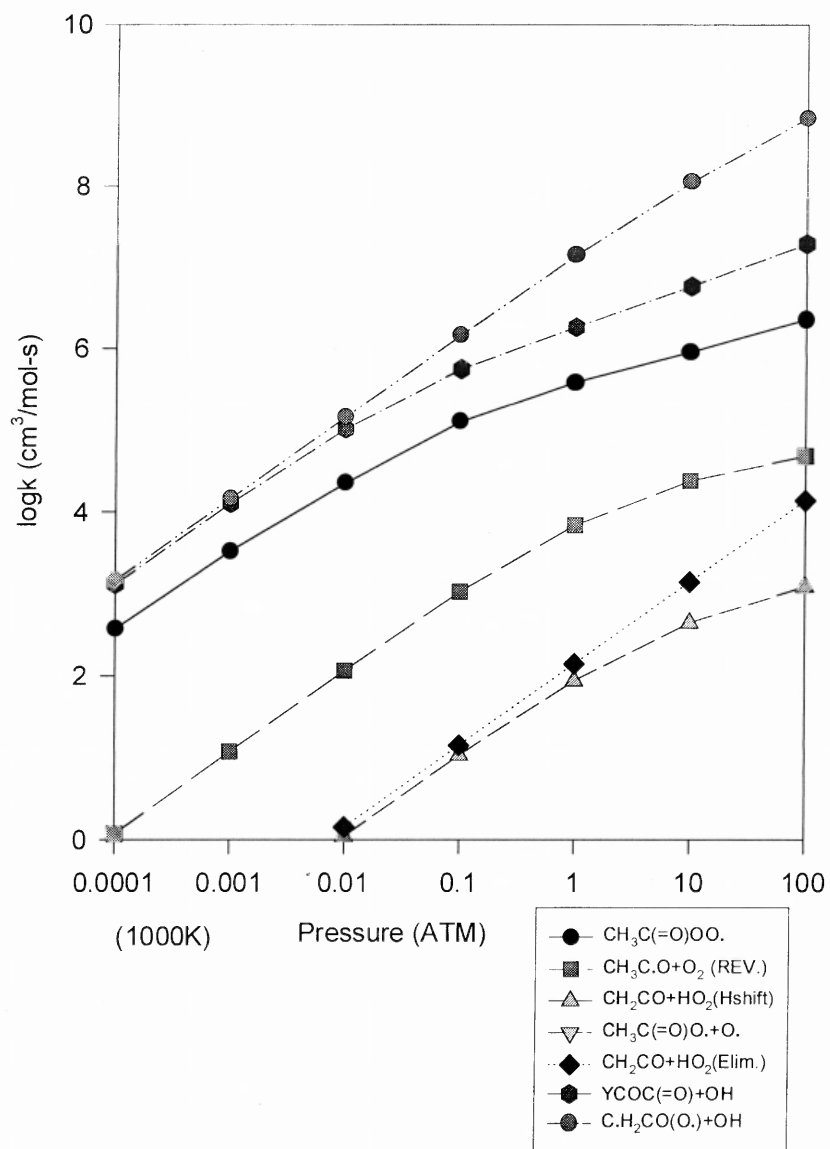
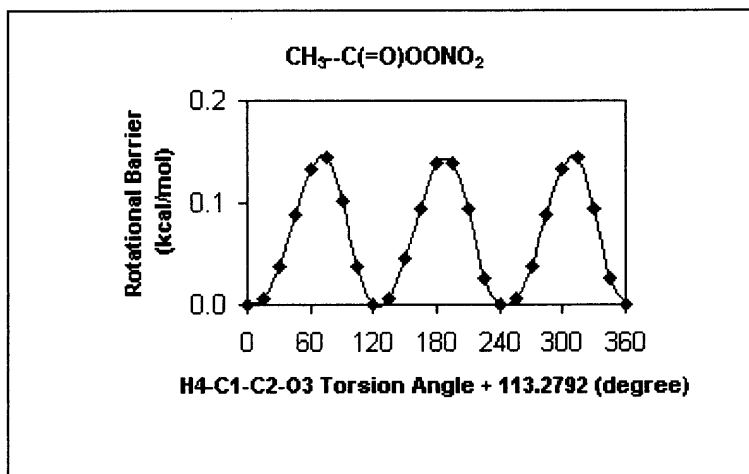


Figure A.6 $\text{C}\cdot\text{H}_2\text{C}(=\text{O})\text{OOH}$ dissociation k vs. pressure at 1000K.

(a) Internal Rotor Contribution

S°_{298}	Cp_{300}	Cp_{400}	Cp_{500}	Cp_{600}	Cp_{800}	Cp_{1000}	Cp_{1500}
5.77	1.01	1.00	1.00	1.00	1.00	1.00	1.00

**(b) Internal Rotor Contribution**

S°_{298}	Cp_{300}	Cp_{400}	Cp_{500}	Cp_{600}	Cp_{800}	Cp_{1000}	Cp_{1500}
4.19	2.13	2.37	2.50	2.54	2.43	2.24	1.74

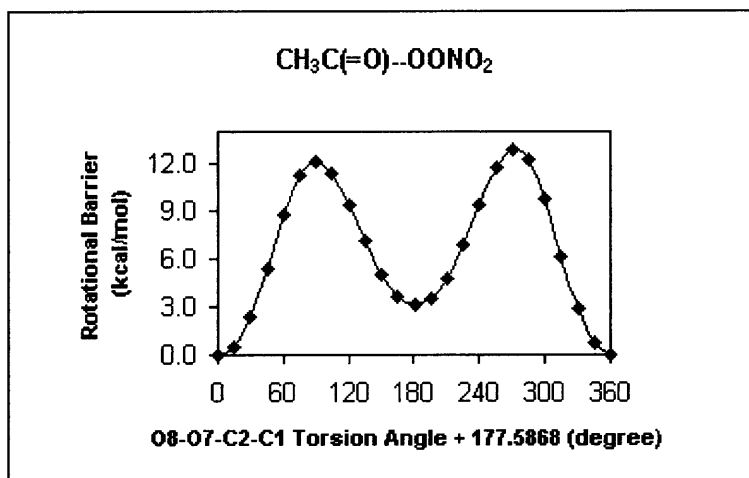
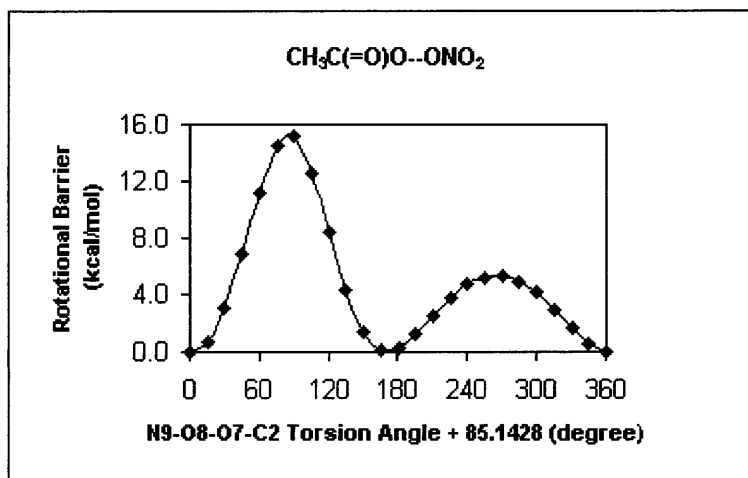


Figure A.7 Potential barriers for internal rotation in CH₃C(=O)OONO₂ at B3LYP/6-31G(d') level of theory.

(c) Internal Rotor Contribution

S_{298}°	Cp_{300}	Cp_{400}	Cp_{500}	Cp_{600}	Cp_{800}	Cp_{1000}	Cp_{1500}
5.93	1.85	1.80	1.75	1.68	1.49	1.29	0.92

**(d) Internal Rotor Contribution**

S_{298}°	Cp_{300}	Cp_{400}	Cp_{500}	Cp_{600}	Cp_{800}	Cp_{1000}	Cp_{1500}
5.42	1.91	1.84	1.77	1.72	1.65	1.59	1.34

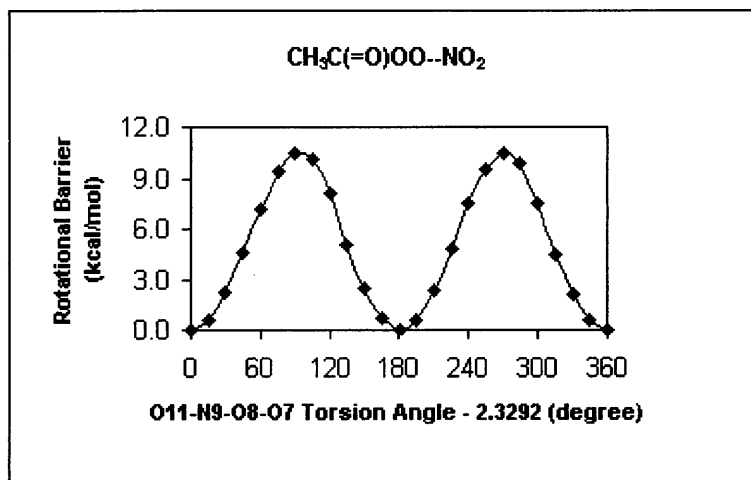
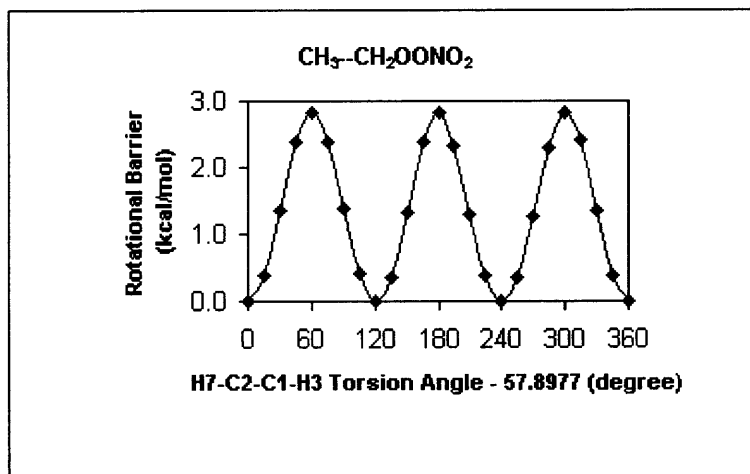


Figure A.7 Potential barriers for internal rotation in CH₃C(=O)OONO₂ at B3LYP/6-31G(d') level of theory (Continued).

(a) Internal Rotor Contribution

S°_{298}	Cp_{300}	Cp_{400}	Cp_{500}	Cp_{600}	Cp_{800}	Cp_{1000}	Cp_{1500}
4.54	2.12	2.07	1.93	1.78	1.54	1.39	1.19

**(b) Internal Rotor Contribution**

S°_{298}	Cp_{300}	Cp_{400}	Cp_{500}	Cp_{600}	Cp_{800}	Cp_{1000}	Cp_{1500}
6.57	2.73	2.30	1.90	1.58	1.11	0.81	0.42

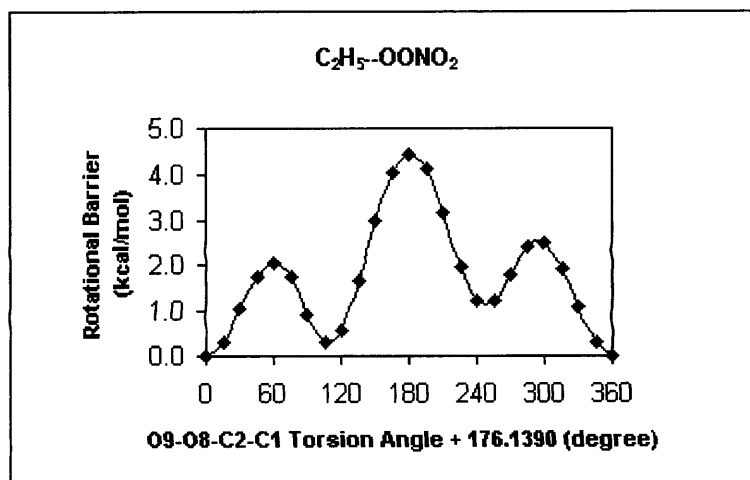
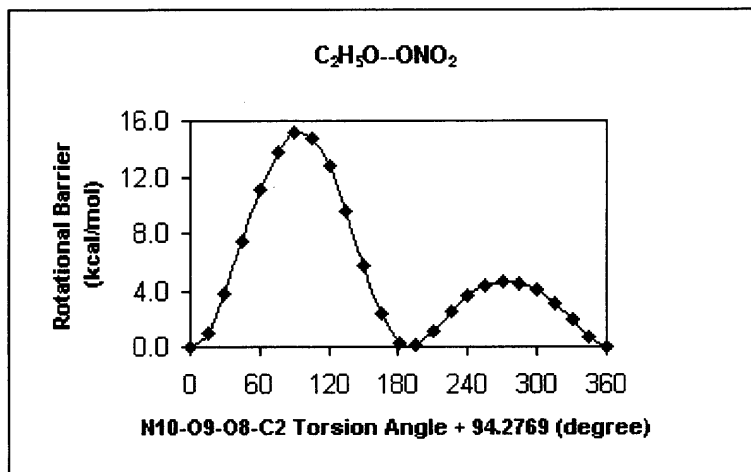


Figure A.8 Potential barriers for internal rotation in C₂H₅OONO₂ at B3LYP/6-31G(d') level of theory.

(c) Internal Rotor Contribution

S°_{298}	Cp_{300}	Cp_{400}	Cp_{500}	Cp_{600}	Cp_{800}	Cp_{1000}	Cp_{1500}
5.42	2.14	2.15	2.09	1.97	1.67	1.41	1.01

**(d) Internal Rotor Contribution**

S°_{298}	Cp_{300}	Cp_{400}	Cp_{500}	Cp_{600}	Cp_{800}	Cp_{1000}	Cp_{1500}
5.33	1.98	1.95	1.90	1.87	1.81	1.72	1.34

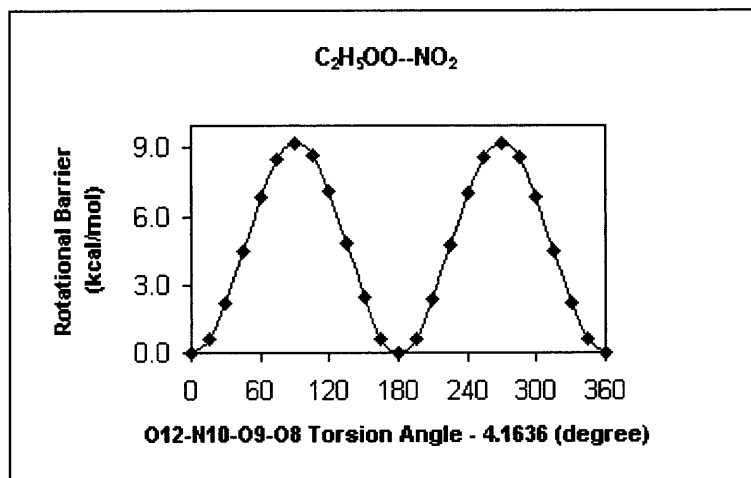


Figure A.8 Potential barriers for internal rotation in C₂H₅OONO₂ at B3LYP/6-31G(d') level of theory (Continued).

APPENDIX B

GEOMETRIES AND $C(OO\bullet)H_2CHO$ AND $C(OOH)H_2C\bullet O$ DISSOCIATIONS

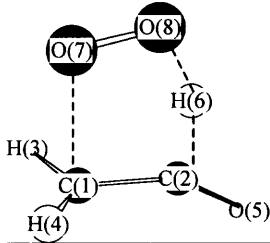
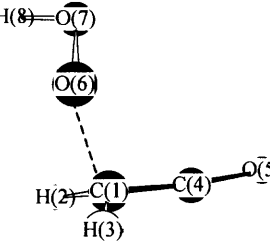
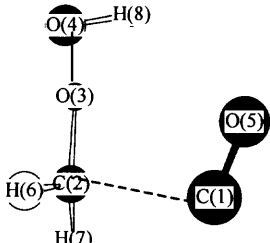
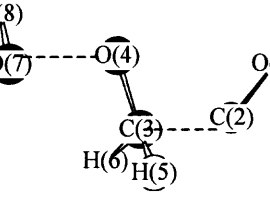
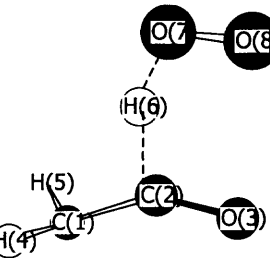
This appendix illustrates optimized geometries of intermediate radicals and transition states and plots of rate constants for $C(OO\bullet)H_2CHO$ and $C(OOH)H_2C\bullet O$ dissociations versus temperature and pressure as discussed in Chapter 4.

Tables B.1 Geometries of Radicals and TS Optimized at MP2/6-31G(d')^a

Species Name & Structure	Bond Length (Å)		Bond Angle (Degree)		Dihedral Angle (Degree)						
[a] C(OOH)H ₂ CHO											
r21							1.51(1.52)				
r31							1.21(1.21)	∠312	123.2(123.3)		
r42							1.41(1.41)	∠421	111.9(112.5)	∠4213	163.7(166.2)
r54							1.47(1.47)	∠542	102.9(104.3)	∠5421	-67.5(-68.6)
r61							1.11(1.11)	∠612	114.4(114.3)	∠6123	178.3(178.3)
r72							1.10(1.10)	∠721	109.7(109.2)	∠7213	-81.0(-78.4)
r85							0.97(0.97)	∠854	98.9(98.9)	∠8542	155.2(145.8)
r92							1.10(1.10)	∠921	110.2(110.2)	∠9213	39.0(40.6)
[b] C(OO•)H ₂ CHO											
r21	1.21(1.20)										
r32	1.52(1.53)	∠321	121.7(122.2)								
r43	1.45(1.44)	∠432	111.1(111.2)	∠4321	179.5(167.2)						
r54	1.30(1.32)	∠543	110.0(110.5)	∠5432	-65.1(-64.2)						
r62	1.11(1.11)	∠625	122.9(123.1)	∠6253	-179.6(-179.1)						
r73	1.10(1.10)	∠732	110.6(109.9)	∠7321	58.3(72.4)						
r83	1.10(1.10)	∠832	110.7(111.0)	∠8321	-63.8(-49.5)						
[c] C(OOH)H ₂ C•O											
r21							1.54(1.54)				
r32							1.41(1.41)	∠321	112.3(112.7)		
r43							1.45(1.45)	∠432	105.1(106.3)	∠4321	66.8(66.4)
r51							1.19(1.19)	∠512	125.9(125.9)	∠5123	178.4(176.0)
r62							1.10(1.10)	∠621	109.1(108.1)	∠6213	-116.4(-124.0)
r72							1.10(1.10)	∠721	108.7(109.0)	∠7213	123.7(116.7)
r84							0.97(0.98)	∠843	100.3(100.1)	∠8432	-105.2(-97.8)
[d] TC•H ₂ CHO-O ₂											
r21							1.09(1.09)				
r31							1.09(1.09)	∠312	117.9(118.7)		
r41							1.49(1.44)	∠412	120.0(121.3)	∠4123	-152.2(-166.6)
r54							1.18(1.23)	∠541	122.5(122.3)	∠5412	178.7(178.7)
r64							1.12(1.11)	∠641	114.8(116.5)	∠6412	-4.8(-2.7)
r71							1.91(2.20)	∠712	99.2(97.2)	∠7123	102.6(93.6)
r87							1.20(1.22)	∠871	115.5(113.6)	∠8712	166.5(162.9)
[e] T ₁ HS											
r21							1.60(1.56)				
r32							1.18(1.18)	∠321	131.6(130.4)		
r42							1.29(1.36)	∠421	90.9(89.8)	∠4213	-176.2(-172.8)
r54							1.36(1.26)	∠542	126.8(129.1)	∠5421	3.3(5.1)
r65							1.37(1.42)	∠654	92.2(93.0)	∠6542	-31.1(-30.6)
r71							1.09(1.09)	∠712	114.5(114.5)	∠7123	-39.8(-45.4)
r81							1.10(1.10)	∠812	104.9(106.0)	∠8123	84.7(78.1)

S²=0.760^b
(0.753)S²=0.764
(0.753)S²=1.579
(1.337)S²=0.800
(0.757)

Tables B.1 Geometries of Radicals and TS Optimized at MP2/6-31G(d')^a (Continued)

Species Name & Structure	Bond Length (Å)		Bond Angle (Degree)		Dihedral Angle (Degree)	
[f] T ₁ E(HO ₂)	S ² = (0.778)					
	r21	(1.39)				
	r31	(1.08)	∠312	(120.8)		
	r41	(1.08)	∠412	(120.8)	∠4123	(-174.9)
	r52	(1.20)	∠521	(146.9)	∠5213	(-92.7)
	r62	(1.31)	∠621	(97.6)	∠6213	(87.4)
	r71	(2.31)	∠712	(93.0)	∠7126	(0.0)
	r87	(1.26)	∠871	(99.2)	∠8712	(0.0)
	[g] T ₂ E(HO ₂)	S ² =0.900 (0.768)				
	r21	1.09(1.09)				
	r31	1.09(1.09)	∠312	117.3(115.2)		
	r41	1.35(1.37)	∠412	114.7(114.0)	∠4123	140.8(135.1)
	r54	1.16(1.17)	∠541	172.8(163.5)	∠5412	107.5(112.3)
	r61	1.86(1.86)	∠612	99.4(99.8)	∠6123	-100.7(-101.2)
	r76	1.40(1.41)	∠761	107.6(108.9)	∠7612	-60.7(-46.4)
	r87	0.97(0.97)	∠876	102.9(102.4)	∠8761	94.9(92.6)
	[h] T ₂ E(C•H ₂ OOH)	S ² = (0.758)				
	r21	(2.32)				
	r32	(1.36)	∠321	(103.4)		
	r43	(1.45)	∠432	(108.6)	∠4321	(-73.8)
	r51	(1.16)	∠512	(106.8)	∠5123	(19.3)
	r62	(1.09)	∠621	(99.5)	∠6213	(-120.7)
	r72	(1.09)	∠721	(103.1)	∠7213	(114.9)
	r84	(0.98)	∠843	(99.6)	∠8432	(92.2)
	[i] T ₂ D(CO+CH ₂ O+OH)	S ² = (0.823)				
	r21	(1.16)				
	r32	(1.69)	∠321	(136.8)		
	r43	(1.31)	∠432	(105.1)	∠4321	(0.1)
	r53	(1.10)	∠532	(101.2)	∠5321	(-123.4)
	r63	(1.10)	∠632	(101.3)	∠6321	(122.7)
	r74	(1.81)	∠743	(105.2)	∠7432	(163.2)
	r87	(0.98)	∠874	(90.5)	∠8743	(-135.8)
	[j] TC•H ₂ CO-HO ₂	S ² =1.628 (1.126)				
	r21	1.42(1.37)				
	r32	1.19(1.21)	∠321	146.0(146.4)		
	r41	1.09(1.08)	∠412	115.9(120.2)	∠4123	108.8(159.8)
	r51	1.09(1.09)	∠512	115.9(118.6)	∠5123	-108.8(-38.0)
	r62	1.35(1.29)	∠621	104.8(106.3)	∠6213	180.0(175.4)
	r76	1.28(1.35)	∠762	152.0(148.6)	∠7621	180.0(155.6)
	r87	1.23(1.25)	∠876	109.8(107.2)	∠8762	-0.2(17.9)

Tables B.1 Geometries of Radicals and TS Optimized at MP2/6-31G(d')^a (Continued)

Species Name & Structure	Bond Length (Å)		Bond Angle (Degree)		Dihedral Angle (Degree)	
[k] TCC•O-H						S ² =0.884 (0.754)
	r21	1.09(1.08)				
	r31	1.09(1.08)	∠312	117.0(119.9)		
	r41	1.34(1.33)	∠412	115.4(119.1)	∠4123	-140.7(164.2)
	r51	1.70(2.16)	∠512	94.4(88.4)	∠5123	97.2(87.2)
	r64	1.17(1.16)	∠641	170.8(177.1)	∠6412	-109.3(-97.8)
[l] TC•CHO-H						S ² =0.899 (0.765)
	r21	1.09(1.08)				
	r31	1.08(1.08)	∠312	121.1(120.5)		
	r41	1.35(1.34)	∠412	117.4(118.1)	∠4123	-168.1(-173.9)
	r54	1.64(1.90)	∠541	89.5(87.7)	∠5412	117.8(126.8)
	r64	1.17(1.17)	∠641	161.1(166.6)	∠6412	-54.5(-44.3)
[m] TC•CHOS						S ² =0.814 (0.754)
	r21	1.40(1.40)				
	r32	1.20(1.21)	∠321	144.5(139.8)		
	r42	1.27(1.30)	∠421	68.1(65.5)	∠4213	127.9(120.4)
	r51	1.10(1.10)	∠512	122.2(122.7)	∠5123	-7.9(-2.6)
	r61	1.08(1.09)	∠612	118.0(118.2)	∠6123	166.2(169.4)
[n] TCH ₃ -CO						S ² =0.812 (0.760)
	r21	2.11(2.34)				
	r31	1.16(1.14)	∠312	115.5(113.4)		
	r41	1.09(1.09)	∠412	102.8(99.0)	∠4123	180.0(170.0)
	r51	1.09(1.09)	∠512	100.0(97.3)	∠5123	59.6(49.6)
	r64	1.09(1.09)	∠641	100.0(96.9)	∠6412	-59.6(-70.0)

^a parenthesis () : B3LYP/6-31G(d)

^b S² : spin contamination from MP2/6-31G(d') and () from B3LYP/6-31G(d)

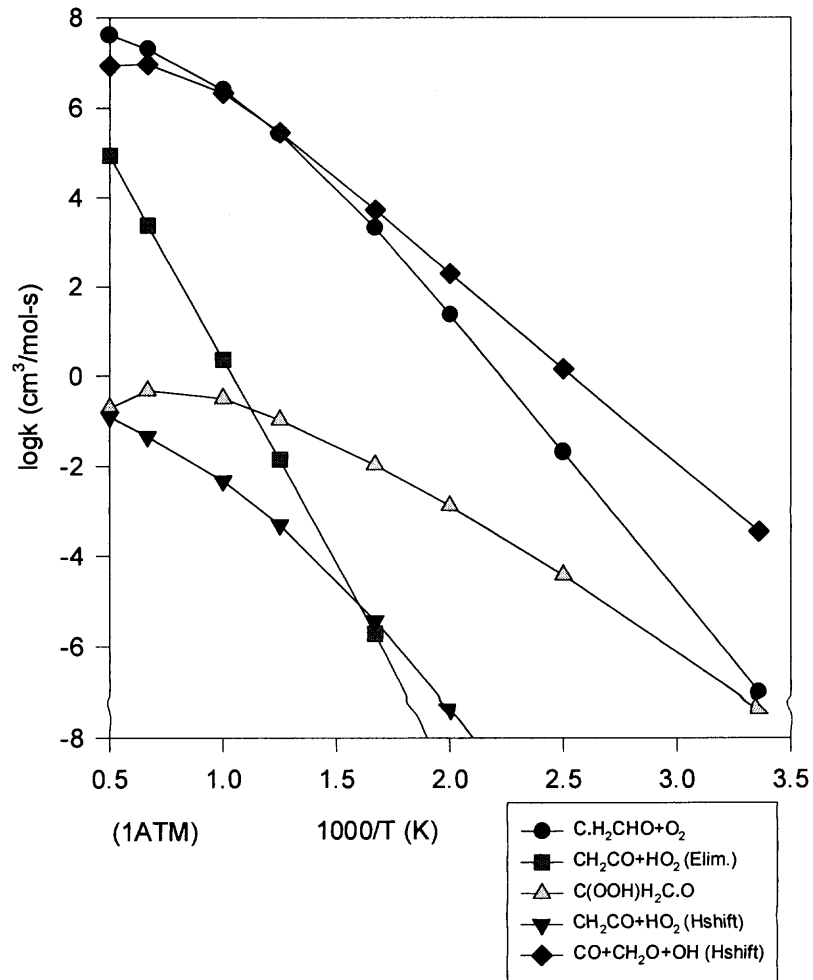


Figure B.1 $\text{C}(\text{OO}\cdot)\text{H}_2\text{CHO}$ dissociation k vs. $1000/T$ at 1 atm.

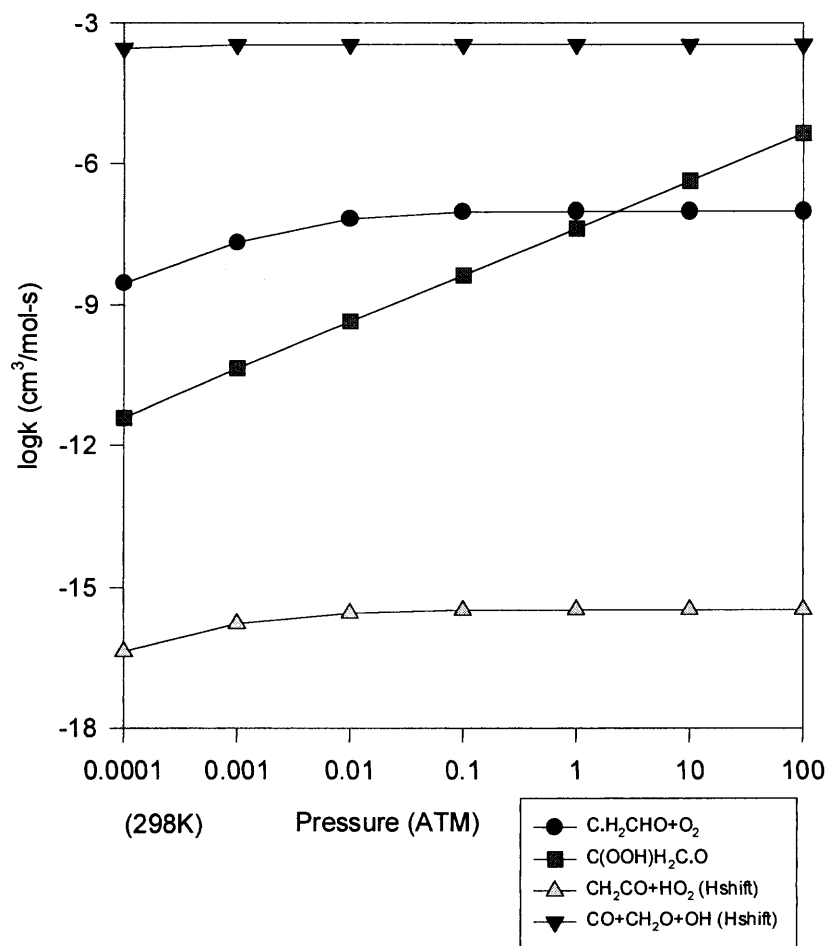


Figure B.2 $\text{C}(\text{OO}\bullet)\text{H}_2\text{CHO}$ dissociation k vs. pressure at 298K.

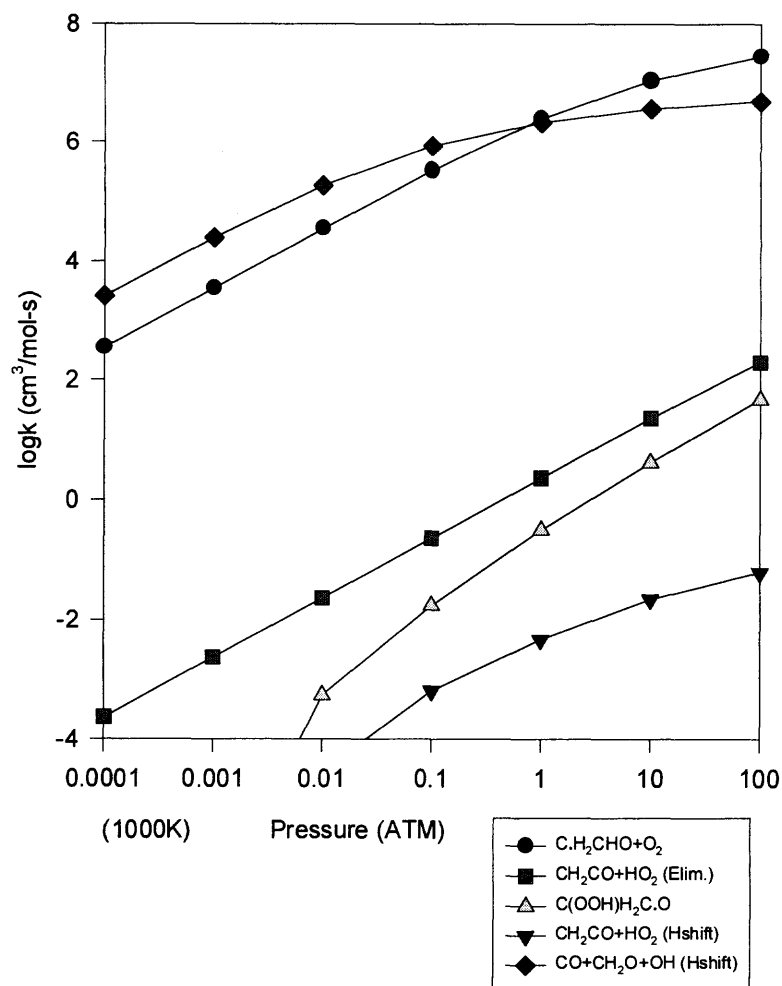


Figure B.3 $\text{C(OO}\bullet\text{)H}_2\text{CHO}$ dissociation k vs. pressure at 1000K.

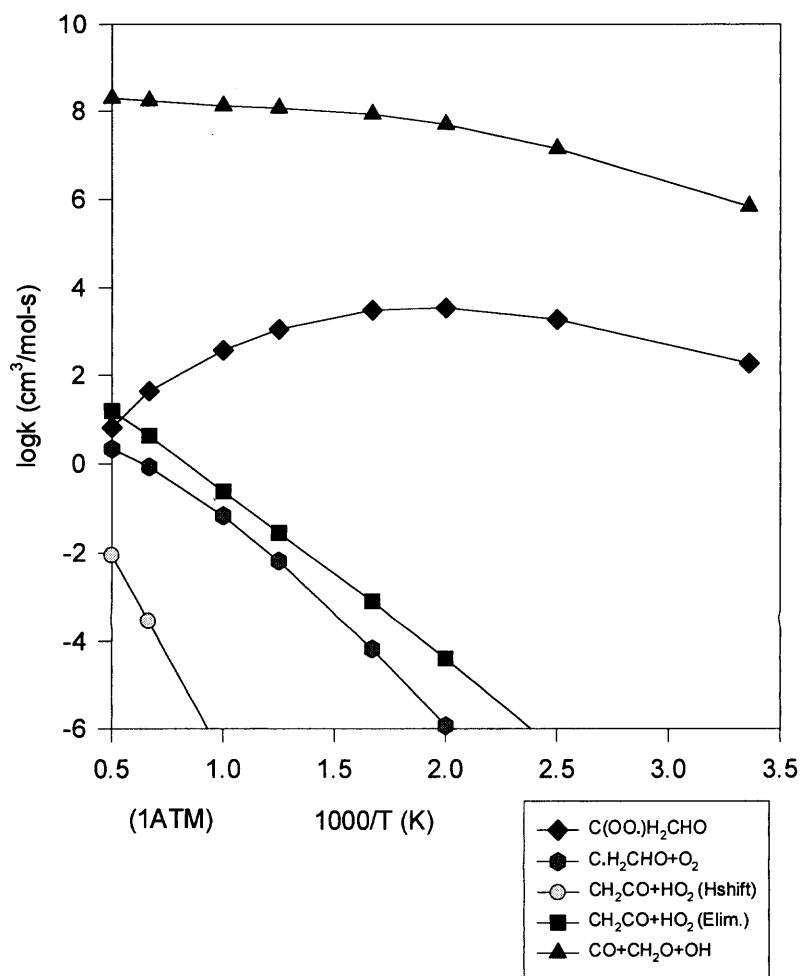


Figure B.4 C(OOH)H₂C•O dissociation k vs. $1000/T$ at 1atm.

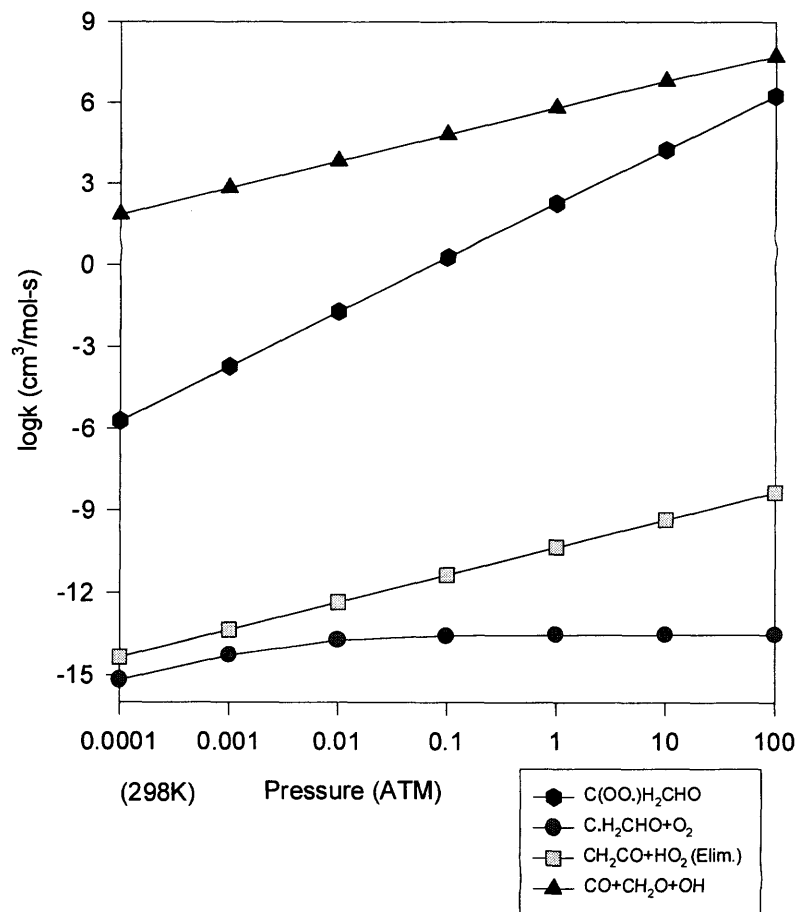


Figure B.5 $\text{C(OOH)H}_2\text{C}\bullet\text{O}$ dissociation k vs. pressure at 298K.

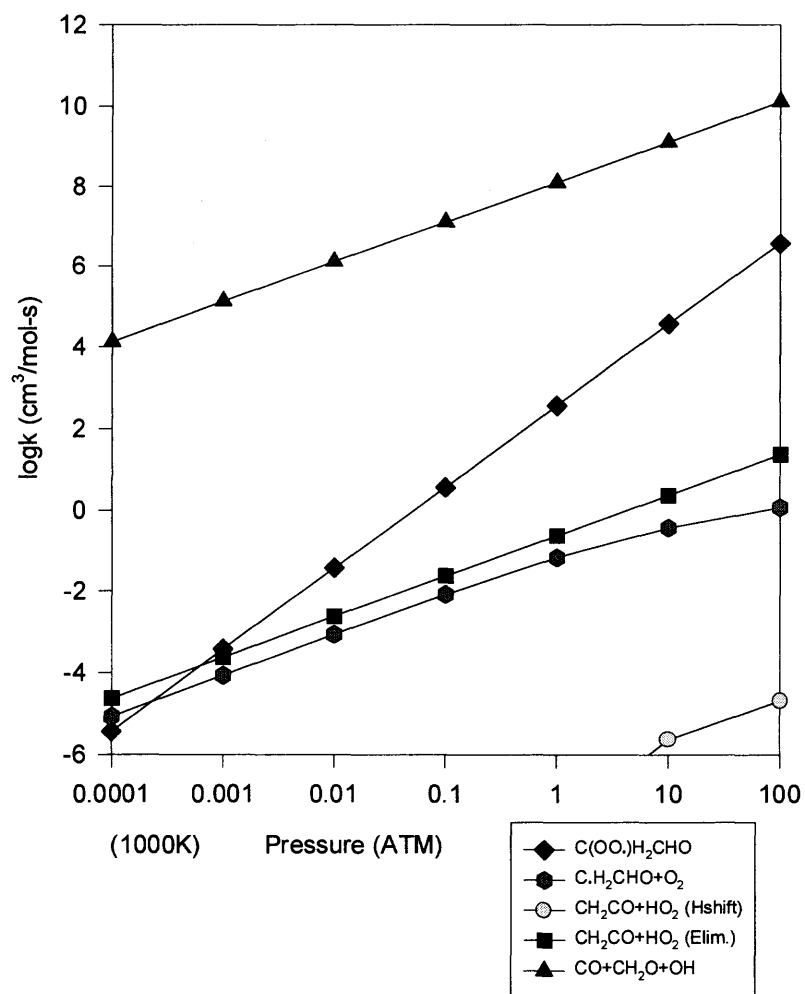


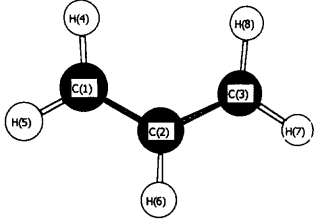
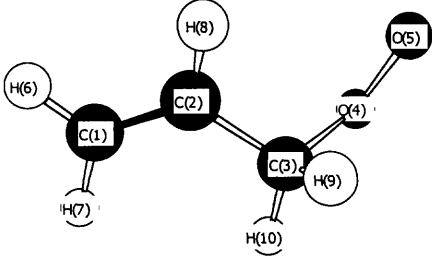
Figure B.6 $\text{C}(\text{OOH})\text{H}_2\text{C}\cdot\text{O}$ dissociation k vs. pressure at 1000K.

APPENDIX C

GEOMETRIES, VIBRATIONAL FREQUENCIES AND MOMENTS OF INERTIA

This appendix illustrates optimized geometries of intermediate radicals and transition states, vibration frequencies and moments of inertia at B3LYP/6-31G(d,p) level as discussed in Chapter 6.

Table C.1 Geometries of Intermediate Radicals and Transition States Optimized at B3LYP/6-31G(d,p)

Species Name & Structure	Bond Length (Å)		Bond Angle (Degree)		Dihedral Angle (Degree)	
[a] CH ₂ =CHC•H ₂	$S^2=0.781$ (0.954) ^a					
	r21	1.39				
	r32	1.39	∠321	125.1		
	r41	1.09	∠412	121.1	∠4123	0.0
	r51	1.08	∠512	121.6	∠5123	180.0
	r62	1.09	∠621	117.5	∠6213	-180.0
	r73	1.08	∠732	121.6	∠7321	-180.0
	r83	1.09	∠832	121.1	∠8321	0.0
	[b] CH ₂ =CHCH ₂ OOH	r21	1.33			
r32	1.50	∠321	124.0			
r43	1.43	∠432	112.4	∠4321	-117.6	
r54	1.45	∠543	107.2	∠5432	72.9	
r61	1.09	∠612	122.0	∠6123	179.9	
r71	1.09	∠712	121.3	∠7123	-0.7	
r82	1.09	∠821	120.1	∠8213	-179.0	
r93	1.10	∠932	111.5	∠9321	6.2	
r103	1.10	∠1032	111.1	∠10321	127.9	
r115	0.97	∠1154	101.1	∠11543	-90.8	
[c] CH ₂ =CHCH ₂ OO•	$S^2=0.753$ (0.766)					
	r21	1.33				
	r32	1.50	∠321	123.8		
	r43	1.47	∠432	110.9	∠4321	122.9
	r54	1.32	∠543	110.8	∠5432	75.0
	r61	1.09	∠612	121.6	∠6123	178.4
	r71	1.09	∠712	121.8	∠7123	-1.1
	r82	1.09	∠821	121.0	∠8213	-179.0
	r93	1.09	∠932	112.4	∠9321	-121.0
	r103	1.09	∠1032	112.3	∠10321	4.4
[d] C•H=CHCH ₂ OOH	$S^2=0.761$ (0.940)					
r21	1.31					
r32	1.51	∠321	124.6			
r43	1.43	∠432	111.9	∠4321	-114.5	
r54	1.45	∠543	107.3	∠5432	74.5	
r61	1.08	∠612	137.9	∠6123	179.8	
r73	1.09	∠732	111.3	∠7321	9.1	
r83	1.10	∠832	110.6	∠8321	131.0	
r95	0.97	∠954	101.2	∠9543	-88.0	
r102	1.10	∠1021	120.0	∠10213	-178.1	

^a S^2 : spin contamination from B3LYP/6-31G(d,p) and () from QCISD(T)/6-31+G(d')

Table C.1 Geometries of Intermediate Radicals and Transition States Optimized at B3LYP/6-31G(d,p) (Continued)

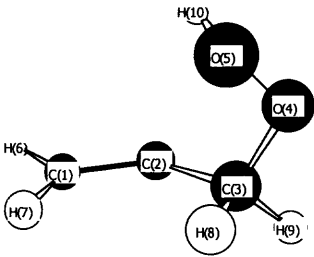
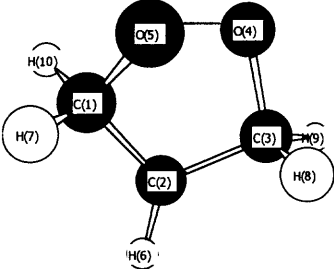
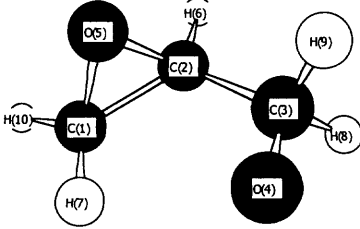
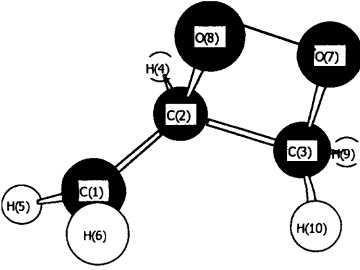
Species Name & Structure	Bond Length (Å)		Bond Angle (Degree)		Dihedral Angle (Degree)		
[e] CH ₂ =C•CH ₂ OOH							S ² =0.760 (0.940)
	r21	1.31					
	r32	1.48	∠321	138.1			
	r43	1.43	∠432	113.7	∠4321	-120.8	
	r54	1.45	∠543	107.1	∠5432	68.5	
	r61	1.09	∠612	122.5	∠6123	-178.2	
	r71	1.10	∠712	121.5	∠7123	1.7	
	r83	1.10	∠832	110.2	∠8321	2.8	
	r93	1.10	∠932	111.1	∠9321	123.0	
	r105	0.97	∠1054	100.8	∠10543	-92.6	
[f] YCC•COO							S ² =0.754 (0.765)
	r21	1.49	∠321	106.5			
	r32	1.49	∠432	103.9	∠4321	-13.3	
	r43	1.43	∠512	103.9	∠5123	-13.4	
	r51	1.43	∠621	126.7	∠6213	179.9	
	r62	1.08	∠712	114.4	∠7123	-128.8	
	r71	1.10	∠832	112.7	∠8321	106.2	
	r83	1.10	∠932	114.4	∠9321	-128.7	
	r93	1.10	∠1012	112.7	∠10123	106.1	
[g] O•CH ₂ YCCO							S ² =0.753 (0.760)
	r21	1.47	∠321	120.8			
	r32	1.52	∠432	115.6	∠4321	-15.8	
	r43	1.37	∠521	59.4	∠5213	-103.4	
	r52	1.43	∠621	119.2	∠6213	153.3	
	r62	1.09	∠712	118.3	∠7123	0.1	
	r71	1.09	∠832	111.1	∠8321	110.9	
	r83	1.10	∠932	109.3	∠9321	-135.2	
	r93	1.11	∠1012	119.9	∠10123	-153.1	
[h] C•H ₂ YCCOO							S ² =0.755 (0.798)
	r21	1.47	∠321	120.5			
	r32	1.54	∠421	112.1	∠4213	135.4	
	r42	1.10	∠512	121.7	∠5123	-128.3	
	r51	1.08	∠612	119.4	∠6123	52.8	
	r61	1.08	∠732	89.7	∠7321	-129.0	
	r73	1.44	∠821	112.8	∠8213	-100.2	
	r82	1.48	∠932	117.6	∠9321	115.9	
	r93	1.09	∠1032	113.5	∠10321	-15.2	
	r103	1.10					

Table C.1 Geometries of Intermediate Radicals and Transition States Optimized at B3LYP/6-31G(d,p) (Continued)

Species Name & Structure	Bond Length (Å)		Bond Angle (Degree)		Dihedral Angle (Degree)			
[i] TC=CC-O ₂								S ² =1.171 (1.879)
	r21	1.37						
	r32	1.39	∠321	121.6				
	r43	2.29	∠432	93.5	∠4321	66.8		
	r54	1.24	∠543	107.0	∠5432	-28.6		
	r61	1.08	∠612	121.8	∠6123	-171.5		
	r71	1.08	∠712	121.2	∠7123	12.2		
	r82	1.09	∠821	118.9	∠8213	168.7		
	r93	1.08	∠932	121.6	∠9321	172.9		
	r103	1.08	∠1032	120.8	∠10321	-18.5		
	[j] TC•=CCOOHS							
	r21	1.31						
	r32	1.53	∠321	120.7				
	r43	1.42	∠432	110.0	∠4321	-28.9		
	r52	1.09	∠521	122.5	∠5213	-179.8		
	r61	1.49	∠612	101.6	∠6123	1.9		
	r71	1.08	∠712	134.8	∠7123	-178.4		
	r83	1.10	∠832	110.3	∠8321	93.6		
	r93	1.09	∠932	111.7	∠9321	-144.8		
	r106	1.10	∠1061	144.9	∠10612	-14.5		
	[k] TC•=CCOOH							
	r21	1.23						
	r32	2.28	∠321	118.3				
	r43	1.36	∠432	107.2	∠4321	159.1		
	r54	1.49	∠543	106.7	∠5432	60.1		
	r61	1.07	∠612	164.9	∠6123	-0.3		
	r73	1.09	∠732	101.0	∠7321	-78.4		
	r83	1.08	∠832	100.1	∠8321	44.9		
	r95	0.97	∠954	98.1	∠9543	163.3		
	r102	1.07	∠1021	153.6	∠10213	-179.1		
	[l] TALLYL-OHSQ							
	r21	1.34						
	r32	1.46	∠321	124.1				
	r43	1.09	∠432	118.4	∠4321	150.0		
	r53	1.39	∠532	118.0	∠5321	7.3		
	r61	1.08	∠612	121.1	∠6123	-179.7		
	r71	1.08	∠712	120.9	∠7123	-0.1		
	r82	1.09	∠821	120.5	∠8213	-178.8		
	r95	1.49	∠953	90.2	∠9532	-118.1		
	r103	1.30	∠1032	112.6	∠10321	-92.1		

Table C.1 Geometries of Intermediate Radicals and Transition States Optimized at B3LYP/6-31G(d,p) (Continued)

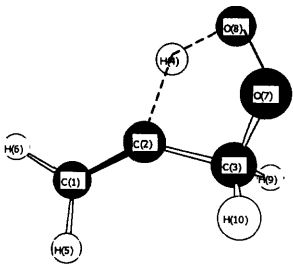
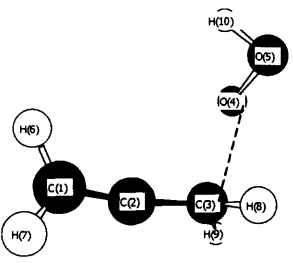
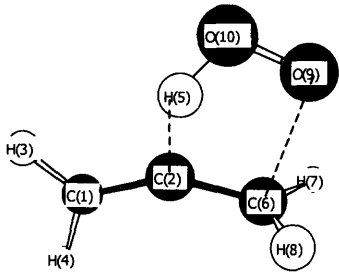
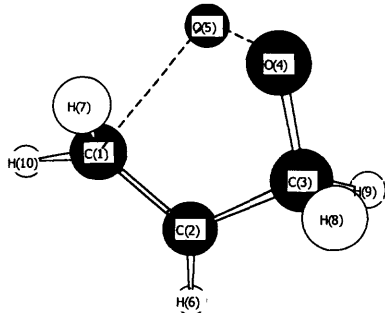
Species Name & Structure	Bond Length (Å)		Bond Angle (Degree)		Dihedral Angle (Degree)		
[m] TC=C•COOHS							$S^2=0.760$ (0.961)
	r21	1.31					
	r32	1.51	∠321	137.9			
	r42	1.41	∠421	134.8	∠4213	179.4	
	r51	1.09	∠512	121.8	∠5123	2.1	
	r61	1.09	∠612	122.0	∠6123	-178.2	
	r73	1.43	∠732	104.3	∠7321	-153.3	
	r84	1.17	∠842	132.7	∠8421	176.6	
	r93	1.10	∠932	109.3	∠9321	87.9	
	r103	1.10	∠1032	114.7	∠10321	-36.5	
[n] TC=C•COOH							$S^2=0.778$ (1.113)
	r21	1.30	∠321	170.4			
	r32	1.36	∠432	108.8	∠4321	0.4	
	r43	1.87	∠543	108.5	∠5432	89.4	
	r54	1.40	∠612	121.8	∠6124	0.4	
	r61	1.09	∠612	121.8	∠6124	0.4	
	r71	1.09	∠712	122.0	∠7126	179.6	
	r83	1.09	∠832	118.7	∠8326	107.6	
	r93	1.09	∠932	118.2	∠9326	-105.1	
	r105	0.97	∠1054	102.6	∠10543	-103.0	
[o] TC=C=C-OOHE							$S^2=0.759$ (1.183)
	r21	1.32	∠312	121.9			
	r31	1.09	∠412	121.4	∠4123	180.0	
	r41	1.09	∠521	114.0	∠5213	0.0	
	r52	1.37	∠621	149.7	∠6213	179.0	
	r62	1.36	∠621	149.7	∠6213	179.0	
	r76	1.09	∠762	122.0	∠7621	88.6	
	r86	1.09	∠862	122.0	∠8621	-88.5	
	r96	2.27	∠962	94.3	∠9625	-0.2	
	r109	1.27	∠1096	97.4	∠10962	0.0	
[p] TYCC•COO							$S^2=0.794$ (1.118)
	r21	1.39	∠321	113.6			
	r32	1.51	∠432	105.2	∠4321	-6.2	
	r43	1.43	∠543	104.9	∠5432	-39.5	
	r54	1.41	∠621	122.2	∠6213	-156.2	
	r62	1.09	∠621	122.2	∠6213	-156.2	
	r71	1.08	∠712	121.2	∠7123	-48.3	
	r83	1.10	∠832	115.9	∠8321	111.3	
	r93	1.10	∠932	109.1	∠9321	-125.5	
	r101	1.09	∠1012	119.8	∠10123	154.3	

Table C.1 Geometries of Intermediate Radicals and Transition States Optimized at B3LYP/6-31G(d,p) (Continued)

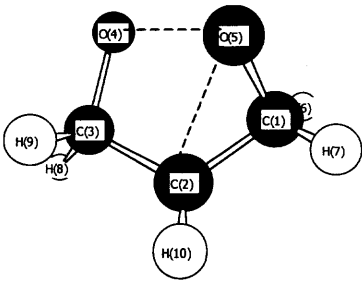
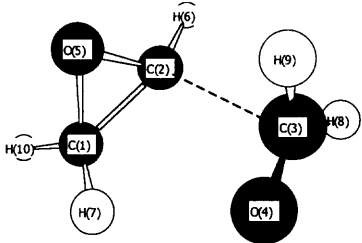
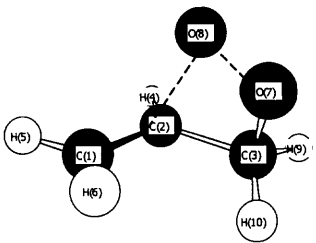
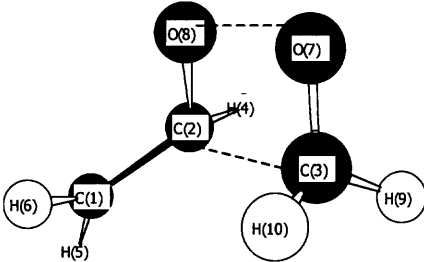
Species Name & Structure	Bond Length (Å)		Bond Angle (Degree)		Dihedral Angle (Degree)	
[q] TO•CH ₂ YCCO	$S^2=0.951$ (1.696)					
	r21	1.49				
	r32	1.49	∠321	112.7		
	r43	1.37	∠432	108.5	∠4321	-4.4
	r51	1.38	∠512	96.7	∠5123	46.0
	r61	1.10	∠612	115.1	∠6123	-76.2
	r71	1.10	∠712	109.8	∠7123	160.0
	r83	1.11	∠832	107.6	∠8321	114.3
	r93	1.11	∠932	110.0	∠9321	-130.2
	r102	1.09	∠1021	123.5	∠10213	-160.6
[r] TYCCO-CH ₂ O	$S^2=0.761$ (0.888)					
	r21	1.45				
	r32	2.28	∠321	108.2		
	r43	1.23	∠432	104.2	∠4321	-2.0
	r52	1.36	∠521	63.7	∠5213	-106.4
	r62	1.09	∠621	134.3	∠6213	142.9
	r71	1.09	∠712	117.8	∠7123	5.1
	r83	1.11	∠832	89.1	∠8321	120.7
	r93	1.11	∠932	88.0	∠9321	-124.6
	r101	1.09	∠1012	121.8	∠10123	-155.6
[s] TC•YCCOO	$S^2=0.779$ (1.042)					
	r21	1.39				
	r32	1.53	∠321	121.8		
	r42	1.09	∠421	118.1	∠4213	161.8
	r51	1.08	∠512	121.0	∠5123	-177.6
	r61	1.09	∠612	120.8	∠6123	10.9
	r73	1.43	∠732	98.0	∠7321	-85.9
	r87	1.45	∠873	95.1	∠8732	-18.3
	r93	1.10	∠932	112.4	∠9321	156.4
	r103	1.10	∠1032	114.7	∠10321	30.2
[t] TC=COOC•	$S^2=0.797$ (1.268)					
	r21	1.37				
	r32	1.95	∠321	121.7		
	r42	1.09	∠421	119.7	∠4213	123.3
	r51	1.08	∠512	120.8	∠5123	-107.4
	r61	1.08	∠612	120.6	∠6123	69.5
	r73	1.38	∠732	81.0	∠7321	-136.8
	r82	1.42	∠821	117.0	∠8213	-92.4
	r93	1.09	∠932	118.9	∠9321	110.5
	r103	1.09	∠1032	104.1	∠10321	-21.6

Table C.1 Geometries of Intermediate Radicals and Transition States Optimized at B3LYP/6-31G(d,p) (Continued)

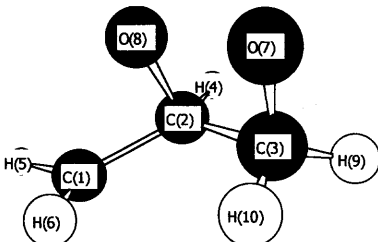
Species Name & Structure	Bond Length (Å)	Bond Angle (Degree)		Dihedral Angle (Degree)		
[u] TYCOCYCO					$S^2=0.890$ (1.472)	
	r21	1.46				
	r32	1.53	∠321	123.3		
	r42	1.10	∠421	115.0	∠4213	148.5
	r51	1.08	∠512	121.1	∠5123	-169.6
	r61	1.08	∠612	119.4	∠6123	21.1
	r73	1.43	∠732	93.7	∠7321	-115.2
	r82	1.43	∠821	91.8	∠8213	-95.2
	r93	1.10	∠932	116.9	∠9321	128.8
	r103	1.10	∠1032	112.5	∠10321	0.8

Table C.2 Vibrational Frequencies and Moments of Inertia at B3LYP/6-31G(d,p) level

Molecule	Frequencies (cm ⁻¹) ^a
CH ₂ =CHC•H ₂ 32.88, 175.25, 208.13 ^b	426, 535, 554, 777, 801, 938, 1017, 1043, 1218, 1278, 1430, 1528, 1535, 3148, 3157, 3164, 3257, 3259
CH ₂ =CHCH ₂ OOH 177.56, 543.48, 644.75	67, 165, 224, 338, 431, 456, 680, 882, 928, 966, 984, 1023, 1039, 1176, 1291, 1319, 1372, 1377, 1459, 1484, 1727, 3037, 3090, 3147, 3157, 3237, 3731
CH ₂ =CHCH ₂ OO• 109.94, 646.65, 696.44	86, 110, 313, 382, 527, 670, 860, 949, 966, 980, 1037, 1162, 1196, 1280, 1312, 1360, 1463, 1485, 1730, 3071, 3138, 3155, 3181, 3243
C•H=CHCH ₂ OOH 171.19, 518.89, 625.66	58, 165, 233, 350, 417, 469, 687, 793, 835, 884, 976, 1021, 1101, 1249, 1293, 1372, 1382, 1475, 1687, 3047, 3051, 3116, 3256, 3723
CH ₂ =C•CH ₂ OOH 163.08, 552.37, 660.96	61, 158, 237, 295, 392, 437, 607, 875, 886, 911, 976, 1025, 1090, 1272, 1354, 1381, 1428, 1449, 1751, 2969, 3063, 3070, 3176, 3727
YCC•COO 220.31, 242.87, 421.76	139, 193, 293, 690, 732, 837, 935, 943, 973, 1005, 1014, 1024, 1183, 1204, 1302, 1329, 1369, 1489, 1495, 2948, 2950, 3054, 3056, 3263
O•CH ₂ YCCO 161.72, 446.39, 483.10	136, 244, 340, 616, 635, 779, 868, 948, 998, 1076, 1103, 1150, 1163, 1201, 1289, 1357, 1375, 1435, 1534, 2902, 2935, 3097, 3106, 3199
C•H ₂ YCCOO 157.51, 381.75, 476.41	147, 174, 328, 445, 579, 701, 861, 879, 936, 952, 1025, 1124, 1149, 1192, 1268, 1334, 1386, 1478, 1528, 3034, 3048, 3108, 3169, 3282
TC=CC-O ₂ 113.92, 856.61, 906.71	269i, 31, 94, 200, 299, 427, 611, 705, 888, 899, 943, 1017, 1037, 1222, 1305, 1428, 1451, 1520, 1587, 3159, 3164, 3173, 3256, 3275
TC•=CCOOHS 211.46, 341.02, 511.34	1178i, 237, 334, 476, 545, 577, 701, 793, 867, 901, 939, 1049, 1072, 1136, 1261, 1272, 1363, 1478, 1623, 1713, 3023, 3100, 3108, 3245
TC•=CCOOH 152.63, 728.23, 837.85	486i, 61, 103, 161, 198, 259, 376, 519, 544, 621, 719, 784, 819, 900, 1108, 1187, 1386, 1458, 1913, 3113, 3259, 3374, 3475, 3771
TALLYL-OHSQ 144.53, 541.18, 588.52	1757i, 119, 209, 258, 566, 616, 636, 869, 918, 950, 964, 1014, 1029, 1152, 1204, 1316, 1379, 1446, 1649, 1963, 3102, 3182, 3192, 3285
TC=C•COOHS 146.04, 518.34, 631.04	2060i, 144, 255, 350, 478, 540, 684, 867, 899, 904, 922, 981, 1025, 1075, 1228, 1313, 1420, 1487, 1739, 1799, 3023, 3098, 3101, 3196
TC=C•COOH 164.60, 676.67, 764.90	553i, 64, 133, 259, 354, 363, 408, 446, 871, 883, 949, 976, 1036, 1055, 1077, 1379, 1435, 1470, 1931, 3099, 3134, 3168, 3214, 3704
TC=C=C-OOHE 177.26, 573.57, 738.59	1053i, 139, 258, 321, 344, 459, 543, 638, 777, 921, 933, 1012, 1056, 1060, 1156, 1364, 1461, 1523, 1644, 1882, 3140, 3153, 3224, 3234
TYCC•COO 227.51, 275.00 435.67	695i, 238, 346, 507, 647, 697, 866, 901, 935, 959, 985, 991, 1089, 1221, 1245, 1358, 1402, 1489, 1533, 3008, 3064, 3155, 3201, 3246

^a Non-scaled. ^b Moments of Inertia in amu-Bohr², 1 Bohr = 0.529177Å.

Table C.2 Vibrational Frequencies and Moments of Inertia at B3LYP/6-31G(d,p) level
(Continued)

Molecule	Frequencies (cm ⁻¹) ^a
TO•CH ₂ YCCO 205.32, 307.79, 445.79	651i, 232, 263, 430, 570, 681, 854, 893, 978, 1045, 1104, 1127, 1165, 1176, 1296, 1319, 1359, 1445, 1462, 2889, 2920, 2975, 3020, 3183
TYCCO-CH ₂ O 164.01, 575.31, 631.27	194i, 63, 153, 174, 321, 555, 767, 836, 984, 1046, 1084, 1112, 1133, 1203, 1258, 1372, 1513, 1528, 1694, 2896, 2951, 3121, 3151, 3228
TC•YCCOO 189.35, 369.07, 452.87	717i, 124, 281, 376, 494, 706, 810, 841, 921, 957, 1000, 1043, 1157, 1198, 1283, 1361, 1436, 1525, 1541, 3030, 3091, 3167, 3188, 3268
TC=COOC• 156.61, 412.72, 509.64	874i, 218, 282, 376, 478, 527, 651, 707, 812, 883, 957, 1041, 1082, 1148, 1180, 1275, 1393, 1501, 1543, 3074, 3108, 3175, 3189, 3276
TYCOCYCO 160.09, 376.99 467.14	793i, 164, 324, 387, 495, 643, 735, 873, 928, 965, 1045, 1143, 1175, 1219, 1258, 1320, 1412, 1488, 1525, 3006, 3053, 3075, 3175, 3291

APPENDIX D

INTERNAL ROTATION, THERMODYNAMIC AND KINETIC ANALYSIS

This appendix lists barriers and coefficients of truncated fourier series expansions for internal rotations, vibration frequencies and moments of inertia at B3LYP/6-31G(d,p) level, and thermodynamic and kinetic analysis vs. temperature as discussed in Chapter 8.

Table D.1 Total Energy and Internal Rotation Barriers of CH₃CH₂SCH₂CH₂Cl and CH₂ClCH₂SCH₂CH₂Cl

torsion angle	total energy ^a	rotational barrier ^b	torsion angle	total energy ^a	rotational barrier ^b	torsion angle	total energy ^a	rotational barrier ^b
CH ₃ --CH ₂ SCH ₂ CH ₂ Cl			CH ₃ CH ₂ --SCH ₂ CH ₂ Cl			CH ₃ CH ₂ S--CH ₂ CH ₂ Cl		
-60	-1016.2503154	0.00	177	-1016.2503154	0.00	80	-1016.2503154	0.00
-45	-1016.2496383	0.42	192	-1016.2500795	0.15	95	-1016.2498753	0.28
-30	-1016.2479461	1.49	207	-1016.2494507	0.54	110	-1016.2489661	0.85
-15	-1016.2461386	2.62	222	-1016.2487760	0.97	125	-1016.2483499	1.23
0	-1016.2453339	3.13	237	-1016.2485175	1.13	140	-1016.2482226	1.31
15	-1016.2460812	2.66	252	-1016.2487938	0.95	155	-1016.2484296	1.18
30	-1016.2478772	1.53	267	-1016.2490807	0.77	170	-1016.2486306	1.06
45	-1016.2495926	0.45	282	-1016.2494115	0.57	185	-1016.2486715	1.03
60	-1016.2503142	0.00	297	-1016.2494087	0.57	200	-1016.2485042	1.14
75	-1016.2496979	0.39	312	-1016.2484416	1.18	215	-1016.2482604	1.29
90	-1016.2480249	1.44	327	-1016.2465985	2.33	230	-1016.2482500	1.30
105	-1016.2461760	2.60	342	-1016.2448865	3.41	245	-1016.2487300	0.99
120	-1016.2453332	3.13	357	-1016.2444854	3.66	260	-1016.2495990	0.45
135	-1016.2461226	2.63	12	-1016.2454484	3.05	275	-1016.2502697	0.03
150	-1016.2479647	1.48	27	-1016.2471393	1.99	290	-1016.2500761	0.15
165	-1016.2496503	0.42	42	-1016.2487999	0.95	305	-1016.2488487	0.92
180	-1016.2503152	0.00	57	-1016.2498554	0.29	320	-1016.2467315	2.25
195	-1016.2496904	0.39	72	-1016.2502725	0.03	335	-1016.2443401	3.75
210	-1016.2480386	1.43	87	-1016.2499715	0.22	350	-1016.2425307	4.88
225	-1016.2461949	2.59	102	-1016.2491630	0.72	5	-1016.2422439	5.06
240	-1016.2453345	3.13	117	-1016.2486925	1.02	20	-1016.2436864	4.16
255	-1016.2460970	2.65	132	-1016.2488893	0.89	35	-1016.2459916	2.71
270	-1016.2479328	1.50	147	-1016.2494943	0.52	50	-1016.2482660	1.29
285	-1016.2496437	0.42	162	-1016.2501083	0.13	65	-1016.2498189	0.31
300	-1016.2503154	0.00	177	-1016.2503153	0.00	80	-1016.2503154	0.00

^a Electronic energies at 0 K. ZPVE and thermal correction to 298 K are not included. Units in Hartree.

^b Rotational barriers are calculated as the difference between the total energy of each conformer and that of the most stable conformer. Units in kcal/mol.

Table D.1 Total Energy and Internal Rotation Barriers of CH₃CH₂SCH₂CH₂Cl and CH₂ClCH₂SCH₂CH₂Cl (Continued)

torsion angle	total energy ^a	rotational barrier ^b	torsion angle	total energy ^a	rotational barrier ^b	torsion angle	total energy ^a	rotational barrier ^b
CH ₃ CH ₂ SCH ₂ --CH ₂ Cl			CH ₂ Cl--CH ₂ SCH ₂ CH ₂ Cl			CH ₂ ClCH ₂ --SCH ₂ CH ₂ Cl		
180	-1016.2503154	0.00	-180	-1475.8431850	0.00	-83	-1475.8431850	0.00
195	-1016.2494349	0.55	-165	-1475.8422553	0.58	-68	-1475.8426285	0.35
210	-1016.2472841	1.90	-150	-1475.8399650	2.02	-53	-1475.8413420	1.16
225	-1016.2450695	3.29	-135	-1475.8374461	3.60	-38	-1475.8394678	2.33
240	-1016.2442155	3.83	-120	-1475.8360114	4.50	-23	-1475.8372397	3.73
255	-1016.2451140	3.26	-105	-1475.8364826	4.21	-8	-1475.8354006	4.88
270	-1016.2467161	2.26	-90	-1475.8382455	3.10	7	-1475.8347690	5.28
285	-1016.2476255	1.69	-75	-1475.8397729	2.14	22	-1475.8358836	4.58
300	-1016.2469341	2.12	-60	-1475.8396832	2.20	37	-1475.8382706	3.08
315	-1016.2446070	3.58	-45	-1475.8379290	3.30	52	-1475.8405600	1.65
330	-1016.2415092	5.53	-30	-1475.8352202	5.00	67	-1475.8418775	0.82
345	-1016.2390530	7.07	-15	-1475.8325591	6.67	82	-1475.8421483	0.65
360	-1016.2382833	7.55	0	-1475.8312347	7.50	97	-1475.8421480	0.65
15	-1016.2395619	6.75	15	-1475.8320127	7.01	112	-1475.8418353	0.85
30	-1016.2421464	5.13	30	-1475.8345924	5.39	127	-1475.8413395	1.16
45	-1016.2448160	3.45	45	-1475.8377840	3.39	142	-1475.8411457	1.28
60	-1016.2464853	2.40	60	-1475.8401356	1.91	157	-1475.8412324	1.23
75	-1016.2465721	2.35	75	-1475.8407690	1.52	172	-1475.8413787	1.13
90	-1016.2452062	3.21	90	-1475.8397172	2.18	187	-1475.8415031	1.06
105	-1016.2435532	4.24	105	-1475.8380815	3.20	202	-1475.8415454	1.03
120	-1016.2432016	4.46	120	-1475.8370542	3.85	217	-1475.8415422	1.03
135	-1016.2446497	3.56	135	-1475.8377823	3.39	232	-1475.8416207	0.98
150	-1016.2471568	1.98	150	-1475.8399948	2.00	247	-1475.8420284	0.73
165	-1016.2494184	0.56	165	-1475.8422696	0.57	262	-1475.8427662	0.26
180	-1016.2503154	0.00	180	-1475.8431849	0.00	277	-1475.8431850	0.00

Table D.2 Coefficients of Truncated Fourier Series Expansions for Internal Rotation Potentials^a

	a ₀	a ₁	a ₂	a ₃	a ₄	a ₅	a ₆	a ₇
CH ₃ --CH ₂ SCH ₂ CH ₂ Cl	1.519	0.010	-0.002	-1.562	0.002	-0.009	0.044	-0.002
CH ₃ CH ₂ --SCH ₂ CH ₂ Cl	1.085	-0.977	0.644	-0.825	0.081	-0.046	0.024	0.015
CH ₃ CH ₂ S--CH ₂ CH ₂ Cl	1.568	0.198	-1.357	-0.426	0.028	0.007	-0.017	-0.006
CH ₃ CH ₂ SCH ₂ --CH ₂ Cl	3.363	-1.919	0.490	-1.885	-0.109	0.032	0.030	0.000
CH ₂ Cl--CH ₂ SCH ₂ CH ₂ Cl	3.301	-1.817	0.539	-1.955	-0.116	0.025	0.023	-0.003
CH ₂ ClCH ₂ --SCH ₂ CH ₂ Cl	1.662	-0.087	-1.379	-0.180	0.095	-0.055	-0.041	-0.003
	b ₁	b ₂	b ₃	b ₄	b ₅	b ₆	b ₇	
CH ₃ --CH ₂ SCH ₂ CH ₂ Cl	0.013	0.004	-0.025	0.004	0.010	0.004	-0.003	
CH ₃ CH ₂ --SCH ₂ CH ₂ Cl	0.178	-0.074	-0.022	-0.012	0.063	-0.041	-0.005	
CH ₃ CH ₂ S--CH ₂ CH ₂ Cl	-1.152	-0.484	0.756	0.022	-0.006	-0.026	0.002	
CH ₃ CH ₂ SCH ₂ --CH ₂ Cl	-0.265	-0.120	0.213	-0.010	-0.002	-0.021	-0.003	
CH ₂ Cl--CH ₂ SCH ₂ CH ₂ Cl	0.260	0.112	-0.217	0.001	-0.005	0.036	0.008	
CH ₂ ClCH ₂ --SCH ₂ CH ₂ Cl	1.372	0.227	-0.680	-0.014	0.074	-0.024	0.020	

^a units in kcal/mol. Values of rotation barriers calculated at the B3LYP/6-31G(d,p) level are used to calculate the coefficients.

Table D.3 Vibrational Frequencies and Moments of Inertia at B3LYP/6-31G(d,p) level

Molecule	Frequencies (cm ⁻¹) ^a
CH ₃ CH ₂ SCH ₂ CH ₃ 126.62, 1064.94, 1146.38 ^b	54, 79, 137,245, 248, 327,335, 685, 689,788, 805, 994,997, 1039, 1054,1062, 1104, 1270,1275, 1288, 1326,1425, 1427, 1499,1507, 1507, 1508,1519, 1520, 3044,3044, 3050, 3050,3088, 3091, 3120,3121, 3130, 3131
CH ₃ CH ₂ SCH ₂ CH ₂ Cl 266.83, 2341.34, 2490.69	43, 66, 87, 206, 220, 246, 259, 379, 663, 693, 743, 763, 795, 979, 996, 1049, 1051, 1082, 1154, 1249, 1272, 1299, 1317, 1335, 1428, 1482, 1499, 1503, 1507, 1518, 3052, 3053, 3078, 3101, 3111, 3123, 3133, 3134, 3179
CH ₂ ClCH ₂ SCH ₂ CH ₂ Cl 938.59, 2681.66, 3256.67	34, 78, 87, 109, 192, 225, 230, 313, 332, 683, 699, 732, 738, 754, 771, 956, 1014, 1047, 1051, 1142, 1159, 1238, 1263, 1302, 1312, 1335, 1336, 1478, 1485, 1500, 1501, 3086, 3087, 3110, 3111, 3140, 3140, 3178, 3178
TS1 160.90, 1330.62, 1352.45	746i, 42, 73, 197, 222, 310, 332, 361, 450, 617, 645, 760, 835, 936, 979, 1030, 1071, 1126, 1190, 1269, 1276, 1285, 1333, 1403, 1422, 1466, 1475, 1505, 1513, 1573, 3034, 3040, 3079, 3105, 3108, 3129, 3190, 3193, 3290
TS2A 530.09, 1842.83, 2250.85	1404i, 41, 67, 91, 170, 243, 297, 312, 338, 363, 641, 677, 709, 796, 803, 995, 1026, 1039, 1059, 1084, 1180, 1275, 1279, 1305, 1348, 1429, 1461, 1502, 1508, 1517, 1577, 3053, 3069, 3118, 3126, 3137, 3140, 3190, 3300
TS2B 321.95, 2484.25 2632.25	911i, 30, 61, 107, 180, 227, 299, 353, 373, 423, 584, 639, 689, 745, 829, 902, 979, 1035, 1053, 1075, 1180, 1259, 1273, 1286, 1352, 1423, 1437, 1465, 1505, 1512, 1525, 3037, 3042, 3082, 3108, 3130, 3155, 3198, 3306
TS2C 646.33, 1534.89, 2034.10	310i, 51, 73, 91, 107, 183, 205, 283, 308, 366, 452, 599, 694, 840, 934, 962, 967, 970, 994, 1068, 1240, 1243, 1270, 1286, 1423, 1434, 1479, 1508, 1511, 1570, 3005, 3044, 3069, 3111, 3135, 3158, 3204, 3249, 3309
TS3A 842.69, 3581.56, 4288.27	1468i, 26, 46, 71, 113, 129, 260, 271, 303, 326, 379, 645, 698, 711, 771, 786, 802, 993, 1025, 1040, 1057, 1147, 1175, 1256, 1276, 1304, 1333, 1355, 1446, 1504, 1507, 1562, 3085, 3104, 3143, 3146, 3171, 3191, 3301
TS3B 351.23, 5310.84, 5487.83	845i, 40, 45, 76, 101, 201, 224, 280, 336, 372, 427, 586, 679, 689, 723, 743, 828, 917, 992, 1037, 1055, 1139, 1182, 1227, 1263, 1298, 1321, 1355, 1434, 1468, 1499, 1527, 3068, 3112, 3116, 3154, 3180, 3197, 3305
TS3C 646.33, 1534.89, 2034.10	310i, 51, 73, 91, 107, 183, 205, 283, 308, 366, 452, 599, 694, 840, 934, 962, 967, 970, 994, 1068, 1240, 1243, 1270, 1286, 1423, 1434, 1479, 1508, 1511, 1570, 3005, 3044, 3069, 3111, 3135, 3158, 3204, 3249, 3309
CH ₃ CH ₂ SCH ₂ C•H ₂ 125.14, 1032.35, 1111.04	45, 73, 135, 190, 247, 307, 326, 551, 659, 686, 784, 802, 994, 1025, 1055, 1064, 1092, 1229, 1257, 1272, 1311, 1426, 1475, 1500, 1507, 1507, 1519, 3044, 3047, 3049, 3089, 3103, 3119, 3131, 3167, 3273
CH ₃ CH ₂ SC•HCH ₃ 113.32, 1052.52, 1129.66	52, 71, 131, 149, 242, 332, 346, 460, 680, 747, 792, 996, 1011, 1035, 1048, 1075, 1122, 1269, 1289, 1325, 1422, 1427, 1486, 1501, 1502, 1507, 1518, 2976, 3051, 3060, 3060, 3104, 3108, 3122, 3134, 3171

^a Non-scaled. ^b Moments of Inertia in amu-Bohr², 1 Bohr = 0.529177Å.

Table D.3 Vibrational Frequencies and Moments of Inertia at B3LYP/6-31G(d,p) level (Continued)

Molecule	Frequencies (cm ⁻¹) ^a
CH ₃ CH ₂ SCH ₂ C•HCl 367.99, 1993.18, 2255.20	25, 57, 110, 173, 242, 249, 283, 372, 428, 662, 717, 761, 797, 892, 996, 1053, 1078, 1102, 1165, 1234, 1271, 1307, 1332, 1426, 1462, 1503, 1508, 1519, 3004, 3050, 3056, 3093, 3105, 3121, 3132, 3236
CH ₃ CH ₂ SC•HCH ₂ Cl 257.34, 2264.29, 2331.80	35, 40, 95, 149, 247, 268, 335, 389, 463, 558, 680, 749, 792, 953, 996, 1052, 1083, 1130, 1183, 1232, 1272, 1302, 1355, 1430, 1496, 1500, 1508, 1518, 3054, 3067, 3116, 3118, 3127, 3139, 3186, 3206
CH ₃ CH ₂ SH 62.53, 348.88, 380.01	233, 267, 328, 649, 741, 877, 988, 1071, 1130, 1287, 1318, 1427, 1493, 1506, 1514, 2677, 3042, 3073, 3107, 3118, 3139
CH ₃ CH ₂ S• 54.45, 339.35, 371.61	228, 331, 491, 660, 910, 981, 1077, 1260, 1294, 1426, 1447, 1502, 1511, 3027, 3044, 3045, 3116, 3137
CH ₃ CH ₂ SCl 249.04, 637.58, 816.09	103, 181, 268, 354, 487, 636, 769, 981, 1060, 1077, 1273, 1312, 1425, 1464, 1504, 1516, 3043, 3052, 3109, 3124, 3145
CH ₃ CH ₂ SCHCH ₂ 249.04, 637.58, 816.09	113, 161, 194, 275, 331, 464, 600, 641, 709, 775, 872, 981, 996, 1033, 1072, 1087, 1283, 1303, 1319, 1426, 1435, 1488, 1506, 1518, 1666, 3048, 3067, 3113, 3120, 3144, 3166, 3179, 3254
CH ₂ ClCH ₂ SCl 308.86, 1949.37, 2173.33	73, 99, 203, 230, 324, 490, 691, 737, 762, 986, 1050, 1148, 1249, 1305, 1341, 1464, 1502, 3066, 3114, 3136, 3183

Table D.4 Thermodynamic and Kinetic Analysis vs. Temperature in Retro-ene and HCl Eliminations**(1) CH₃CH₂SCH₂CH₃ => TS1 (=> CH₃CH₂SH + CH₂CH₂)**

ΔH_f° (kcal/mol)	-20.08	44.33
S° (cal/mol-K)	89.97	86.77

T (K)	ΔH^\ddagger (kcal/mol)	ΔS^\ddagger (cal/mol-K)	ΔG^\ddagger (kcal/mol)	A (s ⁻¹)	T^n	k (s ⁻¹)
300	64.41	-3.19	65.37	1.25E+12	1.21E+04	1.48E-35
400	64.54	-2.83	65.67	2.01E+12	1.94E+04	1.09E-23
500	64.69	-2.49	65.94	2.98E+12	2.80E+04	1.57E-16
600	64.85	-2.20	66.17	4.14E+12	3.78E+04	9.83E-12
800	65.16	-1.76	66.56	6.88E+12	6.07E+04	1.09E-05
1000	65.41	-1.48	66.88	9.92E+12	8.77E+04	5.01E-02
1200	65.60	-1.30	67.16	1.30E+13	1.18E+05	1.46E+01
1500	65.83	-1.13	67.52	1.77E+13	1.71E+05	4.53E+03
2000	66.20	-0.92	68.03	2.63E+13	2.75E+05	1.53E+06

ΔH^\ddagger , ΔS^\ddagger , and ΔG^\ddagger are calculated between reactant and transition state.

$$A = A' T^n$$

Three-parameter model equation: $k(T) = A' T^n \exp(-E_a/RT)$

$$A' = 5.667E+7 \text{ (s}^{-1}\text{)} \quad n = 1.648 \quad E_a = 64.06 \text{ (kcal/mol)}$$

(2) CH₃CH₂SCH₂CH₂Cl => TS2A (=> CH₃CH₂SCHCH₂ + HCl)

ΔH_f° (kcal/mol)	-26.45	30.82
S° (cal/mol-K)	100.53	98.04

T (K)	ΔH^\ddagger (kcal/mol)	ΔS^\ddagger (cal/mol-K)	ΔG^\ddagger (kcal/mol)	A (s ⁻¹)	T^n	k (s ⁻¹)
300	57.27	-2.49	58.02	1.78E+12	7.81E+01	3.37E-30
400	57.20	-2.68	58.28	2.16E+12	9.73E+01	1.20E-19
500	57.15	-2.81	58.55	2.53E+12	1.15E+02	2.65E-13
600	57.09	-2.91	58.84	2.90E+12	1.33E+02	4.61E-09
800	57.01	-3.03	59.43	3.63E+12	1.65E+02	9.65E-04
1000	56.93	-3.12	60.05	4.35E+12	1.96E+02	1.57E+00
1200	56.85	-3.19	60.68	5.02E+12	2.25E+02	2.22E+02
1500	56.69	-3.31	61.65	5.91E+12	2.67E+02	3.25E+04
2000	56.47	-3.44	63.34	7.39E+12	3.33E+02	4.98E+06

Three-parameter model equation: $k(T) = A' T^n \exp(-E_a/RT)$

$$A' = 2.797E+10 \text{ (s}^{-1}\text{)} \quad n = 0.764 \quad E_a = 57.39 \text{ (kcal/mol)}$$

Table D.4 Thermodynamic and Kinetic Analysis vs. Temperature in Retro-ene and HCl Eliminations (Continued)**(3) CH₃CH₂SCH₂CH₂Cl => TS2B (=> CH₃CH₂SH + CH₂CHCl)**

ΔH_f° (kcal/mol)	-26.45	41.32
S° (cal/mol-K)	100.53	93.56

T (K)	ΔH^\ddagger (kcal/mol)	ΔS^\ddagger (cal/mol-K)	ΔG^\ddagger (kcal/mol)	A (s ⁻¹)	T^n	k (s ⁻¹)
300	67.77	-6.98	69.86	1.87E+11	7.18E+02	7.91E-39
400	67.72	-7.12	70.57	2.32E+11	1.00E+03	2.30E-26
500	67.71	-7.13	71.28	2.88E+11	1.29E+03	7.22E-19
600	67.73	-7.10	71.99	3.51E+11	1.60E+03	7.44E-14
800	67.82	-6.98	73.40	4.97E+11	2.23E+03	1.47E-07
1000	67.91	-6.87	74.79	6.55E+11	2.88E+03	9.40E-04
1200	68.00	-6.80	76.15	8.18E+11	3.55E+03	3.37E-01
1500	68.10	-6.72	78.18	1.06E+12	4.60E+03	1.27E+02
2000	68.34	-6.58	81.50	1.52E+12	6.40E+03	5.16E+04

Three-parameter model equation: $k(T) = A' T^n \exp(-Ea/RT)$

$$A' = 1.951E+8 \text{ (s}^{-1}\text{)} \quad n = 1.153 \quad Ea = 67.59 \text{ (kcal/mol)}$$

(4) CH₃CH₂SCH₂CH₂Cl => TS2C (=> CH₃CH₂SCl + CH₂CH₂)

ΔH_f° (kcal/mol)	-26.45	52.16
S° (cal/mol-K)	100.53	97.00

T (K)	ΔH^\ddagger (kcal/mol)	ΔS^\ddagger (cal/mol-K)	ΔG^\ddagger (kcal/mol)	A (s ⁻¹)	T^n	k (s ⁻¹)
300	78.61	-3.53	79.67	1.06E+12	8.46E+01	5.65E-46
400	78.59	-3.57	80.02	1.38E+12	1.06E+02	1.56E-31
500	78.57	-3.64	80.38	1.67E+12	1.26E+02	7.57E-23
600	78.53	-3.70	80.75	1.94E+12	1.45E+02	4.80E-17
800	78.44	-3.83	81.50	2.42E+12	1.81E+02	9.00E-10
1000	78.33	-3.96	82.28	2.85E+12	2.16E+02	2.16E-05
1200	78.22	-4.06	83.09	3.24E+12	2.49E+02	1.84E-02
1500	78.06	-4.17	84.32	3.83E+12	2.96E+02	1.62E+01
2000	77.98	-4.23	86.43	4.97E+12	3.70E+02	1.50E+04

Three-parameter model equation: $k(T) = A' T^n \exp(-Ea/RT)$

$$A' = 1.646E+10 \text{ (s}^{-1}\text{)} \quad n = 0.778 \quad Ea = 78.78 \text{ (kcal/mol)}$$

Table D.4 Thermodynamic and Kinetic Analysis vs. Temperature in Retro-ene and HCl Eliminations (Continued)**(5) CH₂ClCH₂SCH₂CH₂Cl => TS3A (=> CH₂ClCH₂SCHCH₂ + HCl)**

ΔH_f° (kcal/mol)	-31.12	27.99
S° (cal/mol-K)	110.07	109.05

T (K)	ΔH^\ddagger (kcal/mol)	ΔS^\ddagger (cal/mol-K)	ΔG^\ddagger (kcal/mol)	A (s ⁻¹)	T^n	k (s ⁻¹)
300	59.11	-1.02	59.42	3.73E+12	9.43E+01	3.22E-31
400	59.04	-1.21	59.53	4.53E+12	1.19E+02	2.47E-20
500	58.99	-1.33	59.66	5.33E+12	1.42E+02	8.71E-14
600	58.95	-1.41	59.79	6.15E+12	1.64E+02	2.07E-09
800	58.88	-1.51	60.09	7.79E+12	2.06E+02	6.39E-04
1000	58.82	-1.58	60.40	9.41E+12	2.46E+02	1.31E+00
1200	58.74	-1.65	60.72	1.09E+13	2.85E+02	2.18E+02
1500	58.60	-1.75	61.23	1.30E+13	3.40E+02	3.74E+04
2000	58.40	-1.87	62.14	1.63E+13	4.28E+02	6.75E+06

Three-parameter model equation: $k(T) = A' T^n \exp(-Ea/RT)$

$A' = 4.655E+10$ (s⁻¹) $n = 0.797$ $Ea = 59.20$ (kcal/mol)

(6) CH₂ClCH₂SCH₂CH₂Cl => TS3B (=> CH₂ClCH₂SH + CH₂CHCl)

ΔH_f° (kcal/mol)	-31.12	35.87
S° (cal/mol-K)	110.07	104.26

T (K)	ΔH^\ddagger (kcal/mol)	ΔS^\ddagger (cal/mol-K)	ΔG^\ddagger (kcal/mol)	A (s ⁻¹)	T^n	k (s ⁻¹)
300	66.99	-5.81	68.73	3.35E+11	9.19E+02	5.25E-38
400	66.95	-5.92	69.32	4.23E+11	1.30E+03	1.10E-25
500	66.96	-5.91	69.91	5.32E+11	1.69E+03	2.86E-18
600	66.99	-5.85	70.50	6.58E+11	2.11E+03	2.60E-13
800	67.10	-5.70	71.66	9.46E+11	2.97E+03	4.41E-07
1000	67.21	-5.58	72.78	1.26E+12	3.88E+03	2.57E-03
1200	67.30	-5.50	73.89	1.57E+12	4.83E+03	8.70E-01
1500	67.41	-5.41	75.53	2.05E+12	6.30E+03	3.09E+02
2000	67.65	-5.27	78.20	2.93E+12	8.89E+03	1.19E+05

Three-parameter model equation: $k(T) = A' T^n \exp(-Ea/RT)$

$A' = 2.647E+8$ (s⁻¹) $n = 1.196$ $Ea = 66.79$ (kcal/mol)

Table D.4 Thermodynamic and Kinetic Analysis vs. Temperature in Retro-ene and HCl Eliminations (Continued)**(7) CH₂ClCH₂SCH₂CH₂Cl => TS3C (=> CH₂ClCH₂SCl + CH₂CH₂)**

ΔH_f° (kcal/mol)	-31.12	46.52
S° (cal/mol-K)	110.07	106.39

T (K)	ΔH^\ddagger (kcal/mol)	ΔS^\ddagger (cal/mol-K)	ΔG^\ddagger (kcal/mol)	A (s ⁻¹)	T^n	k (s ⁻¹)
300	77.64	-3.68	78.74	9.80E+11	1.09E+02	2.67E-45
400	77.62	-3.73	79.11	1.28E+12	1.38E+02	4.91E-31
500	77.60	-3.77	79.49	1.56E+12	1.65E+02	1.86E-22
600	77.58	-3.81	79.87	1.84E+12	1.92E+02	1.01E-16
800	77.51	-3.91	80.64	2.33E+12	2.43E+02	1.55E-09
1000	77.42	-4.01	81.43	2.77E+12	2.92E+02	3.32E-05
1200	77.32	-4.10	82.24	3.17E+12	3.39E+02	2.62E-02
1500	77.18	-4.21	83.49	3.76E+12	4.08E+02	2.13E+01
2000	77.11	-4.25	85.61	4.91E+12	5.17E+02	1.84E+04

Three-parameter model equation: $k(T) = A' T^n \exp(-Ea/RT)$

$A' = 1.127E+10$ (s⁻¹) $n = 0.822$ $Ea = 77.77$ (kcal/mol)

(8) CH₃CH₂SH + CH₂CH₂ => TS1 (=> CH₃CH₂SCH₂CH₃)

ΔH_f° (kcal/mol)	-10.82	12.54	44.33
S° (cal/mol-K)	70.96	52.42	86.77

T (K)	ΔH^\ddagger (kcal/mol)	ΔS^\ddagger (cal/mol-K)	ΔG^\ddagger (kcal/mol)	A (s ⁻¹)	T^n	k (s ⁻¹)
300	42.61	-36.61	53.59	4.17E+09	5.68E+07	1.39E-22
400	42.69	-36.38	57.24	8.30E+09	1.40E+08	1.44E-14
500	42.85	-36.03	60.87	1.55E+10	2.81E+08	1.06E-09
600	43.06	-35.65	64.45	2.71E+10	4.97E+08	2.05E-06
800	43.55	-34.94	71.51	6.87E+10	1.22E+09	3.19E-02
1000	44.06	-34.38	78.43	1.43E+11	2.46E+09	1.23E+01
1200	44.54	-33.94	85.26	2.56E+11	4.35E+09	7.27E+02
1500	45.24	-33.41	95.36	5.20E+11	8.75E+09	4.89E+04
2000	46.47	-32.71	111.90	1.32E+12	2.15E+10	4.05E+06

Three-parameter model equation: $k(T) = A' T^n \exp(-Ea/RT)$

$A' = 6.858$ (cm³/mol-s) $n = 3.130$ $Ea = 41.78$ (kcal/mol)

Table D.4 Thermodynamic and Kinetic Analysis vs. Temperature in Retro-ene and HCl Eliminations (Continued)**(9) CH₃CH₂SCHCH₂ + HCl => TS2A (=> CH₃CH₂SCH₂CH₂Cl)**

ΔH_f° (kcal/mol)	10.59	-22.06	30.82
S° (cal/mol-K)	86.65	44.65	98.04

T (K)	ΔH^\ddagger (kcal/mol)	ΔS^\ddagger (cal/mol-K)	ΔG^\ddagger (kcal/mol)	A (s ⁻¹)	T^n	k (s ⁻¹)
300	42.29	-33.27	52.27	2.24E+10	6.61E+05	1.28E-21
400	42.16	-33.64	55.62	3.31E+10	1.30E+06	1.12E-13
500	42.11	-33.74	58.99	4.90E+10	2.19E+06	7.01E-09
600	42.13	-33.72	62.36	7.14E+10	3.37E+06	1.18E-05
800	42.28	-33.51	69.09	1.41E+11	6.62E+06	1.46E-01
1000	42.52	-33.25	75.76	2.52E+11	1.12E+07	4.72E+01
1200	42.78	-33.01	82.39	4.09E+11	1.72E+07	2.43E+03
1500	43.17	-32.71	92.24	7.40E+11	2.90E+07	1.40E+05
2000	43.86	-32.32	108.50	1.61E+12	5.70E+07	9.51E+06

Three-parameter model equation: $k(T) = A' T^n \exp(-Ea/RT)$

$A' = 6.046E+3$ (cm³/mol-s) $n = 2.349$ $Ea = 41.84$ (kcal/mol)

(10) CH₃CH₂SH + CH₂CHCl => TS2B (=> CH₃CH₂SCH₂CH₂Cl)

ΔH_f° (kcal/mol)	-10.82	5.00	41.32
S° (cal/mol-K)	70.96	63.08	93.56

T (K)	ΔH^\ddagger (kcal/mol)	ΔS^\ddagger (cal/mol-K)	ΔG^\ddagger (kcal/mol)	A (s ⁻¹)	T^n	k (s ⁻¹)
300	47.14	-40.48	59.28	5.96E+08	8.05E+07	9.90E-27
400	47.26	-40.15	63.32	1.25E+09	2.02E+08	6.92E-18
500	47.44	-39.74	67.31	2.40E+09	4.11E+08	1.61E-12
600	47.67	-39.32	71.26	4.26E+09	7.36E+08	6.75E-09
800	48.19	-38.58	79.05	1.10E+10	1.84E+09	2.76E-04
1000	48.71	-38.00	86.71	2.30E+10	3.76E+09	1.91E-01
1200	49.20	-37.55	94.26	4.16E+10	6.72E+09	1.67E+01
1500	49.91	-37.02	105.40	8.47E+10	1.37E+10	1.66E+03
2000	51.15	-36.31	123.80	2.15E+11	3.43E+10	2.04E+05

Three-parameter model equation: $k(T) = A' T^n \exp(-Ea/RT)$

$A' = 6.781E-1$ (cm³/mol-s) $n = 3.192$ $Ea = 46.31$ (kcal/mol)

Table D.4 Thermodynamic and Kinetic Analysis vs. Temperature in Retro-ene and HCl Eliminations (Continued)**(11) CH₃CH₂SCI + CH₂CH₂ => TS2C (=> CH₃CH₂SCH₂CH₂Cl)**

ΔH_f° (kcal/mol)	-12.95	12.54	52.16
S° (cal/mol-K)	79.28	52.42	97.00

T (K)	ΔH^\ddagger (kcal/mol)	ΔS^\ddagger (cal/mol-K)	ΔG^\ddagger (kcal/mol)	A (s ⁻¹)	T^n	k (s ⁻¹)
300	52.57	-34.69	62.98	1.09E+10	1.47E+07	2.01E-29
400	52.71	-34.30	66.43	2.36E+10	3.39E+07	1.38E-19
500	52.87	-33.94	69.84	4.45E+10	6.46E+07	1.26E-13
600	53.05	-33.61	73.22	7.56E+10	1.10E+08	1.31E-09
800	53.43	-33.07	79.88	1.76E+11	2.52E+08	1.64E-04
1000	53.79	-32.67	86.45	3.37E+11	4.80E+08	2.17E-01
1200	54.13	-32.35	92.96	5.68E+11	8.14E+08	2.89E+01
1500	54.65	-31.97	102.60	1.08E+12	1.55E+09	4.31E+03
2000	55.67	-31.38	118.40	2.57E+12	3.57E+09	7.80E+05

Three-parameter model equation: $k(T) = A' T^n \exp(-Ea/RT)$

$A' = 1.051E+2$ (cm³/mol-s) $n = 2.894$ $Ea = 52.01$ (kcal/mol)

(12) CH₂ClCH₂SCI + CH₂CH₂ => TS3C (=> CH₂ClCH₂SCH₂CH₂Cl)

ΔH_f° (kcal/mol)	-16.75	12.54	46.52
S° (cal/mol-K)	88.86	52.42	106.39

T (K)	ΔH^\ddagger (kcal/mol)	ΔS^\ddagger (cal/mol-K)	ΔG^\ddagger (kcal/mol)	A (s ⁻¹)	T^n	k (s ⁻¹)
300	50.73	-34.88	61.20	9.96E+09	8.26E+06	4.00E-28
400	50.90	-34.39	64.66	2.26E+10	1.84E+07	1.28E-18
500	51.07	-34.03	68.08	4.25E+10	3.44E+07	7.43E-13
600	51.23	-33.73	71.47	7.09E+10	5.72E+07	5.69E-09
800	51.54	-33.29	78.17	1.58E+11	1.28E+08	4.82E-04
1000	51.84	-32.96	84.79	2.91E+11	2.38E+08	5.02E-01
1200	52.14	-32.68	91.35	4.82E+11	3.96E+08	5.66E+01
1500	52.62	-32.33	101.10	9.00E+11	7.39E+08	7.14E+03
2000	53.58	-31.77	117.10	2.11E+12	1.65E+09	1.08E+06

Three-parameter model equation: $k(T) = A' T^n \exp(-Ea/RT)$

$A' = 2.048E+2$ (cm³/mol-s) $n = 2.792$ $Ea = 50.27$ (kcal/mol)

Table D.5 Thermodynamic and Kinetic Analysis vs. Temperature in Bond Cleavage Reactions**(1) $\text{CH}_3\text{CH}_2\text{SCH}_2\text{CH}_3 \Rightarrow \text{CH}_3\text{CH}_2\text{S} \cdot + \text{C}_2\text{H}_5$**

Ar = 1.50E+13 (High-Pressure Limit Rate Constant)				
T (K)	Ea (fwd)	Ar/Af	Af (s ⁻¹)	k (s ⁻¹)
300	74.02	2.30E-04	6.53E+16	7.70E-38
400	73.87	2.83E-04	5.29E+16	2.29E-24
500	73.66	3.59E-04	4.18E+16	2.64E-16
600	73.39	4.57E-04	3.29E+16	6.06E-11
800	72.77	7.17E-04	2.09E+16	2.75E-04
1000	72.06	1.07E-03	1.41E+16	2.50E+00
1200	71.31	1.50E-03	9.99E+15	1.03E+03
1500	70.15	2.32E-03	6.47E+15	3.88E+05
2000	68.17	4.11E-03	3.65E+15	1.29E+08

(2) $\text{CH}_3\text{CH}_2\text{SCH}_2\text{CH}_3 \Rightarrow \text{CH}_3\text{CH}_2\text{SC} \cdot\text{H}_2 + \text{CH}_3$

Ar = 2.63E+13 (High-Pressure Limit Rate Constant)				
T (K)	Ea (fwd)	Ar/Af	Af (s ⁻¹)	k (s ⁻¹)
300	83.36	4.27E-03	6.16E+15	1.14E-45
400	83.60	3.00E-03	8.76E+15	1.83E-30
500	83.76	2.53E-03	1.04E+16	2.53E-21
600	83.84	2.34E-03	1.12E+16	3.23E-15
800	83.84	2.33E-03	1.13E+16	1.40E-07
1000	83.69	2.53E-03	1.04E+16	5.30E-03
1200	83.43	2.85E-03	9.23E+15	5.88E+00
1500	82.87	3.51E-03	7.50E+15	6.31E+03
2000	81.54	5.15E-03	5.11E+15	6.27E+06

(3) $\text{CH}_3\text{CH}_2\text{SCH}_2\text{CH}_2\text{Cl} \Rightarrow \text{CH}_3\text{CH}_2\text{S} \cdot + \text{C} \cdot\text{H}_2\text{CH}_2\text{Cl}$

Ar = 9.12E+12 (High-Pressure Limit Rate Constant)				
T (K)	Ea (fwd)	Ar/Af	Af (s ⁻¹)	k (s ⁻¹)
300	75.61	6.64E-04	1.37E+16	1.13E-39
400	75.32	1.01E-03	9.05E+15	6.31E-26
500	74.98	1.48E-03	6.17E+15	1.03E-17
600	74.61	2.08E-03	4.38E+15	2.90E-12
800	73.81	3.70E-03	2.46E+15	1.68E-05
1000	73.00	5.83E-03	1.56E+15	1.73E-01
1200	72.20	8.43E-03	1.08E+15	7.65E+01
1500	70.99	1.33E-02	6.88E+14	3.12E+04
2000	68.97	2.38E-02	3.84E+14	1.11E+07

Table D.5 Thermodynamic and Kinetic Analysis vs. Temperature in Bond Cleavage Reactions (Continued)**(4) $\text{CH}_3\text{CH}_2\text{SCH}_2\text{CH}_2\text{Cl} \Rightarrow \text{CH}_3\text{CH}_2\text{SC.H}_2 + \text{C.H}_2\text{Cl}$**

Ar = 1.55E+13 (High-Pressure Limit Rate Constant)				
<i>T</i> (K)	Ea (fwd)	Ar/Af	Af (s ⁻¹)	<i>k</i> (s ⁻¹)
300	82.90	1.79E-03	8.66E+15	3.47E-45
400	82.77	2.14E-03	7.25E+15	4.30E-30
500	82.61	2.55E-03	6.07E+15	4.69E-21
600	82.43	3.01E-03	5.14E+15	4.83E-15
800	82.04	4.01E-03	3.87E+15	1.49E-07
1000	81.62	5.07E-03	3.06E+15	4.43E-03
1200	81.18	6.19E-03	2.50E+15	4.10E+00
1500	80.45	8.15E-03	1.90E+15	3.60E+03
2000	78.94	1.26E-02	1.23E+15	2.91E+06

(5) $\text{CH}_3\text{CH}_2\text{SCH}_2\text{CH}_2\text{Cl} \Rightarrow \text{CH}_3\text{CH}_2\text{SCH}_2\text{C.H}_2 + \text{Cl}$

Ar = 3.63E+13 (High-Pressure Limit Rate Constant)				
<i>T</i> (K)	Ea (fwd)	Ar/Af	Af (s ⁻¹)	<i>k</i> (s ⁻¹)
300	80.82	2.05E-03	1.77E+16	2.32E-43
400	80.73	2.33E-03	1.56E+16	1.20E-28
500	80.59	2.71E-03	1.34E+16	7.90E-20
600	80.42	3.17E-03	1.15E+16	5.80E-14
800	80.01	4.26E-03	8.53E+15	1.18E-06
1000	79.54	5.53E-03	6.57E+15	2.71E-02
1200	79.05	6.95E-03	5.22E+15	2.09E+01
1500	78.26	9.34E-03	3.89E+15	1.54E+04
2000	76.90	1.38E-02	2.62E+15	1.04E+07

(6) $\text{CH}_2\text{ClCH}_2\text{SCH}_2\text{CH}_2\text{Cl} \Rightarrow \text{CH}_2\text{ClCH}_2\text{S.} + \text{C.H}_2\text{CH}_2\text{Cl}$

Ar = 9.12E+12 (High-Pressure Limit Rate Constant)				
<i>T</i> (K)	Ea (fwd)	Ar/Af	Af (s ⁻¹)	<i>k</i> (s ⁻¹)
300	73.52	5.81E-04	1.57E+16	4.29E-38
400	73.05	1.14E-03	7.99E+15	9.70E-25
500	72.60	1.89E-03	4.83E+15	8.86E-17
600	72.18	2.79E-03	3.27E+15	1.66E-11
800	71.43	4.82E-03	1.89E+15	5.78E-05
1000	70.78	6.95E-03	1.31E+15	4.44E-01
1200	70.17	9.17E-03	9.94E+14	1.65E+02
1500	69.24	1.30E-02	7.00E+14	5.71E+04
2000	67.55	2.12E-02	4.30E+14	1.78E+07

APPENDIX E

PARTIAL INSTRUCTION SET FOR CHEMRATE

This appendix describes partial instruction set for ChemRate and manual and example output for the NJIT CHEMDIS code. This appendix is related to Chapter 2, Chapter 3 and Chapter 5.

E.1 ChemRate

ChemRate⁴⁶ is a program that contains a master equation solver so that rate constants for unimolecular reactions in the energy transfer region and chemical activation processes under steady and non-steady state conditions can be determined on the basis of Rice-Ramsperger-Kassel-Marcus (RRKM) theory. The ChemRate codes are written and a PC version is distributed by the Chemistry Division of NIST. The Reason for this partial instruction set on ChemRate is to assist other students in this research group who may wish to use it in comparisons of the NJIT programs, CHEMDIS and CHEMASTER. The ChemRate instruction set is not complete, and to our knowledge at this time the help manual for ChemRate is not complete or sufficient for easy use of ChemRate.

ChemRate has several characteristics.⁴⁷

- Calculates high-pressure rate constants of unimolecular reactions on the basis of transition state theory.
- Determines specific rate constants on the basis of RRKM theory.
- Treats multichannel reactions including chemical activation processes under equilibrium and non-equilibrium conditions. Calculates steady state rate constant as well as time-dependent rate constants.
- Computes thermofunctions (C_p , S , H , pK , etc.) at any temperature.
- Treats hindered rotors and tunneling.
- Fits computed results in various ways.
- Compares computed results with experimental data.

ChemRate supports data base of component and reaction and includes complete NIST Kinetic Data Base that contains more than 53000 experimental data for almost 14000 reactions and JANAF Tables.⁴⁸

ChemRate can also create data base of component and reaction when they are not available in the data base. Molecular weight, atomic composition, standard enthalpy of formation, frequencies, external and internal rotations, collision parameters, geometry data, experimental data, etc, are required for component and reaction.

E.1.1 Partial Manual for ChemRate

An outline for use of ChemRate in calculating rate constants and in calculating branching ratios in complex chemical activation and unimolecular dissociation reactions is briefly presented here because ChemRate instruction is not helpful. One must obtain a CD with ChemRate on it from NIST and start it on a pc computer. One can make a folder (ex. C:\Chemrate\)) in Microsoft Windows (ex. MS 98, MS XP) and install it in that folder.

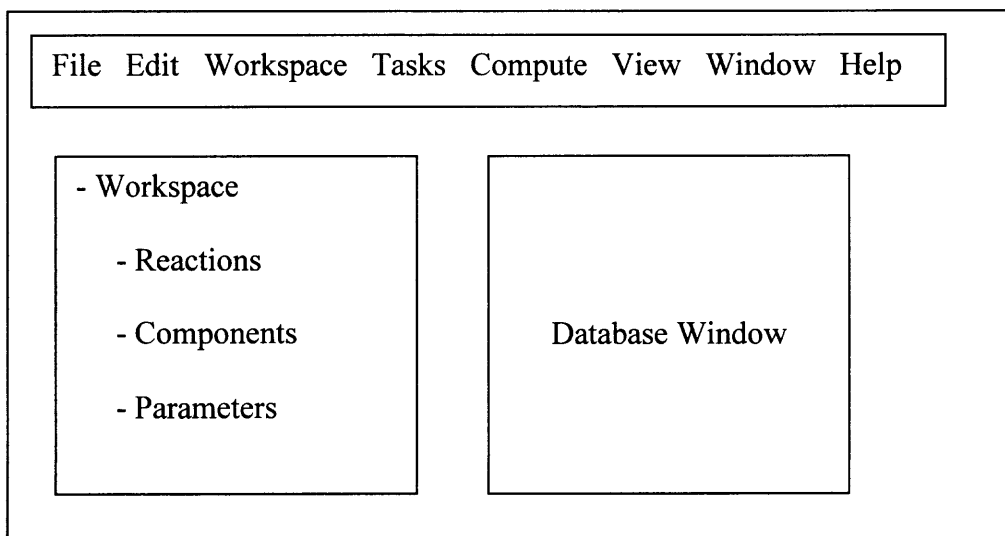
1. Unit options [Click on View and Preferences, see Scheme E.1]:
 - Energy (kcal, kJ, eV)
 - Temperature (K, C, F)
 - Pressure (atm, torr, Pa, bar)
 - Concentration (1/cm³, ol/cm³)
2. Physical condition setting [Click on Parameters, Tasks and Properties]:
 - Temperature, Pressure, Time (Note: time dependent only)

Note: If multiple calculations as functions of temperature and pressure, click on Parameters, Tasks and Add Tasks.
3. Specification of the collisional parameters [Click on Parameters, Collisions and Properties]:
 - Collision model: ex) Exponential-down, $\exp(-dE/\alpha)$
 - Expression for alpha: ex) $\alpha_0 + \alpha_1 \times T + \alpha_2 \times E$
 - Lennard-Jones parameters: ex) N₂, $\delta = 3.798 \text{ \AA}$, $\epsilon/k = 71.4 \text{ K}$
 - Argon is the default buffer gas. One can change it to another one. Then one must add parameters for new species.

4. Specification of reaction [Click on Workspace, Reactions and Add Reaction]:
 - Isomerization, Decomposition, Bimolecular reactions.
 - Choose reaction type and type in thermochemical and structure data for reactant, product, and transition state.

Note: No reaction can be used without transition state. Several components' properties are required for calculation, such as name, atomic composition, mass, enthalpy of formation, frequencies, and rotations. Moment of inertia and symmetry number are needed for rotations. Hindered rotation can be included with barrier and number of minima.
5. Initial mixture composition [Click on Components]:
 - Reactant and buffer gas: ex) $\text{CH}_3\text{C}(=\text{O})\text{OO}\bullet : \text{N}_2 = 1 : 99$
6. Check the Workspace:
 - Before calculating the density and sum of states based on input parameters, it is worth to check the Workspace.
 - The Workspace now contains a list of the reactions and components [reactant (active), product (inactive), transition state, and buffer gas].
7. Calculate the density and sum of states and master equation [Click on Compute and the density and sum of states and master equation].
8. Clicking the reaction of interest gives the results of the rate constants with conditions.

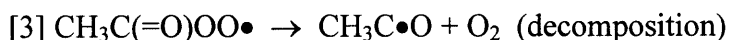
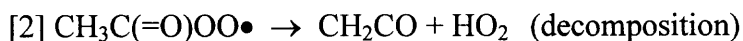
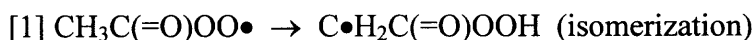
Scheme E.1 Diagram of window in ChemRate



E.1.2 Example for ChemRate

An example for ChemRate in calculating rate constants and branching ratios in unimolecular reactions of acetyl peroxy radical ($\text{CH}_3\text{C}(=\text{O})\text{OO}\bullet$) is presented. This acetyl peroxy radical ($\text{CH}_3\text{C}(=\text{O})\text{OO}\bullet$) unimolecular dissociations and comparison of dissociation rate constants between ChemRate and CHEMASTER are discussed in Chapter 3 (page 50).

Acetyl peroxy radical ($\text{CH}_3\text{C}(=\text{O})\text{OO}\bullet$) has three unimolecular reaction paths:



E.1.2.1 Input Example for ChemRate

1. Units: energy (kcal), temperature (K), pressure (atm), concentration ($1/\text{cm}^3$).
2. Operating condition: 800 K and 1 atm. Steady State.
3. Collision: bath gas (N_2), Exponential-down model: $\exp(-dE/\alpha)$, Expression for α : $\alpha_0 + \alpha_1 \times T + \alpha_2 \times E$, Lennard-Jones parameters: N_2 , $\delta = 3.798 \text{ \AA}$, $\epsilon/k = 71.4 \text{ K}$.
4. Reaction type: Isomerization,
 $\text{CH}_3\text{C}(=\text{O})\text{OO}\bullet \rightarrow \text{C}\bullet\text{H}_2\text{C}(=\text{O})\text{OOH}$,
 Transition State: $\text{TCC}(=\text{O})\text{OO}\bullet$.
5. Thermochemical Data for Reactant ($\text{CH}_3\text{C}(=\text{O})\text{OO}\bullet$), Product ($\text{C}\bullet\text{H}_2\text{C}(=\text{O})\text{OOH}$), and Transition State ($\text{TCC}(=\text{O})\text{OO}\bullet$).

For example, Reactant ($\text{CH}_3\text{C}(=\text{O})\text{OO}\bullet$),

1) Name: $\text{CH}_3\text{C}(=\text{O})\text{OO}\bullet$

2) Atomic composition: C2 O3 H3 .

3) Mass: 75.044 a.m.u.

4) Enthalpy of formation: -38.57 kcal/mol

5) Frequencies: 362.2 559.5 615.9 640.0 860.7 1115.0 1164.2 1283.6 1330.5 1546.2 1598.7 1611.9 2098.5 3229.0 3305.3 3341.2 (cm^{-1}) [Note: frequencies can be imported as a text file]

- Sample data format for frequency

...

```
<frequencies>
  580      1383(2)  3184(2)  3002      345(2)
  643(2)   950(2)   1000      1430      2050
  2990(2)  3380
</frequencies>
```

...

6) Rotations: X 53.46 (moment of inertia (M.I.), amu-Å²), Y 100.53, Z 150.89.

Hindered Rotations:

C--C(=O)OO 3.05 [reduced M.I.; $3.12 \times 126.74 / (3.12 + 126.74)$], 4 kcal (Rotational Barrier Height), 3 (number of minima).

CC(=O)--OO 15.26 [reduced M.I.; $44.19 \times 23.30 / (44.19 + 23.30)$], 7 kcal (Rotational Barrier Height), 1 (number of minima).

E.1.2.2 Output Example for ChemRate

CH₃C(=O)OO• → C•H₂C(=O)OOH at 800 K and 1 atm,

1) Isomerization rate: 85613.3 1/s

2) Branching ratio: 0.723721

3) High pressure rate: 141029 1/s

4) Low pressure rate: 5.38144E-013 cm³/s

5) High pressure rate expression: $k = 5.15245E+012 \exp(-27.6832/RT)$ (1/s)

E.2 Manual and Example Output for the NJIT CHEMDIS Code

The ChemRate program does not give specific output on energy dependent rate constant [k (E)], collision efficiency [β (T)] and other specific parameters needed for the calculation of rate constants in chemical activation reactions and in dissociation reactions where there is pressure dependence. It is need to revert to the NJIT CHEMDIS code for some of this specific data.

Multifrequency quantum Rice-Ramsperger-Kassel (QRRK) analysis with the modified strong collision (CHEMDIS) for the collision efficiency [β (T)] in chemical activation is presented. The energy dependent rate constant [k (E)] is described in Chapter 2 (page 16).

E.2.1 Manual for CHEMDIS

1. General rules:

- First line is file header; this will be put on all output files.
- Leading blanks on all lines are ignored.
- Program uses command keywords; these can appear in any order except when indicated; most keywords require additional information that must follow on subsequent lines.
- Any line at the keyword level whose first non-blank character is a '#' is considered a comment and ignored.
- Blank lines at the keyword level are ignored.

2. Program control options (these are all optional, though some combinations may give no program output; specify as many as desired):

- CHEM (chemact): do chemical activation calculation
- DISS (dissoc): do dissociation calculations
- NOTAB (NoTable): suppress output of rate table file
- RKO (rkold): use original CHEMACT method for stabilization rate
- FITR (fitRange): perform arrhenius fits on all temperature ranges
- SHOW (showShape): show F shape parameters (only invoke with full P range)
- FITG (fitGlobal): calculate Lindeman F functions and (Cray only) fit; uses default fitting form unless TROE and SRI specified.
- TROE: use Troe form for fitting F functions
- SRI: use SRI form for fitting F functions
- INT: integration interval, followed next line by dE (kcal, default=1)
- ROT: include 1-D active rotation in calculations (note: this slows down computation, esp. multi-frequency case)

3. Temperature, pressure specification (these allow override of default):

- TEMP: temperature range; next line contains:
n, t1, t2, ... tn (K)
n should be no more than 20
- PRES: pressure range; next line contains:
m, p1, p2, ... pm (atm)
m should be no more than 40
- CORR: correlated t,p option; next line contains:
n,m

$t(1), p(1,j), j=1,m$
 $t(i), p(i,j), j=1,m$
 $t(n), p(n,j), j=1,m$
 if not specified, program defaults to:
 $T(1..13):300,400,500,600,800,1200,1500,2000,2500,3200,4000,4800$
 $P(1..61): 1E-10, 2E-10, 5E-10, \dots 1E9, 2E9, 5E9, 1D10$
 These are pretty good for fitting F functions

4. Necessary input parameters (specify once only):

- INPUT: overall rate constant into system; next line contains:
 A (cm mol units), n , E (kcal)
 (note: this is forward channel corresponding to REAC specifier)
- MASS: (common) mass for all isomers; next line contains:
 $Mass$ (amu)

5. Specification of collider information (do for each collider):

- COLL (collider); followed by:
 $name$
 (a) mole fraction (or b)
 (b) mole fraction, mass (amu), σ (A), e/k (K), ΔE (cal)
 [if name is preceded by ! program expects (b); else it looks up additional parameters in its data base]
- BETA (optional): do constant beta calculation; next line contains: beta
- Current collider data base:
 $data\ species\ (1)\ /'N2'/$
 $data\ smass\ (1),\ s\ sig\ (1),\ sek\ (1),\ s\ deltaE\ (1)\ / 28.0, 3.621, 97.5, 830.0/$
 $data\ species\ (2)\ /'AR'/$
 $data\ smass\ (2),\ s\ sig\ (2),\ sek\ (2),\ s\ deltaE\ (2)\ / 40.0, 3.33, 136.5, 630.0/$
 $data\ species\ (3)\ /'HE'/$
 $data\ smass\ (3),\ s\ sig\ (3),\ sek\ (3),\ s\ deltaE\ (3)\ / 4.0, 2.6, 10.2, 431.0/$
 $data\ species\ (4)\ /'CH4'/$
 $data\ smass\ (4),\ s\ sig\ (4),\ sek\ (4),\ s\ deltaE\ (4)\ / 16.0, 3.746, 141.4, 2100.0/$
 $data\ species\ (5)\ /'C3H8'/$
 $data\ smass\ (5),\ s\ sig\ (5),\ sek\ (5),\ s\ deltaE\ (5)\ / 44.0, 4.98, 266.8, 4200.0/$
 $data\ species\ (6)\ /'SF6'/$
 $data\ smass\ (6),\ s\ sig\ (6),\ sek\ (6),\ s\ deltaE\ (6)\ / 146.0, 5.13, 222.1, 3400.0/$

NOTE: if no colliders are specified, N2 parameters will be used with a constant beta of 0.2; species name will be 'default'

6. Specification of default well parameters (these are used if not specified in WELL section)

- FREQ (frequency calculation parameters); next line:
 $\#DistinctFreqs, freq1\ (cm^{-1}),\ degen1, \dots freqN\ (cm^{-1}),\ degenN$ [note degen's are assumed reals]

- PARAM: use these collision parameters as default; next line:
Sigma (A), e/k (K)

7. Specification of well info (repeat for each well in system)

- WELL: this starts well loop; next line contains:
Isomer name corresponding to this well

Well loop continues until keyword END encountered

Additional keywords allow reaction channel specification and default overrides, in any order:

Default overrides:

- FREQ (for this well, use:)
#distinctfreqs, freq1 (cm⁻¹), degen1, ... freqN (cm⁻¹), degenN
- PARAM (for this well, use:)
Sigma (A), e/k (K)
Channel specifiers; as follows (Note: n is real):
- REAC
Reactant channel label (e.g. H + O₂)
A (cm mol units), n, E (kcal)
- ISOM
Isomer name of isomerization product
A (cgs), n, E (kcal)
- PROD
Product channel label
A (cgs), n, E (kcal)

ISOM and PROD should be specified for each channel linked to this well

Note: CHEMACT calculation will try to match all isomer product names to fill out array; hence isomer name must be consistent.

REAC channel is that from well back to initial reactants, this is reverse of that specified by INPUT; REAC should be specified only once for whole system. Rate is that out of well; reverse of INPIT

- END terminates well loop
(alternatively, well loop terminates if keyword not recognized, and command is passed to upper level)

8. Main keyword loop terminated by end of file or by keyword COMM (comment); all subsequent lines are ignored

9. New: TAG followed on next line by up to 10 character string (excluding leading blanks): will be added in front of all labels on spreadsheet output file – however, keep it short as legend is truncated at length of 20.

E.2.2 Collision efficiency in CHEMDIS

The collision efficiency (β_c) was evaluated from Troe's expression¹⁹⁷:

$$\frac{\beta_c}{1 - \sqrt{\beta_c}} \cong \frac{-\langle \Delta E_c \rangle}{F_E kT} \quad (1)$$

where $\langle \Delta E_c \rangle$ is the average energy transferred in all collisions and F_E is a temperature-dependent integral involving the density of states $Q_{vib}(E)$ and is expressed;

$$F_E(T) = \frac{\int_{E_0}^{\infty} Q_{vib}(E) \exp(-E/kT) dE}{kT Q_{vib}(E_0) \exp(-E_0/kT)} \quad (2)$$

Troe uses the Whitten-Rabinovitch approximation to calculate the density of states,

$$Q_{vib}(E) = \frac{[E_0 + a(E_0)E_z]^{s-1}}{(s-1)! \prod_{i=1}^s (hv_i)} \quad (3)$$

where s represents the number of vibrational modes, E_z is the zero point energy of the oscillator, E_0 is the barrier height and $a(E)$ is defined through the following:

$$a(E) = 1 - \beta_v w \quad (4)$$

$$\log w = -1.0506 (E/E_z)^{0.25} \quad (E > E_z)$$

$$w^{-1} = 5(E/E_z) + 2.73(E/E_z)^{0.5} + 3.51 \quad (E < E_z)$$

$$\beta_v = (s-1) \frac{\sum_{i=1}^s v_i^2}{(\sum_{i=1}^s v_i)^2}$$

Substituting Eq. (3) into (2) and approximating $a(E)$ by $a(E_0)$, Troe obtains an expression for F_E ,

$$F_E(T) = \sum_{i=0}^{s-1} \frac{(s-1)!}{(s-1-i)!} \left[\frac{kT}{E_0 + a(E_0)E_z} \right]^i \quad (5)$$

Chang et al.³¹ indicate that F_E is close to unity at low temperatures but exhibits an exponential-like dependence on temperature at high temperatures. For larger molecules the departure of F_E from unity starts at lower temperatures as more degrees of freedom are available. Eq. (1) suggests that β_c diminishes as F_E^{-1} in the limit that F_E becomes large. However Gilbert et al.³⁶ show that β_c levels off and even begins to turn around at high F_E . They recommend a higher order approximation for β_c for use with large molecules.

Following Gilbert et al., Chang et al. replace Eq. (1) with

$$\beta_c = \left(\frac{\alpha_c}{\alpha_c + F_E kT} \right)^2 \frac{1}{\Delta} \quad (6)$$

where α_c represents the average energy of down-collisions and is related to $\langle \Delta E_c \rangle$ though,

$$\langle \Delta E_c \rangle = \gamma_c - \alpha_c \quad (7)$$

$$\gamma_c = \frac{\alpha_c F_E kT}{\alpha_c + F_E kT} \quad (8)$$

where γ_c represents the average energy of up-collisions. Although not immediately obvious, Eqs. (6) – (8) are equivalent to Eq. (1) if Δ is set to unity.

The factor Δ in Eq. (6) can be decomposed into two terms,

$$\Delta = \Delta_1 - \left[\frac{F_E kT}{\alpha_c + F_E kT} \right] \Delta_2 \quad (9)$$

where Δ_1 and Δ_2 are temperature-dependent integrals involving the density of states,

$$\Delta_1 = \frac{\int_0^{E_0} Q_{vib}(E) \exp(-E/kT) dE}{\Delta_N} \quad (10)$$

$$\Delta_2 = \frac{\int_0^{E_0} Q_{vib}(E) \exp(-E/kT) \exp[-(E_0 - E)/F_E kT] dE}{\Delta_N} \quad (11)$$

$$\Delta_N = \int_0^{\infty} Q_{vib}(E) \exp(-E/kT) dE \quad (12)$$

Plots of collision efficiency versus temperature for $\text{C}\bullet\text{H}_2\text{CHO}$ and $\text{CH}_3\text{C(=O)OO}\bullet$ stabilization in $\text{CH}_2\text{CO} + \text{H}$ and $\text{CH}_3\text{C}\bullet\text{O} + \text{O}_2$ reaction system are illustrated in Figure E.1 and E.2, respectively. For the calculation of collision efficiency ($F_E = \text{constant}$) Eq. (1) is used, where $F_E = 1.15$ (ref. 198). [Note: RKO command is used for the calculation of collision efficiency ($F_E = \text{constant}$) in a current CHEMDIS input.] However, Eqs. (5) and (6) for F_E and β_c are used for the calculation of collision efficiency [$F_E(T)$].

< Collision Parameters >

1) Bath gas: N_2 , $\delta = 3.621 \text{ \AA}$, $\epsilon/k = 97.5 \text{ K}$, $\langle \Delta E \rangle_{\text{avg}} = 830 \text{ cal/mol}$

2) $\text{C}\bullet\text{H}_2\text{CHO}$: $\delta = 4.34 \text{ \AA}$, $\epsilon/k = 422.61 \text{ K}$

VIBRATION #1: MODES = 3.895 FREQUENCY = 577.3 cm^{-1}

VIBRATION #2: MODES = 5.141 FREQUENCY = 1246.7 cm^{-1}

VIBRATION #3: MODES = 2.964 FREQUENCY = 2979.4 cm^{-1}

GEO MEAN VIBRATION: MODES = 12.000 FREQUENCY = 1204.2 cm^{-1}

3) $\text{CH}_3\text{C(=O)OO}\bullet$: $\delta = 5.19 \text{ \AA}$, $\epsilon/k = 533.08 \text{ K}$

VIBRATION #1: MODES = 6.059 FREQUENCY = 361.7 cm^{-1}

VIBRATION #2: MODES = 8.297 FREQUENCY = 1143.8 cm^{-1}

VIBRATION #3: MODES = 2.645 FREQUENCY = 2566.9 cm^{-1}

GEO MEAN VIBRATION: MODES = 17.000 FREQUENCY = 860.5 cm^{-1}

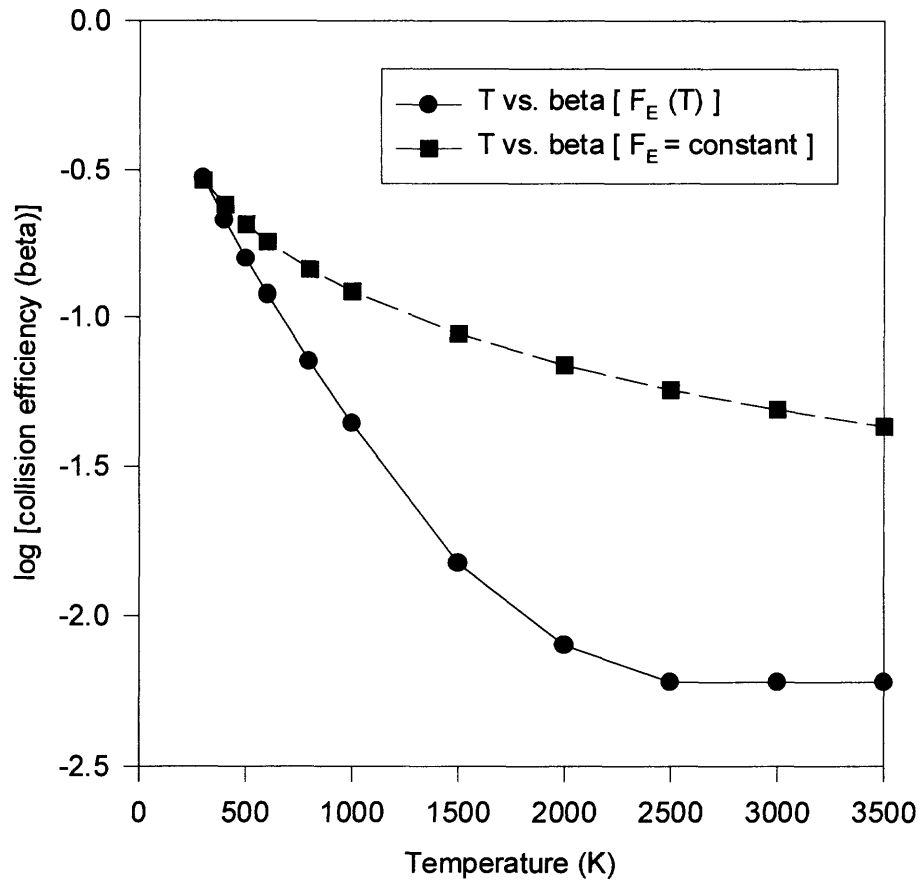


Figure E.1 Collision efficiency vs. temperature for $\text{C}\cdot\text{H}_2\text{CHO}$ stabilization in $\text{CH}_2\text{CO} + \text{H}$ reaction system.

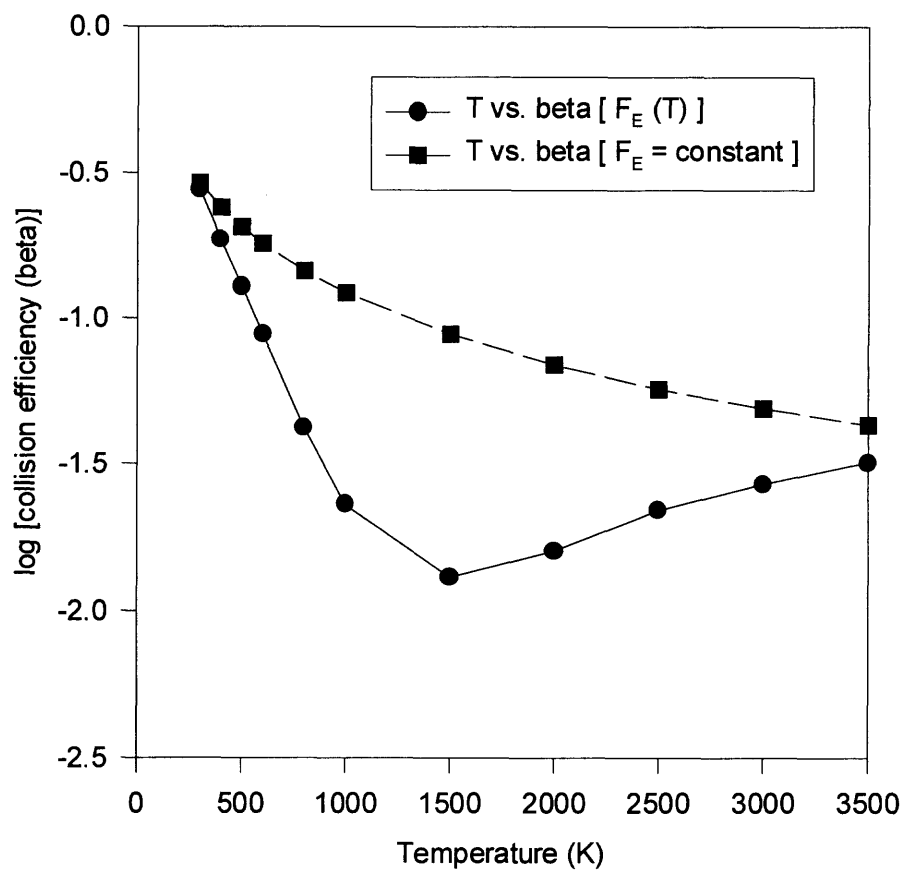


Figure E.2 Collision efficiency vs. temperature for $\text{CH}_3\text{C}(=\text{O})\text{OO}\bullet$ stabilization in $\text{CH}_3\text{C}\bullet\text{O} + \text{O}_2$ reaction system.

REFERENCES

- (1) Benson, S. W. *Thermochemical Kinetics*; John Wiley and Sons: New York, 1976.
- (2) Slagle, I. R.; Ratajczak, E.; Gutman, D. J. *J. Phys. Chem.* **1986**, *90*, 402.
- (3) Lightfoot, P. D.; Cox, R. A.; Crowley, J. N.; Destriau, M.; Hayman, G. D.; Jenkin, M. E.; Moortgat, G. K.; Zabel, F. *Atmos. Environ.* **1992**, *26A*, 1805.
- (4) Atkinson, R. *Atmos. Environ.* **1990**, *24A*, 1.
- (5) Slagle, I. R.; Feng, Q.; Gutman, D. *J. Phys. Chem.* **1984**, *88*, 3648.
- (6) McDade, C. E.; Lenhardt, T. M.; Bayes, K. D. *J. Photochem.* **1982**, *20*, 1.
- (7) Atkinson, R.; Baulch, D. L.; Cox, R. A.; Hampson, R. F.; Kerr, J. A.; Rossi, M. J.; Troe, J. *J. Chem. Phys. Ref. Data* **1997**, *26*, 521.
- (8) Maricq, M. M.; Szente, J. J. *J. Chem. Phys. Lett.* **1996**, *253*, 333.
- (9) Tyndall, G. S.; Staffelbach, T. A.; Orlando, J. J.; Calvert, J. G. *Int. J. Chem. Kinet.* **1995**, *27*, 1009.
- (10) Sehested, I.; Christensen, L. K.; Nielsen, O. J.; Wallington, T. J. *Int. J. Chem. Kinet.* **1998**, *30*, 913.
- (11) Atkinson, R.; Baulch, D. L.; Cox, R. A.; Hampson, R. F., Jr.; Kerr, J. A.; Troe, J. *J. Phys. Chem. Ref. Data* **1989**, *18*, 881.
- (12) Bartels, M.; Hoyermann, K. *An. Asoc. Quim. Argent.* **1985**, *73*, 253.
- (13) Michael, J. V.; Keil, D. G.; Klemm, R. B. *J. Chem. Phys.* **1985**, *83*, 1630.
- (14) Slagle, I. R.; Gutman, D. *J. Am. Chem. Soc.* **1982**, *104*, 4741.
- (15) Alvarez-Idaboy, J. R.; Mora-Diez, N.; Boyd, R. J.; Vivier-Bunge, A. *J. Am. Chem. Soc.* **2001**, *123*, 2018.
- (16) Aloisio, S.; Francisco, J. S. *J. Phys. Chem. A* **2000**, *104*, 3211.
- (17) Zhu, L.; Johnston, G. *J. Phys. Chem.* **1995**, *99*, 15114.
- (18) Bozzelli, J. W.; Dean, A. M. *J. Phys. Chem.* **1993**, *97*, 4427.

- (19) Foresman, J. B.; Frisch, A. *Exploring Chemistry with Electronic Structure Methods*, 2nd ed.; Gaussian Inc.: Pittsburgh, PA, 1996.
- (20) Becke, A. D. *Phys. Rev. A* **1988**, *38*, 3098.
- (21) Lindemann, F. A. *Trans. Faraday Soc.* **1922**, *17*, 598.
- (22) Steinfeld, J. I.; Francisco, J. S.; Hase, W. L. *Chemical Kinetics and Dynamics*; Prentice Hall: NJ, 1989.
- (23) Robinson, P. J.; Holbrook, K. A. *Unimolecular Reactions*; John Wiley and Sons: New York, 1971.
- (24) Hinshelwood, C. N. *Proc. Roy. Soc. A* **1927**, *113*, 230.
- (25) Slater, N. B. *Proc. Comb. Phil. Soc.* **1939**, *56*, 35.
- (26) Rice, O. K.; Ramsperger, H. C. *J. Am. Chem. Soc.* **1927**, *49*, 1617.
- (27) Kassel, L. S. *J. Phys. Chem.* **1928**, *32*, 225.
- (28) Kassel, L. S. *J. Phys. Chem.* **1928**, *32*, 1065.
- (29) Kassel, L. S. *Kinetics of Homogenous Gas Reaction*; Chemical Catalog Co.: New York, 1932.
- (30) Lee, J.; Chen, C.; Bozzelli, J. W. *J. Phys. Chem. A*, **2002**, *106*, 7155.
- (31) Chang, A. Y.; Bozzelli, J. W.; Dean, A. M. *Int. J. Res. Phys. Chem. Chem. Phys. (Zeit. Phys. Chem)* **2000**, *214*, 1533.
- (32) Dean, A. M. *J. Phys. Chem.* **1985**, *89*, 4600.
- (33) Dean, A. M.; Ritter, E. R.; Bozzelli, J. W. *Combust. Sci. Technol.* **1991**, *80*, 63.
- (34) Gilbert, R. G.; Smith, S. C. *Theory of Unimolecular and Recombination Reactions*; Oxford Press: New York, 1990.
- (35) Gilbert, R. G.; Smith, S. C.; Jordan, M. J. T. *UNIMOL Program Suite (Calculation of Fall-off Curve for Unimolecular and Recombination Reactions)*, Sidney, 1993.
- (36) Gilbert, R. G.; Luther, K.; Troe, J. *Ber. Bunsen-Ges. Phys. Chem.* **1983**, *87*, 169.
- (37) Ritter, E. R. *J. Chem. Info. Comp. Sci.* **1991**, *31*, 400.

- (38) Bozzelli, J. W.; Chang, A. Y.; Dean, A. M. *Int. J. Chem. Kinet.* **1997**, *29*, 161.
- (39) Hirschfelder, J. O.; Curtiss, C. F.; Bird, R. B. *Molecular Theory of Gases and Liquids*; Wiley: London, 1963.
- (40) Reid, R. C.; Prausnitz, J. M.; Polling, B. E. *Properties of Gases and Liquids*; McGraw-Hill: New York, 1989.
- (41) Sheng, C. Y.; Bozzelli, J. W.; Dean, A. M.; Chang, A. Y. *J. Phys. Chem. A* **2002**, *106*, 7276.
- (42) Troe, J. *In Combustion Chemistry*; Gardiner, W. C., Jr., Ed.; Springer-Verlag: New York, 1984.
- (43) Heymann, M.; Hippler, H.; Troe, J. *J. Chem. Phys.* **1984**, *80*, 1853.
- (44) Hann, D. K.; Klippenstein, S. J.; Miller, J. A. *Faraday Discuss.* **2001**, *119*, 79.
- (45) Knyazev, V. D.; Slagle, I. R. *J. Phys. Chem.* **1996**, *100*, 5318.
- (46) Mokrushin, V.; Bedanov, V.; Tsang, W.; Zachariah, M.; Knyazev, V. *ChemRate Computer Program*, Version 1.10; NIST: Gaithersburg, MD, 1999.
- (47) Mokrushin, V.; Tsang, W. <http://www.nist.gov/kinetics/chemrate/chemrate.html> December, 2001.
- (48) Chase, M. W. Jr. *NIST-JANAF Thermochemical Tables*, 4th ed., *J. Phys. Chem. Ref. Data* **1998**, Monograph 9, 1-1951.
- (49) Clifford, E. P.; Farrell, J. T.; DeSain, J. D.; Taatjes, C. A. *J. Phys. Chem. A* **2000**, *104*, 11549.
- (50) Tyndall, G. S.; Orlando, J. J.; Wallington, T. J.; Hurley, M. D. *Int. J. Chem. Kinet.* **1997**, *29*, 655.
- (51) McAdam, G. K.; Walker, R. W. *J. Chem. Soc., Faraday Trans. 2* **1987**, *83*, 1509.
- (52) Plumb, I. C.; Ryan, K. R. *Int. J. Chem. Kinet.* **1981**, *13*, 1011.
- (53) Kaiser, E. W.; Rimai, L.; Wallington, T. J. *J. Phys. Chem.* **1989**, *93*, 4094.
- (54) Kaiser, E. W.; Rimai, L.; Wallington, T. J. *J. Phys. Chem.* **1990**, *94*, 3394.
- (55) Gutman, D. *J. Chem. Phys.* **1987**, *84*, 409.
- (56) Gulati, S. K.; Walker, R. W. *J. Chem. Soc., Faraday Trans. 2* **1988**, *84*, 401.

- (57) Rienstra-Kiracofe, J. C.; Allen, W. D.; Schaefer, H. F., III. *J. Phys. Chem. A* **2000**, *104*, 9840.
- (58) Bozzelli, J. W.; Dean, A. M. *J. Phys. Chem.* **1990**, *94*, 3313.
- (59) Wagner, A. F.; Slagle, I. R.; Sarzynski, D.; Gutman, D. *J. Phys. Chem.* **1990**, *94*, 1853.
- (60) Baldwin, R. W.; Dean, C. E.; Walker, R. W. *J. Chem. Soc., Faraday Trans. 2* **1986**, *82*, 1445.
- (61) Chen, C.; Bozzelli, J. W. *J. Phys. Chem. A* **2000**, *104*, 4997.
- (62) McMillan, G. R.; Calvert, J. G. *Oxid. and Combust. Rev.* **1965**, 83.
- (63) Stewart, J. J. P., *MOPAC 6.0*, Frank J. Seiler Research Lab., US Air Force Academy: Colorado, 1990.
- (64) Frisch, M. J.; Trucks, G. W.; Head-Gordon, M.; Gill, P. M. W.; Wong, M. W.; Foresman, J. B.; Johnson, B. G.; Schlegel, H. B.; Robb, M. A.; Peplogle, E. S.; Gromperts, R.; Andres, J. L.; Raghavachari, K.; Binkley, J. S.; Gonzalez, C.; Martin, R. L.; Fox, D. J.; Defrees, D. J.; Baker, J.; Stewart, J. J. P.; Pople, J. A.; *Gaussian 94*, revision C.2; Gaussian Inc.: Pittsburgh, PA, 1995.
- (65) Petersson, G. A.; Bennett, A.; Tensfeldt, T. G.; Al-Laham, M. A.; Shirley, W. A.; Mantzaris, J. *J. Chem. Phys.* **1988**, *89*, 2193.
- (66) Petersson, G. A.; Tensfeldt, T. G.; Montgomery, J. A., Jr. *J. Chem. Phys.* **1991**, *94*, 6091.
- (67) Ochterski, J. W.; Petersson, G. A.; Montgomery, J. A., Jr. *J. Chem. Phys.* **1996**, *104*, 2598.
- (68) Nyden, M. R.; Petersson, G. A. *J. Chem. Phys.* **1991**, *75*, 1843.
- (69) Petersson, G. A. *J. Chem. Phys.* **1994**, *94*, 6081.
- (70) Montgomery, J. A., Jr.; Petersson, G. A. *J. Phys. Chem.* **1994**, *101*, 5900.
- (71) Hehre, W. J.; Radom, L.; Schleyer, P. R.; Pople, J. A. *Ab-Initio Molecular Orbital Theory*; John Wiley & Sons: New York, NY, 1986.
- (72) Pitzer, K. S.; Gwinn, W. D. *J. Chem. Phys.* **1942**, *10*, 428.

- (73) Bozzelli, J. W.; Chang, A. Y.; Dean, A. M. *Int. J. Chem. Kinet.* **1997**, *29*, 161.
- (74) Petersson, G. A. (Hall-Atwater Laboratories of Chemistry, Wesleyan University, Middletown, Connecticut 06459); Schwartz, M. (Department of Chemistry, University of North Texas, Denton, Texas 76203) Personal Communication.
- (75) Eckart, C. *Phys. Rev.* **1930**, *35*, 1203.
- (76) Schwartz, M.; Marshall, P.; Berry, R. J.; Ehlers, C. J.; Petersson, G. A. *J. Phys. Chem. A* **1998**, *102*, 10074
- (77) Rodgers, A. S. *Selected Values for Properties of Chemical Compounds*; Thermodynamic Research Center, Texas A&M University: College Station, TX, 1982.
- (78) Pedley, J. B.; Naylor, R. O.; Kirby, S. P. *Thermodynamic Data of Organic Compounds*, 2nd ed.; Chapman and Hall, London, 1986.
- (79) Stull, D. R.; Prophet, H. *JANAF Thermochemical Tables*, 2nd ed. (NSRDS-NBS37); U.S. Government Printing Office; Washington DC, 1970.
- (80) Stull, D. R.; Westrum, E. F., Jr.; Sinke, G. C. *The Chemical Thermodynamics of Organic Compounds*; Robert E. Krieger Publishing: Malabar, FL, 1987.
- (81) Marshall, P. *J. Phys. Chem. A* **1999**, *103*, 4560.
- (82) Mayer, P. M.; Glukhovtsev, M. N.; Gault, J. W.; Radom, L. *J. Am. Chem. Soc.* **1997**, *119*, 12889.
- (83) Zhu, L.; Bozzelli, J. W. *J. Phys. Chem. A* **2002**, *106*, 345.
- (84) Lay, T. H.; Bozzelli, J. W. *J. Phys. Chem. A* **1997**, *101*, 9505.
- (85) Ritter, E. R.; Bozzelli, J. W. *Int. J. Chem. Kinet.* **1991**, *23*, 767.
- (86) Knyazev, V. D.; Slagle, I. R. *J. Phys. Chem. A* **1998**, *102*, 1770.
- (87) Miller, J. A.; Klippenstein, S. J.; Robertson, S. H. *28th Symposium (Int.) on Combustion*; The Combustion Institute: Edinburgh, U.K., **2000**, 1479.
- (88) Blanksby, S. J.; Ramond, T. M.; Davico, G. E.; Nimlos, M. R.; Kato, S.; Bierbaum, V. M.; Carl Lineberger, W.; Ellison, G. B.; Okumura, M. *J. Am. Chem. Soc.* **2001**, *123*, 9585.

- (89) Reid, R. C.; Prausnitz, J. M.; Sherwood, T. K. *The Properties of Gases and Liquids*; McGraw-Hill Co.: New York, 1979.
- (90) Chen, C.; Bozzelli, J. W. *J. Phys. Chem. A* **1999**, *103*, 9731.
- (91) Kee, R. J.; Rupley, F. M.; Miller, J. A. Chemkin-II: A Fortran Chemical Kinetics Package for the Analysis of Gas Phase Chemical Kinetics; Sandia National Laboratories: CA, 1989.
- (92) Dean, A. M.; Bozzelli, J. W. In *Gas-Phase Combustion Chemistry, Chapter 2: Combustion Chemistry of Nitrogen*; Gardiner, W. C., Jr., Ed.; Springer-Verlag: New York, 1999 (ISBN 0-387-98861-0).
- (93) Baulch, D. L.; Cobos, C. J.; Cox, R. A.; Esser, C.; Frank, P.; Just, Th.; Kerr, J. A.; Pilling, M. J.; Troe, J.; Walker, R. W.; Warnatz, J. *J. Phys. Chem. Ref. Data* **1992**, *21*, 411.
- (94) DeMore, W. B.; Sander, S. P.; Golden, D. M.; Hampson, R. F.; Kurylo, M. J.; Howard, C. J.; Ravishankara, A. R.; Kolb, C. E.; Molina, M. J. *JPL Publication* **1997**, *4*, 1.
- (95) Warnatz, J. In *Combustion Chemistry*, Gardiner, W. C., Jr., Ed.; Springer-Verlag: New York, 1984.
- (96) Taylor, P. H.; Rahman, M. S.; Arif, M.; Dellinger, B.; Marshall, P. *26th Symposium (Int.) on Combustion*; The Combustion Institute: Pittsburgh, PA, **1996**, 497.
- (97) Maricq, M. M.; Szenté, J. J. *J. Phys. Chem.* **1996**, *100*, 12380.
- (98) Tsang, W.; Hampson, R. F. *J. Phys. Chem. Ref. Data* **1986**, *15*, 1087.
- (99) Ernst, J.; Spindler, K.; Wagner, H. Gg. *Ber. Bunsen-Ges. Phys. Chem.* **1976**, *80*, 645.
- (100) Mebel, A. M.; Diau, E. W. G.; Lin, M. C.; Morokuma, K. *J. Am. Chem. Soc.* **1996**, *118*, 9759.
- (101) Bozzelli, J. W.; Sheng, C. *J. Phys. Chem. A* **2002**, *106*, 1113.
- (102) Sebbar, N.; Bockhorn, H.; Bozzelli, J. W. *Phys. Chem. Chem. Phys.* **2002**, *4*, 3691
- (103) Olzmann, M.; Kraka, E.; Cremer, R.; Gutbrod, R.; Andersson, S. *J. Phys. Chem. A* **1997**, *101*, 9421.

- (104) Tuazon, E. C.; Aschmann, S. M.; Arey, J.; Atkinson, R. *Environ. Sci. Technol.* **1997**, *31*, 3004.
- (105) Atkinson, R.; Aschmann, S. M. *Environ. Sci. Technol.* **1993**, *27*, 1357.
- (106) Sun, H.; Bozzelli, J. W. *J. Phys. Chem. A* **2001**, *105*, 9543.
- (107) Sun, H.; Bozzelli, J. W. *J. Phys. Chem. A* **2003**, *107*, 1018.
- (108) Lee, J.; Bozzelli, J. W. *Int. J. Chem. Kint.* **2003**, *35*, 20.
- (109) Tsang, W. *Heats of Formation of Organics Free Radicals by Kinetic Methods in Energetics of Organic Free Radicals*; Martinho Simoes, J. A.; Greenberg, A.; Liebman, J. F., Eds., Blackie Academic Professional: London, 1996.
- (110) Melius, C. <http://z.ca.sandia.gov/~melius/> Unpublished data, January, 2003.
- (111) Petersson, G. A.; Al-Laham, M. A. *J. Phys. Chem.* **1991**, *94*, 6081.
- (112) Ochtowski, J. W.; Petersson, G. A.; Wiberg, K. *J. Am. Chem. Soc.* **1995**, *117*, 11299.
- (113) Chen, C.; Bozzelli, J. W. *J. Phys. Chem. A* **2000**, *104*, 9715.
- (114) Sun, H.; Bozzelli, J. W. *J. Phys. Chem. A* **2001**, *105*, 4504.
- (115) Ervin, K. M.; Deturi, V. F. *J. Phys. Chem. A* **2002**, *106*, 9947.
- (116) Kang, J. K.; Musgrave, C. B. *J. Chem. Phys.* **2001**, *115*, 11040.
- (117) Zhang, Y. K.; Yang, W. T. *J. Chem. Phys.* **1998**, *109*, 2604.
- (118) Johnson, B. G.; Gonzales, C. A.; Gill, P. M. W.; Pople, J. A. *Chem. Phys. Lett.* **1994**, *221*, 100.
- (119) Jursic, B. S. *Chem. Phys. Lett.* **1996**, *256*, 603.
- (120) Carl, S. A.; Sun, Q.; Vereecken, L.; Sumathy, R.; Peeters, J. *Joint Meeting of the Belgian and Deutch Sections of the Combustion Institute*; The Royal Military Academy: Brussels, Belgium, **2002**, 37.
- (121) Vereecken, L.; Sumathy, R.; Carl, S. A.; Peeters, J. *Chem Phys. Lett.* **2001**, *344*, 400.
- (122) Blauwens, J.; Smets, B.; Peeters, J. *16th Symposium (Int.) on Combustion*; The Combustion Institute: Pittsburgh, PA, **1976**, 1055.

- (123) Peeters, J.; Devriendt, K. *26th Symposium (Int.) on Combustion*; The Combustion Institute: Pittsburgh, PA, **1996**, 1001.
- (124) McEnally, C. S.; Pfefferle, L. D. *Combustion and Flame* **2000**, *121*, 575.
- (125) Eickhoff, U.; Temps, R. *Phys. Chem. Chem. Phys.* **1999**, *1*, 243.
- (126) Rim, K. T.; Hershberger, J. F. *J. Phys. Chem. A* **2000**, *104*, 293.
- (127) Miller, J. A.; Durant, J. L.; Glarborg, P. *27th Symposium (Int.) on Combustion*; The Combustion Institute: Pittsburgh, PA, **1998**, 235.
- (128) Marinov, N. M.; Malte, P. C. *Int. J. Chem. Kinet.* **1995**, *27*, 957.
- (129) Carr, R. W., Jr.; Gay, I. D.; Glass, G. P. *J. Chem. Phys.* **1968**, *49*, 846.
- (130) Slemr, F.; Warneck, P. *Ber. Bunsen-Ges. Phys. Chem.* **1975**, *79*, 152.
- (131) Michael, J. V.; Nava, D. F.; Payne, W. A.; Stief, L. J. *J. Chem. Phys.* **1979**, *70*, 5222.
- (132) Frank, P.; Bhaskaran, K. A.; Just, Th. *J. Phys. Chem.* **1986**, *90*, 2226.
- (133) Bencsura, A.; Knyazev, V. D.; Slagle, I.R.; Gutman, D.; Tsang, W. *Ber. Bunsen-Ges. Phys. Chem.* **1992**, *96*, 1338.
- (134) Baldwin, P. J.; Canosa-Mas, C. E.; Frey, H. M.; Walsh, R. *Int. J. Chem. Kinet.* **1987**, *19*, 997.
- (135) Baulch, D. L.; Cobos, C. J.; Cox, R. A.; Frank, P.; Hayman, G.; Just, Th.; Kerr, J. A.; Murrells, T.; Pilling, M. J.; Troe, J.; Walker, R. W.; Warnatz, J. *J. Phys. Chem. Ref. Data* **1994**, *23*, 847.
- (136) Colket, M. B., III; Naegeli, D. W.; Glassman, I. *Int. J. Chem. Kinet.* **1975**, *7*, 223.
- (137) Shokhirev, N. V.
<http://www.chem.arizona.edu/faculty/walk/nikolai/programs.html#programs> July, 2002.
- (138) Lay, T. H.; Krasnoperov, L. N.; Venanzi, C. A.; Bozzelli, J. W. *J. Phys. Chem.* **1996**, *100*, 8240.
- (139) Yamada, T.; Lay, T. H.; Bozzelli, J. W. *J. Phys. Chem. A* **1998**, *102*, 7286.
- (140) Yamada, T.; Lay, T. H.; Bozzelli, J. W. *J. Phys. Chem. A* **1999**, *103*, 5602.

- (141) Hirschfelder, J. O.; Curtiss, C. F.; Bird, R. B. *Molecular Theory of Gases and Liquids*, 2nd ed.; Wiley: London, 1963.
- (142) Bohm, H.; El Kadi, B.; Baronnet, F. *Oxid. Commun.* **1996**, *19*, 25.
- (143) Bach, R. D.; Ayala, P. Y.; Schlegel, H. B. *J. Am. Chem. Soc.* **1996**, *118*, 12758.
- (144) Raiti, M. J.; Sevilla, M. D. *J. Phys. Chem.* **1999**, *103*, 1619.
- (145) Ruiz, R. P.; Bayes, K. D.; Macpherson, M. T.; Pilling, M. J. *J. Phys. Chem.* **1981**, *85*, 1622.
- (146) Morgan, C. A.; Pilling, M. J.; Tulloch, J. M.; Ruiz, R. P.; Bayes, K. D. *J. Chem. Soc. Faraday Trans. 2* **1982**, *78*, 1323.
- (147) Slagle, I. R.; Ratajczak, E.; Heaven, M. C.; Gutman, D.; Wagner, A. F. *J. Am. Chem. Soc.* **1985**, *107*, 1838.
- (148) Knyazev, V. D.; Slagle, I. R. *J. Phys. Chem. A* **1998**, *102*, 8932.
- (149) Lodhi, Z. H.; Walker, R. W. *J. Chem. Soc., Faraday Trans.* **1991**, *87*, 681.
- (150) Stothard, N. D.; Walker, R. W. *J. Chem. Soc. Faraday Trans.* **1992**, *88*, 2621.
- (151) Baldwin, R. R.; Bennett, J. P.; Walker, R. W. *J. Chem. Soc. Faraday Trans. 1* **1980**, *76*, 2396.
- (152) Olivella, S.; Sole, A. *J. Am. Chem. Soc.* **2003**, *125*, 10641.
- (153) Porter, N. A.; Mills, K. A.; Carter, R. L. *J. Am. Chem. Soc.* **1994**, *116*, 6690.
- (154) Porter, N. A.; Caldwell, S. E.; Mills, K. A. *Lipids* **1995**, *30*, 277.
- (155) Scott, A. P.; Radom, L. *J. Phys. Chem.* **1996**, *100*, 16502.
- (156) Boyd, S. L.; Boyd, R. J.; Barclay, L. R. C.; Porter, N. A. *J. Am. Chem. Soc.* **1993**, *115*, 687.
- (157) Barckholtz, T. A. (ExxonMobile Research and Engineering Company, Annandale, New Jersey 08801); Chen, C. and Bozzelli, J. W. (Department of Chemistry and Environmental Science, New Jersey Institute of Technology, New Jersey 07102) Personal Communication.
- (158) Green, J. H. S. *Chem. Ind. (London)*, **1960**, 1215.

- (159) Cox, J. D. ; Pilcher, G. *Thermochemistry of Organic and Organometallic Compound*; Academic Press: New York, 1970.
- (160) Lay, T. H.; Yamada, T.; Tsai, P.; Bozzelli, J. W. *J. Phys. Chem. A* **1997**, *101*, 2471.
- (161) Earl, B. L.; Titus, R. L. *Collect Czech. Chem. Commun.* **1995**, *60*, 104.
- (162) Seetula, J. A.; Gutman, D.; Lightfoot, P. D.; Rayes, M. T.; Senkan, S. M. *J. Phys. Chem.* **1991**, *95*, 10688.
- (163) Seetula, J. A. *J. Chem. Soc. Faraday Trans.* **1998**, *94*, 3561.
- (164) Seetula, J. A. *J. Chem. Soc. Faraday Trans.* **1996**, *92*, 3069.
- (165) Seetula, J. A.; Gutman, D. *J. Phys. Chem.* **1991**, *95*, 3626.
- (166) Timonen, R. S.; Russell, J. J.; Gutman, D. *Int. J. Chem. Kinet.* **1986**, *18*, 1193.
- (167) Petersson, G. A.; Nyden, M. R. *J. Chem. Phys.* **1981**, *75*, 3423.
- (168) Lay, T. H.; Bozzelli, J. W.; Dean, A. M.; Ritter, E. R. *J. Phys. Chem.* **1995**, *99(39)*, 14514.
- (169) Timonen, R. S.; Russell, J. J.; Sarzynski, D.; Gutman, D. *J. Phys. Chem.* **1987**, *91*, 1873.
- (170) Wong, D. K.; Kretkowski, D. A.; Bozzelli, J. W. *Ind. Eng. Chem. Res.* **1993**, *32*, 3184.
- (171) Zhu, L.; Bozzelli, J. W.; Lay, T. H. *Ind. Eng. Chem. Res.* **1998**, *37*, 3497.
- (172) Taylor, P. H.; Dellinger, B.; Tirey, D. A. *Int. J. Chem. Kinet.* **1991**, *23*, 1051.
- (173) Kafafi, S. A.; Hudgens, J. W. *J. Phys. Chem.* **1989**, *93*, 3474. (I took the frequencies in this article for calculating S, Cp.)
- (174) Rayez, M. T.; Rayez, C.; Sawerysyn, J. P. *J. Phys. Chem.* **1994**, *98(44)*, 11342.
- (175) Timonen, R. S.; Gutman, D. *J. Phys. Chem.* **1986**, *90*, 2987.
- (176) Ayscough, P. B.; Cocker, A. J.; Dainton, F. S.; Hirst, S.; Weston, M. *Proc. Chem. Soc.* **1961**, 244.
- (177) Ayscough, P. B.; Dainton, F. S.; Fleischfresser, B. E. *Trans. Faraday Soc.* **1966**, *62*, 1838.

- (178) Bertrand, L.; Bizongwako, J.; Huybrechts, G.; Olbregts, J. *Bull. Soc. Chim. Belg.* **1972**, *81*, 73. (R. + O₂ = 6.31E+10 for k_{ref} was used.)
- (179) Cioslowski, J.; Liu, G.; Moncrieff, D. *J. Am. Chem. Soc.* **1997**, *119*(47), 11452.
- (180) Seetula, J. A. *J. Chem. Soc. Faraday Trans.* **1998**, *94*(7), 891.
- (181) Tschuikow-Roux, E.; Paddison, S. *Int. J. Chem. Kinet.* **1987**, *19*, 15.
- (182) McMurry, J.; Fay, R. C. Chemistry, Prentice-Hall, Upper Saddle River, US, 2001.
- (183) Sinninghe Damste, J. S.; White, C. M.; Green, J. B.; de Leeuw, J. W. *Energy & Fuels* **1999**, *13*, 728.
- (184) Armstrong, D. A. *S-centered radicals*; Wiley: Chichester, UK, 1999; Chapter 2.
- (185) Frisch, M. J.; Trucks, G. W.; Schlegel, H. B.; Scuseria, G.; Robb, M. A.; Cheesman, J. R.; Zakrzewski, V. G.; Montgomery, J. A., Jr.; Stratmann, R. E.; Burant, J. C.; Dapprich, S.; Millam, J. M.; Daniels, A. D.; Kudin, K. N.; Strain, M. C.; Farkas, O.; Tomasi, J.; Barone, V.; Cossi, M.; Cammi, R.; Mennucci, B.; Pomelli, C.; Adamo, C.; Clifford, S.; Ochterski, J.; Petersson, G. A.; Ayala, P. Y.; Cui, Q.; Morokuma, K.; Malick, D. K.; Rabuck, A. D.; Raghavachari, K.; Foresman, J. B.; Cioslowski, J.; Ortiz, J. V.; Baboul, A. G.; Stefanov, R. B.; Liu, G.; Liashenko, A.; Piskorz, P.; Komaromi, I.; Gomperts, R.; Matrin, R. L.; Fox, D. J.; Keith, T.; Al-Laham, M. A.; Peng, C. Y.; Nanayakkara, A.; Gonzalez, C.; Challacombe, M.; Gill, P. M. W.; Johnson, B.; Chen, W.; Wong, M. W.; Andres, J. L.; Head-Gordon, M.; Pople, J. A. *Gaussian 98*; Gaussian Inc.: Pittsburgh, PA, 1998.
- (186) Lias, S. G.; Bartmess, J. E.; Liebman, J. F.; Holmes, J. L.; Levin, R. D.; Mallard, W. G. *J. Phys. Chem. Ref. Data* **1988**, *17*, Supplement No.1.
- (187) Sun, H.; Bozzelli, J. W. *J. Phys. Chem. A* **2002**, *106*, 3947.
- (188) Ruscic, B.; Berkowitz, J. *J. Chem. Phys.* **1992**, *97*, 1818.
- (189) Griller, D.; Martinho Simoes, J. A.; Wayner, D. D. M. *Sulfur-Centered Reactive Intermediates in Chemistry and Biology*; Chatgililoglu, C., Asmus, K. D., Eds.; Nato ASI Series, Plenum: New York, 1990; pp 37-52.
- (190) Nourbakhsh, S.; Norwood, K.; Yin, H. M.; Liao, C. L.; Ng, C. Y. *J. Chem. Phys.* **1991**, *95*, 5014.
- (191) Jefferson, A.; Nicovich, J. M.; Wine, P. H. *J. Phys. Chem.* **1994**, *98*, 7128.

- ~~(192)~~ Yamada, T.; Bozzelli, J. W.; Lay, T. H. *24th Symposium (International) on Combustion*; The Combustion Institute: Pittsburgh, PA, 1996; pp 201-209.
- (193) Montgomery, J. A., Jr.; Frisch, M. J.; Ochtterski, J. W.; Petersson, G. A.; *J. Chem. Phys.* **1999**, *110*, 2822.
- (194) Montgomery, J. A., Jr.; Frisch, M. J.; Ochtterski, J. W.; Petersson, G. A.; *J. Chem. Phys.* **2000**, *112*, 6532.
- (195) Seetula, J. A. *Phys. Chem. Chem. Phys.* **2000**, *2*, 3807.
- (196) Holmes, J. L.; Lossing, F. P. *J. Am. Chem. Soc.* **1988**, *110*, 7343.
- (197) Troe, J. *Ber. Bunsen-Ges. Phys. Chem.* **1983**, *87*, 161.
- (198) Troe, J. *J. Phys. Chem.* **1979**, *83*, 114.